



National Library  
of Canada

Acquisitions and  
Bibliographic Services Branch

395 Wellington Street  
Ottawa, Ontario  
K1A 0N4

Bibliothèque nationale  
du Canada

Direction des acquisitions et  
des services bibliographiques

395, rue Wellington  
Ottawa (Ontario)  
K1A 0N4

Your file    Votre référence

Our file    Notre référence

## NOTICE

The quality of this microform is heavily dependent upon the quality of the original thesis submitted for microfilming. Every effort has been made to ensure the highest quality of reproduction possible.

If pages are missing, contact the university which granted the degree.

Some pages may have indistinct print especially if the original pages were typed with a poor typewriter ribbon or if the university sent us an inferior photocopy.

Reproduction in full or in part of this microform is governed by the Canadian Copyright Act, R.S.C. 1970, c. C-30, and subsequent amendments.

## AVIS

La qualité de cette microforme dépend grandement de la qualité de la thèse soumise au microfilmage. Nous avons tout fait pour assurer une qualité supérieure de reproduction.

S'il manque des pages, veuillez communiquer avec l'université qui a conféré le grade.

La qualité d'impression de certaines pages peut laisser à désirer, surtout si les pages originales ont été dactylographiées à l'aide d'un ruban usé ou si l'université nous a fait parvenir une photocopie de qualité inférieure.

La reproduction, même partielle, de cette microforme est soumise à la Loi canadienne sur le droit d'auteur, SRC 1970, c. C-30, et ses amendements subséquents.

**Canada**

UNIVERSITY OF ALBERTA

**Speciation by Electrospray Mass Spectrometry**

BY



**Ian I. Stewart**

A thesis submitted to the Faculty of Graduate Studies and Research in partial fulfillment of the requirements for the degree of **Doctor of Philosophy**.

**DEPARTMENT OF CHEMISTRY**

**Edmonton, Alberta  
SPRING, 1996**



National Library  
of Canada

Acquisitions and  
Bibliographic Services Branch

395 Wellington Street  
Ottawa, Ontario  
K1A 0N4

Bibliothèque nationale  
du Canada

Direction des acquisitions et  
des services bibliographiques

395, rue Wellington  
Ottawa (Ontario)  
K1A 0N4

Your file    Votre référence

Our file    Notre référence

**The author has granted an irrevocable non-exclusive licence allowing the National Library of Canada to reproduce, loan, distribute or sell copies of his/her thesis by any means and in any form or format, making this thesis available to interested persons.**

**L'auteur a accordé une licence irrévocable et non exclusive permettant à la Bibliothèque nationale du Canada de reproduire, prêter, distribuer ou vendre des copies de sa thèse de quelque manière et sous quelque forme que ce soit pour mettre des exemplaires de cette thèse à la disposition des personnes intéressées.**

**The author retains ownership of the copyright in his/her thesis. Neither the thesis nor substantial extracts from it may be printed or otherwise reproduced without his/her permission.**

**L'auteur conserve la propriété du droit d'auteur qui protège sa thèse. Ni la thèse ni des extraits substantiels de celle-ci ne doivent être imprimés ou autrement reproduits sans son autorisation.**

ISBN 0-612-10641-1

**Canada**

UNIVERSITY OF ALBERTA

LIBRARY RELEASE FORM

NAME OF AUTHOR: **Ian I. Stewart**

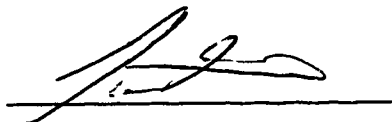
TITLE OF THESIS: **Speciation By Electrospray Mass Spectrometry**

DEGREE: **Doctor of Philosophy**

YEAR THIS DEGREE GRANTED: **1996**

Permission is hereby granted to the University of Alberta Library to reproduce single copies of this thesis and to lend or sell such copies for private, scholarly or scientific research purposes only.

The author reserves all other publication rights and other rights in association with the copyright in the thesis, and except as hereinbefore provided neither the thesis nor any substantial portion thereof may be printed or otherwise reproduced in any material form whatever without the author's prior written permission.



**Department of Chemistry  
University of Alberta  
Edmonton, Alberta  
Canada, T6G 2G2**

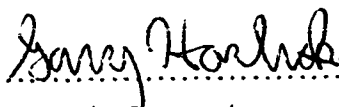
Date: April 16, 1996

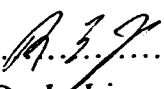


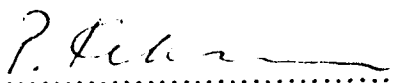
UNIVERSITY OF ALBERTA

FACULTY OF GRADUATE STUDIES AND RESEARCH

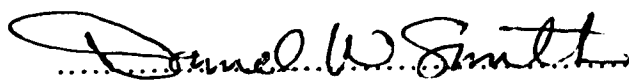
The undersigned certify that they have read, and recommend to the Faculty of Graduate Studies and Research for acceptance, a thesis entitled SPECIATION BY ELECTROSPRAY MASS SPECTROMETRY submitted by Ian I. Stewart in partial fulfillment of the requirements for the degree of Doctor of Philosophy.


  
.....  
Dr. G. Horlick, Supervisor

  
.....  
Dr. L. Li

  
.....  
Dr. P. Kebarle

  
.....  
Dr. R. B. Jordan

  
.....  
Dr. D. W. Smith

  
.....  
Dr. D.W. Koppenaal, External Examiner

DATE:  April 11, 1996

*To my sweetheart Liane,  
and my parents John and Shirley.*

## **Abstract**

An investigation into the use of Electrospray Mass Spectrometry for speciation work is presented. Electrospray's unique ability to transfer pre-existing ions in solution into the gas phase provided the impetus for such studies. An evaluation of the technique's ability to yield useful speciation information based on specific chemical systems is given. Fundamental aspects of the technique were also investigated for the purpose of providing greater insight into the processes responsible for the production of ions.

A characterization of the sampling process is first presented to provide a framework for collisionally induced dissociation (CID) events which occur in this region. A basic understanding of CID at the interface is essential for a correct and useful interpretation of a recorded mass spectrum.

The speciation ability of electrospray was then investigated for two different systems. The first system involved chromium solutions of different oxidation states and molecular forms. It was found that various molecular forms of the two oxidation states Cr(III) and Cr(VI) could be inferred and that useful speciation information could be obtained. The second system involved sulfur containing inorganic molecular ions. A whole range of species was determined in solution. Both of the test systems provided clear evidence that useful speciation information can be obtained in addition to providing insight into further work which would increase the understanding of the technique.

Fundamental studies were undertaken to gain insight into the processes involved in generating a stable electrospray and to better understand the problem of quantitative non-linearity. Several key processes are discussed that contribute to the nonlinearity in relation to mass spectrometry. Other aspects, such as the origin of ion intensity variations and the possible origin of such variations are included. However there are yet to be any definite conclusions.

## **Acknowledgments**

For making all this possible there are many whom I wish to thank.

First and foremost, my deepest thanks goes to Dr. Gary Horlick, for the opportunity to explore my research field without showing (too) much fear. I learned a lot from him on a variety of subjects, such as teaching, scientific philosophy, common sense (I'm still working on this one) and especially pool. These are things I will carry with me forever. For all his help, encouragement and advice throughout my thesis I am truly grateful.

I wish to acknowledge my research group, past and present. Especially the help, advice and friendship of George Agnes which was invaluable.

To all the professors who took the time to answer my frequent questions: I would especially like to thank Dr. R.B. Jordan and Dr. J. Takats for enlightening discussions on certain aspects of inorganic chemistry and Dr. F. Cantwell for his clarification of solution chemistry. My appreciation also goes to Dr. P. Kebarle for some insightful conversations on electrospray.

I am also indebted to all the people in the machine shop and electronics shop, especially Henry Stolk, whose own particular blend of humor and encouragement got me through some difficult situations.

Life in Edmonton was made interesting and enjoyable through my friendships with John Crabtree, John Klassen, Todd DeMone and Christine Szymanski. Thank you for the entertaining conversations over coffee and beer, the parties, and the great soccer games. Working late nights was made all the more bearable due to Dev Pinto and even Darren Lewis. Thanks! You've given me great memories. And my heartfelt appreciation goes to Dr. Edgar Arriaga for always being there.

Finally, my deepest love and gratitude to my sweetheart Liane, for her support and patience throughout all of this, and for believing in me. For this and more I am forever in her debt.

## Table of Contents

Chapter	Page
<b>1 Introduction</b>	<b>1</b>
1.1 Thesis Objective .....	2
1.2 Electrospray .....	2
1.3 Sampling Electrospray Generated ions into a Mass Spectrometer .....	9
1.4 Inorganic Electrospray Mass Spectrometry Studies .....	15
1.5 Conclusions .....	23
1.6 References .....	26
<b>2 Instrumentation</b> .....	<b>29</b>
2.1 Introduction .....	30
2.2 Mass Spectrometer .....	30
2.3 The Vacuum System .....	34
2.4 The Interface .....	36
2.5 The Free Jet Expansion .....	40
2.6 References .....	47
<b>3 The Electrospray Mass Spectra of the Lanthanides</b> .....	<b>48</b>
3.1 Introduction .....	49
3.2 Experimental .....	51
3.3 Results and Discussion .....	54
3.4 Conclusions .....	79
3.5 References .....	81
<b>4 Chromium Speciation</b> .....	<b>84</b>
4.1 Introduction .....	85
4.2 Background .....	87
4.3 Experimental .....	89
4.4 Results and Discussion .....	90
4.4.1 Cr (III) .....	90
4.4.2 Cr (III) solutions .....	92
4.4.3 Polymeric Species .....	10
4.4.4 Kinetic Inertness of Cr (III) .....	10

<b>Chapter</b>	<b>Page</b>
4.4.5 Cr (VI).....	112
4.4.6 Cr (VI) Solutions.....	114
4.4.7 Trichromate Ion.....	125
4.4.8 Chlorochromate.....	127
4.5 Conclusions .....	131
4.5 References.....	133
<b>5 Sulfur Speciation .....</b>	<b>136</b>
5.1 Introduction .....	137
5.2 Experimental .....	139
5.3 Results and Discussion .....	141
5.3.1 General .....	141
5.3.2 Interpreting Reaction Mixtures.....	154
5.3.3 Quantitative Studies: Preliminary Data .....	162
5.4 Conclusions .....	167
5.5 Appendix: Existence of the Bare Peroxodisulfate Ion.....	168
5.6 References.....	175
<b>6 Electrospray: Current Implications.....</b>	<b>178</b>
6.1 Introduction .....	179
6.2 Experimental .....	180
6.3 Results and Discussion .....	183
6.3.1 Electrospray Formation.....	183
6.3.2 Electrospray Current .....	198
6.3.3 Mass Spectral Consequences .....	212
6.3.4 Surface Charging.....	220
6.4 Conclusions .....	231
6.5 References.....	232
<b>7 Surface Tension Gradients .....</b>	<b>235</b>
7.1 Introduction .....	236
7.2 Experimental .....	239
7.3 Discussion.....	240

<b>Chapter</b>	<b>Page</b>
7.3.1 Mass Spectral Ion Intensity .....	240
7.3.2 Surface Tension Gradients .....	243
7.3.3 Surface Tension Measurements.....	245
7.3.4 Implications of the Surface Tension Gradient Measurements.....	246
7.4 Conclusions .....	253
7.5 References.....	254
<b>8 Conclusions</b>	<b>255</b>
8.1 Summary .....	256
8.2 Assesment .....	258
8.3 Future Improvements and Recomendations .....	259

## List of Tables

Table	Page
3.1 Physical Data for the Lanthanide Metals .....	59
4.1 Ionization Potential of Selected Species.....	97
4.2 UV-Vis Absorption Data.....	104
5.1 Relative Isotopic Abundance of Various Sulfate Species .....	165
6.1 Physical Properties and Physical Constants of Methanol.....	225
6.2 Physical Parameters of Electrolytes in Methanol.....	225
7.1 Literature values of $d\gamma/dC_j$ for a variety of electrolytes in water at 298K .....	250
7.2 Anion surface adsorption classification for various anions in water at 298K. ....	250



## List of Figures

Figure	Page
1.1 Schematic profile of an electrospray capillary. With low (a) and high (b.) voltage applied.....	5
1.2 A 60X image of an electrospray capillary in operation. The capillary has a 200 $\mu$ m o.d. and a 100 $\mu$ m i.d. a KCl solution (1x10 <sup>-4</sup> M in methanol) is being pumped through the capillary at 2.00 $\mu$ L/min. The capillary is held at -1900V relative to ground (5mm capillary to counter electrode separation). ....	6
1.3 Electrospray interface schematic showing the expansion region, and an expanded cartoon of the "spray". ....	10
1.4 Electrospray mass spectra of CsCl (1.0x10 <sup>-4</sup> M) in methanol. a) $\Delta V = 5V$ b) $\Delta V = 12V$ , c) $\Delta V = 28V$ . ( $\Delta V$ in all captions refers to the voltage difference between the sampling plate and skimmer).....	12
1.5 Electrospray mass spectrum of a NaCl, NaClO <sub>3</sub> and NaClO <sub>4</sub> solution each at 1.0x10 <sup>-4</sup> M in methanol. ....	17
1.6 Electrospray mass spectra of a) Sn(CH <sub>3</sub> ) <sub>3</sub> Cl $\Delta V = 35V$ b) Sn(CH <sub>3</sub> ) <sub>2</sub> Cl <sub>2</sub> $\Delta V = 30V$ and c) Sn(C <sub>4</sub> H <sub>9</sub> ) <sub>2</sub> Cl <sub>2</sub> $\Delta V = 30V$ each at 1.0x10 <sup>-4</sup> M in methanol. ....	19
1.7 Relative Isotopic distributions of Sn(CH <sub>3</sub> ) <sub>2</sub> OCH <sub>3</sub> <sup>+</sup> and Sn(CH <sub>3</sub> ) <sub>2</sub> Cl <sup>+</sup> .....	21
1.8 Electrospray mass spectra of Sn(CH <sub>3</sub> ) <sub>3</sub> Cl, Sn(CH <sub>3</sub> ) <sub>2</sub> Cl <sub>2</sub> and Sn(C <sub>4</sub> H <sub>9</sub> ) <sub>2</sub> Cl <sub>2</sub> at 1.0x10 <sup>-4</sup> M in methanol. a) $\Delta V = 35V$ b) and c) are just zoomed in portions of a).....	22
2.1 Schematic Diagrams of the modified Perkin Elmer/SCIEX ELAN Model 250 with a.) original ion optics and b.) modified ion optics. ....	31
2.2 Typical intensity improvement a.) before and b.) after ion optic modification. (CrCl <sub>3</sub> : 1x10 <sup>-4</sup> M in methanol, similar operating conditions). ....	33
2.3 A schematic representation of the mass spectrometer and pumping system. ....	34
2.4 Schematic representation of the interface with electrospray. ....	37
2.5 Schematic diagram of the plenum interface chamber showing the a.) profile, and b.) plexiglass front plate.....	38
2.6 Schematic representation of the structure of a continuum free jet expansion originating from a source at pressure P <sub>0</sub> flowing into a region of pressure P <sub>b</sub> . ....	41

Figure	Page
2.7 The center line Mach number (M) dependence on the distance ratio (x/D) for $\gamma = 1.40$ .....	44
2.8 The centerline nitrogen number density dependance on the Mach number (M).....	45
3.1 Schematic diagram of the electrospray interface. ....	51
3.2 Mass Spectra of; $\text{LaCl}_3$ , $\text{CeCl}_3$ , $\text{Pr}(\text{NO}_3)_3$ , $\text{TmCl}_3$ , $\text{YbCl}_3$ , $\text{LuCl}_3$ solutions ( $2.0 \times 10^{-4}\text{M}$ ). Spectra acquired under identical 'bare metal ion' mode conditions. ....	55
3.3 Mass Spectra of $\text{Pr}(\text{NO}_3)_3$ ( $2.0 \times 10^{-4}\text{M}$ ) acquired by varying the sampling plate (S.P.) voltage: (a) 25V, (b) 35V, (c) 45V, (d) 55V, (e) 65V, (f) 75V.....	60
3.4 Mass Spectra of $\text{TmCl}_3$ ( $2.0 \times 10^{-4}\text{M}$ ) acquired by varying the sampling plate (S.P.) voltage: (a) 25V, (b) 35V, (c) 45V, (d) 55V, (e) 65V, (f) 75V.....	66
3.5 Mass Spectra of $\text{Pr}(\text{NO}_3)_3$ , $\text{GdCl}_3$ , $\text{LuCl}_3$ : ( $2 \times 10^{-4}\text{M}$ ). Spectra acquired under bare metal ion mode conditions.....	70
3.6 Mass Spectra of $\text{Pr}(\text{NO}_3)_3$ , $\text{GdCl}_3$ , $\text{LuCl}_3$ : ( $2.0 \times 10^{-4}\text{M}$ ). Spectra acquired under gentle mode conditions by varying the sampling plate voltage (a) 40V, (b) 55V.....	71
3.7 Negative ion mass spectrum of $2.0 \times 10^{-4}\text{M}$ $\text{LaCl}_3$ acquired at a sampling plate voltage of 40V. ....	74
3.8 The mass spectrum of (a) $\text{ScCl}_3$ and (b) $\text{Pr}(\text{NO}_3)_3$ where each are $2.0 \times 10^{-4}\text{M}$ in acetonitrile. The spectrum were both acquired with sampling plate voltages of 30V.....	77
4.1 $\text{CrCl}_3 \cdot 6\text{H}_2\text{O}$ : $1.0 \times 10^{-4}\text{M}$ (~6.6ppm) in methanol/1% $\text{H}_2\text{O}$ . Flowrate: $2.00\mu\text{L}/\text{min.}$ , $\Delta V = 145\text{V}$ .....	94
4.2 $\text{Cr}(\text{ClO}_4)_3 \cdot 6\text{H}_2\text{O}$ : $1.0 \times 10^{-4}\text{M}$ in methanol/1% $\text{H}_2\text{O}$ . Flow rate: $2.00\mu\text{L}/\text{min.}$ a.) $\Delta V = 20\text{V}$ , b.) $\Delta V = 35\text{V}$ , c.) $\Delta V = 55\text{V}$ .....	99
4.3 $\text{Cr}(\text{ClO}_4)_3 \cdot 6\text{H}_2\text{O}$ : $1.0 \times 10^{-4}\text{M}$ in Acetonitrile/1% $\text{H}_2\text{O}$ . Flow rate: $2.00\mu\text{L}/\text{min.}$ a.) $\Delta V = 20\text{V}$ , b.) $\Delta V = 30\text{V}$ , c.) $\Delta V = 45\text{V}$ , d.) $\Delta V = 65\text{V}$ .....	101
4.4 $\text{CrCl}_3 \cdot 6\text{H}_2\text{O}$ : $1.0 \times 10^{-4}\text{M}$ in methanol/1% $\text{H}_2\text{O}$ . $\Delta V = 25\text{V}$ . A $1.0 \times 10^{-2}\text{M}$ stock solution was prepared and allowed to age for 5 months in water, the solution was then diluted and spectra were acquired a.) after 5 min., b.) after 30 min., and c.) after 90 min. ....	106

4.5	CrCl <sub>3</sub> 6H <sub>2</sub> O: 1.0x10 <sup>-4</sup> M in methanol. ΔV = 40V. A 1.0x10 <sup>-2</sup> M stock solution was prepared in methanol and then let stand 12 hours before it was diluted to the final concentration with methanol and run.....	108
4.6	Relative isotopic distribution of a.) CrCl(OCH <sub>3</sub> ) <sup>+</sup> and b.) CrCl <sub>2</sub> <sup>+</sup> .....	109
4.7	Cr(ClO <sub>4</sub> ) <sub>3</sub> 6H <sub>2</sub> O: 1.0x10 <sup>-4</sup> M in acetonitrile/1%H <sub>2</sub> O. Flow rate: 2.00μL/min., ΔV = 25V. A 1.0x10 <sup>-2</sup> M stock solution was diluted and spectra were acquired a.) after 8 min., and b.) after 90 min.....	111
4.8	Effect of pH on the species distribution of Cr(VI) in aqueous solutions for the total concentration of a.) 1.0x10 <sup>-2</sup> M and b.) 1.0x10 <sup>-4</sup> M. ....	113
4.9	CID profile of Na <sub>2</sub> Cr <sub>2</sub> O <sub>7</sub> and HNO <sub>3</sub> each 1.0x10 <sup>-4</sup> M in methanol/1%H <sub>2</sub> O a.) ΔV = 25V, b.) ΔV = 40V.....	115
4.10	CID profile of Na <sub>2</sub> Cr <sub>2</sub> O <sub>7</sub> and HNO <sub>3</sub> each 1.0x10 <sup>-4</sup> M in acetonitrile/1%H <sub>2</sub> O. a.) ΔV = 25V, b.) ΔV = 55V, c.) ΔV = 75V.....	117
4.11	Concentration profiles of Na <sub>2</sub> CrO <sub>4</sub> in acetonitrile. All spectra acquired under identical conditions (ΔV = 25V). a.) 0.5x10 <sup>-4</sup> M, b.) 1.0x10 <sup>-4</sup> M, c.) 2.0x10 <sup>-4</sup> M.....	121
4.12	pH profiles of 0.5x10 <sup>-4</sup> M Na <sub>2</sub> CrO <sub>4</sub> in acetonitrile/0.5% H <sub>2</sub> O with varied pH control. All spectra acquired under identical conditions (ΔV = 25V). a.) 0.5x10 <sup>-4</sup> M NaOH added, b.) no pH adjustment, c.) 0.5x10 <sup>-4</sup> M HNO <sub>3</sub> added. ....	124
4.13	Mass spectrum of the dilution of a concentrated chromate solution. a.) 10μl of a stock solution of Na <sub>2</sub> CrO <sub>4</sub> (1M) and HNO <sub>3</sub> (1M) diluted to 100mL in acetonitrile. ΔV = 17V. b.) the relative isotopic abundances of the various species in a. ....	126
4.14	Mass spectrum of chlorochromate. Na <sub>2</sub> CrO <sub>4</sub> , HNO <sub>3</sub> and KCl each 0.5x10 <sup>-4</sup> M in acetonitrile/1% H <sub>2</sub> O, ΔV = 25V.....	128
4.15	Reaction products of 0.5x10 <sup>-4</sup> M Na <sub>2</sub> CrO <sub>4</sub> in left to age in acetonitrile/0.5% H <sub>2</sub> O for four days. CID profile a.) ΔV = 25V, b.) ΔV = 40V.....	130
5.1	3D CID spectra of ammonium persulfate (1.0x10 <sup>-4</sup> M) in methanol. The plot illustrates the change in the solvated distribution of the persulfate ion going from -10V potential difference to a -30V potential difference.....	144

5.2	Mass spectrum of vanadyl sulfate ( $1.0 \times 10^{-4} \text{M}$ ) in methanol. The spectra were acquired at two different sampling plate to skimmer potential differences a.) -12.5V and b.) -22.5V.....	146
5.3	Mass spectra of sodium thiosulfate ( $1.0 \times 10^{-4} \text{M}$ ) in methanol. The spectra were acquired at different sampling plate to skimmer potential differences; a) -14V, b) -19V and c)-24V.....	149
5.4	Mixture of oxo-sulfur species; ammonium persulfate, sodium thiosulfate and sodium sulfate each $1.0 \times 10^{-4} \text{M}$ in methanol. Spectrum a.) was acquired with a sampling plate to skimmer potential difference of -30V and spectrum b.) was acquired with a sampling plate to skimmer potential difference of -10V ...	151
5.5	Mass spectrum of sodium sulfite ( $1.0 \times 10^{-4} \text{M}$ ) in methanol. The spectrum was acquired with a sampling plate to skimmer potential difference of -20V. ....	153
5.6	Mass spectra of the reaction products from a solution of iodine ( $1.0 \times 10^{-2} \text{M}$ ) and sodium thiosulfate ( $2.0 \times 10^{-2} \text{M}$ ) diluted in methanol 100X. The spectra were acquired at a sampling plate to skimmer potential differences of a.) -22V, and b.) -27V.....	155
5.7	Mass spectrum of the reaction products from a solution of $\text{MnO}_2$ ( $1.0 \times 10^{-2} \text{M}$ ), Sodium sulfite ( $2.0 \times 10^{-2} \text{M}$ ) and nitric acid ( $4.0 \times 10^{-2} \text{M}$ ) diluted in methanol 100X. The spectrum was acquired with a sampling plate to skimmer potential difference of -22V.....	157
5.8	Mass spectra of the reaction products from a solution of silver chloride ( $5.0 \times 10^{-3} \text{M}$ ), dissolved by sodium thiosulfate ( $2.5 \times 10^{-2} \text{M}$ ) in aqueous solution. The sample was then diluted 100X in methanol. The spectra were acquired at different sampling plate to skimmer potential differences; a) -9V, b) -14V (higher resolution) and c) -24V.....	160
5.9	Relative isotopic abundance's silver thiosulfate complexes; a) $\text{Ag}(\text{S}_2\text{O}_3)_2(\text{H}_2\text{O})_5^{3-}$ , b) $\text{Ag}(\text{S}_2\text{O}_3)_2^-$ .....	161
5.10	Log-log calibration curve for sodium sulfate in methanol by ESMS the log of the sulfate intensity as ratioed against a $1.0 \times 10^{-4} \text{M}$ KI internal standard response is plotted versus the log of the sulfate concentration. ....	164
5.11	(Mass spectrum of a waste water sample. The sample was diluted 100X in methanol and acquired with a sampling plate to skimmer potential difference of -40V. ....	164

5.12 Standard addition calibration curve for sulfate ion in a waste water sample by ESMS the total sulfate intensity is ratioed against a $1.0 \times 10^{-4} \text{M}$ KI internal standard response and plotted versus added sodium sulfate concentration.....	166
5.13 Negative ion mass spectra of $2.0 \times 10^{-4} \text{M}$ ammonium persulfate in methanol obtained with a sampler to skimmer potential difference of a.) 20V, and b.) 25V.....	169
5.14 Negative ion mass spectra of $2.0 \times 10^{-4} \text{M}$ ammonium persulfate in methanol obtained with a sampler to skimmer potential difference of a.) 35V, and b.) 40V.....	171
5.15 Negative ion mass spectra of $2.0 \times 10^{-4} \text{M}$ ammonium persulfate in methanol obtained with a sampler to skimmer potential difference of 70V.....	173
5.16 The relative isotopic abundance of $\text{S}_2\text{O}_8^{2-}$ , $\text{SO}_4^-$ and $\text{HSO}_4^-$ .....	174
6.1 CCD image of the stainless steel electrospray capillary tip. O.D. = $200 \mu\text{m}$ , I.D. = $100 \mu\text{m}$ .....	181
6.2 Schematic of the system used to collect the images as well monitor the spray current.....	182
6.3 A CCD picture of the "Taylor cone" (60X, pixel resolution of $1 \mu\text{m}$ ). Solution: KCl at $1 \times 10^{-4} \text{M}$ in MeOH. Flow rate: $2.00 \mu\text{L}/\text{min}$ ., Capillary Voltage: $-2.00 \text{kV}$ , Capillary to plane separation: $5 \text{mm}$ . ....	184
6.4 Unstable Taylor cone profile of; KCl: $3 \times 10^{-4} \text{M}$ , Flow rate $1.50 \mu\text{L}/\text{min}$ ., Electrospray tip biased to $-1.90 \text{kV}$ , held $5 \text{mm}$ from counter electrode.....	189
6.5 The visual response of the electrospray as a function of applied voltage. Acquired at a capillary to planar counter electrode separation of $5 \text{mm}$ , flow rate of $2.00 \mu\text{L}/\text{min}$ . and a solution concentration of $1 \times 10^{-4} \text{M}$ KCl in methanol. a.) $0 \text{V}$ , b.) $-1.55 \text{kV}$ , c.) $-1.60 \text{kV}$ , d.) $-1.70 \text{kV}$ , e.) $-1.80 \text{kV}$ , f.) $-1.90 \text{kV}$ , g.) $-1.95 \text{kV}$ , h.) $-2.00 \text{kV}$ , i.) $-2.10 \text{kV}$ , j.) $-2.20 \text{kV}$ , k.) $-2.30 \text{kV}$ , l.) $-2.40 \text{kV}$ . ....	192
6.6 The chronological sequence of events in the "Pulsed Droplet" mode. Going from an extended form to a relaxed form.....	194
6.7 The main functioning modes of the "Rapid Pulsed Droplet" mode. a.) is the relaxed form and b.) is the extended spray form and c.) reveals some of the fine structure of the spray. 'kink instabilities'.....	196

6.8	The observed current response as a function of applied potential. KCl: $1.0 \times 10^{-4} \text{M}$ in methanol, Flow rate; $2.00 \mu\text{L}/\text{min.}$ , capillary to plane separation; 5mm. ....	200
6.9	The observed cone-jet coordinates as a function of applied potential, a.) filament length b.) cone length. KCl: $1.0 \times 10^{-4} \text{M}$ in methanol, Flow rate; $2.00 \mu\text{L}/\text{min.}$ , capillary to plane separation; 5mm. ....	202
6.10	The effect of hysteresis on the onset potential for a KCl solution of $1.0 \times 10^{-4} \text{M}$ in methanol. Flow rate; $2.00 \mu\text{L}/\text{min.}$ , capillary to plane separation ; 5mm. ....	203
6.11	The current vs applied potential plot for a series of KCl concentrations. Ranging from $2.0 \times 10^{-5} \text{M}$ - $2.0 \times 10^{-4} \text{M}$ KCl in methanol at a Flow rate; $2.00 \mu\text{L}/\text{min.}$ , capillary to plane separation; 5mm. ....	205
6.12	The current vs concentration profile of KCl in methanol. Acquired at a potential of -1.95kV, with a flow rate of $2.00 \mu\text{L}/\text{min.}$ , and a capillary to plane separation of 5mm. ....	205
6.13	A conductivity vs concentration plot for KCl in methanol. ....	206
6.14	a.) Plot of cone angle vs Applied potential for various concentrations of KCl in methanol. b.) The applied potential and observed current at $\theta = 71.6^\circ$ for various concentrations of KCl in methanol. Acquired at a flow rate of $2.00 \mu\text{L}/\text{min.}$ and a capillary to plane separation of 5mm. ....	208
6.15	The affect of Flow rate on the a.) observed current and the b.) observed cone 1/2 angle. The solution is KCl: $1.0 \times 10^{-4} \text{M}$ in methanol, the capillary tip is held at a potential of 1.90kV, and at a separation of 5mm. ....	212
6.16	The total mass spectral ion intensity of chloride vs concentration plot for KCl in methanol. The capillary to front plate separation is 5mm, the flow rate is $2.00 \mu\text{L}/\text{min.}$ and the ssampling plate to skimmer potential was 35V. ....	214
6.17	Pictures acquired of the electrospray phenomena for KCl at a.) $2.0 \times 10^{-5} \text{M}$ and b.) $2.0 \times 10^{-4} \text{M}$ . The hazy vertical illumate at the right of each image is the counter electrode (out od focus) at 5mm separation. The flow rate was $2.00 \mu\text{L}/\text{min.}$ in both cases. ....	215
6.18	Pictures acquired of the electrospray phenomena for KCl at a.) $2.0 \times 10^{-5} \text{M}$ and b.) $2.0 \times 10^{-4} \text{M}$ . The figures are backlit and were acquired at a capillary to counter electrode separation of 5mm at a flow rate of $2.00 \mu\text{L}/\text{min.}$ ....	216

6.19	The total intensity and ratioed intensity of $\text{KClO}_4$ ( $0.5 \times 10^{-4}\text{M}$ ) and $\text{KI}$ ( $1.4 \times 10^{-4}\text{M}$ ) in methanol. Capillary to front plate separation of 5mm, flow rate of $2.00\mu\text{L}/\text{min.}$ , $V_{\text{tip}}$ of $-2.70\text{kV}$ , front plate voltage of $-600\text{V}$ , sampling plate potential of $40\text{V}$ skimmer potential of $-5\text{V}$ .....	219
6.20	The ratioed response calibration curve for varying concentrations of $\text{KI}$ in the presence of $0.5 \times 10^{-4}\text{M}$ $\text{KClO}_4$ . Capillary to front plate separation of 5mm, flow rate of $2.00\mu\text{L}/\text{min.}$ , $V_{\text{tip}}$ of $-2.70\text{kV}$ , front plate voltage of $-600\text{V}$ , sampling plate potential of $40\text{V}$ skimmer potential of $-5\text{V}$ . ....	219
6.21	Observed current profiles for various electrolytes ( $\text{KCl}$ , $\text{KI}$ , $\text{KClO}_4$ , $\text{K}_2\text{SO}_4$ ) in methanol. a.) current versus applied potential and b.) current versus electrolyte.....	224
6.22	Limiting single ion mobility-viscosity product versus the reciprocal of the estimated crystallographic radii for various anions in methanol.....	227
6.23	The electrospray mass spectra of three different solutions acquired at a capillary to front plate separation of 5mm, flow rate of $2.00\mu\text{L}/\text{min.}$ , and a sampling plate to skimmer potential difference of $35\text{V}$ . All electrolyte is present at $1.0 \times 10^{-4}\text{M}$ in methanol. a.) $\text{KClO}_4$ and $\text{KI}$ , b.) $\text{K}_2\text{SO}_4$ and $\text{KI}$ and c.) $\text{KCl}$ , $\text{K}_2\text{SO}_4$ and $\text{KI}$ . ....	229
7.1	The electrospray mass spectra of a) $\text{KCl}$ , $\text{KClO}_4$ and $\text{KI}$ and b) $\text{KClO}_4$ and $\text{K}_2\text{SO}_4$ each at $1.0 \times 10^{-4}\text{M}$ in methanol. The spectra are acquired in negative ion mode with a sampling plate to skimmer potential difference of $35\text{V}$ , at a flow rate of $2.00\mu\text{L}/\text{min.}$ .....	241
7.2	The schematic representation of the system used to acquire surface tension measurements. ....	247
7.3	Ratioed response curves for varying chloride concentrations in the presence of constant concentrations ( $0.5 \times 10^{-4}\text{M}$ ) of iodide and perchlorate.....	252
8.1	The electrospray mass spectrum of sodium dichromate and nitric acid each $1.0 \times 10^{-4}\text{M}$ in acetonitrile. ....	259

## **Chapter 1**

### **Introduction**



## **1.1 Thesis Objective**

The development of new ion sources for mass spectrometry capable of providing more information about solution samples is an ongoing challenge for the analytical chemist.. For inorganic solution analysis, it may not be enough to simply determine the total content of a specified element in solution and so other methods must be sought to accomplish this. Recently there has been interest in the development of inorganic Electrospray Mass Spectrometry (ESMS) as this technique offers the potential to directly determine solution ions. In addition to identifying the type of ion present, the technique also offers information on an ions oxidation state and molecular form, which is not typically possible by established atomic spectroscopic techniques.

The aim of this work is to continue investigations of electrospray as an ion source for elemental and speciation work pertaining to inorganic solutions to further define and provide a guide for further investigations. The scope of this study is not however limited solely to analytical aspects, some important considerations in sampling and of fundamentals of electrospray were examined and will be outlined in the introductory discussion.

## **1.2 Electrospray**

It is fair to say that the development of inorganic Electrospray Mass Spectrometry (ESMS) has largely been overshadowed by the explosive development of ESMS in the organic/biological area. This may be well understood as electrospray offers a unique and relatively simple way of

generating intact gas phase ions from large solution ions and macromolecules. There is a wealth of literature available on a broad range of biological systems. The application of ESMS to inorganic systems has not however been lost and there is a smaller albeit, but strong base of literature available on the subject. In fact the pioneering work on ESMS by Yamashita and Fenn in 1984 examined both positive and negative inorganic ion species [1,2].

Before discussing the actual specifics of inorganic electrospray it is important to first describe the actual processes that are involved in both generating ions by an electrospray process and then sampling these ions into a mass spectrometer.

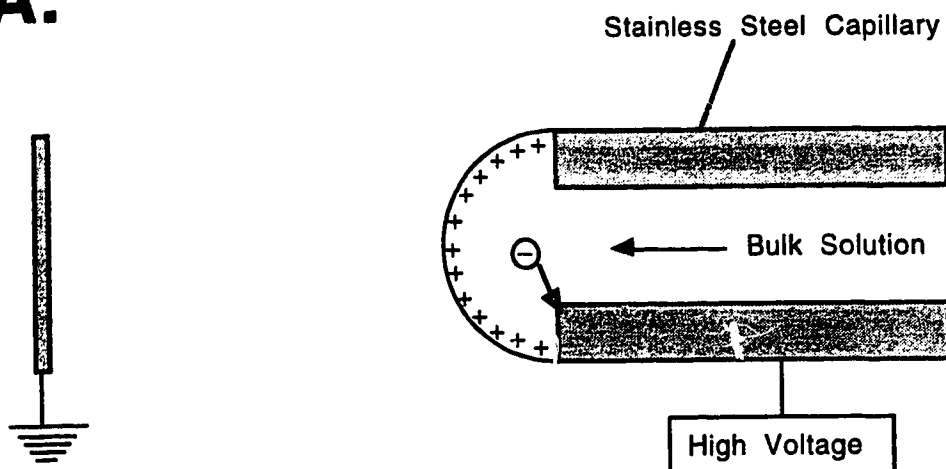
Although electrospray is often referred to as an ion source it cannot truly be thought of as an ionization source in the classical sense. Electrospray does not generally create ions, more it tends to facilitate the transfer of pre-existing solution ions to the gas phase which may then be sampled into a mass spectrometer. Electrospray involves the electrostatic spraying of a liquid, which generates small charged droplets and from which ultimately come gas phase ions. Electrospray may be operated in either a positive ion mode for the generation of positive gas phase ions or a negative ion mode for the generation of negative ions. To implement electrospray an electrolyte solution is pumped through a narrow diameter capillary (usually  $\sim 100\mu\text{m}$ ) at a relatively low flow rate, usually about  $1\text{-}10\mu\text{L}/\text{min}$ . The capillary is held at a high potential relative to a counter electrode (usually a front plate or a sampling orifice on a mass spectrometer). When the potential is positive, positively charged droplets are created and when the capillary is held at a high negative potential, negatively charged

droplets are created. The generation of a charged droplet is dependent on two main processes; a separation of charge yielding an overall net excess charge on the droplet and the liberation of this charged droplet from the bulk solution at the capillary tip.

To understand the first process consider a system where the capillary is charged up to some positive potential and the flow rate is small (Fig. 1.1a). Under the influence of an applied electric field the positive ions at the tip will migrate to the liquid surface whereas the negative ions (counter ions) will migrate away from the surface into the bulk and ultimately to the capillary surface where they are presumably discharged. This charge separation has been discussed in the literature [3] and is sometimes referred to as an "electrophoretic charging" process. The result is that the surface of the solution at the capillary tip will have an overall positive charge and will be drawn towards low field. If the potential on the capillary is increased the field will be stronger and the pull on the positively charged surface will be greater. This force is opposed by the cohesive forces associated with the apparent surface tension of the solution. As the field increases the liquid surface deforms as it is pulled towards the counter electrode and there will come a point when the surface tension is overcome and the bulk in the form of a 'charged droplet' is pulled towards the counter electrode. The surface then relaxes and starts charging up again until a point is reached where another droplet is pulled 'free'. The frequency of this process is dependent on the magnitude of the electric field, the surface tension of the bulk solvent and the conductivity of the solution (necessary to provide the solution ions to charge up the surface). The actual electrospray process onsets at a

higher applied potential (Fig 1.1b) and may be considered a high

**A.**



**B.**

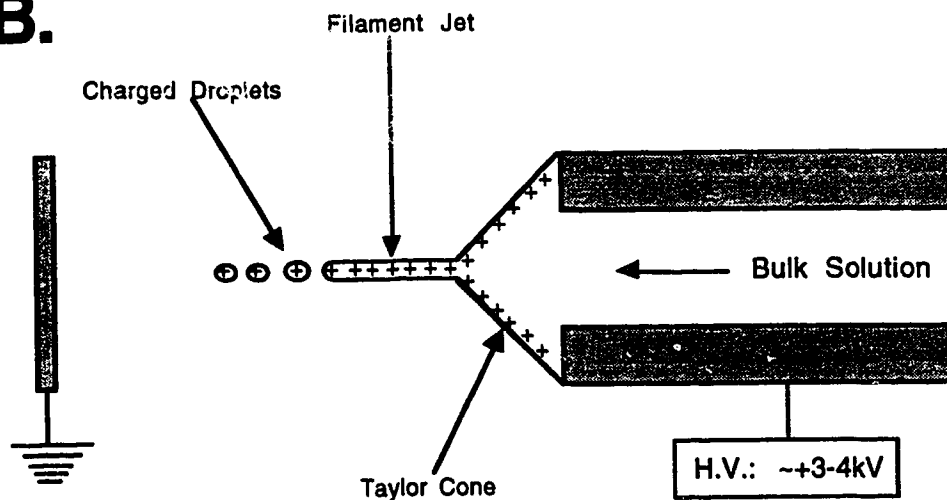


**Figure 1.1** Schematic profile of an electro spray capillary. With low (a) and high (b.) voltage applied.

frequency charged droplet generator. At the tip (assuming the bulk electrolyte concentration is sufficient to charge up the surface fast

enough) solution is both supplied and lost in a sort of steady state process. What typically happens is that at some relatively high potential the shape of the solution surface at the capillary tip changes and forms what is known as a "Taylor Cone" [4] from the tip of which a filament jet emerges and from which charged droplets emerge. An actual electrospray "Taylor Cone" picture of a  $1 \times 10^{-4} \text{M}$  KCl solution as captured by a CCD camera is shown in Fig. 1.2. This "onset potential" has been described in the literature [5,6] for various solvents. The above discussion is a much simplified view of the process and an in depth investigation of the electrospray process, under typical operating conditions was undertaken to better understand the source. The results are presented in chapter 6.

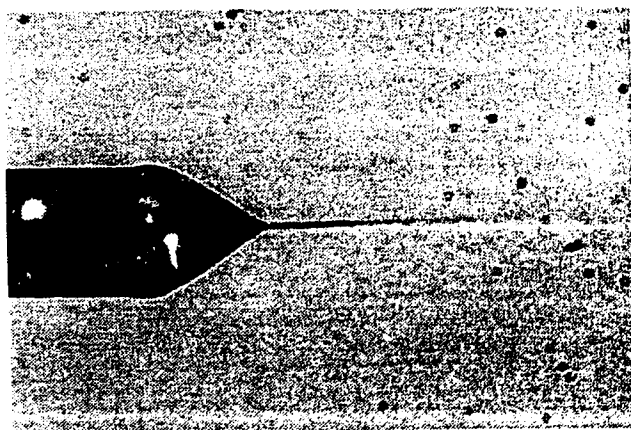


**Fig. 1.2** A 60X image of an electrospray capillary in operation. The capillary has a  $200 \mu\text{m}$  o.d. and a  $100 \mu\text{m}$  i.d.

The formation of the above droplets eventually gives rise to the production of gas phase ions. As a charged droplet travels between electrodes (at atmospheric pressure) the bulk solvent will evaporate at some rate thus reducing the overall radius of the droplet while maintaining the overall charge on its surface. This leads to instability

as the repulsive electrostatic forces on the surface of the droplet start to overcome the attractive surface tension force. This will eventually lead to a rupture of the surface followed by an expulsion of mass and charge from the droplet. The maximum charge ( $Q$ ) a droplet of some radius ( $R$ ) can hold before rupture is given by:

$$Q^2 = 64\pi^2\epsilon_0\gamma R^3 \quad (1.1)$$

where  $\epsilon_0$  is the permittivity of free space, and  $\gamma$  is the surface tension of the droplet. This criterion was first outlined by Lord Rayleigh in 1882 [7] and is commonly known as the Rayleigh limit. This phenomenon has been studied by several groups most notably Taflin et al., [8] and Gomez and Tang [9,10], whose recent work has shown that the droplet does not need to achieve this limit before rupture. In fact it was observed that the rupture occurred at about 80% of the Rayleigh limit and resulted in the expulsion of 2% of the mass with about 15% of the charge. This was usually achieved by the formation of a jet at the liquid surface resulting in the expulsion of many smaller charged droplets. Further the resultant droplets are formed with about one tenth the radius of the parent droplet [9], which assuming mass and charge conservation can lead to some 20 droplets with the corresponding subdivision of charge [11]. Thus the high frequency production of droplets at the capillary tip followed by the subsequent evaporation and fissioning steps leads to the "spray" element of electrospray (see insert Fig 1.3.).

The mechanism responsible for the generation of the eventual gas phase ion product(s) is contentious as it has not been proven

definitively whether it is the ion leaving the droplet or the droplet leaving the ion. After a few cycles of evaporation/fission one can imagine that the resultant droplets will be quite small and it is at this point that the debate stems. The ion evaporation theory first proposed by Iribarne and Thomson [12,13] suggests that when the droplet is small enough and the charge is high enough conditions may be such that the ion with an accompanying solvation sphere of some size is able to evaporate directly from the surface. The Dole theory which was first proposed in a paper by Dole *et al.* in 1968 [14] suggests that the evaporation/fissioning cycle eventually leads directly to drops that contain only one charge, this of course consists of an ion with some mass of solvent as well perhaps some bulk paired electrolyte. Most researchers in the field even though they may not side directly with one view or the other, have theories based on or as extensions of the two models [5, 15, 16, 17]. In any case the result is that solvated gas phase ions reflective of solution ions are generated. Therefore if an ion is soluble and stable in an appropriate solvent it may be "electrosprayed" and detected by mass spectrometry. A particular ion's response however is not straightforward in the sense that equal concentrations of strong electrolytes present in the original stock solution do not necessarily yield equal intensities as observed by mass spectrometry (barring any space charge effects or transmission losses inside the mass spectrometer). This is an important point and has important implications regarding the mechanism of electrospray and subsequently the quantitative aspects of electrospray. This type of phenomena has probably been observed by just about every researcher who uses

electrospray and has also been discussed by Tang and Kebarle [11]. Chapters 6 and 7 discuss these particular phenomena.

### **1.3. Sampling Electrospray Generated Ions into a Mass Spectrometer**

With the appropriate atmospheric pressure interface virtually any mass spectrometer may be used to sample and mass analyse electrospray ions. Most atmospheric pressure interfaces involve a two or multiple stage pumping system in order to handle the gas load. The actual interface is usually based on a narrow diameter orifice in a sampling plate (nozzle) through which the gas is expanded, the resultant jet expansion (a molecular/ion beam) is then skimmed and guided with the appropriate ion optics into the mass analyser. The ion optics may be simple electrostatic beam guides or more commonly, rf quadrupoles, hexapoles or octapoles. These latter rf beam guides are prevalent in most of the newer atmospheric pressure sampling mass spectrometers. The type of optics and pumping systems are largely determined by the type of mass spectrometer as well the manufacturer and these latter rf beam guides are prevalent in most of the newer atmospheric pressure sampling mass spectrometers some references which discuss these aspects are given [18,19]. A side profile of the type of sampling configuration used for these studies is illustrated in Fig. 1.3. Other common types of interfaces are based on capillary tube/nozzle inlets as described by Whitehouse *et al.* [20]. A brief but thorough discussion of the source is presented in chapter 2 of the thesis.



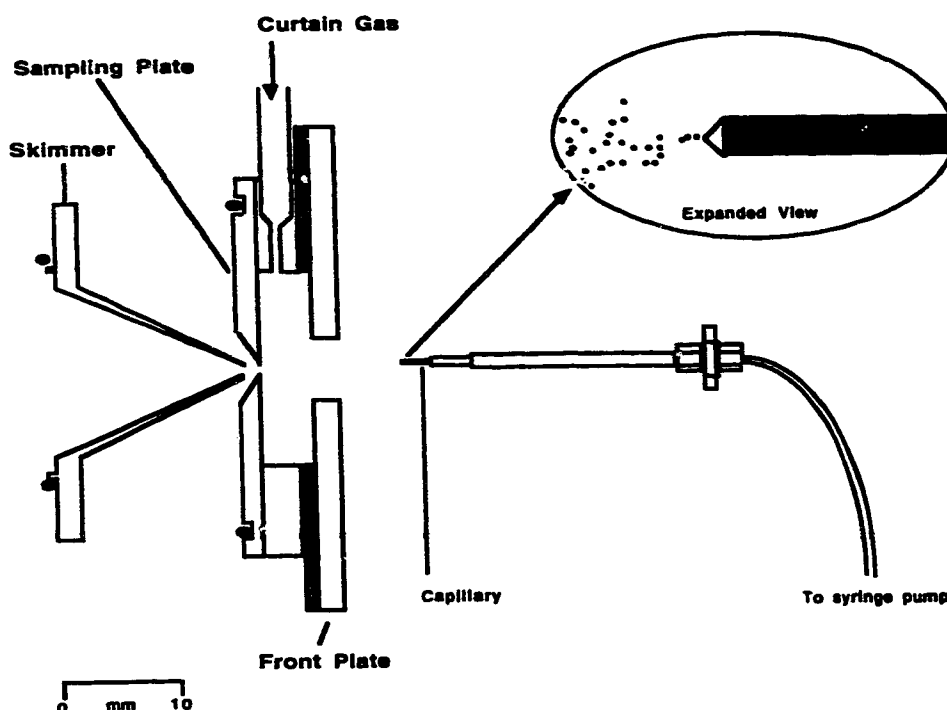


**Figure 1.3** Electrospray interface schematic showing the expansion region, and an expanded cartoon of the "spray".

For positive ion generation the field is created to go from high positive potential (capillary tip) to a low positive potential (skimmer). The opposite is true for negative ion generation. For the interface shown in Fig. 1.3, some common applied potentials are, capillary tip: 3-5 kV, front plate: 400-800V, sampling plate (nozzle): 0-200V and skimmer: 0-10V. In addition, there is a flow of curtain gas (usually nitrogen) supplied to the interface region whose purpose is primarily to exclude the entrainment of neutrals such as solvent or water vapors from the expansion region thus minimizing any Van der Waals clustering as the ion beam cools and expands. The curtain gas does have other important roles such as to aid in the drying of the droplets

as they travel this region, as well to provide a source of neutral collision gas in the expansion region.

The region between the sampling plate and skimmer Fig. 1.3. is very important as it provides a collision region. Into this region both the electrospray ions and neutral curtain gas (nitrogen) are entrained, and if there is an electric field present the ions will be accelerated relative to the neutral gas. This in effect will lead to neutral/ion collisions, the energy of which is dependant on the acceleration of the ions and hence the magnitude of the electric field. For example if a solvated metal ion is entrained into this region and an electric field exists then energetic collisions will lead, in the simplest case, to loss of solvent ligands. This is commonly referred to as Collisionally Induced Dissociation or CID. The result at the detector of course is that an ion different to what was originally sampled is observed. Depending on the application the sampling of a metal ion with eleven or six solvent ligands may or may not be critical. In order to reduce CID one must therefore minimize the potential drop in areas of significant carrier gas pressure, ie. between the sampling plate and skimmer for the most part and as well between the skimmer and ion optics. The CID in the interface region is usually referred to as high pressure (~0.5 torr) CID and depending on the magnitude of the field, can be quite efficient at stripping solvated metal ions down to their bare elemental form. This is illustrated for Cs in Fig. 1.4.

Fig. 1.4 is comprised of three spectra (a., b., and c.) where each was acquired under different conditions: for spectrum a. the sampling plate to skimmer potential difference was 5V, for b. 13V and for c. 28V. These spectra were therefore acquired going from "relatively"

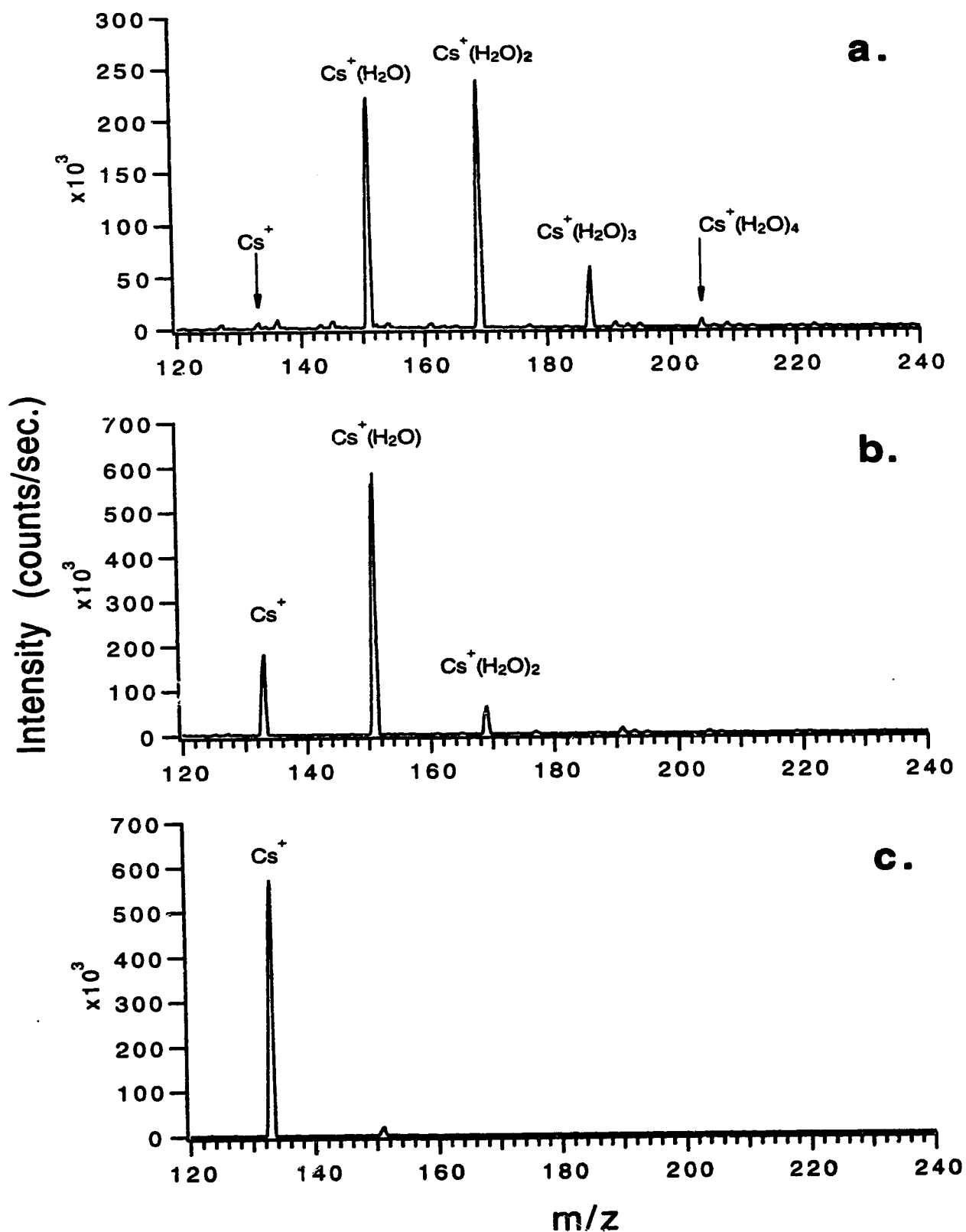


**Figure 1.4** Electrospray mass spectra of  $\text{CsCl}$  ( $1.0 \times 10^{-4} \text{ M}$ ) in methanol. a.)  $\Delta V = 5 \text{ V}$ , b.)  $\Delta V = 12 \text{ V}$ , c.)  $\Delta V = 28 \text{ V}$ .

gentle CID conditions to harsher conditions. In Fig. 1.4a. the spectrum is comprised of a distribution of water solvated cesium ions and as the potential is increased (Fig. 1.4b.) the distribution is narrowed and centers around one water molecule with a sizable contribution by the bare cesium ion. Finally in Fig. 1.4c. we see that under "harsh" conditions the dominant ion is the bare metal cesium ion with only a minor contribution by the mono-solvated species. In all the above cases the species observed is the cesium ion however its form, whether it be a simple bare metal species or a solvated metal species, is determined by the sampling conditions.

The above discussion centered around a very simple system, where the solvating ligands are removed sequentially leaving only a 'bare' metal ion. This process becomes more complicated for higher charged metal ions such as  $3^+$  species. For example imagine a  $3^+$  metal ion species that has just been "liberated" from a drop. It will of course be accompanied by a solvation sphere and we will assume it is of some size ( ie. some number of solvating ligands) that is capable of stabilizing the charge (and this size persists to the CID region for arguments sake). As the ion enters the CID region it will invariably lose some of its solvation sphere due to collision, and there will come a point where the existing solvation sphere is no longer able to stabilize the charge and so a "charge reduction" reaction occurs as exemplified below:



In the above case we have arbitrarily chosen water as the ligand and shown the reaction in its most simple form. A charge reduction

reaction may occur for other ligands such as methanol in a similar fashion. These types of reactions have been discussed in the literature by Blades *et al* [21,22], and Stewart *et al* [23]. An in depth study of the behaviour of highly charged metal ion centers under high pressure CID conditions is presented in Chapter 3.

It should be noted with respect to the above example that the authors have never seen a 3<sup>+</sup> metal ion stabilized by methanol or water ligands alone to preserve the species overall charge. However, by choosing a different electrospray solvent such as acetonitrile the solvated lanthanum 3<sup>+</sup> ion may be observed, as illustrated by Stewart *et al* [23] and Cheng *et al* [24]. Triply charged ions may be observed in the aprotic solvent acetonitrile because it is not capable of the stabilizing charge reduction step that protic solvents are and must undergo a higher energy charge transfer reaction. For the lanthanides one can observe the bare 3<sup>+</sup> ion with as little as 3-4 acetonitrile solvent ligands. In fact a number of authors have used a wide variety of other solvents such as dimethyl sulfoxide (DMSO), dimethyl formamide (DMF), acetone, ethanol and propanol to successfully electrospray inorganic species [21,22, 24,25]. Another method that has been employed by several groups is to complex the the metal ion with stabilizing ligands such as sepulchrate [22], 2,2'-bipyridyl [26,27] and other complexing agents [28] to observe "metal ions" with electrospray. There are a wide number of different solvents or solvent systems that may be used and care should be taken in selecting an appropriate one in order to avoid reactions with the analyte upon dilution with the solvent and ensure stable spray to maximize the information obtained.

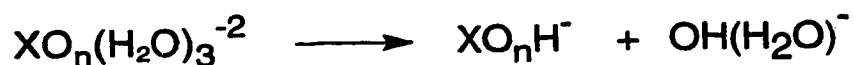
## **1.4 Inorganic Electrospray Mass Spectrometry Studies**

In terms of analytical studies of inorganic solution ions by electrospray mass spectrometry, Agnes and Horlick have published a series of papers on a wide variety of subjects ranging from elemental applications [29,30], speciation [31] and quantitation [32], to parametric studies [33]. For the most part these studies focus on uncomplexed solution ions. They have shown that one can successfully determine simple metal ions such as the alkali and alkaline earth metals as well as multivalent transition metals such as row three transition metals and the lanthanides. In addition elements of special concern such as vanadium, lead, uranium, cadmium, tin and arsenic may be determined. The speciation of these elements includes both the oxidation state and the form of the ion in solution whether it exists as a simple solvated metal ion or in a more complex molecular ion species such as  $\text{MnO}_4^-$  or  $\text{HCrO}_4^-$ . The combination of the work done in these papers and the references provided therein provides an excellent overview into some of the work that has been done to date in inorganic ESMS.

Some very interesting work involving metal ion complex species on more of an applied front has been performed by Colton and co-workers. Their work has focussed primarily on the identification and examination of labile and non labile inorganic and organometallic complexes [see for example 34,35,36 and references within] not normally observable by other techniques.

Negative ions can be generated and sampled in much the same way as positive ions. One potential problem with negative ion ES is that it is more susceptible to discharge formation ( ie. corona discharge

from capillary tip to ground), and the use of a discharge suppressing gas [2] has been commonly employed, however it is not necessary if the conditions are selected properly. ES mass spectrum of a mixture of chlorine species; chloride, chlorate and perchlorate each  $1.0 \times 10^{-4} \text{M}$  in methanol is shown in Fig. 1.5. Under the conditions in which the spectrum was acquired it is seen that all ions being singly charged can be stripped down to their bare molecular/atomic form. The above example is representative of electrospray's ability to examine inorganic anionic mixtures without first separating the compounds on a chromatographic column. For multiply charged negative ion centers similar reactions to positive ion species occur as the stabilizing solvent ligand sphere is removed. These stabilization reactions are highly dependant on the ions specific chemistry but a typical reaction for a multiply charged oxoanion is perhaps best described as 'charge separation':



Here water was chosen arbitrarily as the ligand, for methanol or other protic solvents the above reaction also holds. Non protic solvents will act to suppress this type of reaction.

In the case of an oxoanion like sulfate which may exist in solution as either  $\text{HSO}_4^-$  or  $\text{SO}_4^{2-}$ , depending on the pH, great care must be taken in sampling such a species. If the sampling conditions are too harsh it will appear via the charge separation as described above that the only species present is  $\text{HSO}_4^-$ . In order to best observe the ions

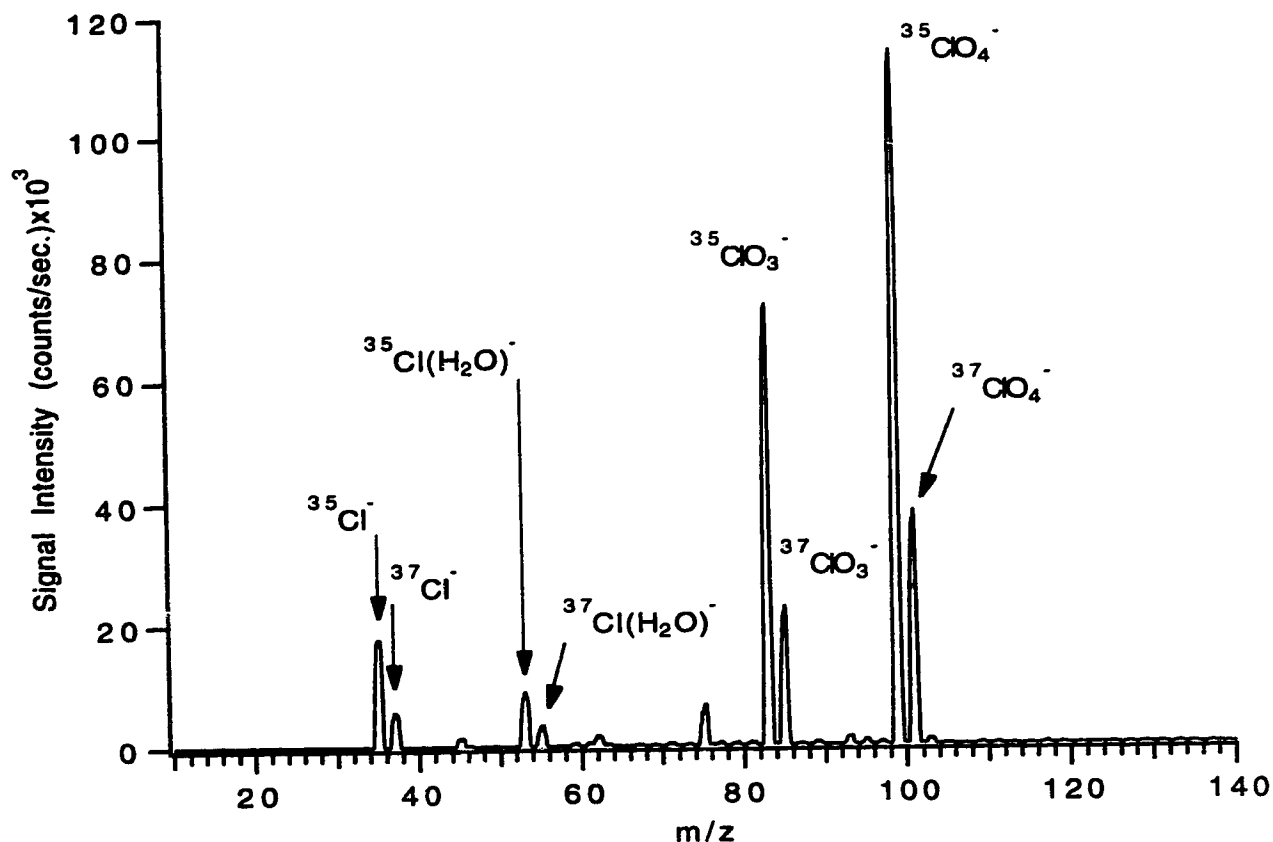


**Fig. 1.5.** Electrospray mass spectrum of a NaCl, NaClO<sub>3</sub> and NaClO<sub>4</sub> solution each at  $1.0 \times 10^{-4}$  M in methanol.

present in solution it is therefore necessary to use very gentle conditions, where it is possible to observe the solvated forms of both the HSO<sub>4</sub><sup>-</sup> and the SO<sub>4</sub><sup>2-</sup> ions to confirm their existence. This point is illustrated and discussed in some detail in chapter 5 of the thesis. Chapter 5 is an extension of the preliminary results presented by Agnes *et al* [31] on sulfur speciation with some analytical applications.

The pioneering work by Yamashita and Fenn explored negative ion production of simple inorganic and organic anions [2] and recently Agnes *et al* [30,31] have investigated more elaborate inorganic anionic species ranging from complexes to mixed systems. Rose *et al* [37] have



also used electrospray to examine borate ions. To date there has been considerably less work done on inorganic negative ions than on their positive ion counterparts. It should be emphasized that electrospray offers a direct method of determination for anionic species whether they be simple monatomic halides or more complex molecular species such as peroxodisulfate or iodate. In addition it is possible to distinguish between the various anionic species present in a complex mixture.

In the case of environmentally sensitive samples, the need for a direct unambiguous determination of species becomes critical. Thus a technique that is readily able to distinguish between ions of the same element but different form is desirable. Electrospray has the potential to offer this. For example organo-tin compounds have a wide range of chemical and toxicological properties and therefore it is not enough to know that tin is present but one must know which form of tin is present. The electrospray mass spectra of three different organotin species are given in Fig. 1.6, trimethyltinchloride, dimethyltinchloride and dibutyltinchloride. The spectrum of the trimethyltin ion is shown in Fig. 1.6a.. As this ion has only one charge overall it does not undergo any of the stabilization reactions that were seen for lanthanum above, and it can be stripped down from a solvated form to its bare form quite easily. For the dimethyltin ion (Fig. 1.6b.), the spectrum (stripped down) shows clearly that tin is present as Sn(IV) in the dimethyl form, however the variety of charged reduced species ( $\text{Sn}(\text{CH}_3)_2(\text{OH})^+$ ,  $\text{Sn}(\text{CH}_3)_2(\text{OCH}_3)^+$ ) and as well counterion associated species ( $\text{Sn}(\text{CH}_3)_2\text{Cl}^+$ ) tends to complicate the spectrum. It should be noted at this point that the observed charge reduced species may not be

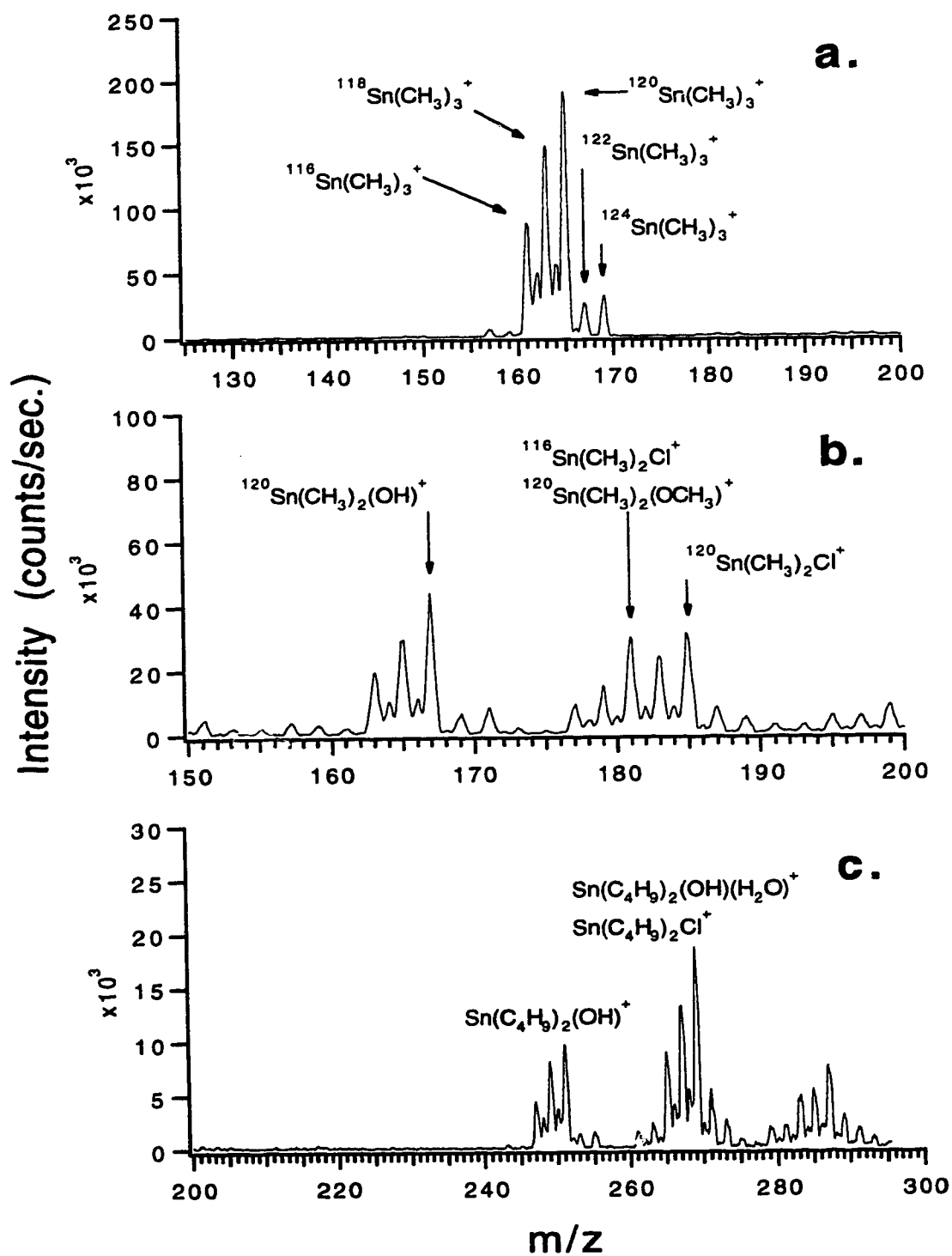


**Fig. 1.6** Electro spray mass spectra of a)  $\text{Sn}(\text{CH}_3)_3\text{Cl}$   $\Delta V = 35\text{V}$ , b)  $\text{Sn}(\text{CH}_3)_2\text{Cl}_2$   $\Delta V = 30\text{V}$  and c)  $\text{Sn}(\text{C}_4\text{H}_9)_2\text{Cl}_2$   $\Delta V = 30\text{V}$  each at  $1.0 \times 10^{-4}\text{M}$  in methanol.

the result of gas phase charge reduction solely and it is possible that hydrolysis/solvolysis occurs in the solution directly. For dibutyltin we see a similar range of species (Fig. 1.6c). The fact that the later species do not generally strip down to one dominant molecular ion, presents the obvious complication of isobaric overlap especially for an element such as tin that is wealthy in isotopes. Examination of the isotopic distributions for the dimethyltinmethoxide ion and the dimethyltinmonochloride ion in Fig. 1.7 illustrate this fact. Regardless, the spectra in Fig. 1.6 illustrate that each of the components may be positively identified. If a mixture of these species is examined by ESMS (Fig. 1.8) it can be seen that there is a considerable amount of isobaric overlap of both inter- and intra-species, especially in the case of trimethyltin and dimethyltinhydroxide ions whose dominant isotopes are at  $m/z$  165 and 167 respectively (Fig. 1.8b.). The dibutyltin contribution (Fig. 1.8c.) is fairly well isolated and its isotopic peak distributions in the  $m/z$  245-280 range are similar to what is observed in Fig 1.6c. from the simple dibutyltin chloride solution. In any case, if the knowledge obtained from Fig. 1.6 is applied then assignments may be made to Fig. 1.8 where all of the individual species have been clearly identified. If very intense CID conditions are applied, then the species may be stripped down to bare  $\text{Sn}^+$ . In real life samples the actual matrix and concentration of a particular analyte may not be amenable to electrospray and therefore it may be necessary to couple ESMS to chromatographic methods. Some interesting work by Huggins *et al* [38] demonstrates this, where they coupled capillary electrophoresis to a mass spectrometer using a nitrogen assisted electrospray source or "ion spray" sheath flow

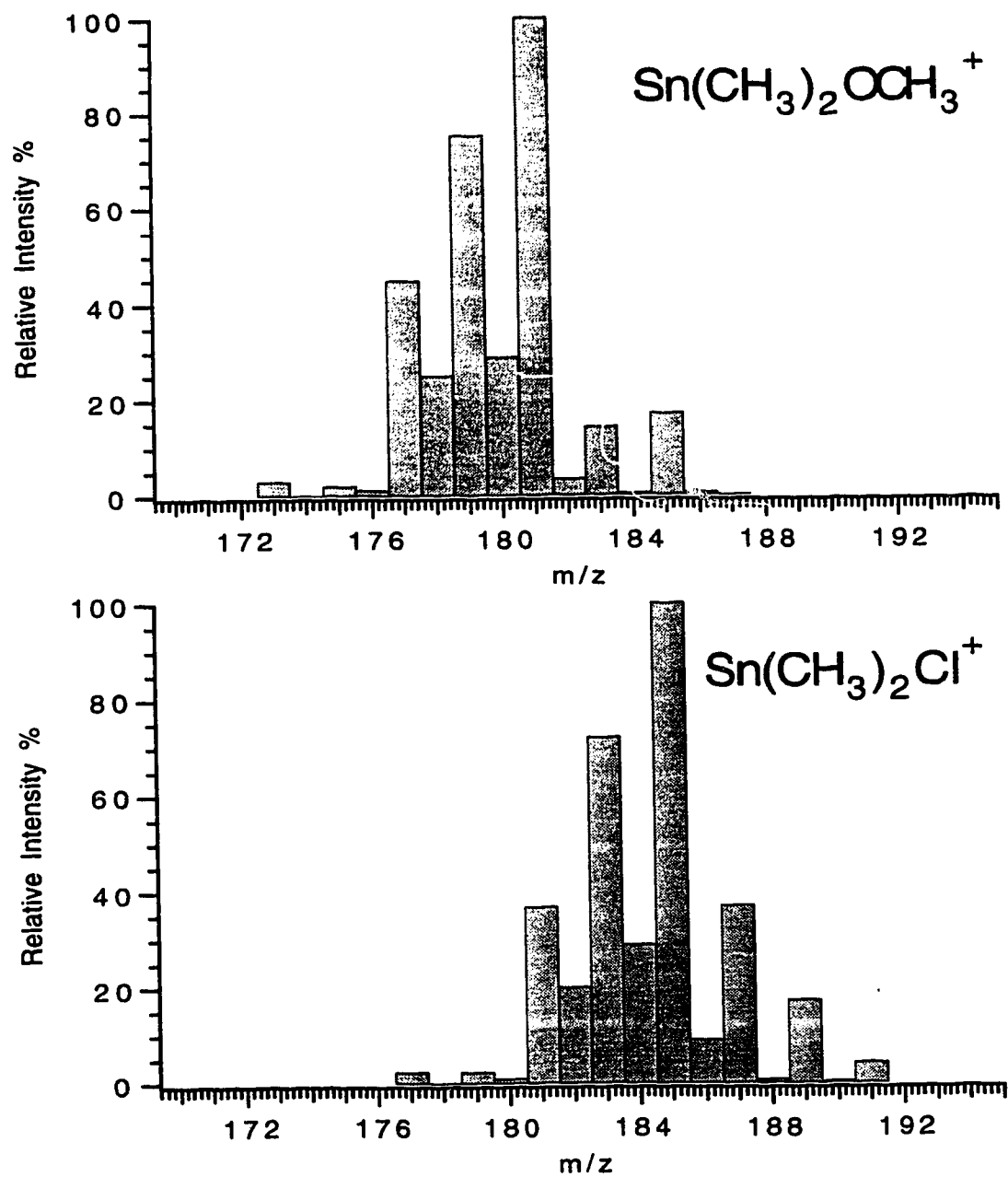


**Fig. 1.7.** Relative Isotopic distributions of  $\text{Sn}(\text{CH}_3)_2\text{OCH}_3^+$  and  $\text{Sn}(\text{CH}_3)_2\text{Cl}^+$ .

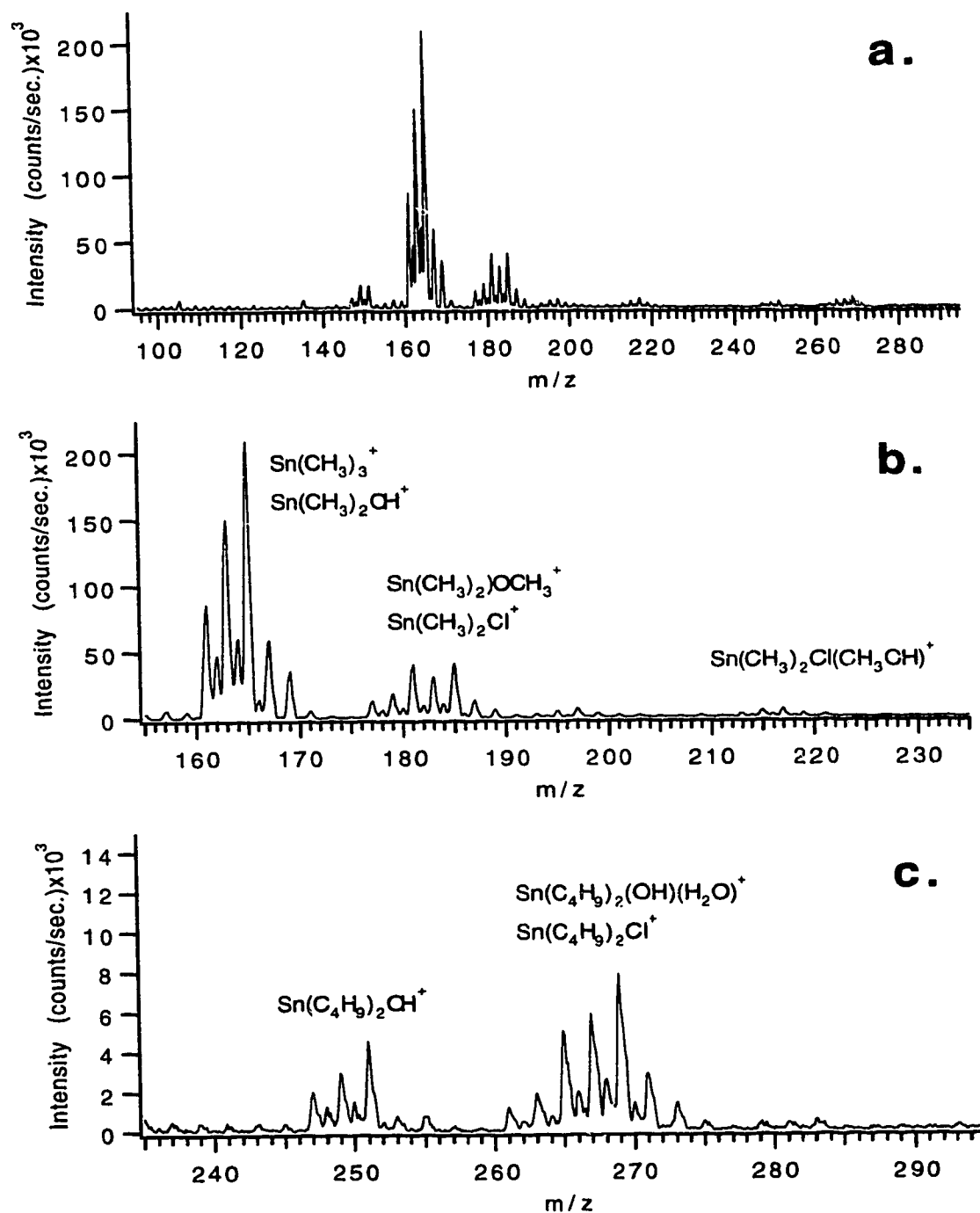


**Fig. 1.8.** Electrospray mass spectra of  $\text{Sn}(\text{CH}_3)_3\text{Cl}$ ,  $\text{Sn}(\text{CH}_3)_2\text{Cl}_2$  and  $\text{Sn}(\text{C}_4\text{H}_9)_2\text{Cl}_2$  at  $1.0 \times 10^{-4}\text{M}$  in methanol. a)  $\Delta V = 35\text{V}$  b) and c) are just zoomed in portions of a).

interface. This modified electrospray interface is discussed in some detail by Bruins *et al.* [39]. In the study Huggins *et al* examined a whole range of inorganic cations and anions and compared results to indirect-UV capillary electrophoresis analysis. Siu *et al* however when examining tributyltin in PACS-1, a sediment reference material, did not have to resort to chromatography [40]. Solvent extraction was performed and 0.5mL sample sizes were fed to an ionspray source by FIA for MS/MS analysis. The monitoring of both the parent isotopic peak and daughter fragment enabled the specific detection of tributyltin. This degree of selectivity is lost with elemental techniques.

A comprehensive study of chromium, an environmentally sensitive element, was undertaken, where species present in both of its two common oxidation states (Cr (III) and Cr (VI)) were studied. The results of the investigation are presented in chapter 4.

## **1.5 Conclusion**

Since 1980, the inductively coupled plasma (ICP) has been the primary source coupled to a mass spectrometer for the purpose of elemental analysis [41]. In fact, inductively coupled mass spectrometry went very rapidly from laboratory experiments to commercial development and wide-spread analytical application. While its success and rapid development has lent considerable credibility to the utilization of mass spectrometry as a general technique for elemental analysis, the ICP is not an ideal source for such a coupling. In the high temperature environment of the plasma essentially all analytes are converted to singly ionized gas phase atoms. It is a strange dichotomy that this most successful coupling to-date of a source to a mass spectrometer for the

purpose of elemental analysis thus destroys key chemical information about the nature of the element in the sample that mass spectrometry is capable of determining (*i.e.* molecular form (molecular weight) and charge state ( $m/z$ )). The answer to many chemical questions these days is not simply obtained by a knowledge of just the elemental composition of the sample. We may need to know if the element is present as a cation or an anion, what is its molecular or chemical form, and what is its oxidation state. It would certainly be more ideal if an MS source could be developed that would retain more detailed information about the "elemental" composition of a sample. Clearly, as outlined above, an electrospray ion source has the potential to provide such capability.

The ability of electrospray to generate intact gas phase ions representative of solution ions opens up a whole new avenue for speciation work. This in effect illustrates its potential to avoid the ambiguity associated with other speciation techniques, as a direct determination of a given stable solution species is offered. The form, whether it be a simple solvated species or a complex molecular species may be deduced. In addition the technique allows both positive and negative ion speciation. In certain cases mixtures may be evaluated directly or in conjunction with a chromatographic method. In either case the result is an unambiguous assignment based on  $m/z$  values and relative isotopic contributions rather than relative retention times. Great care however must be taken in selecting the optimum ES conditions to ensure a meaningful determination, as has been discussed and illustrated in this chapter. As yet the full potential of this technique has not been realized, and considerable work must be done to

further characterize and better understand it. This thesis was written in partial fulfillment of this goal.



## 1.6 References

1. M. Yamashita and J.B. Fenn, *J. Phys. Chem.*, **88**, 4451 (1984).
2. M. Yamashita and J.B. Fenn, *J. Phys. Chem.*, **88**, 4671 (1984).
3. A.T. Blades, M.G. Ikonomou and P. Kebarle, *Anal. Chem.*, **63**, 2109 (1991).
4. G.I. Taylor, *Proc. Roy. Soc. Lond.A.*, **313**, 453 (1969).
5. P. Kebarle and L. Tang, *Anal. Chem.*, **65**, 972A (1993).
6. D.P.H. Smith *IEEE Trans. Ind. Appl.*, **63**, 527 (1986).
7. Lord Rayleigh, *Philos. Mag.*, **14**, 184 (1882).
8. D.C. Taflin, T.L. Ward and E.J. Davis, *Langmuir*, **5**, 376 (1989).
9. A. Gomez and K. Tang, *Phys. Fluids*, **6**, 404 (1994).
10. K. Tang and A Gomez, *Phys. Fluids*, **6**, 2317 (1994).
11. L. Tang and P. Kebarle, *Anal. Chem.*, **65**, 3654 (1993).
12. J.V. Iribarne and B.A. Thomson, *J. Chem. Phys.*, **64**, 2287 (1976).
13. B.A. Thomson and J.V. Iribarne, *J. Chem. Phys.*, **71**, 4451 (1979).
14. M. Dole, L.L. Mack, R.L. Hines, R.C. Mobley, L.D. Ferguson and M.B. Alice, *J. Chem. Phys.*, **49**, 2240 (1968).

15. K.W.M. Siu, R. Guevremont, J.C.Y. LeBlanc, R.T. O'Brien and S.S. Berman, *Org. Mass Spectrom.*, **28**, 579 (1993).
16. J. B. Fenn, *J. Am. Soc. Mass Spectrom.*, **4**, 524 (1993).
17. M.S. Wilm and M. Mann, *Int. J. Mass Spectrom. Ion Processes*, **136**, 167 (1994).
18. A.P. Bruins, *Mass Spectrom. Rev.*, **10**, 53 (1991).
19. D.J. Douglas and J.B. French, *J. Am. Soc. Mass Spectrom.*, **2**, 398 (1991).
20. C.M. Whitehouse, R.N. Dreyer, M. Yamashita and J.B. Fenn, *Anal. Chem.*, **57**, 675 (1985).
21. A.T. Blades, P. Jayaweera, M.G. Ikonomou and P. Kebarle, *Int. J. Mass Spectrom. Ion Processes*, **101**, 325 (1990).
22. A.T. Blades, P. Jayaweera, M.G. Ikonomou and P. Kebarle, *Int. J. Mass Spectrom. Ion Processes*, **102**, 251 (1990).
23. I.I. Stewart and G. Horlick, *Anal. Chem.*, **66**, 3983 (1994).
24. Z.L. Cheng, K.M.W. Siu, R. Guevremont and S.S. Berman, *Org. Mass Spectrom.*, **27**, 1370 (1992).
25. Z.L. Cheng, K.M.W. Siu, R. Guevremont and S.S. Berman, *J. Am. Soc. Mass Spectrom.*, **3**, 281 (1992).
26. V. Katta, S.K. Chowdhury and B.T. Chait, *J. Am. Chem. Soc.*, **112**, 5348 (1990).
27. R. Arakawa, T. Matsuo, H. Ito, I. Katakuse, K. Nozaki, T. Ohno and M. Haga, *Org. Mass Spectrom.*, **29**, 289 (1994).

28. C.L. Gatlin, F. Turecek and T. Vaisar, *Anal. Chem.* **66**, 3950 (1994).
29. G.R. Agnes and G. Horlick, *Appl. Spectrosc.*, **46**, 401 (1992).
30. G.R. Agnes and G. Horlick, *Appl. Spectrosc.*, **48**, 655 (1994).
31. G.R. Agnes, I.I. Stewart and G. Horlick, *Appl. Spectrosc.*, **48**, 1347 (1994).
32. G.R. Agnes and G. Horlick, *Appl. Spectrosc.*, **48**, 649 (1994).
33. G.R. Agnes and G. Horlick, *Appl. Spectrosc.*, **49**, 324 (1995).
34. T.J. Cardwell, R. Colton, S. M. Mitchell and J.C. Traeger, *Inorg. Chim. Acta*, **216**, 75 (1994).
35. R. Colton, W. Klaui, *Inorg. Chim. Acta*, **211**, 235 (1993).
36. R. Colton, D. Dakternieks, *Inorg. Chim. Acta*, **208**, 173 (1993).
37. M.E. Rose, D. Wycherley and S.W. Preece, *Org. Mass Spectrom.*, **27**, 876 (1992).
38. T.G. Huggins and J.D. Henion, *Electrophoresis* **14**, 531 (1993).
39. A.P. Bruins, T.R. Covey and J.D. Henion, *Anal. Chem.*, **59**, 2642 (1987).
40. K.W.M. Siu, G.J. Gardner and S.S. Berman, *Anal. Chem.*, **61**, 2320 (1989).
41. R.S. Houk, *Acc. Chem. Res.*, **27**, 33 (1994).

## **Chapter 2**

### **Instrumentation**

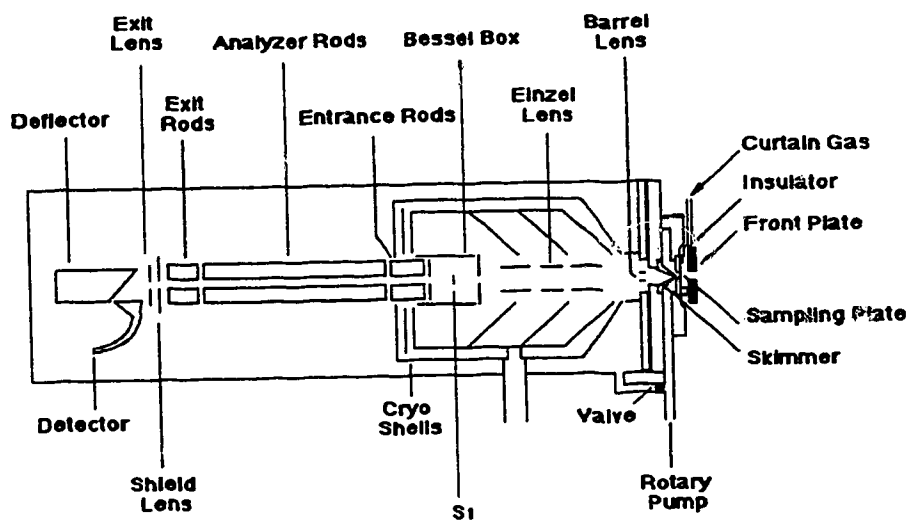
## **2.1 Introduction**

This chapter is devoted to the description of the instrumentation used. In addition to a general description of the system and its components, any additions or modifications that were implemented during the course of experimentation will be described. It is designed to give the reader a frame of reference for the latter chapters.

## **2.2 Mass Spectrometer**

The mass spectrometer used in all experiments is a quadrupole mass spectrometer. A Perkin Elmer/SCIEX ELAN Model 250 ICP-MS was modified previously by Agnes and Horlick [1] so that it could be interfaced with an electrospray ion source. This involved removing the ICP at the front end and modifying the atmospheric pressure interface. The interface will be described in more detail in section 2.4. A schematic of the quadrupole mass spectrometer is given in Fig. 2.1a below. The ions are sampled through a sampling plate (nozzle) -skimmer configuration. They are then guided through the ion optics to the entrance rods, then through the analytical rods (quadrupole), out the exit rods and into the deflector/detector configuration where they are detected. The mass to charge ( $m/z$ ) working range of the analytical rods is  $\sim 1$ -295  $m/z$  units. The working range was so defined as the mass spectrometer was designed originally for elemental analysis by ICP-MS.

a.



b.

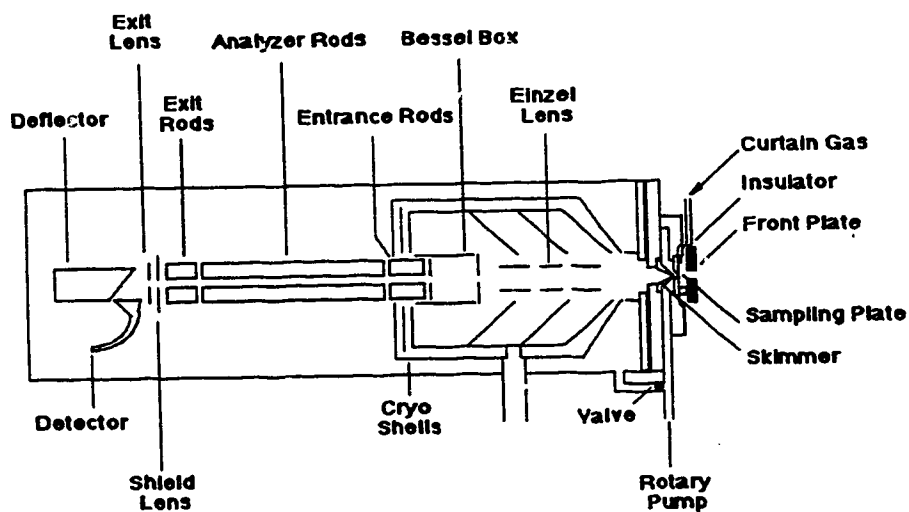


**Figure 2.1** Schematic Diagrams of the modified Perkin Elmer/SCIEX ELAN Model 250 with a.) original ion optics and b.) modified ion optics.

The ion optics prior to the mass analyzer were designed specifically for the transport of ions created by the ICP source and consist of a series of einzel lenses followed by a bessel box, which act together as an energy filter. The voltages on the various lens elements of the energy filter may then be set to pass only ions of a set energy into the mass analyzer. This was discussed in some detail by Vaughan and Horlick [2,3].

This configuration may also be used with the electrospray source. However because the total ion throughput of the electrospray source at the interface is significantly less (as a result of orifice size and ion density), the number of ions reaching the detector of a given mass will also be significantly less. In an effort to improve the total ion transport the ion optics were modified where the first barrel lens located just after the skimmer and the center stop located in the bessel box were removed. The new configuration is given in Fig. 2.1b. The net result is that optics no longer function strictly as an energy filter but more as beam guide, and the net signal at the detector is increased. This is illustrated in Fig. 2.2 where two spectra of  $\text{CrCl}_3$  were acquired under similar conditions, but Fig. 2.2a was acquired before the modification to the energy filter and Fig. 2.2b was acquired after the modification. The figure is scaled to illustrate the increase in signal and for the most part an increase of one order of magnitude was achieved as a result of this modification.

Data are presented in this thesis which were acquired on both of the configurations and will be noted where necessary.

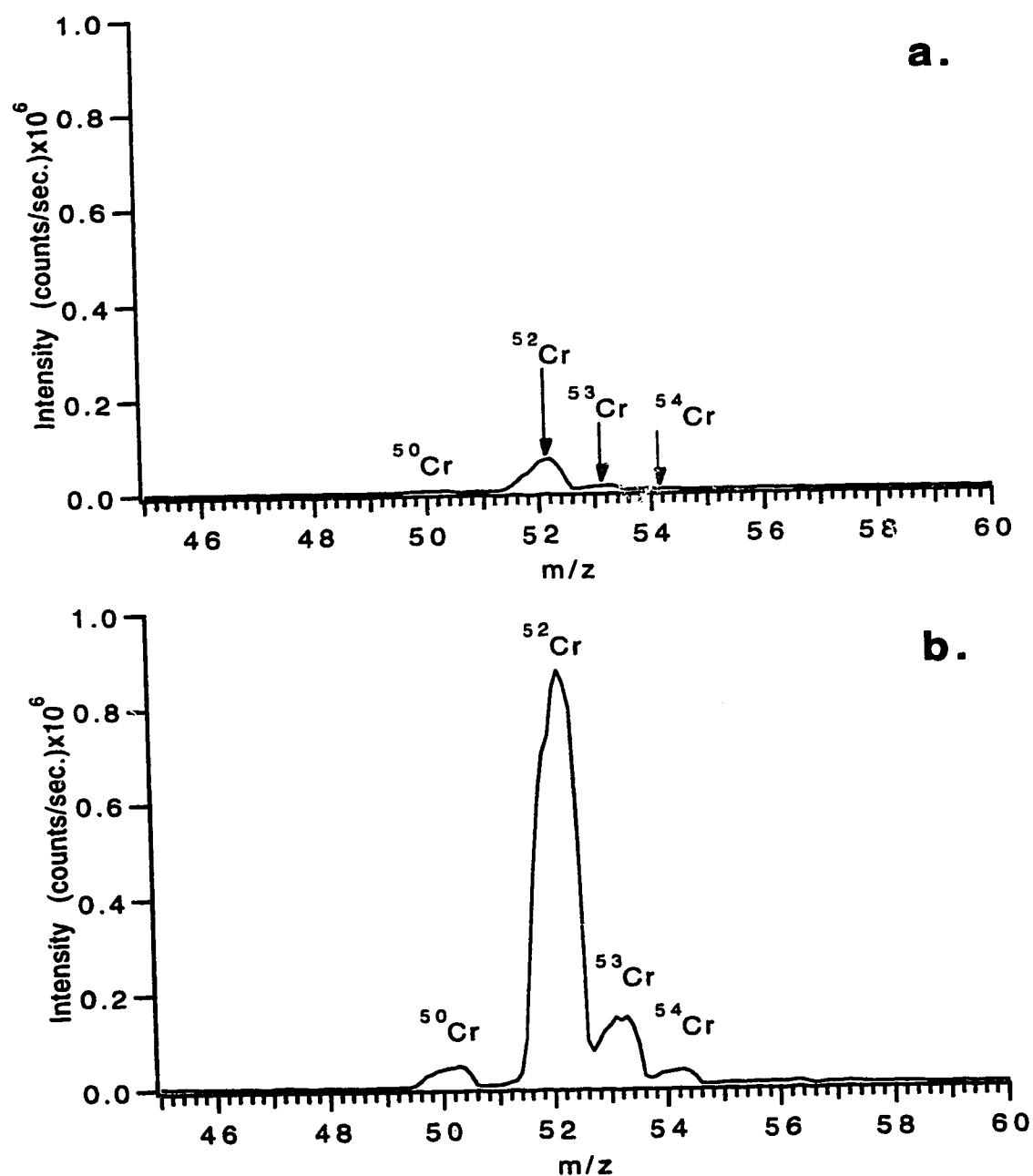


**Figure 2.2** Typical intensity improvement a.) before and b.) after ion optic modification. ( $\text{CrCl}_3$ :  $1 \times 10^{-4}\text{M}$  in methanol, similar operating conditions).



## 2.3 The Vacuum System

A schematic representation of the vacuum system is shown in Fig. 2.3. The system is based on a two stage pumping system, where the interface region is evacuated by an Edwards E2M18 double stage roughing pump (1), ( $\sim 7\text{L/sec.}$ ) and the main vacuum chamber is pumped by a Cryo-torr 8 cryopump ( $\sim 3500\text{ L/sec.}$ ).

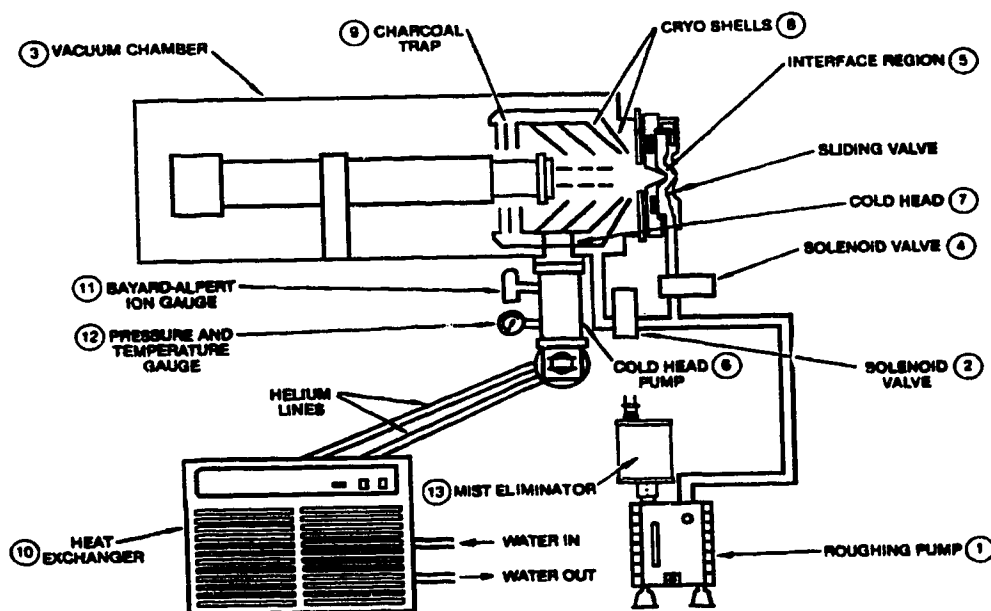


**Figure 2.3** A schematic representation of the mass spectrometer and pumping system

The cryopump is a vacuum pump which consists of a surface which is cooled down to very low temperatures ( $<120\text{K}$ ), so that gases or vapours may condense at this surface. This surface is cooled by a cold head. In the refrigerated cryopump (Fig. 2.3) the

cold is produced by a two stage refrigerator cold head (7) located in the cold head pump (6). The cold head pump uses helium as a refrigerant to cool the cold head. The cooling surface or cryoshells (8) consist of polished copper, as well a series of charcoal traps (9) are incorporated to trap or cryosorb non condensables such as hydrogen or helium. The cold head pump is connected to a heat exchanger (10) which transfers the heat from the cold head to the circulating water.

The cold head as stated above consists of two stages where the first stage provides cooling for an 80K condensing array and the second stage provides cooling for a 15K condensing array. The pump usually operates at a temperature of 16K at the second stage. The ultimate pressure attainable when nitrogen is pumped is given by the following formula;

$$p_{ult} = p_s (T_w/T_k)^{1/2} \quad (2.1)$$

where  $p_s$  is the saturation pressure of the pumped gasses ( $N_2 = 1.0 \times 10^{-11}$  torr at 20K [4]) at the cold head temperature ( $T_k$ ) and  $T_w$  is the temperature of the vacuum vessel wall ( $T_w = 298K$ ). Which translates to  $2.9 \times 10^{-11}$  torr. The theoretical pumping speed may then be calculated as;

$$S_{th} = A_k \times S_a \times \alpha(1-p_{ult}/p) \quad (2.2)$$

where  $A_k$  is the effective area of the cold surface,  $S_a$  is the area related pumping speed,  $\alpha$  is the condensation probability ( $\alpha = 1$  for low temperatures) and  $p$  is the vacuum pressure. As the pressure in

the vacuum chamber is  $\sim 5 \times 10^{-6}$  torr during routine operation the formula simplifies to;

$$S_{th} = A_k \times S_a \quad (2.3)$$

where  $S_a$  may be calculated from the kinetic theory of gasses as;

$$S_a = (RT_g/2\pi M)^{1/2} \quad (2.4)$$

Where  $R$  is the molar gas constant,  $T_g$  is the gas temperature and  $M$  is the molar mass of the gas. Thus for nitrogen at 298K,  $S_a = 11.9$  L/(s·cm<sup>2</sup>). Nitrogen gas entering an expansion experiences a cooling and therefore this value may only be considered an upper limit. As the cold surface area is not given in the manufacturers literature a theoretical pumping speed cannot be calculated. The manufacturers pumping speed is listed as 3500 L/s for nitrogen. The closed vacuum chamber pressure as measured by a Bayard-Alpert ion gauge is  $\sim 1 \times 10^{-8}$  torr, and when the interface is open to atmosphere is  $\sim 5 \times 10^{-6}$  torr.

## 2.4 The Interface

A schematic of the mass spectrometers interface is given in Figure 2.4. It is a modified version of the original sampling plate skimmer configuration present on the initial ICP interface. The various components (i.e. front plate, sampling plate, skimmer) are all electrically isolated so that individual potentials may be applied. The electrospray capillary is usually positioned a variable distance from

the front plate ( $\sim 0.5 - 2.0$  cm). The curtain gas (nitrogen) enters from a slot at the top at some specified rate ( $\sim 1.0-1.5$  L/min.).

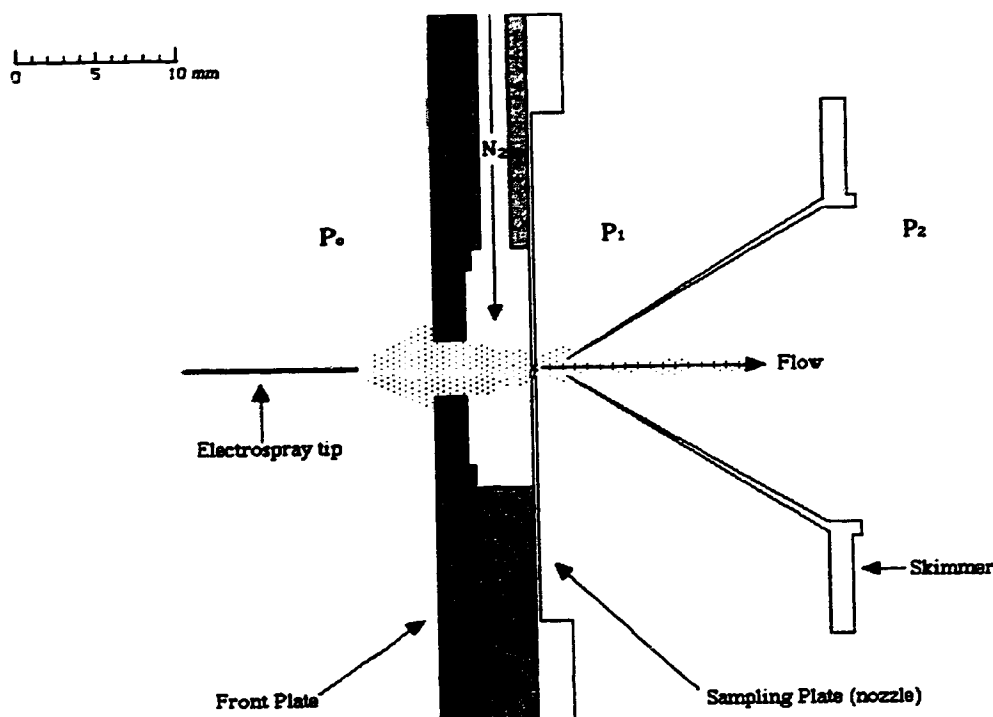


**Figure 2.4** Schematic representation of the interface with electrospray.

In order to better control the conditions at the interface a plenum chamber was designed. The chamber was designed to isolate the interface from disturbances originating in the laboratory, as well to provide a stable consistent evacuation of the interface region, which would help eliminate both a build up of solvent vapour around the interface, and the efficient removal of potentially toxic substances generated via the electrospray process. A schematic of this interface is presented in Figure 2.5.

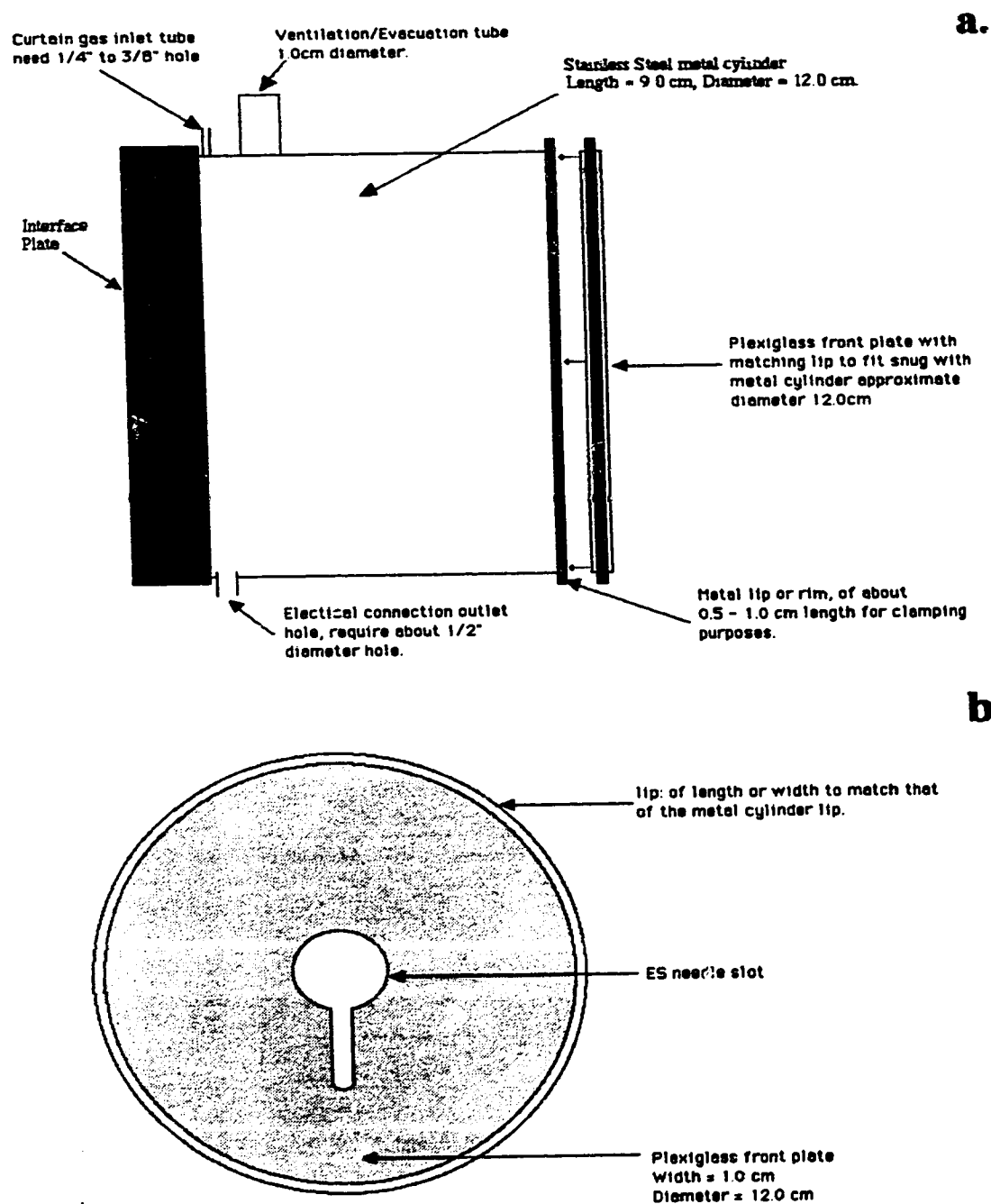


**Figure 2.5 Schematic diagram of the plenum interface chamber showing the a.) profile, and b.) plexiglass front plate.**

The keyhole electrospray needle slot was designed to allow the interface plate to move up and down, as the mass spectrometer goes from atmospheric to non atmospheric operating conditions.

The interface is of critical importance as not only does its design allow for the transfer of atmospheric gas phase ions into the vacuum chamber for mass spectrometric determination but it also allows for efficient high pressure CID for stripping solvent off of ion-solvent clusters and to break apart molecular species. The curtain gas typically used at the interface is nitrogen. When other gases such as argon were used discharge was more noticeable. In terms of CID efficiency however a larger monatomic gas like argon would be preferred as it allows for more efficient energy transfer upon collision. Consider the case where an analyte ion is entrained into a jet expansion of a neutral curtain gas ( $N_2$  or Ar), if the analyte is not too large then we can assume that it travels with the velocity of the expanding molecular beam. Now couple in an electric field, which serves to accelerate the ions in the beam relative to the neutral curtain gas, the result is energetic collision of the analyte ion with and the curtain gas (assuming sufficient number density to limit the mean free path). The more energetic the collisions the more kinetic energy of the ion may be converted into internal energy and hence excite the ion and lead to fragmentation. For example the maximum amount of kinetic energy that may be converted into internal energy for the purposes of decomposition may be deduced from the conservation of energy and momentum as:

$$E_k = eV \times m/(m + M) \quad (2.5)$$

where  $eV$  refers to the kinetic energy of the ion,  $m$  is the mass of neutral collision gas and  $M$  is the mass of target ion. Therefore for argon of mass 40 and nitrogen of mass 28 the total kinetic energy converted into internal energy upon collision of an ion of mass 236 ( $\text{La}(\text{OH})(\text{H}_2\text{O})_5^{2+}$ ) is  $\sim eV/7$  and  $\sim eV/9.5$ . This equation does not take into account the fact that energy may be absorbed by nitrogen through its vibrational mode, and so the total energy that is converted into internal energy in the  $\text{La}(\text{OH})(\text{H}_2\text{O})_5^{2+}$  complex may be less. Regardless of differences in collisional energy, efficient stripping may be achieved in expansion region due to number collisions when either curtain gas is used. Lubman *et al.* [5] have compared the collisional frequencies of monoatomic and diatomic gases in an isentropic jet. They report a 3X increase in collisional frequency going from a monoatomic to diatomic gas at a  $x/D$  distance of 20. The deciding factor however becomes which leads to a more stable electrospray, in this case nitrogen was selected.

## 2.5 The Free Jet Expansion

As was stated above the interface consists of a sampling plate (nozzle) and skimmer configuration. The sampling plate or nozzle allows a high pressure source to be expanded into a low pressure ambient background, which results in a supersonic free jet expansion. A skimmer may be placed in front of the expansion in

order to sample the centerline beam. A schematic representation of a continuum free jet expansion is given in Fig. 2.6. As the beam consists primarily of nitrogen we shall model the expansion after a nitrogen expansion.

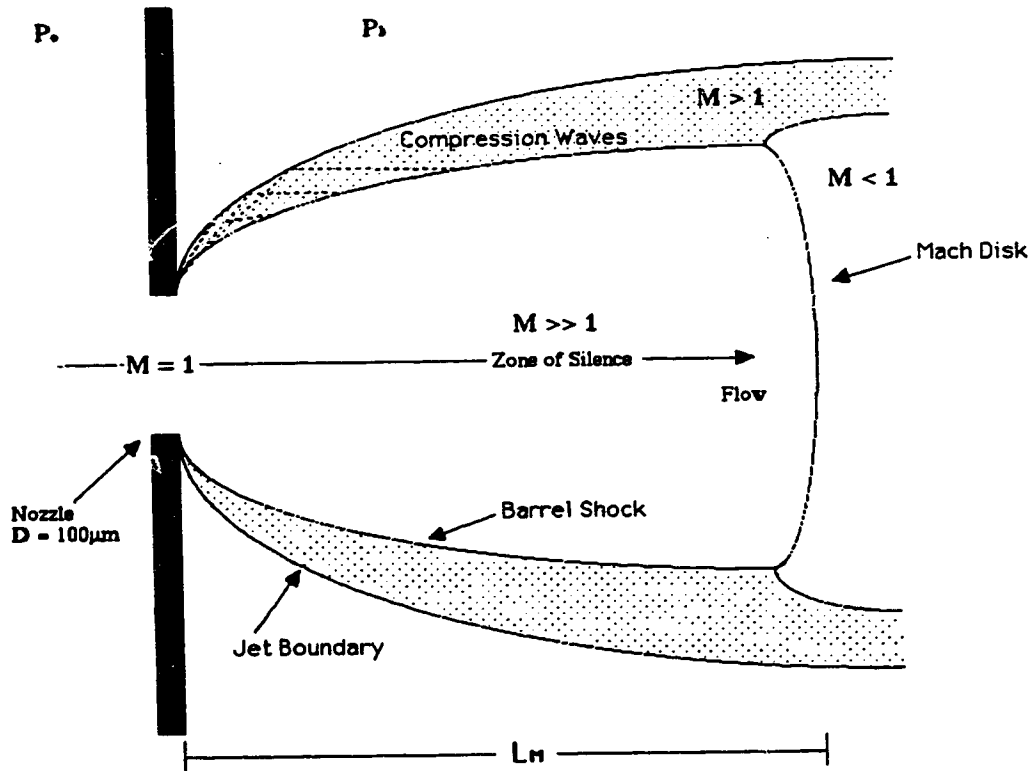


**Figure 2.6** Schematic representation of the structure of a continuum free jet expansion originating from a source at pressure  $P_0$  flowing into a region of pressure  $P_b$ .

From Fig. 2.6 it is shown that the Mach number is equal to 1 in the orifice, or that gas flow at this point has reached sonic velocity or the local speed of sound. This condition is satisfied when;

$$\frac{P_0}{P_b} > ((\gamma + 1)/2)^{\gamma/(\gamma-1)} \quad (2.6)$$



where  $\gamma$  is the ratio of the heat capacities ( $C_p/C_v = 1.4$  for nitrogen) for various gases. For a nitrogen expansion the value is  $\sim 1.9$ , therefore a ratio of greater than 1.9 is required to satisfy this condition. The pressure inside the expansion chamber is not known exactly, however it is measured off of the chamber as 300 mtorr. This number is probably too low and therefore it will be estimated as  $\sim 500$  mtorr (which may still be too low). If the source pressure is taken as 760 torr then the ratio becomes 1520 which is much in excess of 1.9, and therefore we can conclude sonic flow through the orifice. The local speed of sound may then be calculated from;

$$a_0 = \left( \frac{\gamma k T_0}{m} \right)^{1/2} \quad (2.7)$$

where  $k$  is Boltzmann's constant,  $T_0$  is the source temperature (298K), and  $m$  is the mass of the gas (nitrogen). Using these values  $a_0$  is calculated to be 35190 cm/s. The flow through the orifice may then be calculated [6] using the equation below;

$$F = 0.445 n_0 a_0 D^2 \quad (2.8)$$

where  $n_0$  is the nitrogen number density at  $P_0$  and  $T_0$  ( $n_0 = 2.43 \times 10^{19}$  molecules/cm<sup>3</sup>) and  $D$  is the orifice or nozzle diameter. This results in  $3.81 \times 10^{19}$  molecules/s flowing through the orifice.

The skimmer is usually placed such that it may skim or sample from the isentropic region of the expansion or the "zone of silence". This region is defined by the orifice on one end and the Mach disk at the other end, a cartoon representation often found in the literature [7,8] is given in Fig. 2.6. It is thus advantageous to calculate where

the Mach disk is located. Ashkenas and Sherman [7] have shown that the Mach disk forms at a distance  $L_m$  from the orifice as given by equation (2.9);

$$L_m = 0.67 D (P_o/P_b)^{1/2} \quad (2.9)$$

If  $P_b$  is taken as 500 mtorr then  $L_m = 2.61$  mm. The skimmer is mounted 2 mm from the orifice, which might not be the most effective placement of the skimmer but is within the Mach disk.

For an isentropic, ideal gas expansion, with constant  $\gamma$  equations may be deduced to relate the source temperature, pressure, and number density, to corresponding expansion values located some distance ( $L_m/D$ ) from the orifice and are given below [8]:

$$\frac{T}{T_0} = \left( 1 + \frac{(\gamma - 1) M^2}{2} \right)^{-1} \quad (2.10)$$

$$\frac{P}{P_0} = \left( \frac{T}{T_0} \right)^{\gamma/(\gamma-1)} \quad (2.11)$$

$$\frac{n}{n_0} = \left( \frac{T}{T_0} \right)^{1/(\gamma-1)} \quad (2.12)$$

where  $M$  refers to the Mach number ( $M = V/a_0$ ) which is the ratio of the beam velocity at a given point ( $x$ ) over the local speed of sound. The Mach number may be deduced from the following equation. It should be noted that this refers to a centerline Mach number [8];

$$M = A \left( \frac{x - x_0}{D} \right)^{(\gamma-1)} - \frac{1/2 \left( \frac{\gamma+1}{\gamma-1} \right)}{A \left( \frac{x - x_0}{D} \right)^{(\gamma-1)}} \quad (2.13)$$

where  $A$  is a constant ( $A = 3.65$  for  $\gamma = 1.40$ ). A plot of Mach number versus the distance ratio is given in Fig. 2.7. As the skimmer distance is located 2 mm from the orifice the distance ratio is 20 at this point which corresponds to a Mach number of 12!

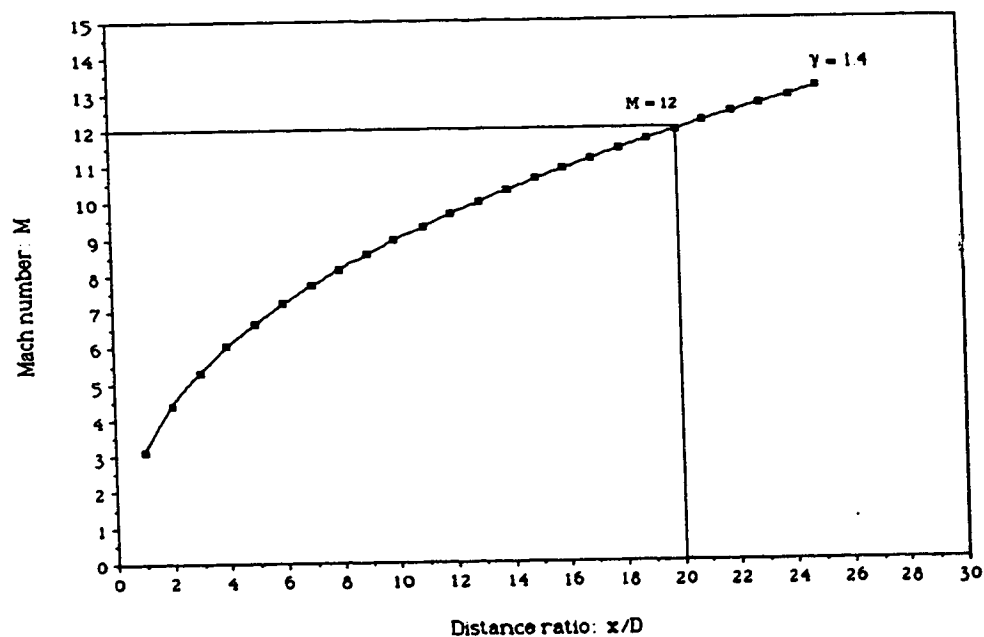


**Figure 2.7** The center line Mach number ( $M$ ) dependence on the distance ratio ( $x/D$ ) for  $\gamma = 1.40$ .

Thus, based on this equation, the nitrogen beam has a centerline value of Mach 12 at the skimmer which may seem quite high. These numbers are not presented to be hard and fast however and should be viewed with caution. If this relationship is translated

into nitrogen number density and equation 2.12 is plotted as a function of Mach number then the relationship may be plotted as in Figure 2.8.

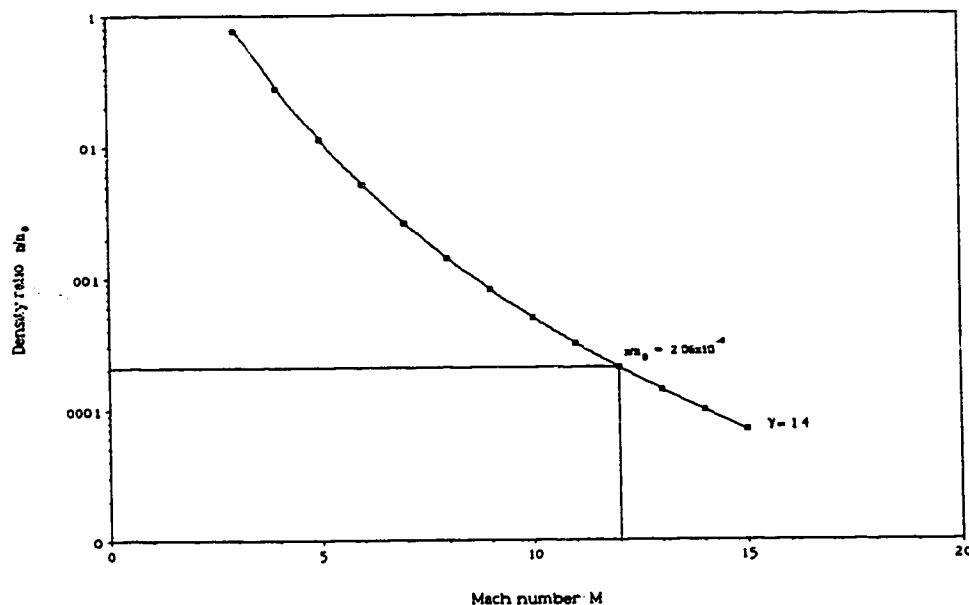


**Figure 2.8** The centerline nitrogen number density dependence on the Mach number (M).

It is seen from Fig. 2.8 that the number density of the centerline beam is only  $\sim 2 \times 10^{-4}$  that of the number density in the source ( $n_0 = 2.43 \times 10^{19}$  molecules/cm<sup>3</sup> at  $T_0 = 298$  and  $P_0 = 760$  torr) which corresponds to a value of  $\sim 5.0 \times 10^{15}$  molecules/cm<sup>3</sup>. This is important as it gives information on the nature of the CID collisions in the expansion region. The mean free path is directly related to the gas number density. For example, consider an ion of some mass and cross sectional area, if we assume (for simplicity) hard sphere

collisions, then the ion and collision gas (in this case nitrogen) have a collisional cross section denoted as  $\sigma_{\text{collision}}$  and expressed as;

$$\sigma_{\text{collision}} = \pi(r_{\text{ion}} + r_{\text{nitrogen}})^2 \quad (2.14)$$

The collisional mean free path may thus be expressed as;

$$\lambda = 1 / (\sigma_{\text{collision}} n) \quad (2.15)$$

Therefore as would be expected the mean free path ( $\lambda$ ) increases with decreasing number density for a particular collision pair. In the expansion where the number density is high the mean free path is small and therefore an ion accelerated under the influence of an electric field in this region will not achieve a significant energy before it collides with the expansion gas. As the ion travels toward the skimmer its mean free path increases in accord with the decrease in number density (Fig. 2.8) and thus the energy of collision also increases (due to acceleration to higher velocities). Thus the more energetic collisions and hence the more effective CID occurs further from the orifice at the expense of collisional frequency. It should be noted that the above collisional cross section is for hard sphere collisions and does not take into account the polarization of the curtain gas or ions which will serve to increase this area. The discussion above indicates that the CID region may be described best in a qualitative way and a quantitative description of this region is difficult at best.

## 2.6 References

1. G.R. Agnes and G. Horlick, *Appl. Spectrosc.*, **46**, 401 (1992).
2. M.A. Vaughan and G. Horlick, *Spectrochim. Acta*, **45B**, 1289 (1990).
3. M.A. Vaughan and G. Horlick, *Spectrochim. Acta*, **45B**, 1301 (1990).
4. B.W., Rossiter and J.F. Hamilton, Foundations of Vacuum Technology; In Physical Methods of Chemistry; W. Bryant Ed., Wiley Interscience: New York, Vol. 1, p. 121, (1986).
5. D.L. Lubman, C.T. Rettner and R.N. Zare, *J. Phys. Chem.*, **86**, 1129 (1982)
6. J.B. French, *C.A.S.I. Transactions*, **3**, 77 (1970).
7. H. Ashkenas and F.S. Sherman, Rarefied Gas Dynamics, Proc. 4th Int. Symp. Rarefied Gas Dynamics; J.H.de Leeuw, Ed.; Academic Press: New York, **2**, 84 (1966).
8. D. R. Miller, Free Jet Sources. In Atomic and Molecular Beam Methods; J. Scolas Ed., Oxford University Press: Oxford, Vol. 1, p. 14 (1988)

## **Chapter 3**

### **The Electrospray Mass Spectra of the Lanthanides**

### 3.1 Introduction

Since the introduction of electrospray-mass spectrometry (ES-MS) by Yamashita and Fenn [1,2] the majority of interest has been in the analysis of organic compounds, primarily biomolecules[3,4]. The technique is not however limited to this field of study and has successfully been applied to a variety of metal ion species. A number of researchers [5-10] especially Colton *et al* [11-18] have successfully examined complexed and organometallic metal ion species. Similarly others [19-23] have examined uncomplexed metal ions in solution also incorporating a variety of solvents. Recently Horlick and Agnes, [24-26] have examined both the qualitative and quantitative aspects of ES-MS as a technique for elemental analysis. In particular they illustrated the typical ion species observable and as well indicated that ES-MS could be used for the complete determination of inorganic solution components.

In this study uncomplexed lanthanide (III) metal ion solutions are examined, with the primary focus being on the type of information that may be obtained, and how this relates to the chemistry of the elements. The evolution of mass spectra starting from solvated ions down to the bare metal and molecular ions will be followed. This is achieved by varying the potential difference between the sampling plate and the skimmer ( see Figure 3.1). Given a significant potential difference between the sampling plate and the skimmer in the 500 mtorr region there will be a large number of energetic collisions between the neutral curtain gas and analyte ions that are entrained into the vacuum. By increasing the potential difference the energy of these



collisions is increased and declustering of the entrained ions is promoted (ie. collision induced dissociation (CID)).

These studies were pioneered by Kebarle and coworkers [19,20, 27-29] who have investigated  $M^{+1}$ ,  $M^{+2}$  and  $M^{+3}$  metal ions. In particular they investigated some of the lanthanides (La, Nd and Sm) and reported the species observed, which were clusters or charge reduced clusters. They also illustrated that the choice of solvent or incorporation of stabilizing ligands, had a great effect on whether the type of cluster observed was in a  $3^{+}$  or reduced  $2^{+}$  charge state. Siu *et al.* also have studied aqueous metal ion solutions with electrospray mass spectrometry [21,22] and as well a selection of lanthanide metal ions has been examined in complexed form by Curtis et al [9,10].

For the most part, elemental analysis of metal ion solutions has been conducted by using atomic-based techniques such as atomic absorption spectrometry (AAS), inductively coupled plasma-atomic emission spectrometry (ICP-AES), and inductively coupled plasma-mass spectrometry (ICP-MS). Since the development of ICP-MS there have been a number of studies of the lanthanides [see references 30-32 for example]. However although ICP-MS is quite sensitive, its focus is on the determination of the total amount of an element present in a solution and information concerning valence state, counterions, or complexation is not directly available. As illustrated by Horlick and Agnes [24,25], this type of information may be obtained from elemental electrospray mass spectrometry and these capabilities will be shown here for the lanthanides.

### 3.2 Experimental

The electrospray interface used for this study is shown in Fig. 3.1. The SCIEX/Perkin Elmer ELAN Model 250 ICP-MS mass spectrometer used for these studies has been described previously [24,25]. The critical parameters are the biases applied to the ES tip, front plate, sampling plate, skimmer and ion extractor lens as well as curtain gas flow rate. Unless indicated these parameters were kept constant except for the sampling plate voltage which was varied.

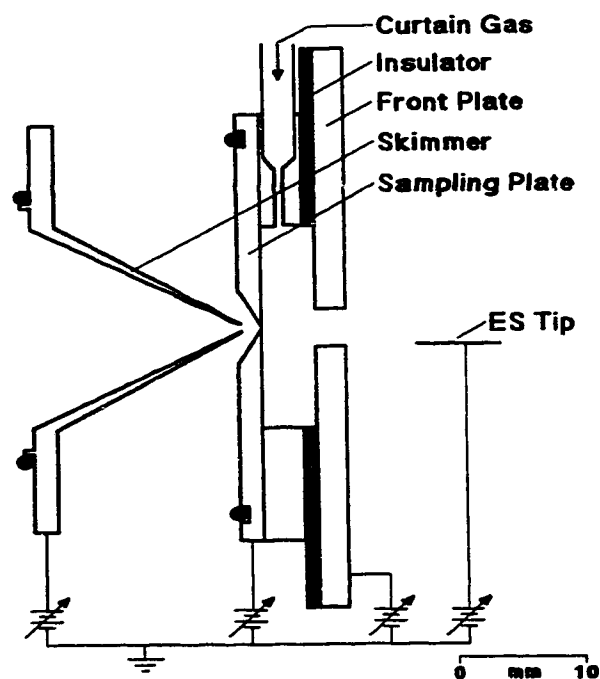


**Figure 3.1** Schematic diagram of the electrospray interface.

The ES tip was positioned 5mm from the front plate and about 2-4 mm off axis with respect to the central axis of the mass spectrometer and was set to deliver sample solution at either 4.5

$\mu\text{L}/\text{min}$  or  $10 \mu\text{L}/\text{min}$ . The tip voltage was supplied by a Glassman high voltage supply (EH series, 0-10kV). Both the front plate and sampling plate were independently biased by Glassman High Voltage supplies (EH series, 0-2kV). The skimmer was biased by a Hewlett Packard 6215A power supply, and any potential applied to the ion extractor lens was supplied via the voltage regulator board on the mass spectrometer.

As the droplets/solvated ion clusters which are produced as a result of the electrospray process drift through the atmospheric region there is a tendency for exchange to occur with any water present as vapor in the ambient atmosphere. Thus if there is a significant water vapor pressure there will be significant exchange in this region and the resultant ions sampled should reflect this. For these experiments a 'dry' (water free) atmosphere was used in order to minimize this effect.

There were two main modes of operation; a 'bare metal ion' mode, where the ions were essentially stripped or declustered down to elemental or molecular form, and gentle conditions where cluster conditions are allowed to predominate depending on the potential difference between the sampling plate and skimmer. It should be pointed out that the term 'gentle condition' is a relative one as compared to the 'bare metal ion' mode. In addition it should also be pointed out that the conditions for 'bare metal ion' mode represented in the spectra presented in this paper are not extreme. Conditions can be changed such that all molecular ions other than the bare  $1^+$ ,  $2^+$  and oxide are totally eliminated, in addition the oxide level can be reduced to such levels that the dominant ions in all cases are the bare metal ion.

The conditions used in this study were chosen to illustrate and exemplify the processes involved in stripping down the lanthanide species. Bare metal ion spectra have been presented in other publications by this group [24,26]. Both modes of operation however are considered to be quite harsh in terms of the potential difference between the sampling plate and skimmer which was typically 10 - 180V. Typical voltages applied for the 'bare metal ion' mode are: tip 4.5kV, front plate 900V, sampling plate 180V, skimmer 7V, and barrel lens -6V. For gentle conditions applied voltages were: tip 3.6kV, front plate 550V, sampling plate 20-100V, skimmer 9V, and the barrel lens at ground potential.

The curtain gas was prepurified nitrogen ( <4ppm H<sub>2</sub>O ). For this study a flow rate of 1.5 L/min was used for the gentle mode and 0.8 L/min for the bare metal ion mode. The curtain gas has two main purposes; first to minimize the entrance of solvent and other unwanted neutrals into the mass spectrometer and second to provide a source of neutrals for CID. It has been found that once past a minimum flow rate the curtain gas can have an effect on the metal ion cluster distribution as well spray stability for this system [25].

The metal salts used were commercially available from: Fischer, Ventron (Alfa products), and Nuclear Corporation of America. The specific metal solutions were prepared by dissolving the metal salt (indicated where necessary, for example, in discussion and figure captions) in nanopure water and diluting to  $1.0 \times 10^{-2}$ M. An aliquot of this solution was then diluted with either H.P.L.C. grade methanol, or H.P.L.C. grade acetonitrile to  $2.0 \times 10^{-4}$ M. Typical water content in these solutions was 1-2% by volume.

### 3.3 Results and Discussion

Lanthanide solutions were first studied under 'bare metal ion' mode conditions. The mass spectra of a selection of lanthanide metal ions are shown in Fig. 3.2 where all spectra were acquired under identical conditions. The first and last three elements of the lanthanide row were selected. This was done in order to highlight the differences in element chemistry along the series from low to high mass. There are noticeable differences in the spectra. In the lower mass region of the mass spectra a peak due to the bare  $2^+$  metal ion is evident in all cases except for lutetium. Note that the relative intensity of this peak is similar for the lower mass lanthanides (La, Ce, and Pr) as compared to the  $1^+$  ions ( $M^+$  and  $MO^+$ ). The relative intensity of the  $M^{2+}$  signal for the higher mass lanthanides (Tm and Yb) is greater than for the lower mass lanthanides, and in the case of ytterbium even exceeds that of the bare metal ( $M^+$ ) and oxide species ( $MO^+$ ).

The second noticeable difference is in the higher mass or  $1^+$  region of the mass spectra. For the lower mass lanthanides (La, Ce, and Pr), the oxide peak ( $MO^+$ ) is the dominant mass of the spectra whereas for the higher mass lanthanides (Tm, Yb, and Lu), the bare metal ion peaks ( $M^+$ ) are more intense than the corresponding oxide peaks ( $MO^+$ ).

These spectra pose the question; how do  $3^+$  lanthanide ions go from their solvated form in solution to the distribution of molecular and bare metal ion species observed in the mass spectrum? Obviously a whole series of events occurs before the final products observed in Fig. 3.2 are formed. Kebarle and coworkers [19, 20, 33, 34] have

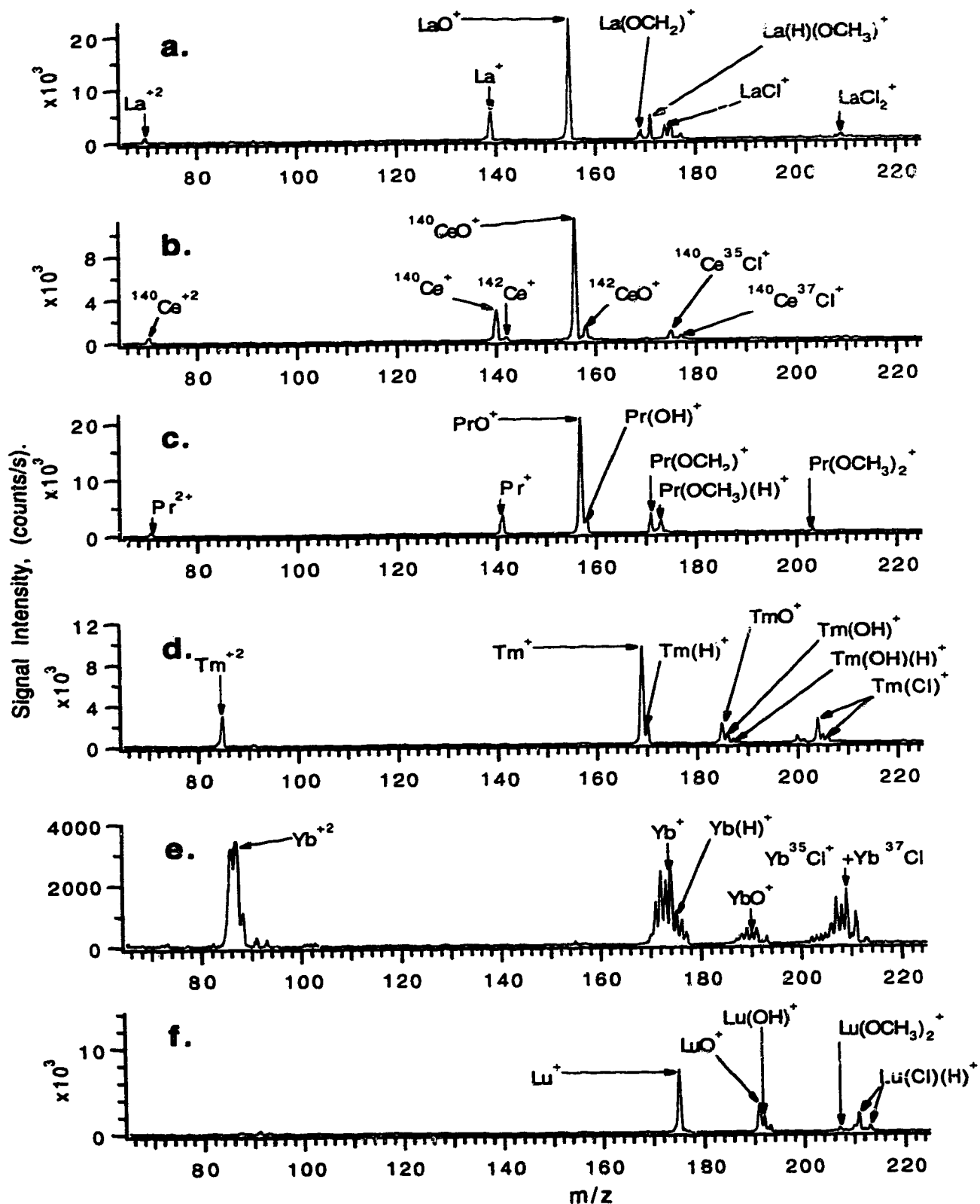


**Figure 3.2.** Mass Spectra of:  $\text{LaCl}_3$ ,  $\text{CeCl}_3$ ,  $\text{Pr}(\text{NO}_3)_3$ ,  $\text{TmCl}_3$ ,  $\text{YbCl}_3$ ,  $\text{LuCl}_3$  solutions ( $2 \times 10^{-4} \text{ M}$ ). Spectra acquired under identical 'bare metal ion' mode conditions.

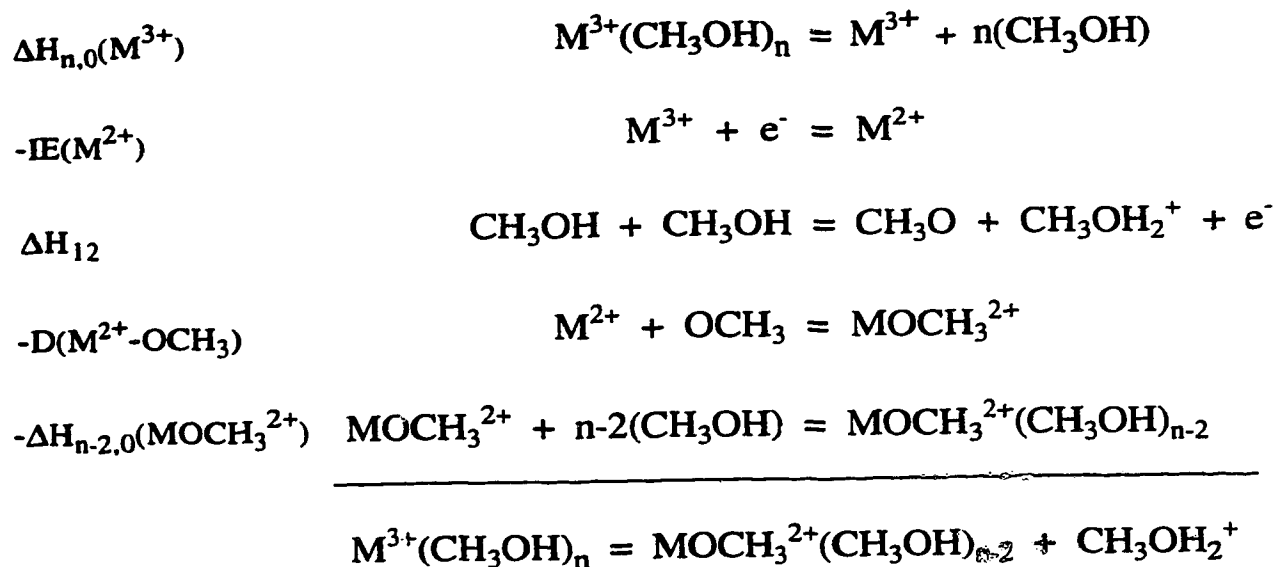
outlined some of the steps required for the production of molecular and bare metal ion products from their original solvated form in the gas phase. The initial step is the desorption/fission of a solvated gas phase ion from a larger charged parent droplet [35-37]. This ion will be solvated to some degree  $n$  ( $n$  refers to the number of solvent molecules). As the ion travels the interface region it will become declustered or lose solvent molecules. This will occur until a certain minimum value of  $n$  is reached. At this stage charge reduction will start competing with simple ligand loss as the solvation sphere in the gas phase can no longer stabilize the charge on the metal ion. Expressions to account for the charge reduction process where the metal ion is solvated by a ligand, in our case methanol, have been deduced:



The energy for such a process ( $\Delta H_{10}$ ) may be described by a thermochemical cycle the [19];

$$\begin{aligned} \Delta H_{10} = & \Delta H_{n,0}(M^{3+}) - IE(M^{2+}) + \Delta H_{12} - D(M^{2+}-OCH_3) \\ & - \Delta H_{n-2,0}(MOCH_3^{2+}) + E_{coul.} \end{aligned} \quad (3.2)$$

which may be deduced from the following scheme which relates the above values to thermodynamic equations;



Scheme 3.1

All the terms are self explanatory, one thing to note is the incorporation of a non thermodynamic  $E_{coul.}$  into equation (3.2) which accounts for the energy associated with the coulombic repulsion of the two positive ions  $CH_3OH_2^+$  and  $M(OCH_3)^{2+}(CH_3OH)_{n-2}$  which are formed. For the most part the above values are poorly defined or unknown.

The importance of equation (3.2) however is not lost in that it highlights the dominant processes involved in charge reduction. The charge reduction process, assuming the number of stabilizing ligands does not equal 0, is in competition with simple ligand loss. One of the dominant parameters that the equation highlights is the ionization potential of the metal ion. As a rule of thumb, charge reduced species form when  $IE(M^{n+}) > IE(L)$  (where L refers to ligand or coordinating solvent), and the tendency to form charge reduced species declines as  $IE(M^{n+}) < IE(L)$ . Conversely as the tendency for



the solvated ion to undergo charge reduction increases its ability to undergo simple ligand loss decreases. The dissociation energy of the ligand metal bond is another important parameter and in this case is related to the ease with which the metal ion will form an oxide. It is well known that the lanthanides are strong oxide formers [38].

It should be pointed out that these reactions described above refer to the solvated metal gas phase ions. Other species such as complexed ones present in solution may also undergo charge reduction provided the charge reduction criterion are satisfied (i.e.;  $\text{Pr}(\text{NO}_3)(\text{OCH}_3)(\text{HOCH}_3)_1^+$  shown in Fig. 3.3 spectrum b). As the decomposition energy is increased these ions may also become precursors for the oxide ions observed under harsh conditions. These species tend to be minor but are clearly documented in the appropriate spectra, the focus of discussion however is on the purely solvated species.

To understand how the properties of an individual lanthanide relate to the evolution of its ES mass spectrum some important physical information about the lanthanide series must be given (see Table 3.1). Notice that in Table 3.1 there is a general trend in the metal-oxide dissociation energy where the bond is stronger for the low mass end and weaker for the high mass end of the series. There is also a trend in regards to the second ionization potential where it tends to be lower at the low mass end and higher at the high mass end of the series. If two elements from opposite ends of the series are selected they should then exhibit different behaviour. With this in mind the evolution of praseodymium (Pr), and thulium (Tm) spectra as a function of sampling plate voltage is shown in Figs. 3.3 and 3.4

respectively. The spectra a-f. in Figs. 3.3 and 3.4 were obtained by increasing the sampling plate voltage in 10V steps. These stages are to be considered precursor steps to the generation of the spectra associated with the 'bare metal ion' mode as shown in Fig. 3.2.

**Table 3.1.** Physical Data for the Lanthanide Metals.

	Dissociation Energies <sup>a</sup> (eV)		Ionization Potentials <sup>b</sup> (eV)			
	(M-O)	(M <sup>+</sup> -O)	I	II	III	IV
La	8.24	8.89	5.58	11.06	19.18	49.95
Ce	8.15	8.80	5.47	10.85	20.20	36.76
Pr	7.59	8.20	5.42	10.55	21.62	38.98
Nd	7.24	7.76	5.49	10.73	22.10	40.41
Sm	5.90	5.98	5.63	11.07	23.40	41.40
Eu	4.86	4.03	5.67	11.24	24.92	42.60
Gd	7.37	7.80	6.14	12.09	20.63	44.00
Tb	7.15	7.67	5.84	11.52	21.91	39.79
Dy	6.33	6.29	5.93	11.67	22.80	41.47
Ho	6.24	6.11	6.02	11.80	22.84	42.50
Er	6.24	6.07	6.10	11.93	22.74	42.65
Tm	5.29	5.03	6.18	12.05	23.68	42.69
Yb	4.12	3.82	6.25	12.18	25.03	43.74
Lu	6.90	5.51	5.43	13.90	20.96	45.19

a.) Murad, E.; Hilderbrand, D.L. *J. Chem. Phys.* **1980**, 73, 4005-4011.

b.) *CRC Handbook of Chemistry and Physics*, 1993 edition.

Examination of the praseodymium spectrum acquired under gentle conditions (Fig. 3.3a) shows a distribution of 2<sup>+</sup> cluster ion species ie.: [Pr(OCH<sub>3</sub>)(CH<sub>3</sub>OH)<sub>n</sub>]<sup>2+</sup> where n=2 to n=10. Note that there are no 3<sup>+</sup> cluster ion species as one stage of charge reduction has already occurred. In methanolic solutions 2<sup>+</sup> as opposed to 3<sup>+</sup> ion clusters are expected because the third ionization potential of Pr (21.62 eV) is much greater than the ionization potential of methanol (10.84 eV). Thus, unless sufficient solvent molecules are present to simulate solution conditions the ion cluster will not be stable and

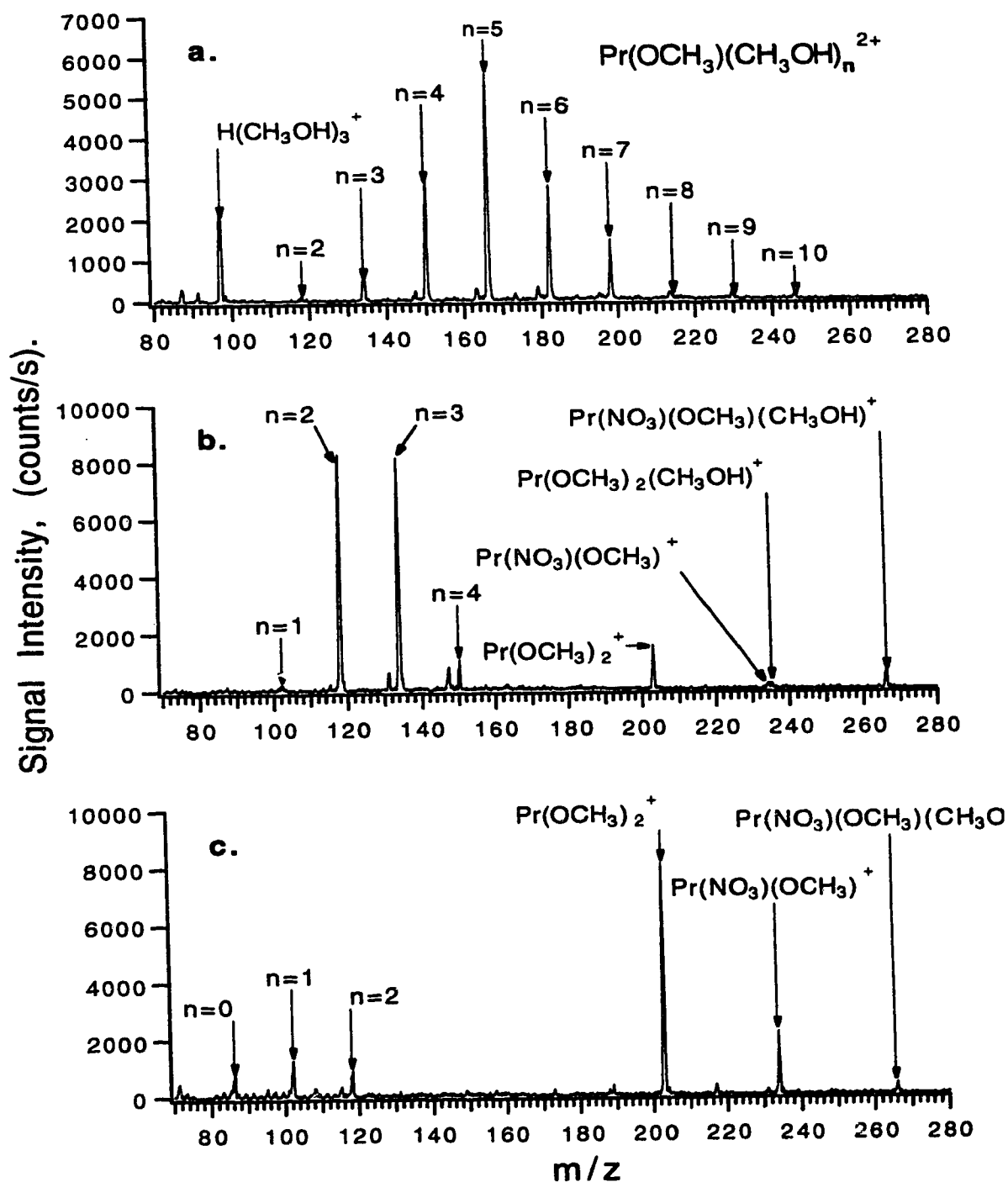


**Figure 3.3** Mass Spectra of  $\text{Pr}(\text{NO}_3)_3$  ( $2.0 \times 10^{-4}\text{M}$ ) acquired by varying the sampling plate (S.P.) voltage: (a) 25V, (b) 35V and (c) 45V.

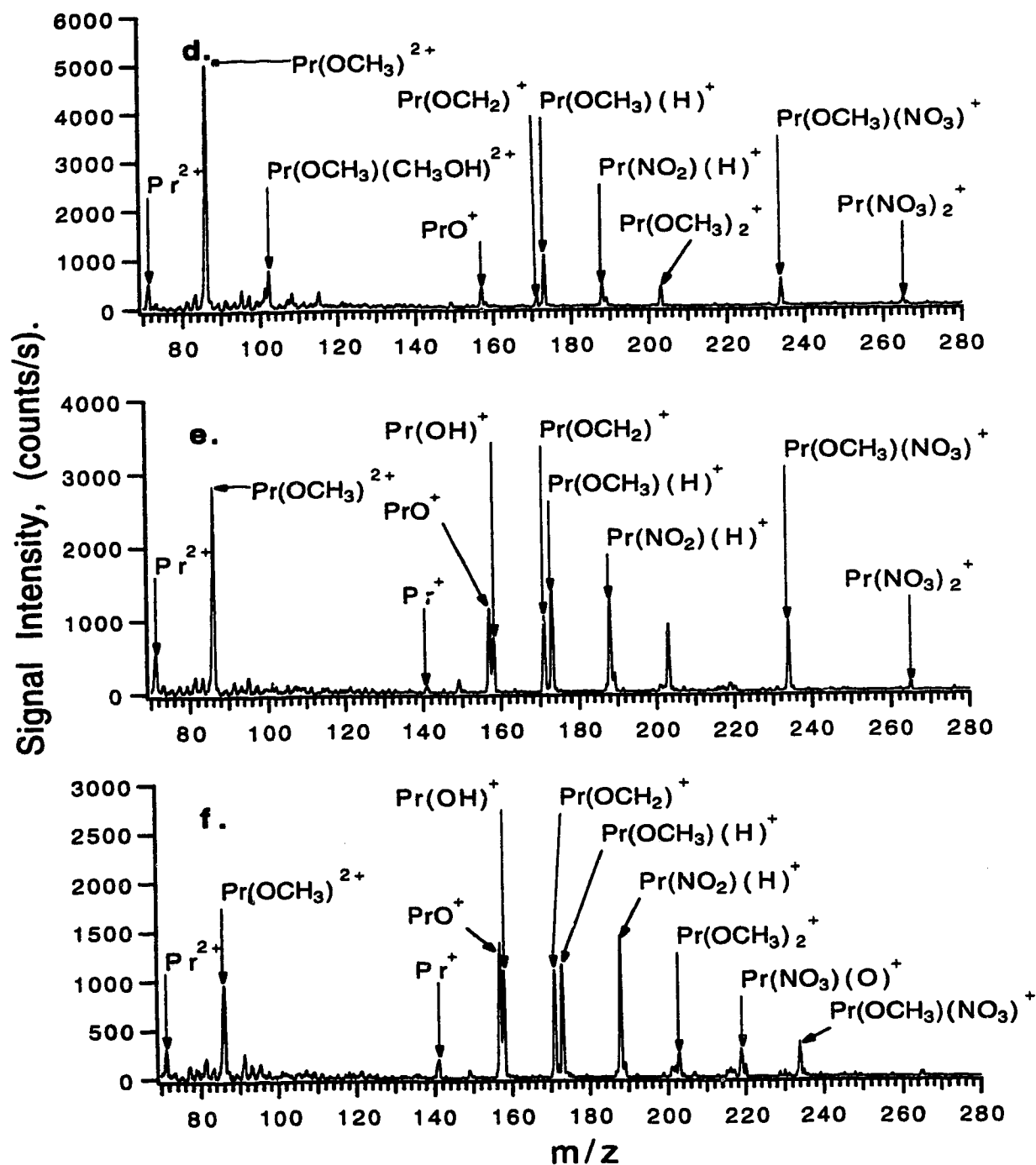


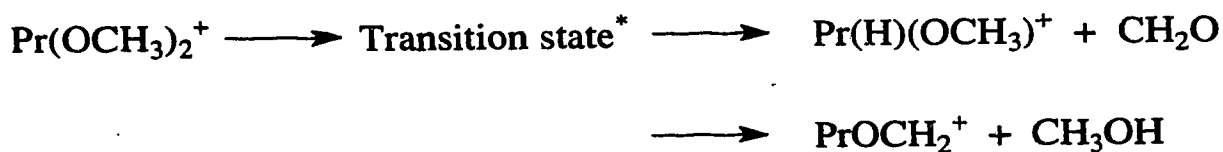
**Figure 3.3** Mass Spectra of  $\text{Pr}(\text{NO}_3)_3$  ( $2.0 \times 10^{-4} \text{M}$ ) acquired by varying the sampling plate (S.P.) voltage: (d) 55V, (e) 65V, (f) 75V.

charge reduction will occur. In a (Fig. 3.3) the distribution maximum is at  $n = 10$  which is just larger than the number associated with the typical inner solvation sphere of a lanthanide which may be either eight (ie.  $[\text{Ln}(\text{H}_2\text{O})_8]^{3+}$ ) or nine (ie.  $[\text{Ln}(\text{H}_2\text{O})_9]^{3+}$ ) [39]. Therefore it may be concluded that the minimum solvation required to preserve the  $3+$  charge state is greater than  $n = 10$ . For ions of similar IE (18-20 eV) it has been predicted [8] that the minimum solvation number is greater than 15.

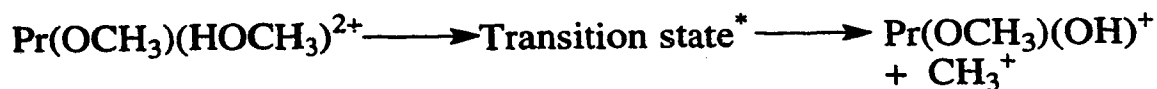
In spectrum b (Fig. 3.3) the distribution of the clusters has been narrowed considerably to  $n=1$  to  $n=4$  as a result of CID. At this stage declustering and charge reduction are in competition and as a result some  $1+$  charge reduced species (second stage) are seen at  $m/z$  203 and greater. With a further increase in voltage (Figure 3.3c) the dominant ions observed in the spectrum are the doubly charge reduced  $1+$  ions ( $[\text{Pr}(\text{OCH}_3)_2(\text{CH}_3\text{OH})_n]^{+1}$ ), and species such as;  $[\text{Pr}(\text{OCH}_3)(\text{X})(\text{CH}_3\text{OH})_n]^{+1}$  (where  $\text{X} = \text{Cl}^-$  or  $\text{NO}_3^-$  for example) with smaller contributions by  $2+$  ion species. These species may be the result of ion pairing which occurs at the later stages in the lifetime of a charged droplet or they may exist as an equilibrium population in solution (see the discussion later on). Note that the upper mass limit is  $\sim 295$   $m/z$  (ie. that corresponding to a converted ICP-MS). This effectively limits information on the occurrence of higher mass cluster distributions, in particular those corresponding to the heavier nitrate anion species. Spectrum d (Fig. 3.3) shows that the  $2+$  ion clusters have been fully desolvated down to the charge reduced ion,  $[\text{Pr}(\text{OCH}_3)]^{2+}$ . It is at this stage that the effect of the elements chemistry may be seen fairly well. The two important and competing

parameters are the ionization potential (IE) and the strength of the oxide bond that is formed upon charge reduction. For Pr the second IP (10.55 eV) is slightly less than the IE of methanol (10.84 eV) and the oxide bond is actually quite strong (8.20 eV). If the second IE had been a couple of eV higher with the same oxide formation potential a much smaller contribution of 2<sup>+</sup> species would be observed. Further evolution of the mass spectrum is shown in Figs. 3.3e and 3.3f, in particular the further decomposition of doubly charge reduced and complex species. If we consider that the spectrum in Fig. 3.2c is a later stage for the mass spectrum, then a dominant ion formed is the molecular species PrO<sup>+</sup>. This may be expected as Pr is a fairly strong oxide former [38].

Some interesting products of the decomposition to note are [Pr(OCH<sub>2</sub>)]<sup>+</sup> at m/z 171 and [Pr(OCH<sub>3</sub>)(H)]<sup>+</sup> at m/z 173. These ions are probably formed as a result of β-hydride transfer [40] reactions from the doubly charge reduced precursor species [Pr(OCH<sub>3</sub>)<sub>2</sub>]<sup>2+</sup>. The reaction is postulated in scheme 3.2 below. The formation of the hydroxyl/alkoxyl cation [Pr(OCH<sub>3</sub>)(OH)]<sup>+</sup> at m/z 189 is also interesting and its formation sequence is proposed in scheme 3.3 below.



Scheme 3.2



Scheme 3.3

The dialkoxide species will first form a transition state complex of unknown structure. This structure(s) can then afford two different decomposition products as shown above. The first being the alkoxide/hydride species and the second being a three membered formaldehyde type species. Upon formation, the two products are then capable of reductive elimination with the first scheme giving  $\text{Pr}^+$  and methanol, and the second giving  $\text{Pr}^+$  and formaldehyde or  $\text{PrO}^+$  and carbene. The peak at  $m/z$  189 is probably formed by the decomposition of the solvated  $2^+$  ion. The relatively large  $2^+$  ion peak at  $m/z$  86 ( $[\text{Pr}(\text{OCH}_3)]^{2+}$ ) will undoubtedly decompose to one of two products, the bare  $2^+$  metal ion ( $\text{Pr}^{2+}$ ) or  $\text{PrO}^+$  and  $\text{CH}_3^+$ . As the element is a fairly strong oxide former, it could be speculated that the dominant product would be the oxide ( $\text{PrO}^+$ ) with the lesser component being the bare metal ion ( $\text{Pr}^+$ ). If the element had not been a strong oxide former a larger relative  $\text{Pr}^{2+}$  ion contribution may have been expected. The above decomposition schemes are generally consistent with a formation scheme of rare earth metal ions with methanol in the gas phase as presented by Azzaro *et al* [41]. In that paper they present reaction mechanisms for the production of solvated gas phase di-alkoxide rare earth metals by reacting gas phase  $\text{M}^+$  metal ions with a partial pressure of methanol and recording the resultant mass spectra. The products and intermediates are consistent with the decomposition products and intermediates observed in this study.

Knowing that the physical properties of praseodymium and thulium are different, differences in the evolution of the spectrum for thulium can be expected. For thulium its second ionization potential is

12.05 eV which is  $\sim 1.5$  eV above that of methanol and Tm is not as strong an oxide former as Pr with its  $D(M^+-O)$  being 5.03 eV vs 8.20 eV for Pr.

The first three spectra (a., b., and c.) in Fig. 3.4 show the typical cluster distribution associated with gentle conditions. A comparison of these spectra with the corresponding praseodymium spectra (Figs. 3.3 a-c) shows a difference in the type of distribution observed. In going from gentle to harsher conditions; a to c in both figures there is an obvious shift in the cluster distribution. For thulium it is noted that there is no  $2^+$  cluster species with  $n$  less than 2 (note the peak at  $m/z$  119 is due to a sodium cluster species that is formed as a result of impurities in the solvent) whereas for Pr there are species present with  $n$  as low as 0 ( Fig. 3.3c). This is probably because the second IE of Tm is higher than that of methanol and Pr, so as the cluster distribution edges towards a less solvated state the cluster will undergo a second charge reduction preferentially to further ligand loss. The fact that the extent of the distribution of the clustered species (Fig. 3.4c) at this stage ( $n = 2 - 5$  vs  $n = 0 - 2$  ) is larger than that of the Pr (Fig. 3.3c) may be explained by the lower relative oxide formation potential of Tm ie.; the energy necessary for charge reduction (eq. (2)) although favourable in terms IE is not as favourable in terms of oxide formation potential relative to that of Pr. The two terms set a sort of +/- balance in terms of the energy required for charge reduction. As illustrated in Fig. 3.4 spectra d, e and f, the energy barrier for complete charge reduction is overcome via the energy provided by CID and the main contribution is due to



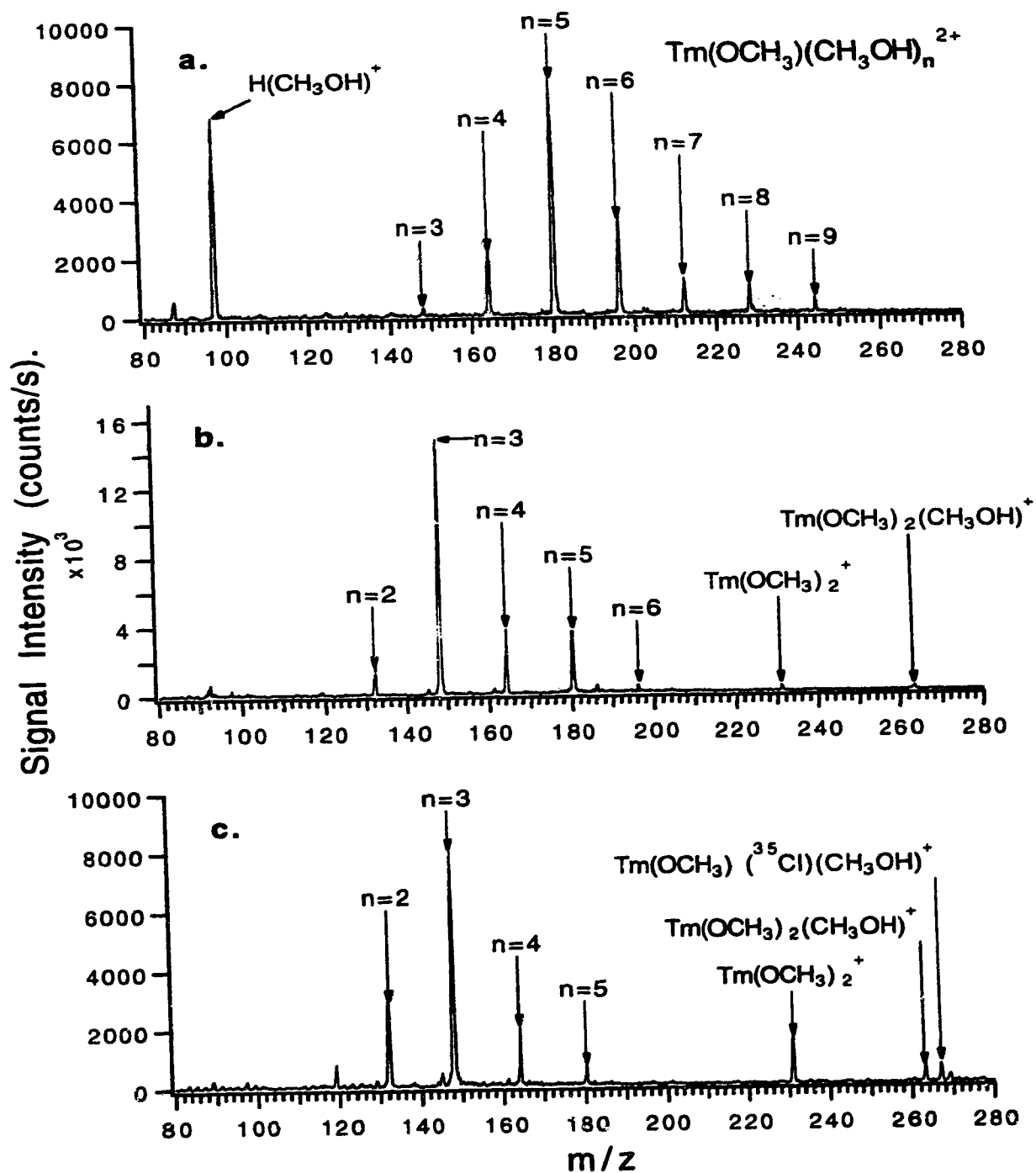


**Figure 3.4** Mass Spectra of  $\text{TmCl}_3$  ( $2.0 \times 10^{-4}\text{M}$ ) acquired by varying the sampling plate (S.P.) voltage: (a) 25V, (b) 35V, (c) 45V.

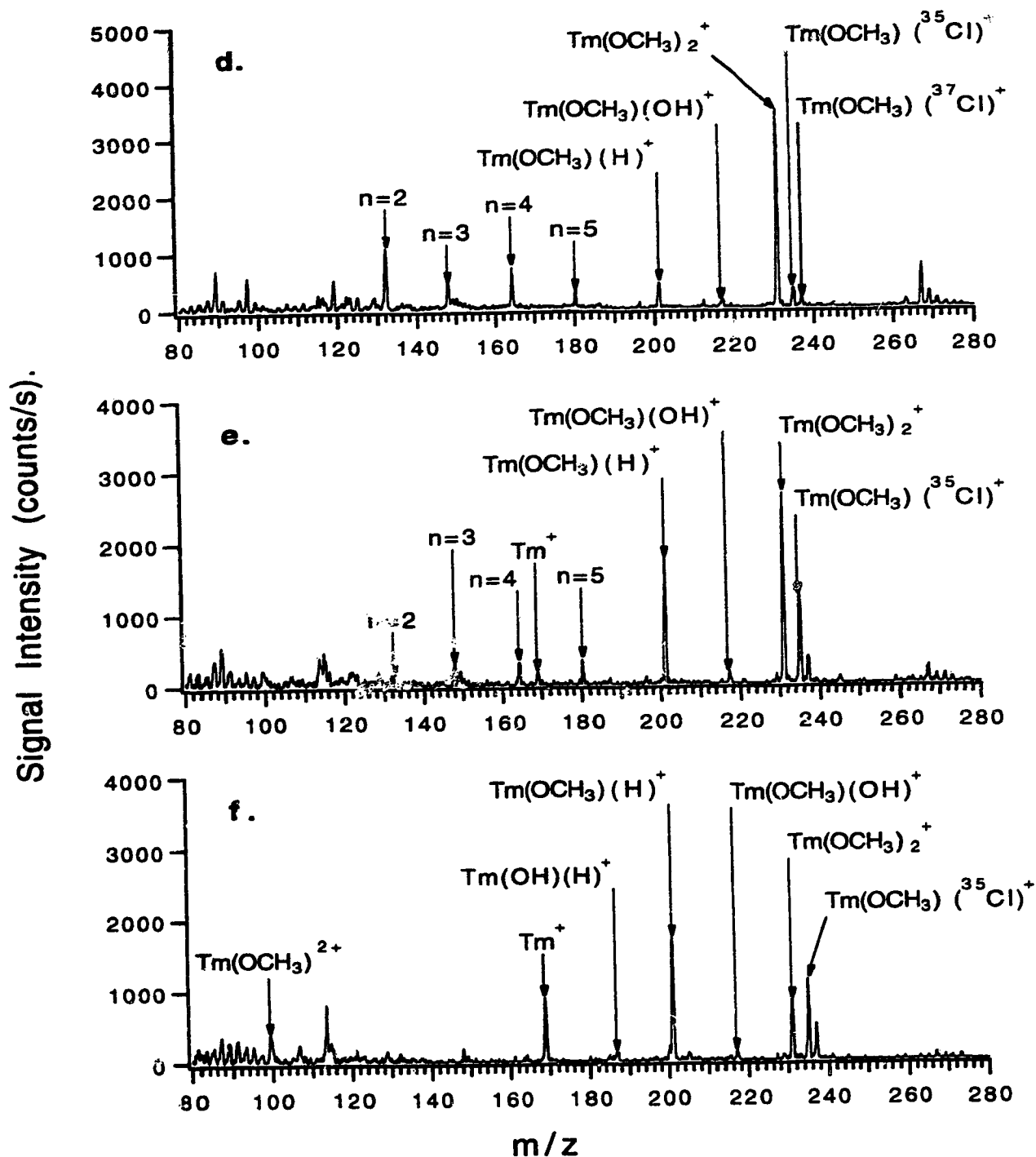
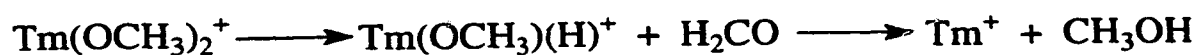


**Figure 3.4** Mass Spectra of  $\text{TmCl}_3$  ( $2.0 \times 10^{-4} \text{M}$ ) acquired by varying the sampling plate (S.P.) voltage: (d) 55V, (e) 65V, (f) 75V.

doubly charge reduced species which eventually give way to other molecular species. In particular the reductive elimination process based on Scheme 3.2 is dominant:



Scheme 3.4

This scheme is useful in understanding the dominant contribution of  $\text{Tm}^+$  in Fig. 3.2d. The large contribution by  $\text{Tm}^{2+}$  ion in the spectrum shown in Fig. 3.2d is explained by the fact that the higher energy conditions associated with the 'bare metal ion' mode will ultimately yield distributions of smaller cluster numbers not evident in Fig. 3.4 a-c. Thus any  $2^+$  cluster ion species (ie.  $[\text{Tm}(\text{OCH}_3)(\text{CH}_3\text{OH})_n]^{2+}$ ) that reach the  $n=0$  state (Fig. 3.4f) will tend to dissociate to a larger extent to the bare  $\text{Tm}^{2+}$  ion than to the oxide ( $\text{TmO}^+$ ) as Tm is not as strong an oxide former as Pr.

Having illustrated the essential aspects that are involved in the the evolution of the 'bare metal ion' mode mass spectrum it is now possible to better understand the results shown in Fig. 3.2. Similar spectra are seen for La, Ce, and Pr in Figs. 3.2a-c. This may be expected as the dissociation energies of their corresponding oxides and their ionization potentials are all quite similar (see Table 1). Therefore if we review the evolution of the Pr spectra in Fig. 3.3 it is not surprising that La and Ce will also yield intense oxide ion peaks relative to the bare  $1^+$  and  $2^+$  ion peaks. The ytterbium spectra in Fig. 3.2e shows a more intense  $2^+$  bare ion peak relative to that of Tm. The second ionization potential of Yb is 12.18 eV which is similar to that of Tm (12.05 eV), however its oxide forming potential (3.82 eV)

is much lower than that of Tm (5.03 eV). It should therefore be expected that charge reduction will not be as favourable as in the case of Tm (eq. 3.2), and therefore an intense  $\text{Yb}^{2+}$  bare ion peak should be observed. For Lutetium (Fig. 3.2f) the spectrum reveals little or no contribution from the  $\text{Lu}^{2+}$  ion but a dominant contribution by the  $\text{Lu}^+$  ion. Lutetium is a relatively weak oxide former (5.51 eV) as compared to the other lanthanides however its second ionization potential is the largest of all the lanthanides being 13.90 eV. The high second IE, therefore, is the dominant variable and as  $[\text{Lu}(\text{OCH}_3)(\text{CH}_3\text{OH})_n]^{2+}$  ion species approach lower values of  $n$ , the ion will undergo charge reduction in preference to ligand loss down to the  $n = 0$  state.

Next the examination of a mixture of lanthanides was undertaken. The spectrum for a mixture of Pr, Gd, and Lu is shown in Fig. 3.5. The interface conditions were set so as to generate a 'bare metal ion' spectrum. The spectrum is somewhat complex with a large amount of isobaric overlap caused by the presence of oxides. In particular note the overlap of  $\text{PrO}^+$  with the bare  $\text{Gd}^+$  isotope distribution as well as the overlap of the  $\text{GdO}^+$  isotope distribution with the bare  $\text{Lu}^+$  ion. This kind of overlap is common in other mass spectral determinations of lanthanides such as ICP-MS where in addition to the bare metal ion, oxides and hydroxides are also found but at considerably lower levels [30-32]. In order to overcome these isobaric overlaps in ICP-MS correction procedures are typically required [30]. This problem may be overcome in ES-MS by running the mixture under gentle source and interface conditions. Spectral

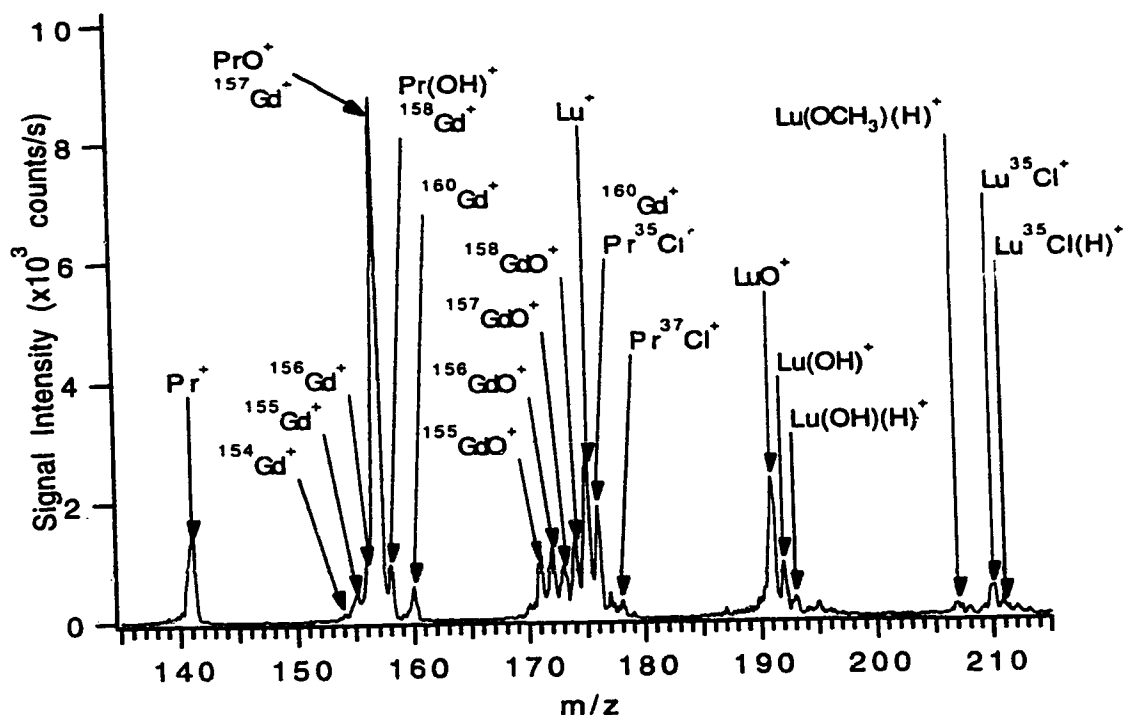


**Figure 3.5** Mass Spectra of  $\text{Pr}(\text{NO}_3)_3$ ,  $\text{GdCl}_3$ ,  $\text{LuCl}_3$ : ( $2.0 \times 10^{-4}\text{M}$ ). Spectra acquired under bare metal ion mode conditions.

overlap may be avoided by sampling the cluster ion species, where the individual distributions do not overlap with other distributions or any doubly charge reduced species (see Fig. 3.6a). In this case the singly charge reduced clusters are illustrated with Pr (X), Gd (Y) and Lu (Z) all present with varying solvation spheres. At another set of conditions (see Fig. 3.6b) the voltage on the sampling plate was increased in order to promote further charge reduction. The typical solvent derived molecular ions and also the complex ion species are seen with little isobaric overlap. In the original solution both chloride and nitrate anions were present. This spectrum (Fig. 3.6b) reveals both chloride and nitrate metal ion species. Most notable are those due to  $[\text{Pr}(\text{OCH}_3)(\text{NO}_3)]^+$  ( $m/z = 234$ ) and  $[\text{Lu}(\text{OCH}_3)(\text{Cl})]^+$  ( $m/z =$

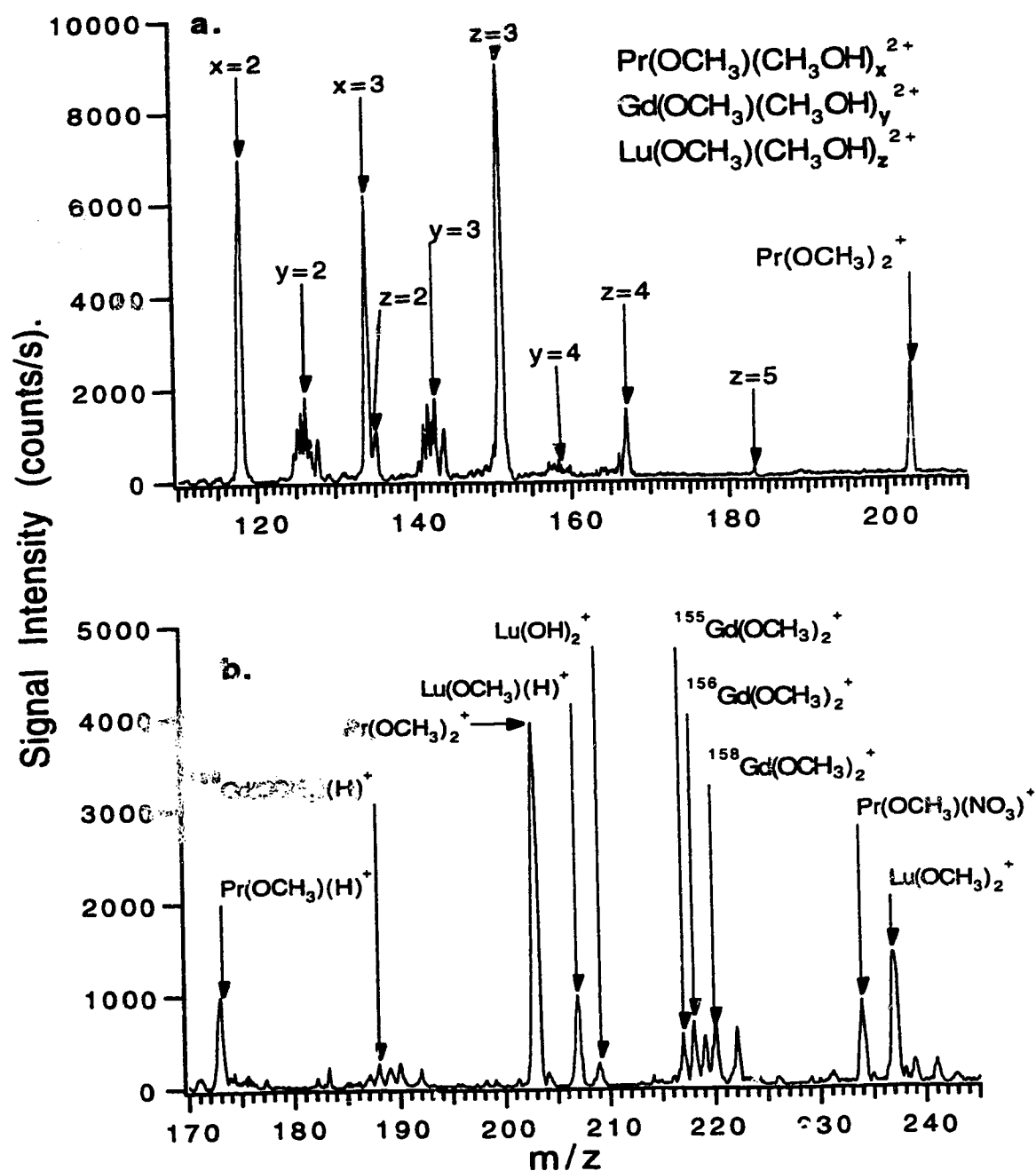


**Figure 3.6** Mass Spectra of  $\text{Pr}(\text{NO}_3)_3 \text{GdCl}_3, \text{LuCl}_3$ : ( $2.0 \times 10^{-4} \text{M}$ ). Spectra acquired under gentle mode conditions by varying the sampling plate voltage (a) 40V, (b) 55V.

241,243). As both anions are present in solution we would expect to see both species.

It has been illustrated above (and in some earlier spectra) that the mass spectra do not just consist of dissociation products of ( $[Ln(MeOH)_n]^{3+}$ ) species, but also species such as  $[Ln(X)(OCH_3)(MeOH)_n]^+$  (where  $X = Cl^-$ , or  $NO_3^-$ ). It is useful to understand the origin of such species. First the original solution chemistry must be examined. The samples are run in predominantly methanolic solutions (only  $\sim 1-2\%$   $H_2O$ ) and so the solution chemistry will be somewhat different from that of an aqueous solution. In dilute aqueous solutions the species present is exclusively  $[Ln(H_2O)_8]^{3+}$ , in fact Wertz and coworkers [42,43] have shown that even in 10N HCl there is only minor inner-sphere bonding. When they investigated methanolic solutions there was evidence for extensive inner-sphere bonding by  $Cl^-$ . The methanolic solutions under investigation were however  $\sim 10^4$  times more concentrated relative to those run under normal electrospray conditions. Therefore in dilute methanolic solutions one may assume that the extent of inner-sphere coordination will be greater than that of aqueous solutions but still only minor and for the most part any association in solution will be some form of ion pairing. This reasoning would seem to be supported by examination of the spectra shown in Fig. 3.4. Under gentle conditions (Figs. 3.4a and 3.4b) it is expected that if there was inner-sphere coordination then there would be a fairly strong distribution due to the species  $[LnX(CH_3OH)_n]^{2+}$ . This is not observed. When the sampling plate voltage is increased significantly (Figs. 3.4c-f) however, we see

contributions due to the doubly charge reduced or  $1^+$  ion species ( $[\text{LnX}(\text{OCH}_3)(\text{MeOH})_n]^+$ ).

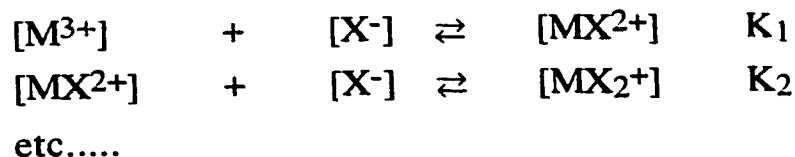
This may be understood by going to the literature, primarily some recent work by Tang and Kebarle [33,34], that is based on work by several groups [35-37]. In this work droplet formation and fission processes are described in some detail and stepwise sequences are developed to help illustrate the formation of gas phase ions. There are typically two possible scenarios, the first being uneven fission processes. It was found that in the case of uneven fission processes ~15% of the charge is lost with ~2% of the mass. This translates into some twenty droplets with ~10% of the radius of the parent droplet. The second scenario is where even fission will occur which yields two droplets of even charge and mass.

Ultimately the droplets will continue the fission/evaporation cycle until they reach a critical radius [37]. Given a 1 : 1 strong electrolyte this is thought to be ~80 angstroms with a corresponding excess charge of ~70 and it is at this stage that single ion ejection is thought to occur. Through continuous solvent evaporation and fissioning processes one will end up with droplets that are excess in surface cations with a concentrated bulk ion pair concentration. This occurs as a result of volume decrease in the droplets due to solvent evaporation. It was shown that the initial concentration is related to the eventual concentration of ion pair species in the droplet [33,34].

At the later stages of the droplets life one may imagine that the increased concentration may afford conditions that are conducive to complex formation. If this is the case, then in addition to formation of solvated bare surface ions one should see a distribution of solvated



complex ion species, the extent of which will be determined by the formation constants under the given conditions ie.:



This is indeed the case, where minor contributions due to these complex species under somewhat harsh CID conditions are observed. In support of this argument a weak but distinct signal (ie. correct isotopic pattern) due to the formation of the  $[\text{LaCl}_4]^-$  species in negative ion mode ES has been observed in other studies in our laboratory.

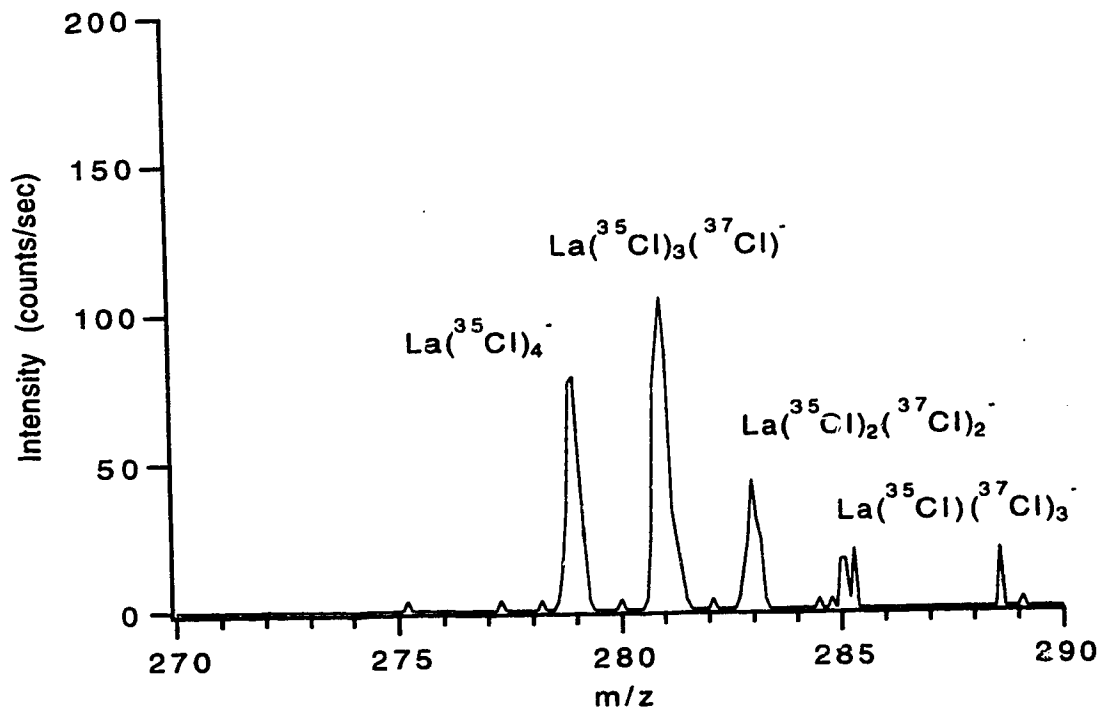


**Figure 3.7** Negative ion mass spectra of  $2.0 \times 10^{-4} \text{ M}$   $\text{LaCl}_3$  acquired at a sampling plate voltage of 40V.

In general it was not until a relatively high potential difference between the sampler and skimmer was reached that these species were observed. To explain this, the intensities of the spectra observed must be considered. Under gentle conditions where complex species are not readily observable, the overall signal intensity is rather low, however when the potential difference is increased the complex signal intensity as well as the overall signal intensity is increased. It may be speculated that the increase in potential is not necessarily responsible for generating more ions but serves to focus the ion beam and thus results in greater ion throughput to the detector. Ultimately, if these ions originate from the bulk or more appropriately as a result of the preconcentration ions in the droplet then they will be the last ions to be formed at the end of a droplets life [33]. It would thus seem reasonable to assume that these species would also be in the minority as compared to ions that would be found at the surface of the droplet. In addition these ions formed last may carry away more of the droplets mass and so may exist more as a singly charged droplet than a well solvated ion. This may generate several sampling problems; such as will the mass spectrometer be able to pass the 'ion droplet' through the energy filter or will the vacuum serve to cool and ultimately freeze the 'ion droplet' to a crystalline form making it 'immune' to CID.

Some evidence that supports the complexation theory is presented in Fig. 3.8. The upper mass range of the instrument poses a restriction in observing the higher  $m/z$  cluster species of the lanthanides. Therefore it was necessary to find a lower mass alternative, but one that still resembles the lanthanides as closely as

possible. Thus the rare earth element scandium seemed a good choice. It however has a smaller ionic size and a correspondingly lower average coordination number ( typically  $\sim 6$  ) than the other rare earth elements. Scandium also exhibits a higher degree of covalency in its complexes as compared to the elements of the lanthanide series. It seems to follow the d-type transition metals [44] and will probably have a different chemistry in methanol than the elements in the lanthanide series [41]. Lanthanides are thought to be more ionic in nature with only slight covalent tendency and thus similar in character to the alkali metals. This is illustrated by the fact that the typical free electronic configuration is  $f^n s^2$  and thus in its ionic form its charge is well shielded making most interactions electrostatic in nature. The ES mass spectrum of scandium however, did confirm the above speculation, in that the lower mass of scandium enables us to examine higher mass product ions, and there is indeed a low intensity distribution of mono-chloro, and even di-chloro species.

To further confirm these speculations Pr was examined in acetonitrile. It has been shown [22] that when the lanthanides are electrosprayed in acetonitrile,  $3^+$  ions may be easily observed. This would enable observation of charge transfer  $2^+$  counterion species, which neatly circumvents the restriction of a mass ceiling. Spectrum b (Fig. 3.8) is for  $\text{Pr}(\text{NO}_3)_3$  in acetonitrile solution run under gentle conditions, and as expected there is a strong contribution due to the  $3^+$  cluster ion distribution, and by the counterion  $2^+$  charge transfer distribution. It should be pointed out that because acetonitrile is a different solvent it will have different physical characteristics in its solvation of the metal ion. Also note that at  $m/z$  145, 147 and 104, 106

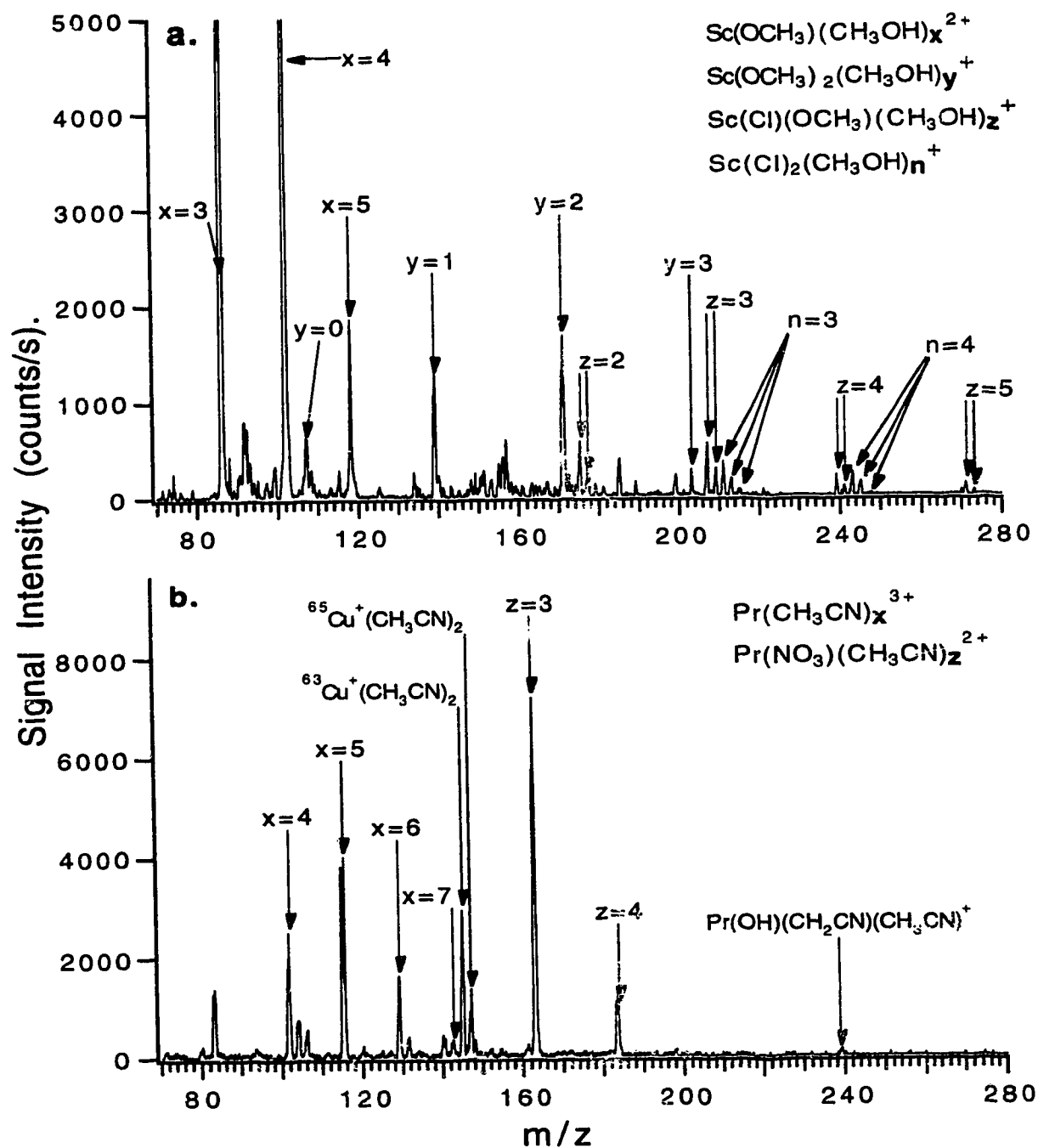
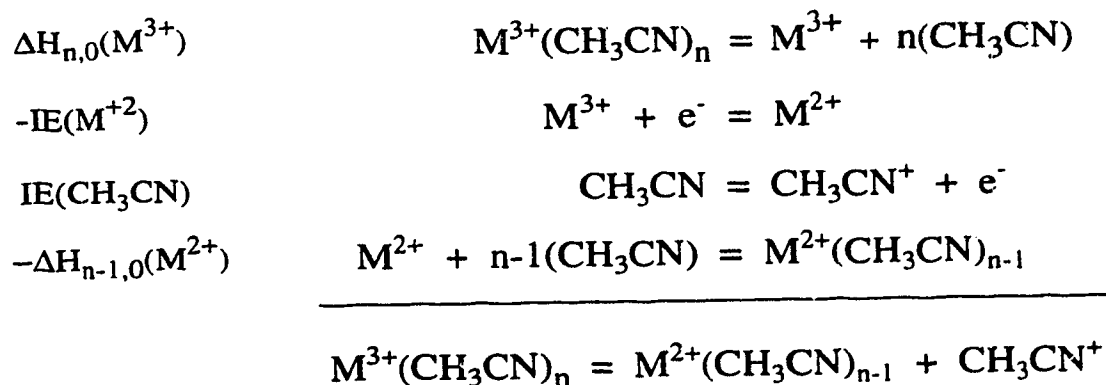


**Figure 3.8** The mass spectrum of (a)  $\text{ScCl}_3$  and (b)  $\text{Pr}(\text{NO}_3)_3$  where each are  $2.0 \times 10^{-4} \text{ M}$  in acetonitrile. The spectrum were both acquired with sampling plate voltages of 30V.

there are peaks present due to Cu (I) acetonitrile adducts. This impurity has been seen in other studies [22]. The copper may originate from two sources; the solution and or copper or brass fittings present in our electrospray setup. Recent experiments indicate the later as the source of impurity.

The 3+ cluster ion species is probably observed due to a high energy requirement for charge reduction. The ionization potential of acetonitrile is higher than methanol being ~12.2 eV. This is not the primary reason for the lack of charge reduction, rather it stems from the fact that unlike methanol or water the charge reduction (charge transfer) does not yield strong covalent M-O bonds such as Ln-OCH<sub>3</sub> and therefore the overall energy given up as a result of the charge transfer is less. The resultant products are usually just complexed species, however Ln-CH<sub>2</sub>CN bonds are seen under strong CID conditions (under investigation in future work). The overall effect is a 'protection' of charge or a seeming stabilization of the ion. Similar to equations 3.1 and 3.2, the process may be described thermodynamically and is given in Scheme 5 below;



Scheme 5

To explain the complexed species in acetonitrile the physical properties of the solvent must be considered. The dielectric constant of acetonitrile (~36) has a value similar to that of methanol (~33) both of which are considerably less than water (~80). Thus in both cases more inner sphere coordination of a counterion species as compared to water is expected. Examining the intensity of the complex species ( $[\text{Pr}(\text{NO}_3)(\text{CH}_3\text{CN})_z]^{2+}$ ) in spectrum b (Fig. 3.8) it is obvious that it is much greater in intensity than that of the associated species in methanol (Fig. 3.4). To explain this the solvents donicity [45] must be considered. The donor number for acetonitrile (~14) is less than methanol (~19) both of which are less than water (~33). Low donor numbers will typically afford a greater inner sphere coordination of the counter ion [45]. Thus the extent of complexation may be attributed to not only the dielectric constant but also to the relative donor strength of the solvent. Thus these species may be present at the surface of the droplet and not just restricted to the bulk of the droplet. The stabilizing effect is quite dramatic as the  $3^+$  ion cluster distribution persists even with  $n$  as low as 4 in the spectrum and can even be seen with  $n$  as low as 2.

### 3.4 Conclusion

It is clear that the exact character of the electrospray mass spectra of the lanthanides is quite complex. The species observed and their relative intensities are highly dependant on the physical and chemical properties of the lanthanide metal, the solvent, declustering conditions and instrumental design characteristics. These particular spectra were

acquired on the existing system and may vary from system to system however the underlying physical principles should remain intact. While it is difficult to achieve conditions that yield clean singly charged metal ion spectra (ie. spectra containing only  $\text{Ln}^+$  ions), it is possible to determine the lanthanides as charge reduced cluster species, to establish the original solution oxidation state of the lanthanide based on the nature of the observed charge reduced species and to determine the anions present in solution by observation of complex ions. As well, the general nature of the spectra can be explained based on straight forward properties of the lanthanides and the solvent. Overall, ES-MS is an information rich technique for the determination of these metal ions.

### 3.5 References

1. M. Yamashita and J.B. Fenn, *J. Phys. Chem.*, **88**, 4451 (1984).
2. M. Yamashita and J.B. Fenn, *J. Phys. Chem.*, **88**, 4671 (1984).
3. R. D., Smith, J. A., Loo, C. G., Edmonds, C. J. Barinaga, and H. R. Udseth, *Anal. Chem.*, **62**, 882 (1990).
4. M. Mann *Org. Mass Spectrom.*, **25**, 575 (1990).
5. V. Katta, S.K. Chowdhury and B.T. Chait, *J. Am. Chem. Soc.*, **112**, 5348 (1990).
6. X. Xu, S.P. Nolan and R.B. Cole, *Anal. Chem.*, **66**, 66 119 (1994).
7. C.L. Gatlin, F. Turecek and T. Vaisar, *Anal. Chem.*, **66**, 712 (1994).
8. R. Arakawa, T. Matsuo, H. Ito, I. Katakuse, K. Nozaki, T. Ohno and M. Haga, *Org. Mass Spectrom.*, **29**, 289 (1994).
9. J.M. Curtis, P.J. Derrick, A. Schnell, E. Constantin, R.T. Gallagher, and J.R. Chapman, *Inorg. Chim. Acta*, **21**, 197 (1992).
10. J.M. Curtis, P.J. Derrick, A. Schnell, E. Constantin, R.T. Gallagher, and J.R. Chapman, *Inorg. Chim. Acta*, **217**, 1176 (1992).
11. R. Colton, and J.C. Traeger, *Inorg. Chim. Acta*, **201**, 153 (1992).
12. R. Colton, B.D. James, I.D. Potter, and J.C. Traeger, *Inorg. Chem.*, **32**, 2626 (1993).
13. R. Colton, V. Tedesco, and J.C. Traeger, *Inorg. Chem.*, **31**, 3865 (1992).
14. A.M. Bond, R. Colton, J.C. Traeger, and J. Harvey, *Inorg. Chim. Acta*, **212**, 233 (1993).



15. R. Colton, D. Dakternieks, *Inorg. Chim. Acta*, **208**, 173 (1993).
16. R. Colton, W. Klaui, *Inorg. Chim. Acta*, **211**, 235 (1993).
17. A.J., Canty, P.R. Traill, R. Colton, and I.M. Thomas, *Inorg. Chim. Acta*, **210**, 91 (1993).
18. A.J., Canty, R. Colton, *Inorg. Chim. Acta*, **215**, 179 (1993).
19. A.T. Blades, P. Jayaweera, M.G. Ikonomou and P. Kebarle, *Int. J. Mass Spectrom. Ion Processes*, **101**, 325 (1990).
20. A.T. Blades, P. Jayaweera, M.G. Ikonomou and P. Kebarle, *Int. J. Mass Spectrom. Ion Processes*, **102**, 251 (1990).
21. Z.L. Cheng, K.M.W. Siu, R. Guevremont and S.S. Berman, *Org. Mass Spectrom.*, **27**, 1370 (1992).
22. Z.L. Cheng, K.M.W. Siu, R. Guevremont and S.S. Berman, *J. Am. Soc. Mass Spectrom.*, **3**, 281 (1992).
23. J.J. Corr and D.J. Douglas, "Elemental Ion Spray-Mass Spectrometry: Analysis of Solutions of Metal Salts", in *Abstracts and Index of Authors of the 41 st ASMS conference of Mass Spectrometry and Applied topics*, San Francisco, p.202 (1993).
24. G.R. Agnes and G. Horlick, *Appl. Spectrosc.*, **46**, 401 (1992).
25. G.R. Agnes and G. Horlick, *Appl. Spectrosc.*, **48**, 649 (1994).
26. G.R. Agnes and G. Horlick, *Appl. Spectrosc.*, **48**, 655 (1994).
27. P. Juhasz, M.G. Ikonomou, A.T. Blades and P. Kebarle, "Methods and Mechanisms for Producing Ions from Large Molecules", Edited by K.G. Standing and W. Ens, Plenum Press, New York (1991).
28. A.T. Blades, P. Jayaweera, M.G. Ikonomou and P. Kebarle, *J. Chem. Phys.*, **92**, 5900 (1990).
29. A.T. Blades, P. Jayaweera, M.G. Ikonomou and P. Kebarle, *J. Am. Chem. Soc.*, **112**, 2452 (1990).

30. P. Moller, P. Dulski, and J. Luck, *Spectrochimica Acta*, **47B**, 1379 (1992).
31. I. Roelandts, *Spectrochimica Acta*, **46B**, 79 (1991).
32. W. Doherty, *Spectrochimica Acta*, **44B**, 263 (1989).
33. L. Tang and P. Kebarle, *Anal. Chem.*, **65**, 3654 (1993).
34. P. Kebarle and L. Tang, *Anal. Chem.*, **65**, 972A (1993).
35. D.C. Taflin, T.L. Ward and E.J. Davis, *Langmuir*, **5**, 376 (1989).
36. A. Gomez and K. Tang, *Phys. Fluids*, **6**, 404 (1994).
37. J.V. Iribarne and B.A. Thomson, *J. Chem. Phys.*, **64**, 2287 (1976).
38. M.A. Vaughan and G. Horlick, *Appl. Spectrosc.*, **44**, 587 (1990).
39. C. Cossy, L. Helm, D.H. Powell and A.E. Merbach, *New J. Chem.*, **19**, 27 (1995).
40. F.A. Cotton and G. Wilkinson, "*Advanced Inorganic Chemistry. A Comprehensive Text*" Fifth Edition, Interscience, New York N.Y., p.1134 (1988).
41. M. Azzaro, S. Breton, M. Decouzon, and S. Geribaldi, *Int. J. Mass Spectrom. Ion Processes*, **128**, 1 (1993).
42. L.S. Smith, D.C. McCain, and D.L. Wertz, *J. Am. Chem. Soc.*, **98**, 5125 (1976).
43. M.L. Steele, and D.L. Wertz, *Inorg. Chem.*, **16**, 1225 (1977).
44. K.A. Gschneider, and L. Eyring, "*Handbook on the Physics and Chemistry of the Rare Earths*", Elsevier Science, New York N.Y., Vol. 8, Chapter 56, (1986).
45. V. Gutmann, *Electrochimica Acta*, **21**, 661 (1976).

## **Chapter 4**

### **Chromium Speciation**

## 4.1 Introduction

From a toxicological standpoint, it is well known that different species of the same element will follow different metabolic pathways. Thus the toxicity of an element can and will depend on its speciation in a sample. Speciation as a term is one yet to be wholly defined, however in the literature it is commonly referred to as the specific form (monatomic or molecular) or configuration in which an element can occur. The element chromium is one of many elements that fall into this category where its toxicity is species dependent. In solution chromium primarily exists in either the Cr(III) or Cr(VI) oxidation states. For the most part chromium (III) is non toxic and even considered to be an essential nutrient for most mammals. Chromium (VI) on the other hand is a powerful oxidizing agent and is considered to be quite toxic. There are of course multiple species possible for each oxidation state which are usually dependent on such factors as matrix, concentration and pH.

The determination of chromium has been performed by numerous flame and plasma spectroscopic techniques with detection limits ranging from the parts per billion (ppb) to the sub parts per billion levels [1]. The most sensitive technique to date is however inductively coupled plasma mass spectrometry (ICP-MS), with detection limits on the most recent commercial instruments being reported in the 0.001-0.1 ppb range [2-4]. Inductively coupled plasma atomic emission spectrometry (ICP-AES) will typically have higher detection limits however recent reports on the 'end-on' or axially viewed plasma by Ivařdi and Tyson [5] report detection limits as low

as 0.068ppb using ultrasonic nebulization. The only drawback to these techniques is that when they are used 'alone' they provide only the total chromium content and speciation information is lost. Therefore when speciation is critical other methods must be incorporated.

One solution to this problem is through the incorporation of chromatographic methods. A variety of separation techniques have been coupled to the ICP such as high performance liquid chromatography (HPLC) [6], ion chromatography (IC) [7], and capillary electrophoresis (CE) [8] for example. It should be pointed out that the list of coupling ICP with chromatographic techniques and others is quite extensive and dates back to the 1970's. Mention should also be made of coupled flame atomic absorption (FAA) measurements by *Sperling et al* [9] who report ppb to sub ppb detection limits for both Cr (III) and Cr (VI) species. The goal of these techniques is obviously not to provide complete separation and subsequent determination, as differentiation is only required between same element species. Therefore rapid separation times may be achieved at the cost of chromatographic resolution. However in order to properly realize the high sensitivity that techniques such as ICP-MS or ICP-AES are capable of, the interface must be designed to provide a means to yield complete nebulization/atomization with a high transport efficiency into the plasma. For the most part these techniques provide rapid determinations on the ppb level for Cr (III) and Cr (VI) species.

The speciation in the above cases tends simply to differentiate between the two oxidation states with potentially ambiguous information provided on the actual chemical species present. It would therefore be advantageous to determine specifically the species present

in solutions. Recently the use of electrospray mass spectrometry (ESMS) for elemental and speciation work has been investigated by *Agnes et al* [10-14] as well a brief review on the subject on the electrospray of inorganic solutions has been given by Stewart and Horlick [15]. In terms of speciation the technique shows great promise as solution information tends to be preserved rather than destroyed during analysis. Evidence has however been presented where in special cases species may undergo electrochemical reactions at the solution capillary interface, thus creating new ions [16]. By nature, electrospray is a relatively simple ion source that does not typically create ions but merely takes pre-existing ions in solution and transfers them to the gas phase. This fact is critical as information on a particular target ~~analyte~~ such as oxidation state and molecular form will be preserved. Investigations of ~~chromium solution~~ species in both the Cr (III) and Cr (VI) states will be provided with some fundamental discussion of the processes that are involved in the generation and sampling of these ions.

## 4.2 Background

The electrostatic spraying of liquids is by no means a new phenomena, researchers have been studying it since the turn of the century [17]. It was not however until Yamashita and Fenn [18,19] reported the results of coupling electrospray to mass spectrometry in the 1980's that its potential as an analytical tool was realized. Since then the field has literally exploded, with the majority of the focus being applied to biological studies. Its use as a probe for inorganic solution species has

not however taken off as fast and this is probably because so many excellent and proven techniques already exist for elemental determination.

Electrospray has been described extensively in the literature [20-27] and so only a qualitative description will be given here. Simply put, electrospray is an electrostatic spraying process, where a liquid surface becomes disrupted when an intense electric field is applied resulting in a spray of charged droplets. In electrospray a solution of some minimum conductivity (typically a methanolic electrolyte solution on the order of  $10^{-5}\text{M}$  -  $10^{-3}\text{M}$ ) is pumped ( $\sim 1$ - $10\mu\text{L}/\text{min.}$ ) through a stainless steel capillary ( $\sim 100\mu\text{m}$  i.d.) which is held at some high potential relative to a counter electrode (the mass spectrometer sampling orifice). The capillary to counter electrode separation is usually between 0.5-3.0 cm and the potential difference in this region is usually  $\sim 2$ - $4\text{kV}$ . This spraying phenomena at the capillary tip affords the transfer of solution ions to the gas phase where they may be sampled by a mass spectrometer. A negatively biased capillary results in negatively charged droplets and ultimately negative gas phase ions, the opposite is true for a positively biased capillary. The formation of the spray, the charging of the droplets and formation of gas phase ions from such droplets are described in some detail in the literature. In particular a review article by Kebarle and Tang [28] summarizes most of the current thought on the processes involved in ESMS.

### 4.3 Experimental

The electrospray source and mass spectrometer have been previously described [10] (as well chapter 2 of this thesis). The high pressure sampling region of the modified Sciex/Perkin-Elmer ELAN Model 250 ICP-MS mass spectrometer, is based on a sampling plate/skimmer configuration. There have, however, been some modifications inside the mass spectrometer; the shadow or first photon stop in the ion optics as well as the second stop located in the Bessel box have been removed. This has led to an increase in sensitivity of one to one and a half orders of magnitude. As both cations and anions are being studied the mass spectrometer was operated in both positive and negative ion modes. In the negative ion mode the ES tip was typically biased at -3000V, the front plate at -600V, the sampling plate was varied to minimize or maximize collisionally induced dissociation (CID) in the high pressure region (typically between -2 and -60V) and the skimmer was held at -2V. For positive ion mode the potentials were similar but of opposite polarity and as well the sampling plate voltage was typically run at higher potentials. As the skimmer potential is held constant, the potential drop and hence energy is proportional to the sampling plate voltage (see ref. 29 for discussion). The curtain gas used for these experiments was nitrogen at a flow rate of about 1.3 L/min. The ES needle tip had a 100 $\mu$ m i.d. and was operated at a flow rate of 1.0-2.0 $\mu$ L/min via a syringe pump (Harvard Apparatus 22). The tip position although optimized for each set of experiments was usually set 5 mm from the front plate and 0-1 mm off axis. It was found that careful selection of flow rate (usually a low



flow rate) and applied capillary potential, led to stable signals without the use of discharge suppressing gasses for negative ion mode.

Measurements of pH were taken by a Fisher Accumet Mini pH Meter Model 955. The probe (Corning general purpose combination) was standardized through pH 4, pH 7 or pH 10 buffer solutions depending on the range studied.

UV-visible absorption measurements were acquired on a Hewlett-Packard 84542A Diode Array Spectrometer. The cell had a 1.0 cm path length. Absorption spectra were acquired with 1 second integration times over the wavelength range of 190-820nm.

All solutions were prepared by dissolving the ACS grade salts in distilled deionized water to form a stock solution except where specified. Aliquots of the stock solution were then diluted with HPLC-grade methanol or HPLC-grade Acetonitrile to the desired concentration. These procedures result in the solution being primarily methanol or acetonitrile with water content in the range of 0.5-2.0% by volume depending on the sample.

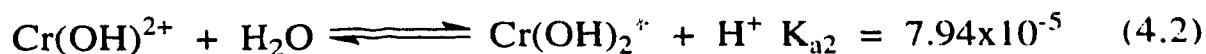
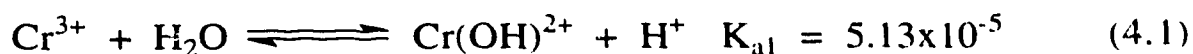
## **4.4 Results and Discussion**

### **4.4.1 Cr (III)**

The chemistry of chromium (III) is quite extensive, as it may exist in a wide number of complexes all of which with little exception are hexacoordinate. The chemistry of Cr(III) as a metal salt dissolved in aqueous solutions is not as simple or uninteresting as one might initially anticipate. The aqua ion is quite acidic and will readily

hydrolyse in solution. This in itself is not unique as many other transition metals such as iron and vanadium hydrolyse in aqueous solutions. Chromium is unique however in its kinetic inertness, where ligand exchange in the inner coordination sphere is quite slow and can have half lives in the range of several hours [30]. These attributes lead to some quite complex solution chemistry.

When chromium is dissolved in aqueous solution it readily hydrolyses to an extent which is determined by its pK<sub>a</sub> values [31]:



Under certain conditions (of concentration, pH, and temperature) the hydrolysis products can polymerize to yield dimers, trimers, tetramers, etc. For example one scheme for forming the dimer is given below by equation (4.3);



The above reaction has a reported rate constant of about  $k_{11} = 2.0 \times 10^{-4} \text{ M}^{-1}\text{s}^{-1}$  [32] under experimental conditions. The above dimer also has an approximate stability constant of [32];

$$\beta = \frac{[\text{Cr}_2(\text{OH})_2^{+4}][\text{H}^+]^2}{[\text{Cr}^{+3}]^2} = 10^{-5.26} \text{ M} \quad (4.4)$$

These systems have been studied quite extensively by Marty *et al.* [31-34] as well Rai *et al.* [35] have studied aqueous chromium chemistry. There is still some debate as to what extent polynuclear chromium species are present, especially in systems of low total chromium content. In most natural water samples or samples collected under neutral to acidic pH's chromium would probably only be present in dilute concentrations and so would exist primarily as the aqua ( $\text{Cr}(\text{H}_2\text{O})_6^{3+}$ ) or hydroxo species ( $\text{Cr}(\text{OH})(\text{H}_2\text{O})_5^{2+}$ ). For the most part the normal working concentrations for electrospray are between  $10^{-3}\text{M}$  and  $10^{-5}\text{M}$ .

#### 4.4.2 Cr (III) Solutions

The electrospray mass spectra of chromium III solutions may vary in complexity. Electrospray when operated in the stable cone-jet mode will ultimately produce gas phase ions independent of the sampling process. It is the sampling interface that allows some flexibility in obtaining either simplified or complex mass spectra. The use of a sampling plate skimmer configuration similar to that of most early commercial ICP-MS's to sample the atmospheric pressure gas phase ions allows for this. The use of this configuration allows for efficient high pressure collisionally induced dissociation (CID) which has been discussed with respect to the electrospray of metal ions [11,29] and so only a cursory discussion will be given here. Simply put, the sampling plate allows both ions and curtain gas to be entrained into the expansion, a potential drop between the sampling plate and skimmer accelerates the ions relative to the neutral curtain gas ( $\text{N}_2$ ). This

ultimately produces energetic collisions, the energy of which is proportional to the potential drop between the sampling plate and skimmer. Thus a large potential difference affords complete stripping of a solvated metal ion down to its bare form, whereas a small potential drop results in minimal stripping and therefore preserves solution information.

A mass spectrum of a chromium solution is given in Fig. 4.1. Here a relatively mature solution of chromium chloride (aged ~5 months) was diluted with methanol (~6ppm) and run under conditions that resulted in very efficient CID (i.e. large potential difference between sampling plate and skimmer) by electrospray mass spectrometry. Similar to an ICP mass spectrum, Fig. 4.1 consists of a 'bare' or atomic chromium isotope packet signal centered at  $m/z$  52 with an associated oxide peak at  $m/z$  68. The  $MO^+/M^+$  ratio in this case is ~2%. This ratio is sampling condition dependent, and may be made lesser or greater depending on the magnitude of the potential drop or severity of the CID conditions.

Casual inspection of Fig. 4.1, may give the impression that similarly to an ICP mass spectrum very little solution information may be obtained other than the fact that chromium is present. If one however considers the fact that electrospray run in a positive ion mode will 'liberate' only positive solution ions, then one can assume that this mass spectrum is due to a positive solution ion chromium species. Further, in natural waters under neutral to mildly acidic conditions this would imply a Cr(III) ion as Cr(VI) species exists predominantly in anionic form. In either case this may be confirmed by changing the

sampling conditions to gentler ones in order to preserve the solution form.

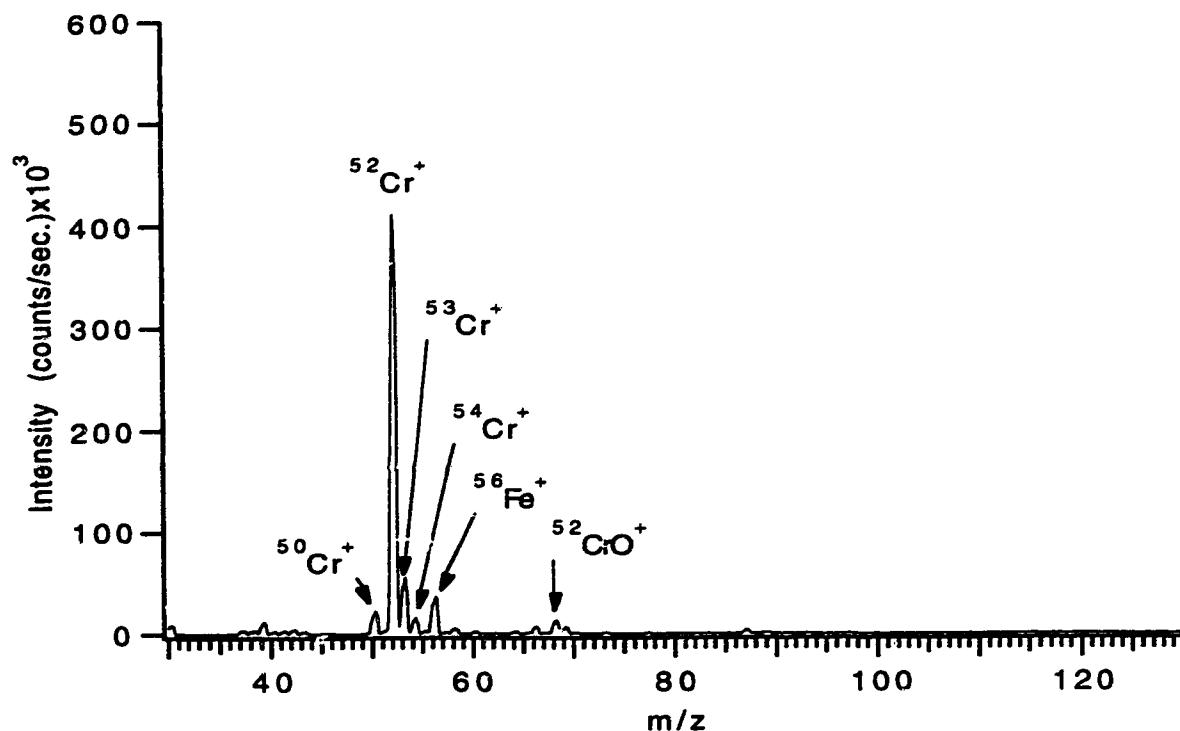
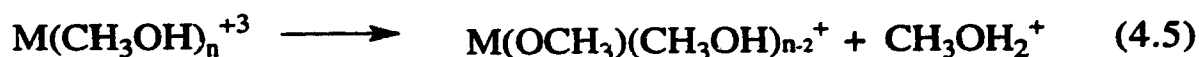


**Figure 4.1**  $\text{CrCl}_3 \cdot 6\text{H}_2\text{O}$ :  $1.0 \times 10^{-4}\text{M}$  (~6.6ppm) in methanol/1% $\text{H}_2\text{O}$  Flow rate:  $2.00\mu\text{L}/\text{min.}$ ,  $\Delta V = 145\text{V}$ .

The pH of the  $1.0 \times 10^{-2}\text{M}$   $\text{CrCl}_3$  stock solution was measured and found to be 3.02. This is indicative of solution phase hydrolysis as would be predicted by the  $K_{a1}$  value given in equation (4.1) above. Indeed calculation using the above constant for a  $1.0 \times 10^{-2}\text{M}$  stock solution yields  $[\text{Cr}^{3+}] = 9.31 \times 10^{-3}\text{M}$ ,  $[\text{Cr}(\text{OH})^{2+}] = 6.91 \times 10^{-4}\text{M}$  and  $\text{pH} = 3.16$  units. One would therefore predict that the above stock solution consists primarily of  $\text{Cr}^{3+}$  ion with some  $\text{Cr}(\text{OH})^{2+}$  ion. Dilution 100X in methanol will have an unknown effect, in that we are diluting it in a solvent of lower dielectric and solvating properties. It might be fair to say that methanol being a protic solvent should have at

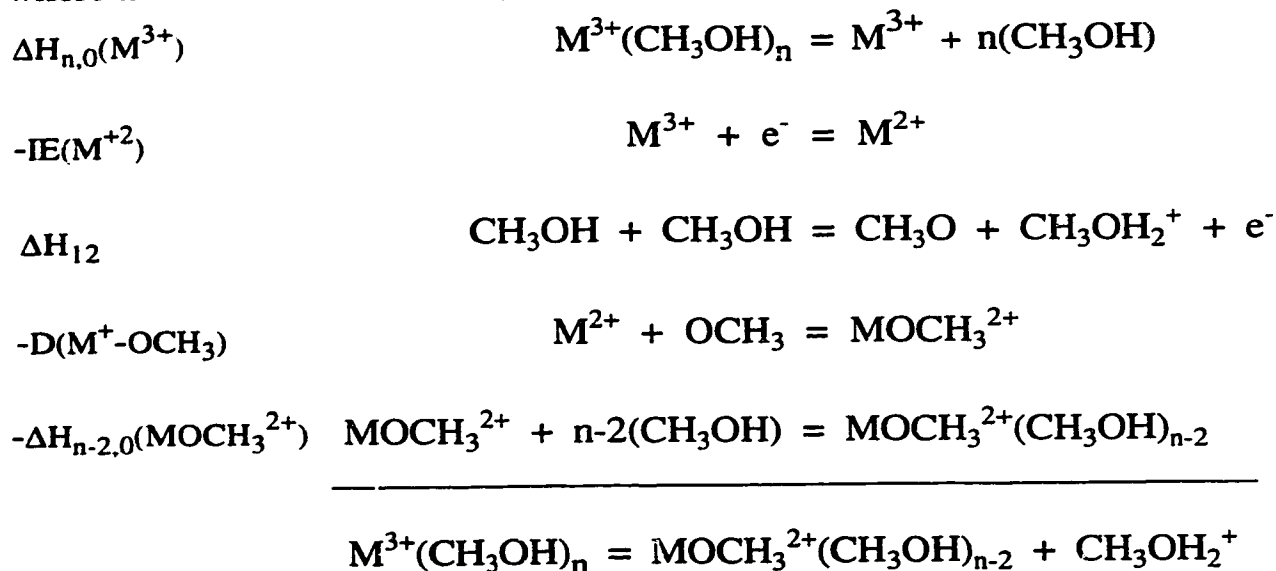
least similar solvating properties as that of water and that the major difference might lie in a potential for increased complexation with counter ion. This however should be small for dilute solutions of electrolytes. Solvolysis should still occur, however the associated constants for these events are unknown. It will be assumed that for this case methanol just acts to dilute the sample.

A second consideration that should be discussed is that of gas phase solvolysis or charge reduction. This topic has been discussed in the literature especially with regards to metal ions [29, 36]. A bare 3+ metal ion, which is unsolvated in the gas phase will be quite unstable. These ions typically are much more stable when solvated by a medium in which it may delocalize a portion of this charge. Consider the case where such a metal center is 'liberated' from a droplet with an accompanying solvation sphere of some size or number, if these solvent ligands are gradually stripped off there will come a point where the solvation sphere no longer provides the stability of the bulk solution and so the metal ion becomes less stable. Eventually there will come a point where the solvent is stripped down to a minimum number such that the metal centered complex is no longer stable and thus a 'charge reduction' reaction occurs which is represented in equation (4.5) below;



In effect what happens is that, in an attempt to better delocalize its charge, the metal center forms a more localized covalent bond with one of the immediate inner sphere ligands. This effectively reduces the net

charge but not the oxidation state associated with the metal center. The above reaction may be described thermodynamically as shown below where methanol is the solvent;



Scheme 4.1

Although in many cases all the above values are not known, a rough rule of thumb is that when the ionization potential (IE) of the metal ion is greater than the ionization potential of the ligand (related to  $\Delta H_{12}$  here), charge reduction becomes increasingly favored as solvation is lost and this is typically aided or hindered by the ligands ability to form a covalent bond (i.e., M-OCH<sub>3</sub> or M-OH) with the metal center. When large differences between ionization potentials are experienced large solvent or ligand numbers will typically be required to stabilize the charge center. The ionization potential for chromium and various ligands is given in Table 4.1. The third ionization potential of chromium is about three times in excess of the ionization potential for methanol, this coupled with the fact that chromium readily forms Cr-O bonds indicates that charge reduction will be favored unless excessive

solvation is present. The ability of methanol to stabilize a  $\text{Cr}(\text{OCH}_3)_n^{3+}$  species is however likely for some minimum ligand number. Therefore, under gentle sampling conditions, species like  $\text{Cr}(\text{CH}_3\text{OH})_n^{3+}$  are unlikely (even though they may exist in solution) whereas solvated species like  $\text{Cr}(\text{OCH}_3)(\text{CH}_3\text{OH})_n^{2+}$  would be expected exclusively. The above example has assumed that the only species present in solution is the  $3^+$  ion where the solvent consists solely of methanol. Where water is present  $\text{Cr}(\text{OH})_2^{2+}$  species of mixed ligand spheres will also exist, this will be observed below.

**Table 4.1 Ionization Potentials of Selected Species.**

	Ionization Potential (eV) <sup>a.)</sup>					
	I	II	III	IV	V	VI
chromium	6.76	16.49	30.95	50	73	91
methanol	10.84					
water	12.6					
acetonitrile	12.2					

a.) *CRC Handbook of Chemistry and Physics*, 1993 edition.

Figure 4.2 shows a CID profile for chromium perchlorate solutions diluted in methanol. The three spectra Fig 4.2a-c were acquired under different conditions ranging from a fairly gentle (Fig. 4.2a) to a fairly harsh set of conditions (Fig. 4.2c). Under the gentle conditions of Fig 2a ( $\Delta V = 20\text{V}$ ) it is observed that the dominant ion is the  $\text{CrOH}^{2+}$  ion with a mixed water methanol solvation sphere, ranging



in total ligand number from 5-7. This spectrum indicates the oxidation state of chromium as it exists in solution i.e., Cr (III). The species distributions are typically separated by 9 m/z units indicative of a  $2^+$  ion separated in mass by 18 units or 1  $\text{H}_2\text{O}$  ligand. This  $\text{CrOH}^{2+}$  ion is the predicted ion that we should observe based on the above discussion. It has been assumed that the ion is the  $\text{CrOH}^{2+}$  ion and not the  $\text{Cr}(\text{OCH}_3)^{2+}$  ion, which may or may not be entirely true and will be addressed in a later section. Regardless of the which ligand has formed the covalent bond, gentle conditions indicate that the ion observed is chromium in the (III) formal oxidation state and the overall charge of the species is  $2^+$ , consistent with predictions. Figs. 4.2b and 4.2c are the resultant mass spectra acquired with increased potential differences. They illustrate the typical steps which the chromium  $2^+$  species of Fig. 4.2a goes through as it gets stripped down to a bare  $\text{Cr}^+$  ion as observed in Fig. 4.1. The proposed steps based on the the various species recorded by the mass spectrometer are summarized in the schemes below where Schemes 4.2 and 4.3 are for hypothetical systems consisting of pure methanol and water solvation spheres respectively. The schemes illustrate the type of sequences that are observed and the processes in Scheme 4.2 have been discussed in some detail previously [29]. These schemes are representative of pure systems and a variety of CID products are possible when mixed solvent spheres are present initially. The final step proposed in Scheme 4.2 is observed under CID conditions that are less intense as compared to the final step in Scheme 4.3. In either case the Schemes show possible mechanisms to explain how the original Cr (III) gas phase ion becomes 'stripped' down to the

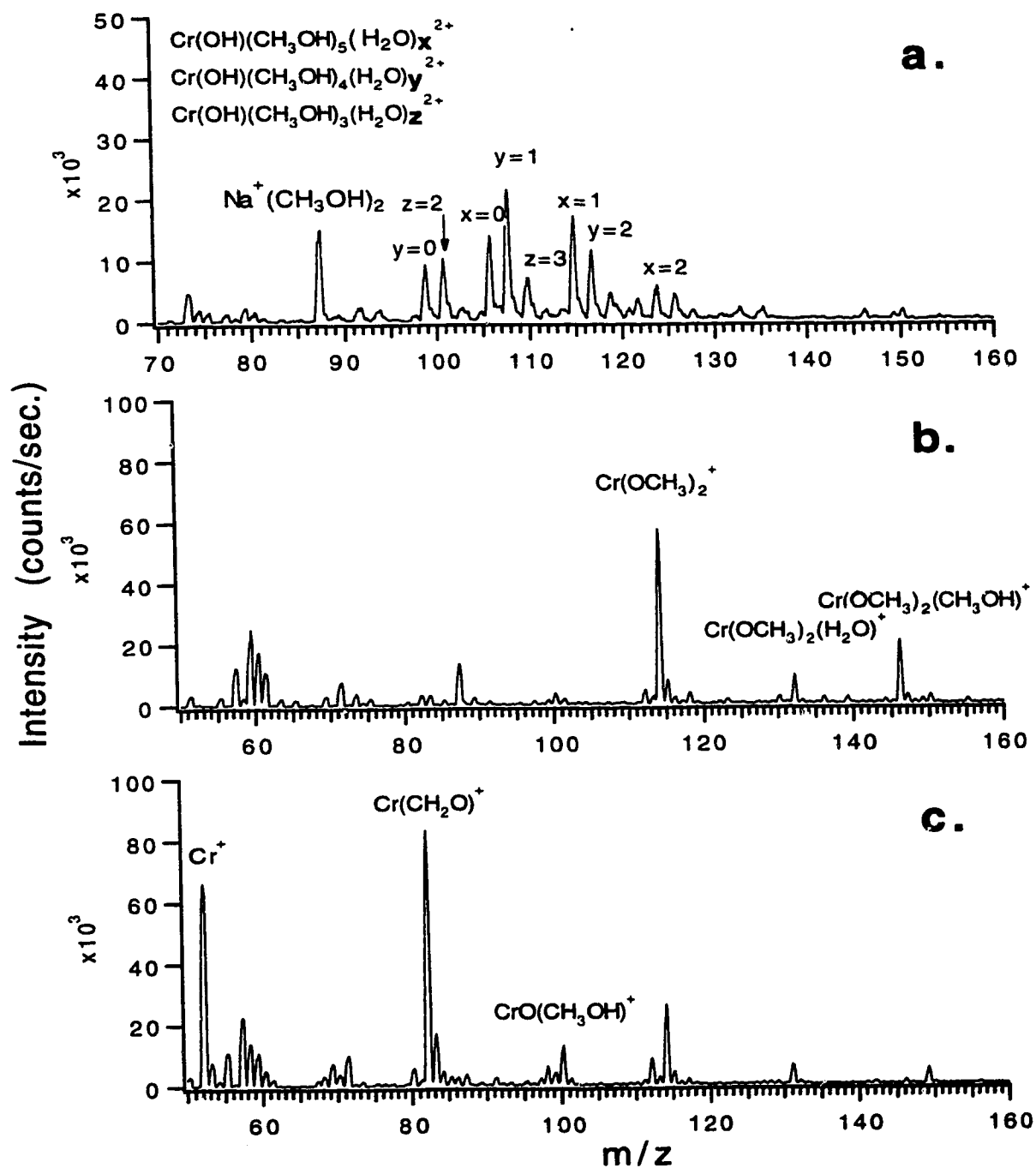
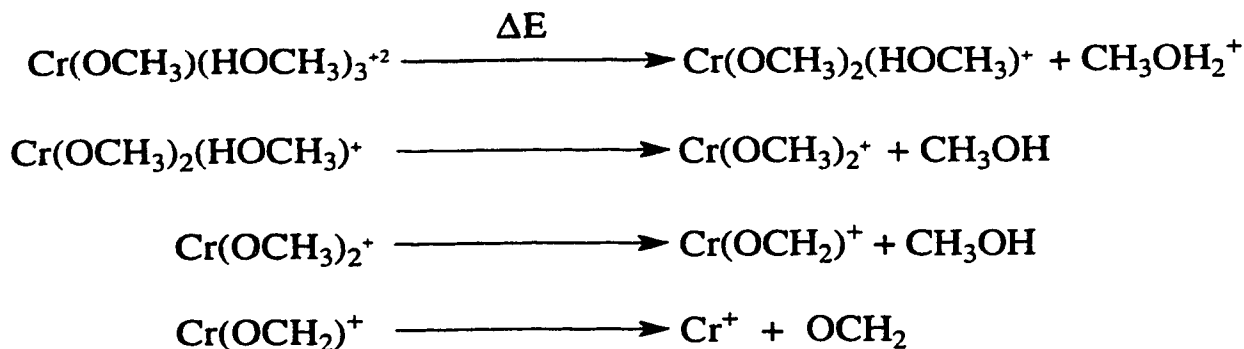
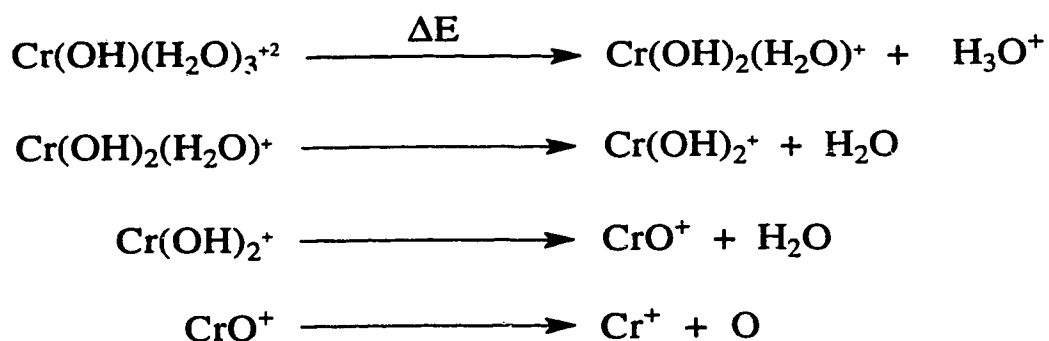


**Figure 4.2**  $\text{Cr}(\text{ClO}_4)_3 \cdot 6\text{H}_2\text{O}$ :  $1.0 \times 10^{-4}\text{M}$  in methanol/1%  $\text{H}_2\text{O}$ . Flow rate:  $2.00 \mu\text{L}/\text{min}$ . a.)  $\Delta V = 20\text{V}$ , b.)  $\Delta V = 35\text{V}$ , c.)  $\Delta V = 55\text{V}$ .

Cr (I) species observed in the mass spectrum.



Scheme 4.2



Scheme 4.3

When the same chromium perchlorate solution is diluted in acetonitrile similar species are observed. A CID profile is given in Fig. 4.3. Fig. 4.3a is acquired under relatively gentle conditions ( $\Delta V = 20\text{V}$ ) and the expected  $\text{CrOH}^{2+}$  ion is observed. In this case the stabilizing ligand will be  $\text{H}_2\text{O}$  rather than  $\text{CH}_3\text{CN}$ , this may be expected as both ligands have similar ionization potentials however acetonitrile cannot form a stabilizing covalent bond similar to the M-O bond that water can and therefore acts to hinder the charge reduction process or 'protect' the charge. It should be noted that under the gentle conditions of Fig. 4.3a (and gentler) the  $\text{CrOH}^{2+}$  ion was observed with mixed solvation spheres of water and acetonitrile, however in all cases there were only two distributions observed; one containing 3 acetonitrile ligands

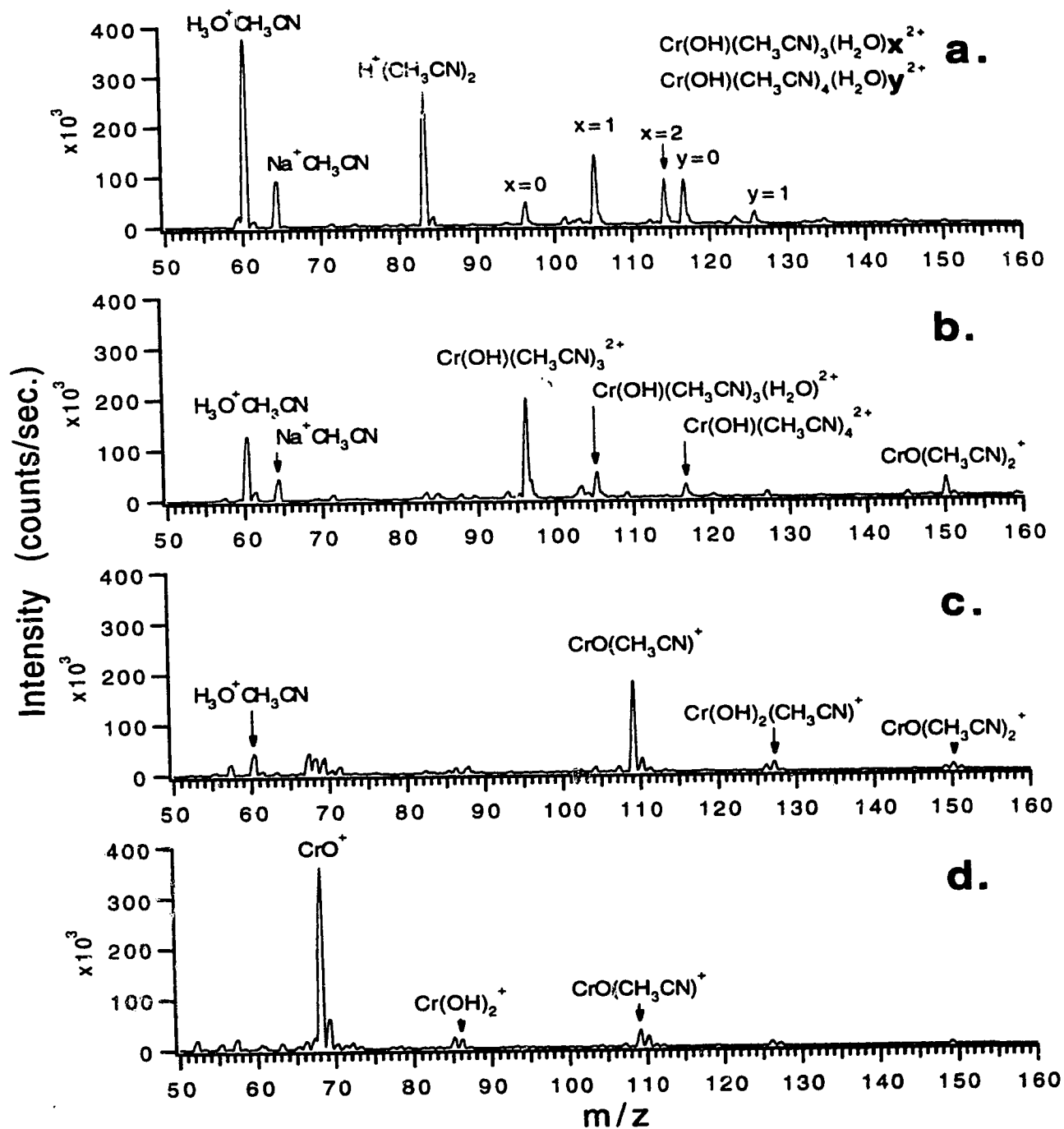
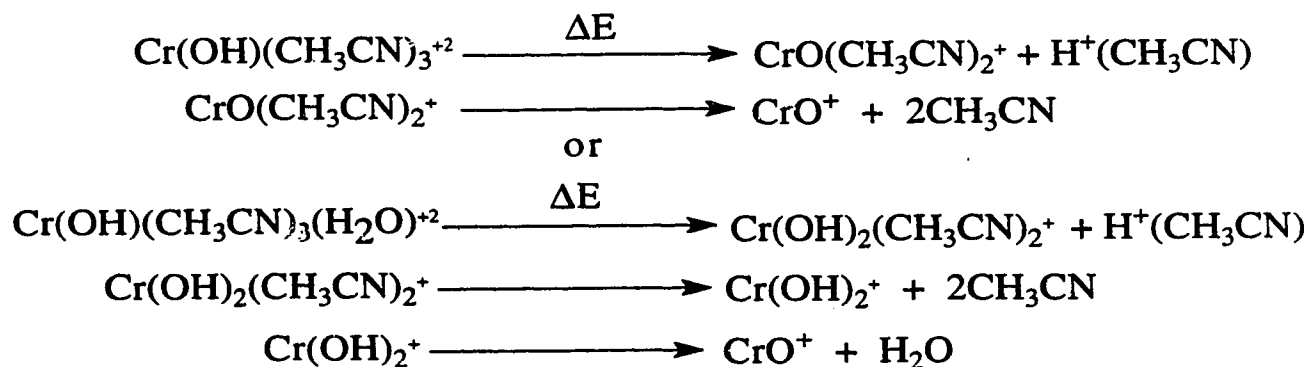


**Figure 4.3**  $\text{Cr(ClO}_4)_3 \cdot 6\text{H}_2\text{O}$ :  $1.0 \times 10^{-4}\text{M}$  in Acetonitrile/1% $\text{H}_2\text{O}$ . Flow rate:  $2.00 \mu\text{L/min}$ . **a.)**  $\Delta V = 20\text{V}$ , **b.)**  $\Delta V = 30\text{V}$ , **c.)**  $\Delta V = 45\text{V}$ , **d.)**  $\Delta V = 65\text{V}$ .

(Cr(OH)(CH<sub>3</sub>CN)<sub>3</sub>(H<sub>2</sub>O)<sub>x</sub><sup>2+</sup>) and one containing 4 acetonitrile ligands (Cr(OH)(CH<sub>3</sub>CN)<sub>4</sub>(H<sub>2</sub>O)<sub>y</sub><sup>2+</sup>) with accompanying water. Under conditions gentler than that of Fig. 4.3a these two distributions were observed but with correspondingly more water ligands. This observation was consistent and made on several different occasions. In addition during CID stripping it was the extraneous water ligands that were lost in preference to one of the 3 or 4 acetonitrile ligands. Both of the 2<sup>+</sup> solvated chromium species (Cr(OH)(CH<sub>3</sub>CN)<sub>3</sub>(H<sub>2</sub>O)<sub>x</sub><sup>2+</sup>, Cr(OH)(CH<sub>3</sub>CN)<sub>4</sub>(H<sub>2</sub>O)<sub>y</sub><sup>2+</sup>) are typically stripped down to a Cr(OH)(CH<sub>3</sub>CN)<sub>3</sub><sup>2+</sup> species before further charge stabilization reactions occur (Fig. 4.3b) however there is some minor contribution by hydrated species (Cr(OH)(CH<sub>3</sub>CN)<sub>3</sub>(H<sub>2</sub>O)<sub>2</sub><sup>2+</sup>). The CID processes of chromium in acetonitrile as shown in Fig. 4.3 are illustrated in Scheme 4.4 below where the first part represents the major process and the second represents the minor process:



Scheme 4.4

Chromium (III) acetonitrile solutions typically produce "cleaner" spectra than the corresponding methanol solutions. Complexation of Cr (III) with a large organic chelating agent may serve to clean up the spectra even further.

From the above discussion it has been demonstrated that chromium (III) may be observed where its oxidation state may be verified conclusively as well its solution form may be inferred.

#### 4.4.3 Polymeric Species

A series of solutions were prepared in an attempt to investigate polymeric chromium species, under certain conditions where such species are thought to exist. Four stock solutions of  $1.0 \times 10^{-2} \text{M}$   $\text{Cr}(\text{ClO}_4)_3 \cdot 6\text{H}_2\text{O}$  were prepared where to the first no base was added, to the second  $1.0 \times 10^{-4} \text{M}$  NaOH was added, to the third  $1.0 \times 10^{-3} \text{M}$  NaOH was added and to the fourth  $1.0 \times 10^{-2} \text{M}$  NaOH was added. The solutions were then allowed to age for 10 months at room temperature, at which time their pH's and UV-visible absorption spectra were acquired. All four solutions were acidic, with the solution with no base and  $1.0 \times 10^{-4} \text{M}$  base having pH's both of 2.79 and the  $1.0 \times 10^{-3} \text{M}$  base and  $1.0 \times 10^{-2} \text{M}$  base having pH's of 2.89 and 3.23 respectively. The colours of the solutions ranged from violet blue to a green colour with increasing pH. According to Stunzi and Marty [31] the ratio of the extinction coefficients of the two d-d band maxima at  $\sim 420 \text{ nm}$  and  $\sim 580 \text{ nm}$  provide an easy identification and check on the purity of the oligomers. The ratio of the band maxima  $\epsilon_{\text{max}}(\text{ca. } 420 \text{ nm})/\epsilon_{\text{max}}(\text{ca. } 580 \text{ nm})$  for the different species are: monomer = 1.17, dimer = 1.18, trimer = 1.60 and tetramer = 1.95 (easy distinction between monomer and dimer seems dubious). The spectral data collected in Table 4.2 provide evidence for species other than the monomer being present, especially for the solution with

$1.0 \times 10^{-2} \text{M}$  base added. These solutions were then diluted with both acetonitrile and methanol and then electrosprayed. ESMS analysis did not yield any conclusive evidence that would support the presence of polymeric species in these solutions (there were however some unexplained peaks which may or may not be due to the presence of polymeric species). The stability constant of the dimer ( $5.5 \times 10^{-6} \text{M}$ ) given in eqn. (4.4) is highly dependant on the conditions in which it was measured. Under the dilute conditions of these experiments it is difficult to predict the total concentration of the dimer present. In the literature however, polymeric species have been reported under the dilute conditions associated with natural waters [37]. With this in mind these experiments were carried out as it was not known quantitatively how much dimer (or other oligomer) was present initially, nor at what rate the reverse reaction occurred in the electrospray solvents; methanol or acetonitrile. No direct evidence was found to support the presence of polymeric species at the concentrations examined.

**Table 4.2 Absorption Data.**

$10^{-2} \text{M Cr}(\text{ClO}_4)_3$ with:	$\epsilon_{\text{max}} (\text{M}^{-1} \text{cm}^{-1})$ $\lambda$ (~420nm)	$\epsilon_{\text{max}} (\text{M}^{-1} \text{cm}^{-1})$ $\lambda$ (~580nm)	Ratio pH (final)	
1. no base	14.30	11.83	1.21	2.79
2. $1.0 \times 10^{-4} \text{M NaOH}$	15.05	12.44	1.21	2.79
3. $1.0 \times 10^{-3} \text{M NaOH}$	15.46	12.64	1.22	2.89
4. $1.0 \times 10^{-2} \text{M NaOH}$	21.60	15.99	1.35	3.23

#### 4.4.4 Kinetic Inertness of Cr(III)

It is known that one of the unique characteristics of chromium (III) is its relative kinetic inertness towards exchange. As a result of this many different Cr (III) complexes can be isolated and studied. This will have direct consequences on the resultant electrospray mass spectra of such solutions. When stock solutions of chromium (III) (which are not strictly controlled by low pH's) are examined it is fair to say that the investigation is of the solution at that particular time, as some time later whether it is a couple of hours or months the solution composition will change. This can act to complicate a determination, because for chromium (III) it may take several hours or days before a state of semi-equilibrium is reached or perhaps a full equilibrium is never established. To illustrate this case a relatively mature stock solution of  $\text{CrCl}_3 \cdot 6\text{H}_2\text{O}$  was diluted in methanol and then run immediately by electrospray, the spectra were acquired under identical conditions as a function of time and are given in Fig. 4.4. In the first spectrum (Fig. 4.4a) acquired about 5 minutes after dilution the spectrum consists for the most part of fully water solvated species ( $\text{Cr}(\text{OH})_2(\text{H}_2\text{O})_x^+$ ) as well there are some mixed ligand species present. For simplicity only the  $1^+$  region of the mass spectrum is being shown. However under these conditions  $2^+$  species are also present (i.e.  $\text{Cr}(\text{OH})(\text{H}_2\text{O})_x^{2+}$ ) at correspondingly lower  $m/z$ . Examination of Figs. 4.4b and 4.4c at 30 minutes and 90 minutes after dilution respectively show marked contrasts where the later contains species that are indicative of almost exclusive solvation by methanol, and the former contains species that are intermediate between water



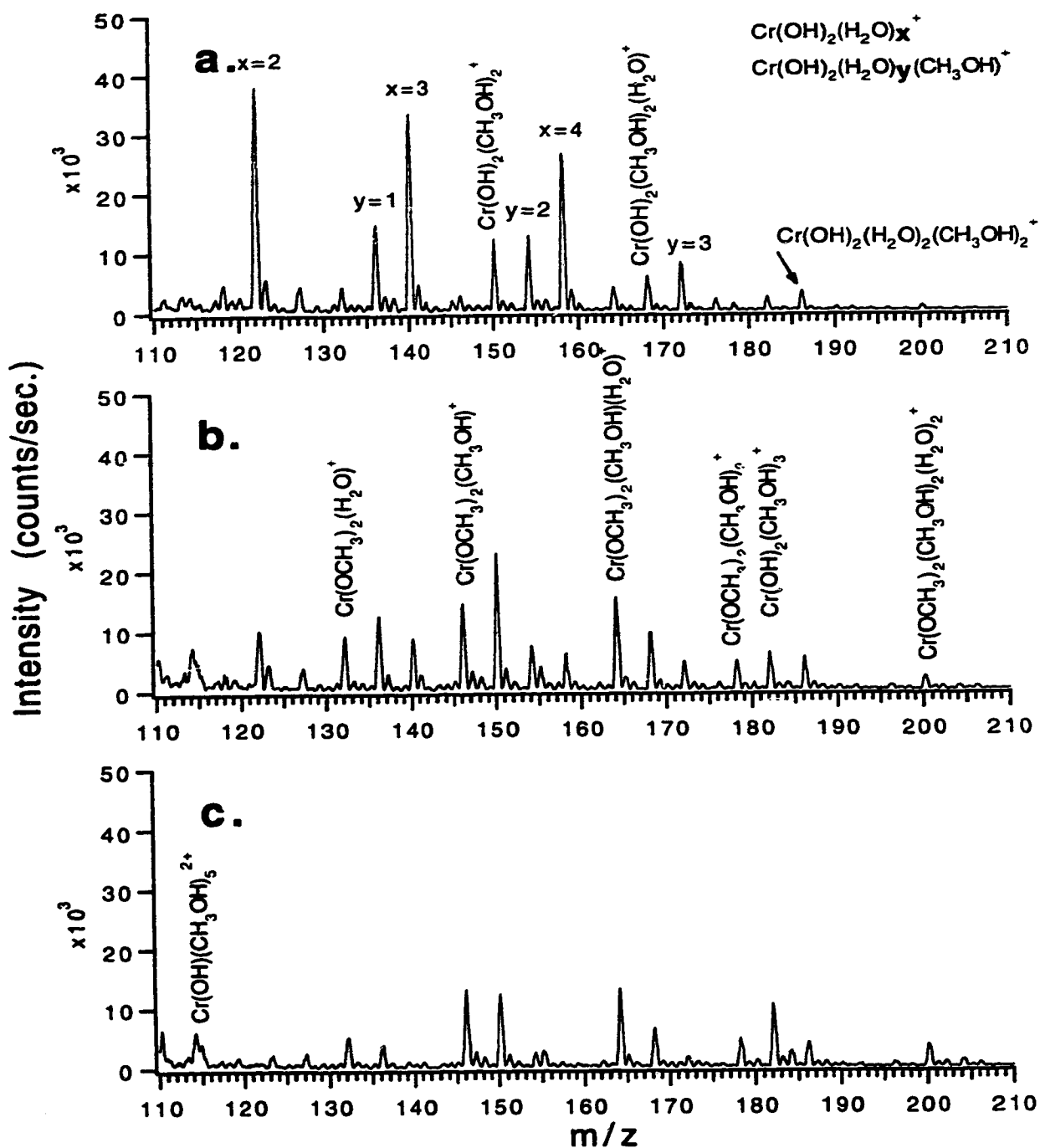


**Figure 4.4**  $\text{CrCl}_3 \cdot 6\text{H}_2\text{O}$ :  $1.0 \times 10^{-4}\text{M}$  in methanol/1%  $\text{H}_2\text{O}$ .  $\Delta V = 25\text{V}$ . A  $1.0 \times 10^{-2}\text{M}$  stock solution was prepared and allowed to age for 5 months in water, the solution was then diluted and spectra were acquired a.) after 5 min., b.) after 30 min., and c.) after 90 min.

rich and water poor species. Upon reexamination of Fig. 4.2 at this point it should become clear why Fig. 4.2b contains almost exclusively methanolic species such as  $\text{Cr}(\text{OCH}_3)_2^+$  as opposed to hydrolytic species  $\text{Cr}(\text{OH})_2^+$ . The series of spectra in Fig. 4.2 were of course collected in chronological order where Fig. 4.2a was acquired about 20 minutes after dilution and Fig. 4.2b was acquired about 50 minutes after dilution.

The above solution (Fig. 4.4) was a chromium chloride solution prepared in water, and allowed to mature for 5 months, when it was diluted with methanol the dominant ion observed was a solvated  $2^+$  species or  $1^+$  species depending on the sampling conditions. A fresh stock solution of the same  $\text{CrCl}_3 \cdot 6\text{H}_2\text{O}$  salt was then prepared in methanol and allowed to stand for 12 hours, at which time it was diluted to  $10^{-4}\text{M}$  with methanol and observed by electrospray as given in Fig. 4.5. The spectrum was acquired under moderately harsh CID conditions ( $\Delta V = 40\text{V}$ ). There is a marked contrast between the two experiments. The data presented in Fig. 4.5 is a relatively simple spectrum which consists almost exclusively of the mono and di-chloride species;  $\text{Cr}(\text{OCH}_3)\text{Cl}(\text{CH}_3\text{OH})_n^+$  and  $\text{CrCl}_2(\text{CH}_3\text{OH})_n^+$ , with some contribution by the uncomplexed  $\text{Cr}(\text{OCH}_3)_2(\text{CH}_3\text{OH})_n^+$  species where  $n$  is some arbitrary ligand number. The bar graphs in Fig. 4.6 illustrate the relative isotopic contribution of the two chloro complexes observed in Fig. 4.5. From the above two examples it should be apparent that when methanol is used as an electrospray solvent for Cr (III) species the kinetic inertness of the metal centre is maintained. In addition methanol also seems to yield increased complexation with counter ion.

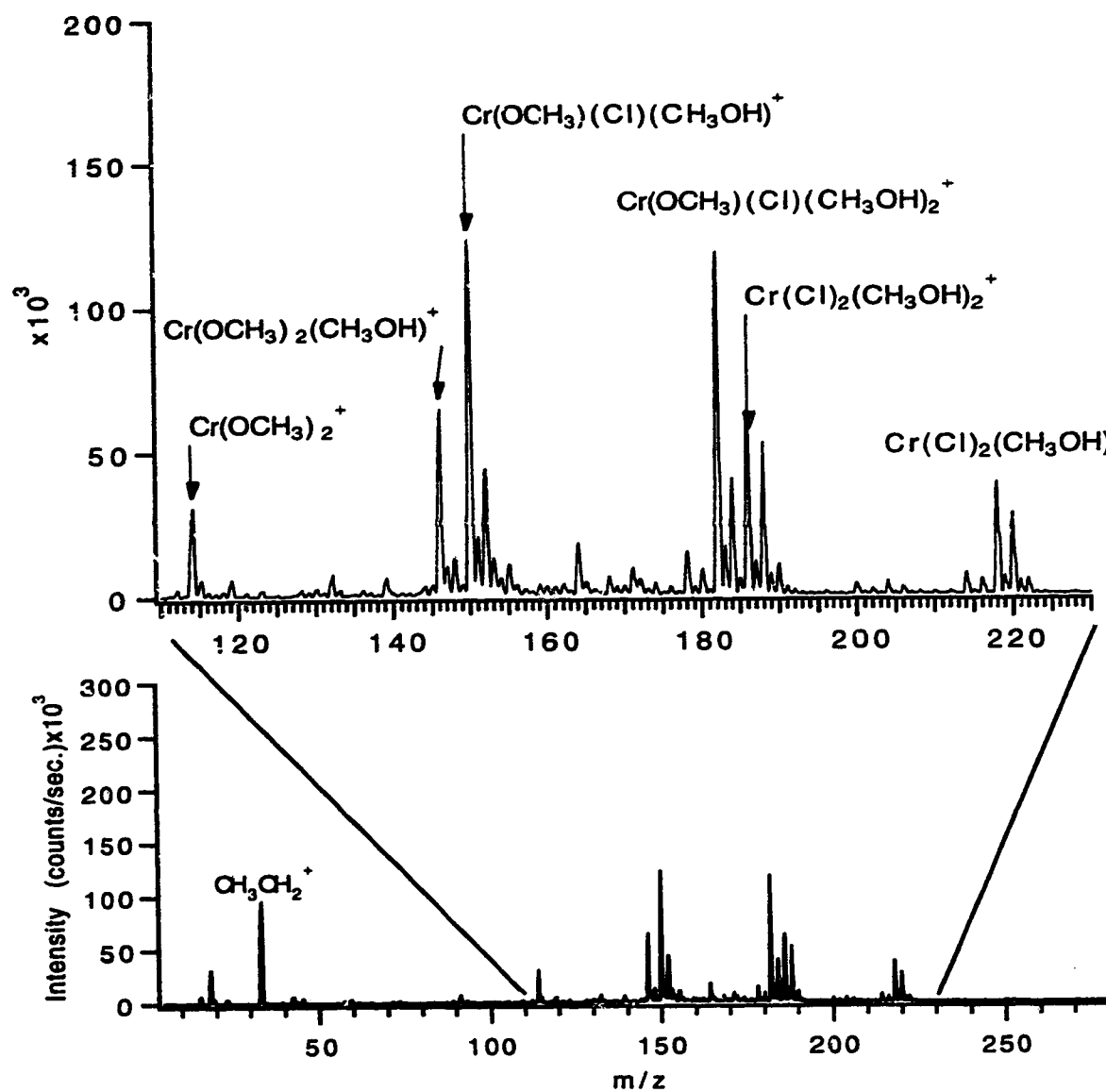


**Figure 4.5**  $\text{CrCl}_3 \cdot 6\text{H}_2\text{O}$ :  $1.0 \times 10^{-4}\text{M}$  in methanol.  $\Delta V = 40\text{V}$ . A  $1.0 \times 10^{-2}\text{M}$  stock solution was prepared in methanol and then let stand 12 hours before it was diluted to the final concentration with methanol and run.

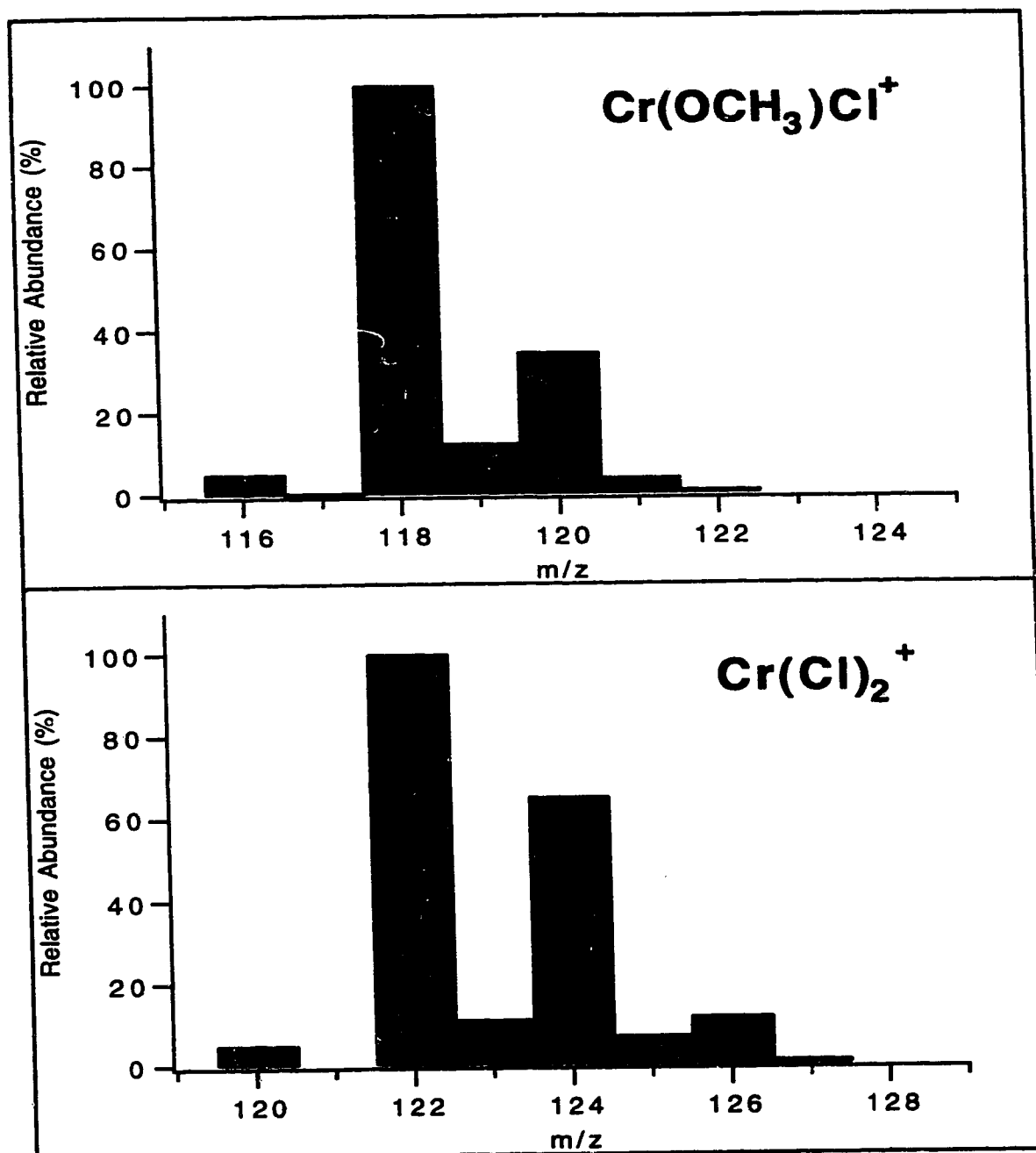


**Figure 4.6** Relative isotopic distribution of a.)  $\text{CrCl}(\text{OCH}_3)^+$  and b.)  $\text{CrCl}_2^+$ .

When the same chronological experiments were conducted with acetonitrile as the solvent the results were not as dramatic. Figure 4.7 contains two mass spectra acquired 8 minutes (Fig. 4.7a) and 90 minutes (Fig. 4.7b) after the dilution of a mature  $\text{Cr}(\text{ClO}_4)_3 \cdot 6\text{H}_2\text{O}$  stock solution. For the most part there are no major differences and the mass spectra consist in both cases of the two distributions  $\text{Cr}(\text{OH})(\text{CH}_3\text{CN})_3(\text{H}_2\text{O})_x^{2+}$  and  $\text{Cr}(\text{OH})(\text{CH}_3\text{CN})_4(\text{H}_2\text{O})_y^{2+}$  as discussed previously. The only real difference is that the species seem to have shifted to lower water content i.e. the change in intensity of the  $x=0$  and  $x=2$  species. Investigations of this phenomenon using absorption spectrophotometry indicated that the spectra acquired immediately upon dilution of the same stock solution with acetonitrile and one hour later showed no extreme changes. The 2 d-d absorption maxima remained constant at  $\lambda = 414\text{nm}$  and  $\lambda = 578\text{nm}$  as well there was only a ~5% increase in the molar absorptivities over this time. This minimal change is consistent with that of the ESMS experiments where little change was observed over the given time period, however these results should be viewed with caution as lower concentrations of the chromium perchlorate solutions were used.

From the above discussion it was shown that Cr(III) solutions could be investigated by electrospray mass spectrometry. Where both the oxidation state and the indirect solution form (owing to gas phase stabilization reactions) of the ion could be determined by selecting the appropriate conditions. The characteristic chemistry of Cr (III) in aqueous solutions was also discussed especially with regards to the

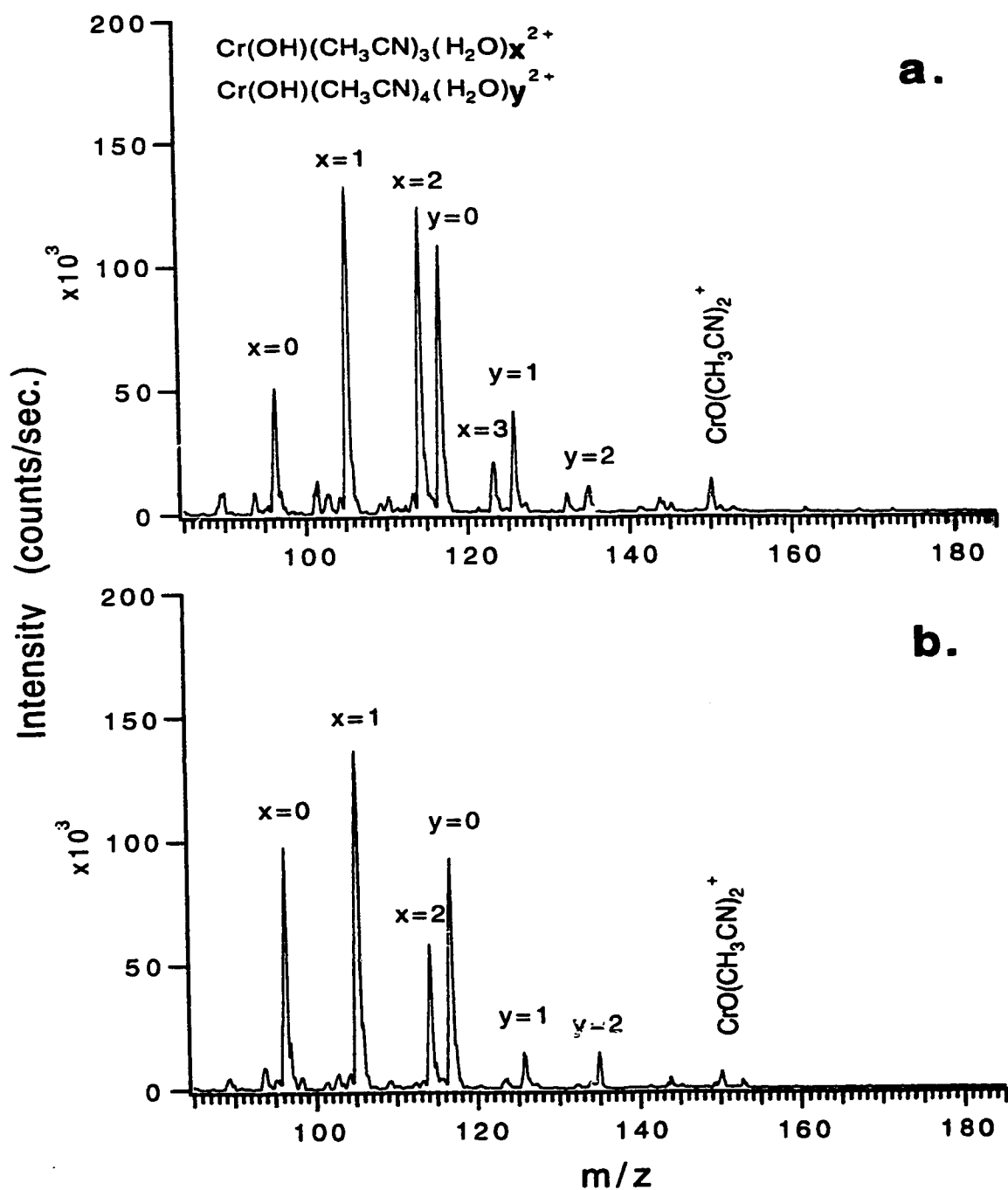
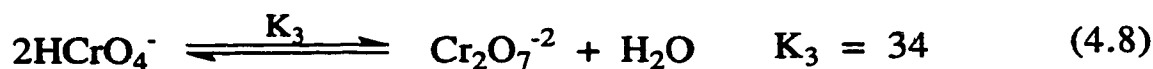
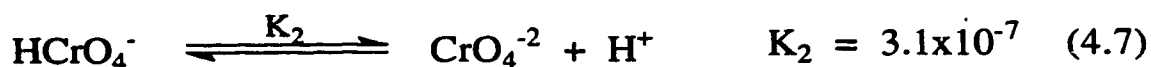
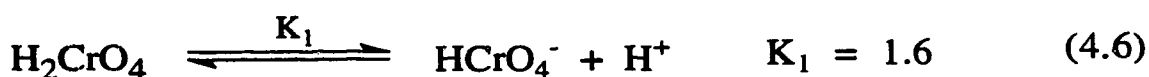


**Figure 4.7** Cr(ClO<sub>4</sub>)<sub>3</sub>·6H<sub>2</sub>O: 1.0×10<sup>-4</sup>M in acetonitrile/1%H<sub>2</sub>O. Flow rate: 2.00μL/min., ΔV = 25V. A 1.0×10<sup>-2</sup>M stock solution was diluted and spectra were acquired a.) after 8 min., and b.) after 90 min.

electrospray process. It was found that specific characteristics of the metal center such as its kinetic inertness could be observed directly which is important to consider as it will have direct consequences on the solution composition at any given time. The use of electrospray to probe the solution chemistry of chromium is a unique and informative method which allows direct and indirect information to be gained on a variety of chromium complexes with minimal sample volumes.

#### 4.4.5 Cr(VI)

The chemical form of Cr (VI) in aqueous solutions is highly dependant on its concentration and the solution pH. Recently Tandon *et al.* [38] presented data on the effects of pH and concentration on Cr (VI) species in solution that were later corrected by Shen-Yang and Ke-An [39]. From the various equilibrium constants listed below;



which are reported for conditions of 0 ionic strength [39], the pH and concentration dependance is obvious. Figure 4.8 presents a graphical interpretation of the above constants between the pH ranges of 2 and 12 for  $1.0 \times 10^{-2}\text{M}$  and  $1.0 \times 10^{-4}\text{M}$  total chromium concentrations. It should

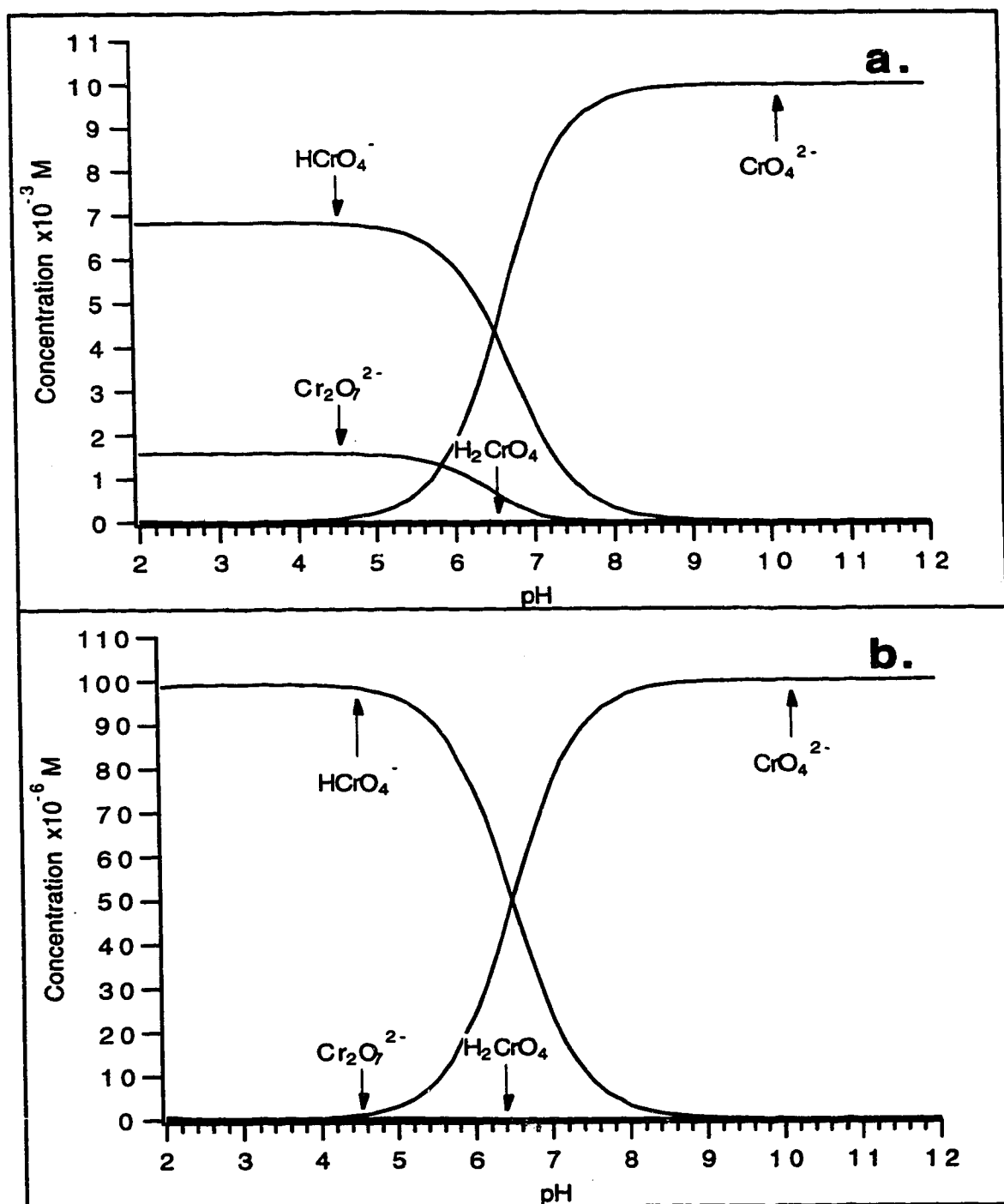


**Figure 4.8** Effect of pH on the species distribution of Cr(VI) in aqueous solutions for the total concentration of a.)  $1.0 \times 10^{-2}$  M and b.)  $1.0 \times 10^{-4}$  M.



be noted that the effect of total ionic strength on the equilibrium constants is known to be rather large and therefore these representations should be viewed with caution.

In terms of the equilibrium distribution of Cr(VI) species in solution, it does seem that the above equilibria (equations (4.6)-(4.8)) are fairly well accepted, however they have been criticised in that there has never been direct evidence to support all of the postulated species in aqueous solution. Michel *et al* [40,41] however have done extensive studies on these systems using Raman spectroscopy, a technique which should allow for the direct determination of such species if they existed. In particular they focussed on the existence of the  $\text{HCrO}_4^-$  ion in aqueous solutions, and they were able to conclude that, "the presence of the entity  $\text{HCrO}_4^-$  in acidic Cr(VI) solutions was very doubtful". They then went on to determine their own equilibrium constants with this knowledge in mind. Therefore it would seem that the solution chemistry of the Cr(VI) is still somewhat undefined, and is still open for debate.

#### 4.4.6 Cr(VI) Solutions

With this limited knowledge the solution chemistry of Cr(VI) solutions was studied by ESMS. It will be assumed that for the sake of comparison the above equilibria (equations (4.6)-(4.8)) are valid. One of the first experiments undertaken was to examine a mixture of  $\text{Na}_2\text{Cr}_2\text{O}_7$  and  $\text{HNO}_3$  (each  $1.0 \times 10^{-4}\text{M}$ ) in methanol. The result, given in Fig. 4.8, is not surprising and it emphasizes a very important point that must be taken under consideration when using electrospray.

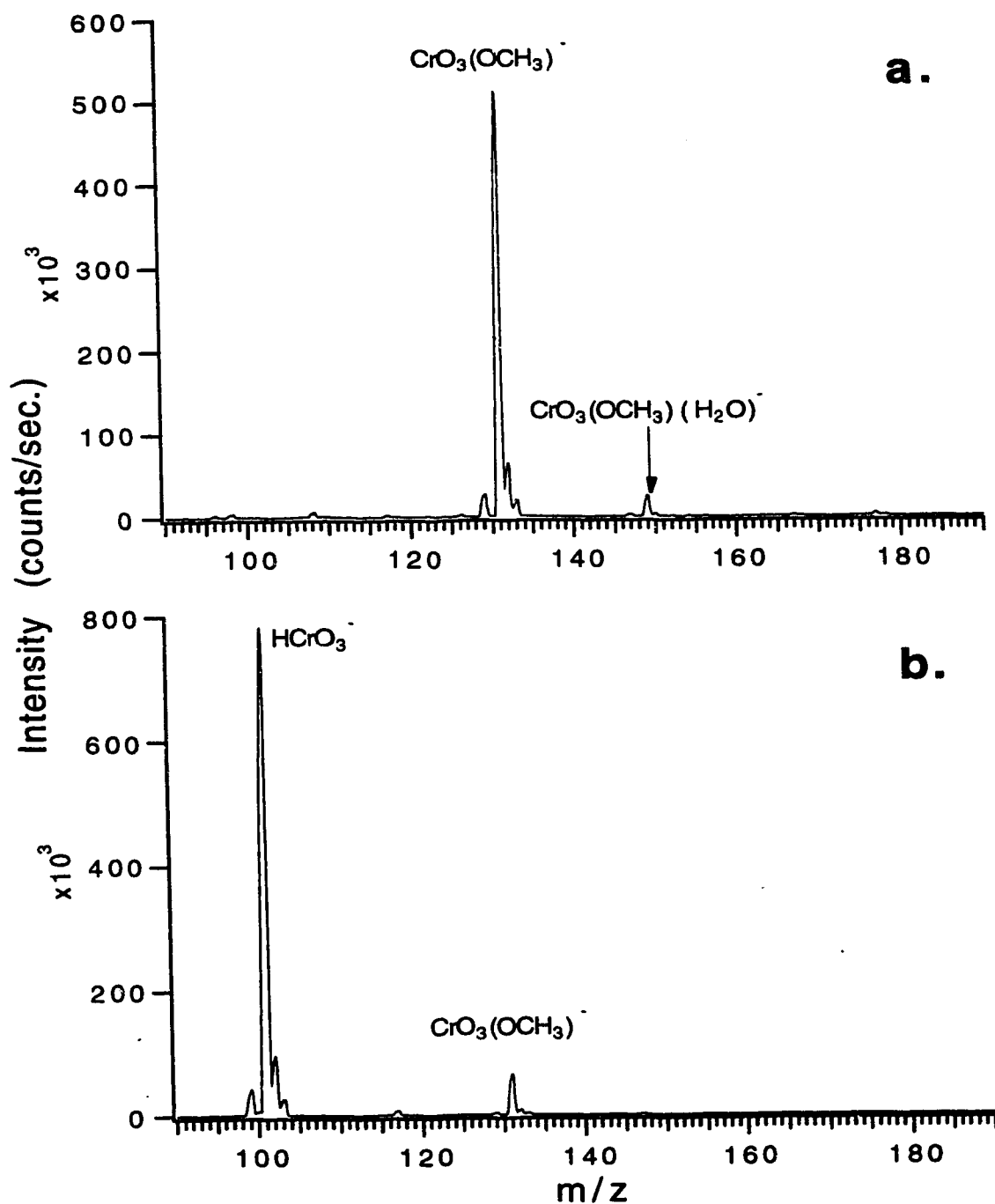
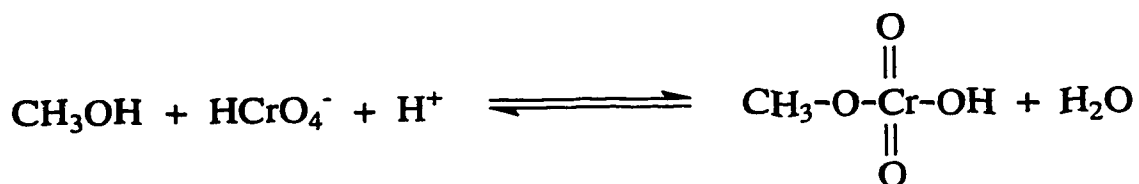


**Figure 4.9** CID profile of  $\text{Na}_2\text{Cr}_2\text{O}_7$  and  $\text{HNO}_3$  each  $1.0 \times 10^{-4} \text{M}$  in methanol/1%  $\text{H}_2\text{O}$ . **a.**)  $\Delta V = 25 \text{V}$ , **b.**)  $\Delta V = 40 \text{V}$ .

In this case as would be expected Cr(VI) will react with methanol, in fact Cr(VI) is used rather routinely in organic synthesis to oxidize alcohols to aldehydes or ketones. Fig. 4.9a shows the chromate ester which is an intermediate step in the oxidation of the alcohol to in this case an aldehyde and is represented in Scheme 4.5 below;



Scheme 4.5

When the potential difference in the sampling region is increased to 40V (Fig. 4.9b) the chromate ester decomposes to the  $\text{CrO}_3^-$  species probably via the loss of  $\text{CH}_2\text{O}$ . Although this presents a potential problem it also opens up new avenues to explore the solution reactions of Cr(VI) especially with regards to oxidation products and intermediates. This however is not the focus of this paper.

In order to better study these systems a more suitable electrospray solvent must be used. Acetonitrile was selected and it was found to be suitable for the most part however it too suffers some limitations as will be discussed later. The same stock solution of  $1.0 \times 10^{-2}$  M  $\text{Na}_2\text{Cr}_2\text{O}_7$  and  $\text{HNO}_3$  was diluted 100X in acetonitrile and was examined by electrospray and the results are presented in Fig. 4.10. Fig. 4.10 is a CID profile where Fig. 4.10a was acquired at  $\Delta V=25\text{V}$ , Fig. 4.10b, and Fig. 4.10c are acquired at  $\Delta V=55\text{V}$  and  $\Delta V=75\text{V}$  respectively. The spectrum in Fig. 4.10a is a solvent stripped spectrum, where conditions were such that all the solvent ligands were stripped from the molecular ions with minimal

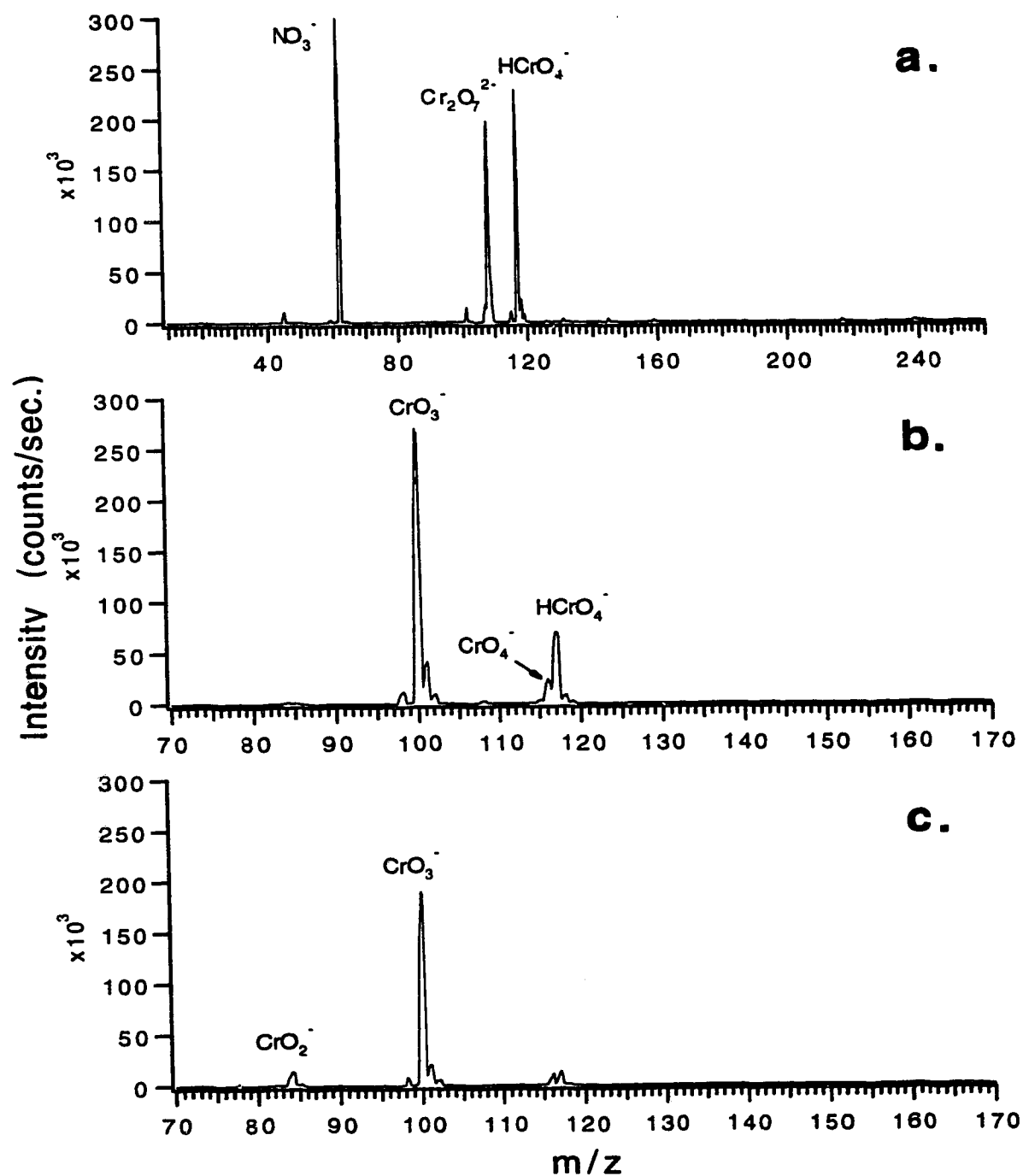
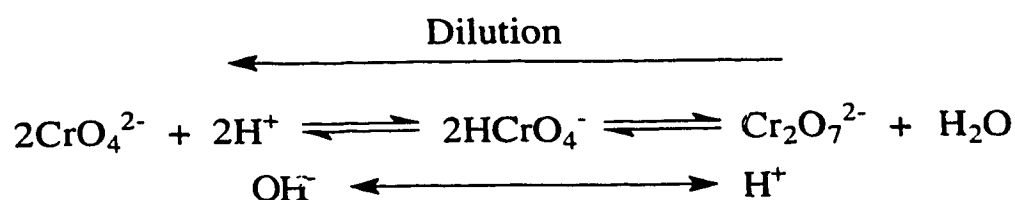


**Figure 4.10** CID profile of  $\text{Na}_2\text{Cr}_2\text{O}_7$  and  $\text{HNO}_3$  each  $1.0 \times 10^{-4} \text{M}$  in acetonitrile/1%  $\text{H}_2\text{O}$ . a.)  $\Delta V = 25 \text{V}$ , b.)  $\Delta V = 55 \text{V}$ , c.)  $\Delta V = 75 \text{V}$ .

decomposition. In this spectrum we see the characteristic ions;  $\text{NO}_3^-$ ,  $\text{Cr}_2\text{O}_7^{2-}$ , and  $\text{HCrO}_4^-$  which are more or less indicative of the ions present in the stock solution. At this point it is necessary to consider some fundamental aspects of the process to better understand or interpret results. In particular those pertaining to equilibrium discrepancies.

In the above experiment the stock solution had a total Cr(VI) content of  $2 \times 10^{-4}\text{M}$ , and a pH of 2.15. Based on the equilibrium constants given in equations (4.6)-(4.8), the relative ratio of  $[\text{Cr}_2\text{O}_7^{2-}]/[\text{HCrO}_4^-]$  is  $\sim 0.77$ . For a similar solution of only  $1 \times 10^{-4}\text{M}$  total Cr(VI) this ratio is  $\sim 0.24$ . Now if these stock solutions are diluted 100X in aqueous media with the decrease in concentration would also come an increase in pH. The net result would be a shift to an almost complete solution content of the  $\text{HCrO}_4^-$  species under mildly acidic conditions. This shift in equilibrium species is not observed when the stock solution is diluted in acetonitrile as shown in Fig. 4.10a. In fact the actual distribution is more representative of the stock solution, which might be expected. The comparison to dilution in acetonitrile, an aprotic solvent, is not wholly appropriate. There is only  $\sim 1\%$  water after dilution and so the equilibria as described by equations (4.6)-(4.8) will not strictly apply. The second consideration is the proposed droplet preconcentration that occurs as a result of solvent evaporation during a droplets lifetime [28]. Consider a charged droplet of some radius  $R$ , the free charge will occupy a surface layer of some thickness, and the interior of the droplet will consist primarily of bulk solution ions. Now if the droplet starts evaporating both the surface area and the droplet volume will decrease, where the former

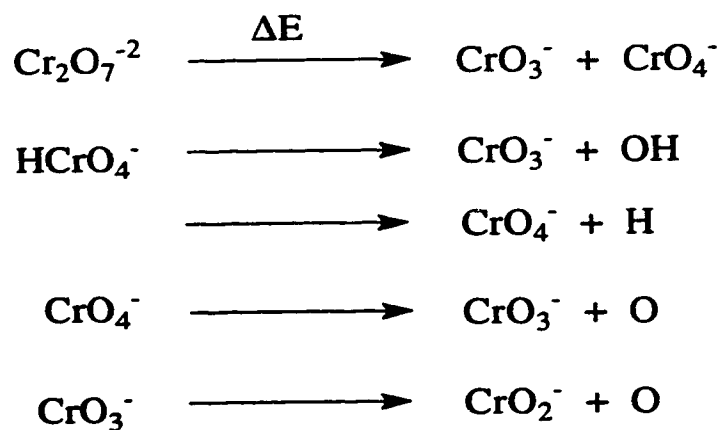
contributes to a higher surface charge density and the later contributes to an increase in bulk concentration. The rate of droplet evaporation determines the rate at which the surface charge density increases and ultimately to what point the droplet is stable before a fission event occurs. While this is occurring the bulk concentration is simultaneously increasing, and so the solution composition of the bulk inside the droplet will begin to differ from that of the original solution. As a rough guide consider the following scheme;



Scheme 4.5

Thus any increase in concentration will favour an increase in  $\text{Cr}_2\text{O}_7^{2-}$ . In acidic conditions the proton becomes concentrated as well and thus will serve to shift the equilibrium to the right. To further complicate this the low initial water content present in the solution (~1%) may act to further retard the reverse reaction going from extreme right. Ultimately new equilibria will depend to a large extent on the solvent media and its effect. The above discussion has been focused on bulk concentration effects and does not take into account any intensity differences due to the actual gas phase ion production, which will probably act to complicate the matter further. This particular aspect of a particular ions intensity related to its solution concentration has been discussed in some detail by Kebarle and Tang [28]. The above considerations have to be understood before a real assessment of the ion intensities may be made. This study is however a qualitative one

and its goal is to determine whether or not ions that are present in solution may be observed in the gas phase. A third possibility which may account for the unexpected appearance of the dichromate ion is by collision of two  $\text{HCrO}_4^-$  ions in the jet expansion. These types of collisions may be possible in ion rich beams however they would have to overcome substantial electrostatic repulsive potential energy barriers. Figs. 4.10b and 4.10c, illustrate the decomposition pathway of these species where scheme 4.6 given below is probably representative of what is occurring;



Scheme 4.6

Two experiments were performed to explore the concentration and pH dependence of Cr(VI) species under conditions of electrospray. The first experiment was a concentration profile where the amount of  $1.0 \times 10^{-2} \text{M}$   $\text{Na}_2\text{CrO}_4$  stock solution diluted in acetonitrile was varied. The stock solution had a pH of 7.76, which from Fig. 4.8a indicates the dominant ions are  $\text{CrO}_4^{2-}$  and  $\text{HCrO}_4^-$ . Fig. 4.11 contains three spectra where Fig. 4.11a-4.11c are of  $0.5 \times 10^{-4} \text{M}$ ,  $1.0 \times 10^{-4} \text{M}$  and  $2.0 \times 10^{-4} \text{M}$   $\text{Na}_2\text{CrO}_4$  respectively. The dilution of the stock solution

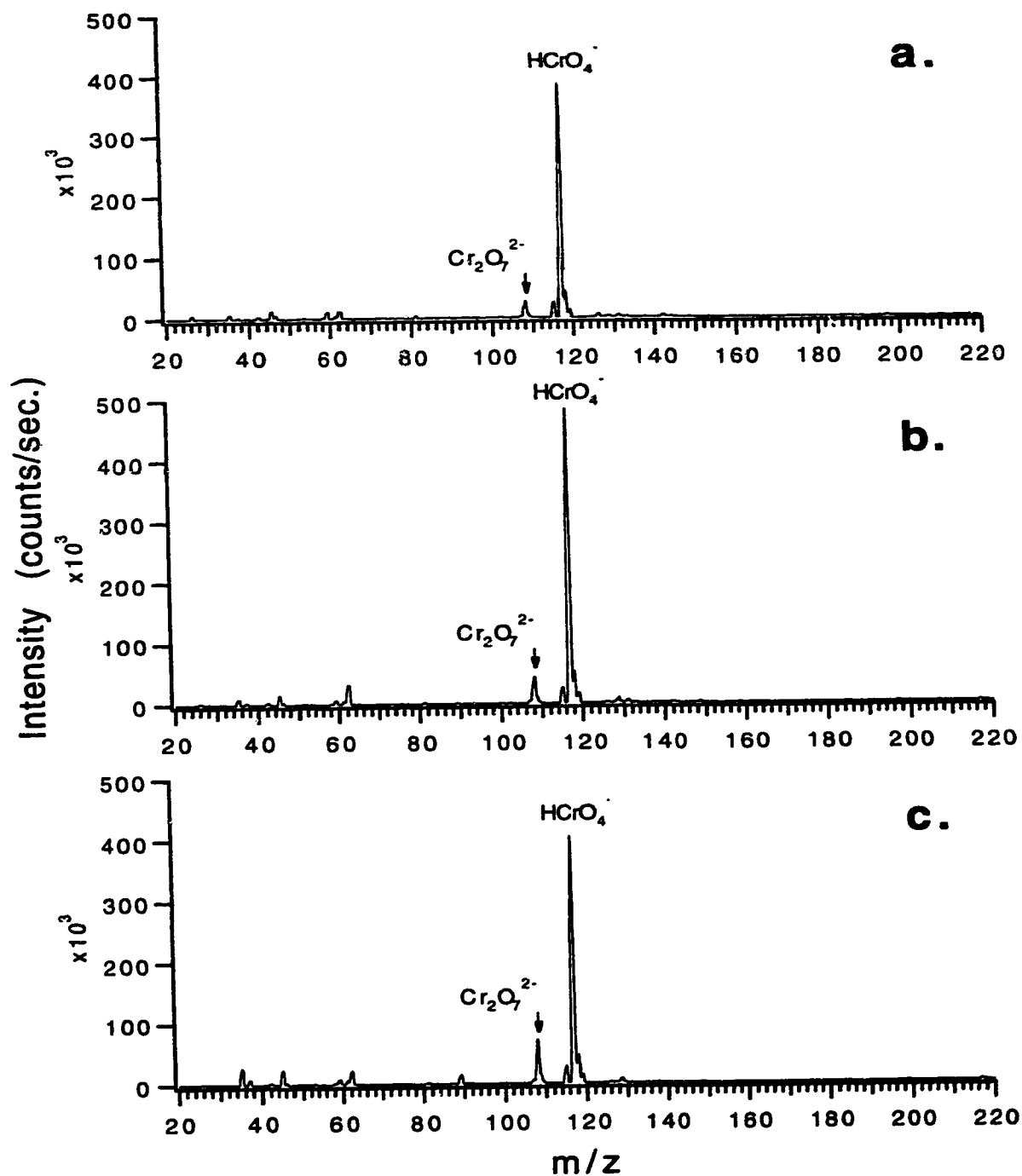
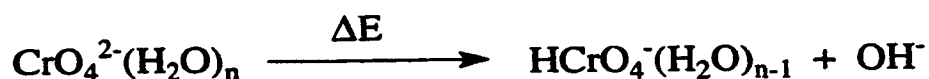


**Figure 4.11** Concentration profiles of  $\text{Na}_2\text{CrO}_4$  in acetonitrile. All spectra acquired under identical conditions ( $\Delta V = 25\text{V}$ ). a.)  $0.5 \times 10^{-4}\text{M}$ , b.)  $1.0 \times 10^{-4}\text{M}$ , c.)  $2.0 \times 10^{-4}\text{M}$ .



would favour a shift in the equilibrium to the left as represented in Scheme 4.5. The spectra were acquired under identical conditions and it was found that the ratio of  $\text{Cr}_2\text{O}_7^{2-}$  to  $\text{HCrO}_4^-$  increased with concentration. For the three concentrations going from low to high, the ratios expressed as percents are 7.0%, 9.0% and 18.0% respectively. This of course would not be expected based on the equilibrium constants, however it may be understood from the above discussion of droplet preconcentration. The dominant ion expected when the aqueous equilibria would be obeyed (based on Fig. 4.8a) is the chromate ion  $\text{CrO}_4^{2-}$  which is not observed. This however may be understood if one considers the fact that if the ion is generated by electrospray then it would probably be 'liberated' from the droplet with an accompanying solvation sphere of some number  $n$ , i.e.,  $\text{CrO}_4^{2-}(\text{L})_n$  (where  $\text{L}$ = some ligand either water or acetonitrile). If the solvation sphere contains water then a competitive reaction might occur between ligand loss and charge separation as illustrated in Scheme 4.7 below;



Scheme 4.7

Charge separation occurs readily in ions that are not able to effectively stabilize the charge without solvation. For example it is obvious, based on Fig. 4.9, that the large dichromate ion is able to exist in the gas phase as a stable ion. This might not be and probably isn't the case for the smaller chromate ion, in a similar case the sulfate ion ( $\text{SO}_4^{2-}$ ) is unable to sustain a bare gas phase  $2^-$  charge and will charge separate

below a ligand number of 4 [15]. Under gentle conditions of  $\Delta V \sim 0V$ , a chromate distribution is not observed and the only distribution observed is the  $HCrO_4^-(L)_n$  distribution of some low ligand number. It is difficult to say whether the conversion of  $CrO_4^{2-}$  to  $HCrO_4^-$  occurs in the gas phase or in the solution phase. It would seem reasonable that in order to form more  $Cr_2O_7^{2-}$  as observed in Fig. 4.11 there must also exist a correspondingly greater amount of the precursor  $HCrO_4^-$  which would indicate that it must be present in solution to some degree.

The second experiment explored the pH dependence of the Cr (VI) solutions. Three stock solutions of  $1.0 \times 10^{-2}M$   $Na_2CrO_4$  each were prepared. The first contained  $1.0 \times 10^{-2}M$   $NaOH$ , the second no additive and the third  $1.0 \times 10^{-2}M$   $HNO_3$ . The corresponding pH's were found to be 11.65, 7.76, and 3.57. The electrospray mass spectra of all three solutions diluted 200X in acetonitrile are given in Fig. 4.12 where each was acquired under identical conditions. There is a corresponding increase in the ratio of  $Cr_2O_7^{2-}$  to  $HCrO_4^-$  (expressed as a percent) going from high to low pH being 4.0%, 7.0% and 38.0% respectively. Again this trend may be expected based on Scheme 4.5 and the above discussion on droplet preconcentration. The large jump from 7.0% to 38% as exhibited in the difference between Figs. 4.12b and 4.12c may be due to the effective preconcentration of both the Cr(VI) ion and the  $H^+$  ion.

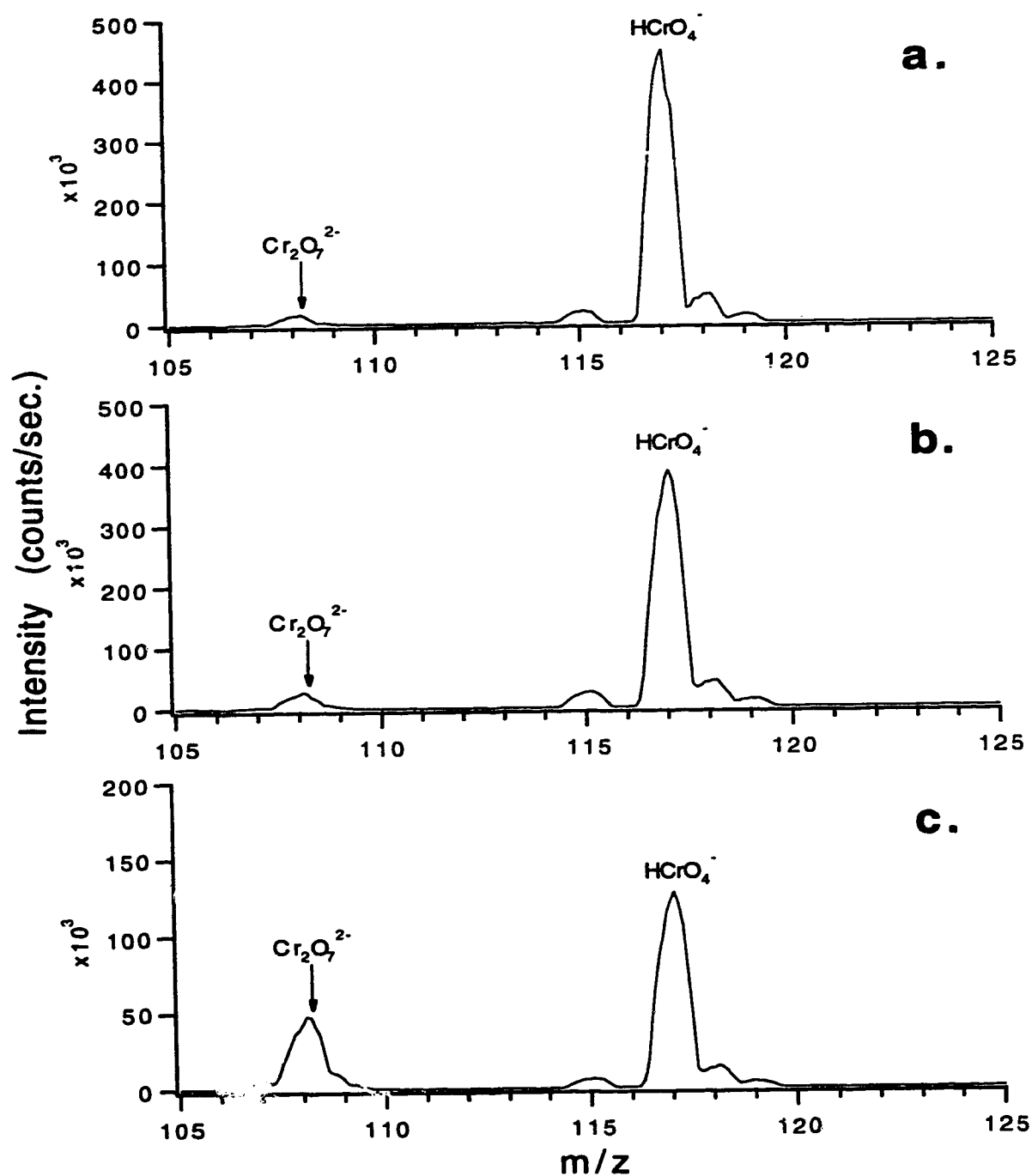


**Figure 4.12** pH profiles of  $0.5 \times 10^{-4} \text{ M Na}_2\text{CrO}_4$  in acetonitrile/0.5%  $\text{H}_2\text{O}$  with varied pH control. All spectra acquired under identical conditions ( $\Delta V = 25 \text{ V}$ ). **a.**)  $0.5 \times 10^{-4} \text{ M NaOH}$  added, **b.**) no pH adjustment, **c.**)  $0.5 \times 10^{-4} \text{ M HNO}_3$  added.

#### 4.4.7 Trichromate Ion

The existence of the trichromate ion ( $\text{Cr}_3\text{O}_{10}^{2-}$ ) has only been detected at high concentrations ( $\sim 1\text{M}$  or greater  $\text{Na}_2\text{CrO}_4$ ) and pH's less than 0. Based on the above knowledge where dilution of Cr(VI) solutions in acetonitrile does not have the same effect as it would with water it was thought that this system could be studied, or at least probed. A stock solution of  $1\text{M}$   $\text{Na}_2\text{CrO}_4$  with a corresponding  $1\text{M}$   $\text{HNO}_3$  concentration was prepared, which had the characteristic dark orange red colour. From this solution  $10\mu\text{L}$  was diluted to  $100\text{ mL}$  in acetonitrile keeping the effective water content down to  $\gg 1\%$ . This dilution gives an overall concentration of  $1.0 \times 10^{-4}\text{M}$  in acetonitrile and the corresponding mass spectrum acquired under gentle conditions of this solution is given in Fig. 4.13a. In this mass spectrum the characteristic  $\text{Cr}_2\text{O}_7^{2-}$  and  $\text{HCrO}_4^-$  ions are observed as well the  $\text{HCr}_2\text{O}_7^-$  ion at  $m/z$  217 and the trichromate ion ( $\text{Cr}_3\text{O}_{10}^{2-}$ ) at  $m/z$  158 are also observed. A relative isotopic distribution (normalized to 100%) of these species is presented immediately below in Fig. 4.13b, which seem to agree favourably with the proposed ions.

It was found that the trichromate ion may also be observed from solutions prepared from more dilute stock solutions (i.e.,  $1.0 \times 10^{-2}\text{M}$  with  $1.0 \times 10^{-2}\text{M}$   $\text{HNO}_3$ ). When these are diluted in acetonitrile, to give overall concentrations of  $\geq 2.0 \times 10^{-4}\text{M}$   $\text{Na}_2\text{CrO}_4$  and  $2.0 \times 10^{-4}\text{M}$   $\text{HNO}_3$ , there does appear to be evidence for the trichromate ion. The intensities however are not as great as those observed in Fig. 4.13a. Again this may be understood as a result of preconcentration of the Cr(VI) species in the droplets, especially under conditions (higher

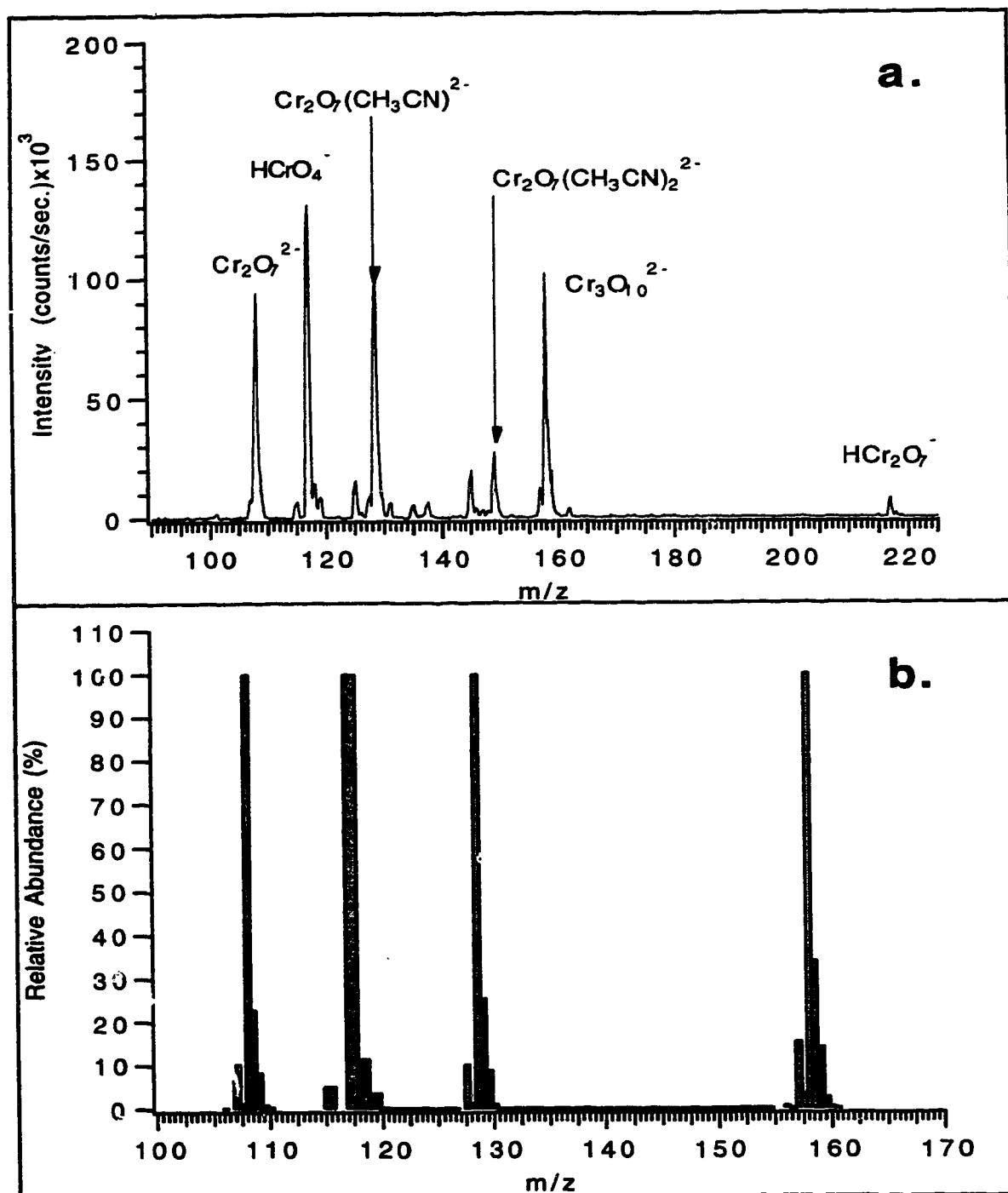
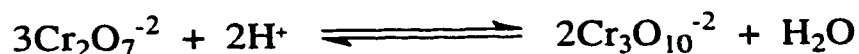


**Figure 4.13** Mass spectrum of the dilution of a concentrated chromate solution. a.) 10  $\mu\text{L}$  of a stock solution of  $\text{Na}_2\text{CrO}_4$  (1M) and  $\text{HNO}_3$  (1M) diluted to 100mL in acetonitrile.  $\Delta V = 17\text{V}$ . b.) the relative isotopic abundances of the various species in a.

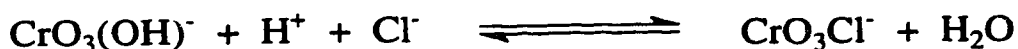
concentration and lower pH) favourable to the existence of the  $\text{Cr}_2\text{O}_7^{2-}$  ions, as given by reaction Scheme 4.8:



Scheme 4.8

#### 4.4.8 Chlorochromate Ion

For the most part Cr(VI) in aqueous solution will exist as species dictated by the equilibria given above (equations (4.6)-(4.8)). These equilibria may be perturbed by the presence of certain matrix ions which can give rise to the existence of other species. Notably the presence of halides such as chloride under concentrated conditions can give rise to chlorochromate complexes as illustrated in Scheme 4.9 below.



Scheme 4.9

This reaction is reversible as it may be hydrolyzed in water. Other complexes include sulfato complexes which can be formed upon reaction with sulfuric acid or acid sulfate. To see if the chlorochromate species may be observed by electrospray a solution of  $\text{Na}_2\text{CrO}_4$ ,  $\text{HNO}_3$  and  $\text{KCl}$  each  $0.5 \times 10^{-4}\text{M}$  in acetonitrile/1%  $\text{H}_2\text{O}$  was prepared. The mass spectrum is presented in Fig. 4.14 and it clearly shows the presence of the chlorochromate species at  $m/z$  135 as well

the other characteristic equilibrium species. Michel and Machiroux [40] also observed the chlorochromate species by Raman spectroscopy and it was determined that it became the dominant species in solution when HCl was in excess of Cr(VI) in concentrated solutions. The data presented in Fig. 4.14 is from dilute equal molar solutions and reflect the effects of droplet preconcentration. It becomes important to consider these species when solution control for such purposes as chromatographic separation is required.

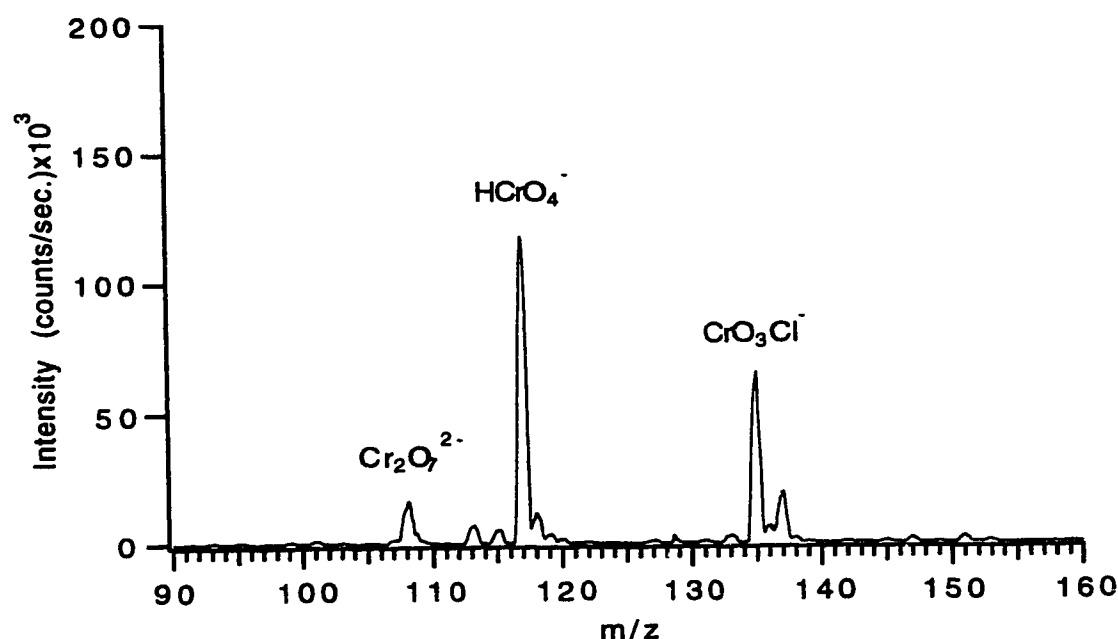
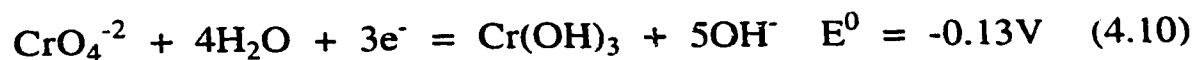
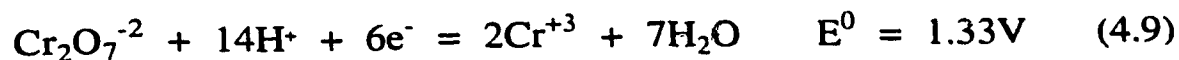


**Figure 4.14** Mass spectrum of chlorochromate.  $\text{Na}_2\text{CrO}_4$ ,  $\text{HNO}_3$  and  $\text{KCl}$  each  $0.5 \times 10^{-4} \text{M}$  in acetonitrile/1%  $\text{H}_2\text{O}$ ,  $\Delta V = 25 \text{V}$ .

The very nature of Cr (VI) is that of a strong oxidizer. The oxidation strength of the species is pH dependant, where under acidic conditions it behaves as a stronger oxidant than under basic conditions as given by equations (4.9) and (4.10) below [30];



In acetonitrile Cr(VI) is not completely stable and will react with the solvent over time. The rate of reaction is dependant on the pH of the solution where the more acidic the solution the quicker the decomposition. When Cr(VI) is allowed to mature in acetonitrile the solution turns to a pink/violet colour indicative of a reaction. The mass spectra of a solution allowed to age 4 days in acetonitrile ( $1.0 \times 10^{-4}$  M  $\text{Na}_2\text{CrO}_4$ ) is given in Fig. 4.15, where Fig. 4.15a is acquired under gentle conditions and Fig. 4.15b is acquired under harsh conditions and shows the CID decomposition products of the precursors (Fig. 4.15a). The three major reaction products observed are at  $m/z$  126, 142 and 158 and are tentatively assigned  $\text{CrO}_3\text{CN}^-$ ,  $\text{Cr}(\text{O}_2)_2\text{CN}^-$ , and  $\text{CrO}(\text{O}_2)_2\text{CN}^-$  respectively. This assignment is supported in part by the decomposition products observed in Fig. 4.15b however these assignments should be viewed with caution. The purpose of the experiment is to illustrate the potential shortcomings of acetonitrile as an electrospray solvent for Cr(VI) species. The decomposition seems to be accelerated in the cases of solutions (initial stock solutions) of lower pH. In choosing an appropriate solvent for Cr(VI) determination by ESMS it would seem highly unlikely that any organic solvent would be immune to oxidation, and therefore the best solvent might be the one with the slowest solution decomposition.



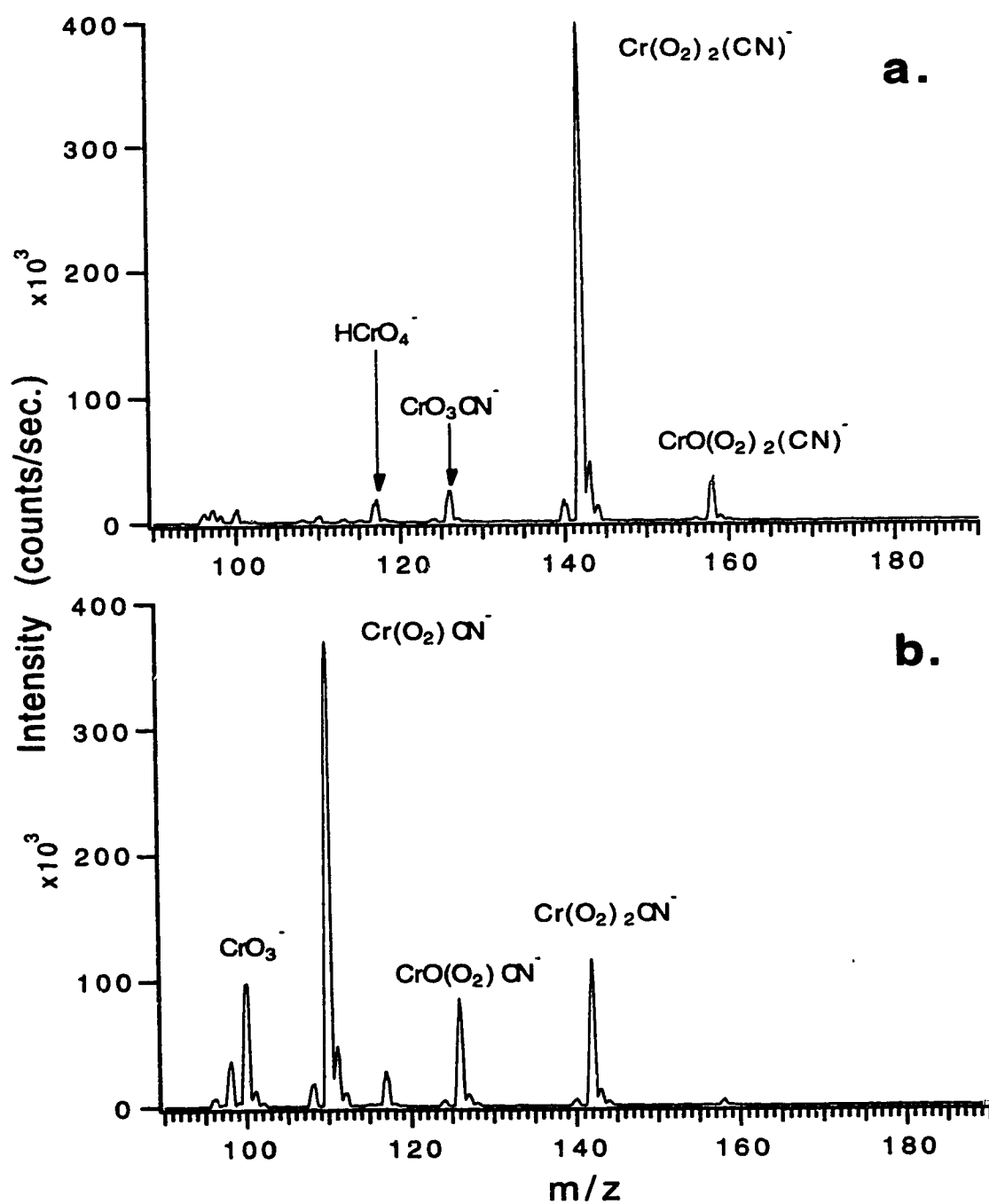


**Figure 4.15** Reaction products of  $0.5 \times 10^{-4} \text{ M Na}_2\text{CrO}_4$  in left to age in acetonitrile/0.5%  $\text{H}_2\text{O}$  for four days. CID profile **a.**)  $\Delta V = 25 \text{ V}$ , **b.**)  $\Delta V = 40 \text{ V}$ .

Overall the electrospray mass spectra of the Cr (VI) species seem to be reflective of the stock solution concentration however the species distribution is understandably shifted based on the above discussion. The mass spectra presented can be used effectively to directly show the existence of Cr (VI) species in solution however the equilibria involved with such species becomes complicated. The one species that was not directly observed was the  $\text{CrO}_4^{2-}$  ion, this may be due to a gas phase (i.e., charge separation) or a solution phase conversion to the  $\text{HCrO}_4^-$  ion. As a corollary of this it is difficult to say that the  $\text{HCrO}_4^-$  ion exists in solution however it cannot be argued that it exists in the gas phase. However for acidic solutions where  $\text{CrO}_4^{2-}$  is expected to be absent, the  $\text{HCrO}_4^-$  ion is observed as expected and so probably does not form as a result of gas phase charge separation. The evidence that it exists however is more favourable than not based on the results obtained.

## 4.5 Conclusions

The use of electrospray mass spectrometry to probe the solution speciation of chromium ions was examined. Electrospray's ability to generate intact gas phase ions representative of solution ions was studied. The results at times are not clear and usually require some interpretation. At other times they can be quite simple as is illustrated by Fig. 4.10a. Considering the fact that this solution consists of sodium dichromate with nitric acid run in the negative ion mode, the dominant ions expected of course would be nitrate, and Cr (VI) ions (dictated by equilibrium). In looking at the spectrum acquired over a

$m/z$  range of 10 to 260 it is a remarkably clean spectrum containing essentially only these ions. In addition it was shown that the technique is able to offer other avenues for exploring certain aspects of solution chemistry not wholly realized by other techniques. The differentiation of Cr(III) from Cr(VI) in a solution sample may be achieved by changing the operating modes between positive and negative ion mode where the individual species present may be determined. The list of possible solution forms for these two oxidation states is quite extensive, and this work can only be regarded as a minor exploration of the possible species. It would seem that the use of electrospray for speciation work has the potential to provide direct information not normally obtainable by other techniques.

#### 4.6 References

1. M.L. Parsons, S. Major, and A.L. Forster, *Appl. Spectrosc.*, **37**, 411 (1983).
2. Technical Summary report: Perkin-Elmer-SCIEX, ELAN 5000.
3. Technical Summary report: VG Elemental Limited System, VG Plasma Quad PQ2 Turbo Plus.
4. Technical Summary report: Hewlett Packard, HP 4500.
5. J.C. Ivaldi, and J. F. Tyson, *Spectrochim. Acta , Part B* **50**, 1207 (1995).
6. K. E. La Ferniere, V. A. Fassel, and D. E. Eckels, *Anal. Chem.*, **59**, 879 (1987).
7. M. J. Tomlinson, J. Wang, and J.A Caruso, *J. Anal. At. Spectrom.*, **9**, 957 (1994).
8. J.W. Olesik, J.A. Kinzer, and S. V Olesik. *Anal. Chem.*, **67**, 1 (1995).
9. M. Sperling, S. Xu, and B. Welz, *Anal. Chem.*, **64**, 3101 (1992).
10. G.R. Agnes and G. Horlick, *Appl. Spectrosc.*, **46**, 401 (1992).
11. G.R. Agnes and G. Horlick, *Appl. Spectrosc.*, **48**, 655 (1994).
12. G.R. Agnes, I.I.Stewart and G. Horlick, *Appl. Spectrosc.*, **48**, 1347 (1994).
13. G.R. Agnes and G. Horlick, *Appl. Spectrosc.*, **48**, 649 (1994).

14. G.R. Agnes and G. Horlick, *Appl. Spectrosc.*, **49**, 324 (1995).
15. I. I. Stewart and G. Horlick, *Trends in Anal. Chem.*, **15**, 80 (1996).
16. G. J. Van Berkel, S.A. McLuckey, and G.L. Glish, *Anal. Chem.*, **64**, 1586 (1992 ).
17. J. Zeleny *Phys. Rev.*, **10**, 1 (1917 ).
18. M. Yamashita and J.B. Fenn, *J. Phys. Chem.*, **88**, 4451 (1984).
19. M. Yamashita and J.B. Fenn, *J. Phys. Chem.*, **88**, 4671 (1984).
20. D.P.H. Smith *IEEE Trans. Ind. Appl.*, **63**, 527 (1986).
21. I. Hayati, A.I Bailey, and TH. F. Tadros, *J. Colloid. Interface Sci.*, **117**, 205 (1987).
22. I. Hayati, A.I Bailey, and TH. F. Tadros, *J. Colloid. Interface Sci.*, **117**, 222 (1987).
23. D.C. Taflin, T.L. Ward and E.J. Davis, *Langmuir*, **5**, 376 (1989).
24. A. Gomez and K. Tang, *Phys. Fluids*, **6**, 404 (1994).
25. J.V. Iribarne and B.A. Thomson, *J. Chem. Phys.*, **64**, 2287 (1976).
26. B.A. Thomson and J.V. Iribarne, *J. Chem. Phys.*, **71**, 4451 (1979).
27. M. Dole, L.L. Mack, R.L. Hines, R.C. Mobley, L.D. Ferguson and M.B. Alice, *J. Chem. Phys.*, **49**, 2240 (1968).

28. P. Kebarle and L. Tang, *Anal. Chem.*, **65**, 972A (1993).
29. I.I. Stewart and G. Horlick, *Anal. Chem.*, **66**, 3983 (1994).
30. F.A. Cotton, and G. Wilkinson, "*Advanced Inorganic Chemistry. A Comprehensive Text*" Fifth Edition, Interscience, New York N.Y., p.687, 1988.
31. H. Stunzi, and W. Marty, *Inorg. Chem.*, **22**, 2145 (1983).
32. Rotzinger, F.P., Stunzi, H., and Marty, W., *Inorg. Chem.*, **25**, 489 (1986).
33. L. Spiccia, and W. Marty, *Inorg. Chem.*, **25**, 266 (1986).
34. L. Spiccia, H. Stoeckli-Evans, W. Marty, and R. Giovanoli, *Inorg. Chem.*, **26**, 474 (1986).
35. D. Rai, B.M. Sass, and D.A Moore, *Inorg. Chem.*, **26**, 345 (1986).
36. A.T. Blades, P. Jayaweera, M.G. Ikonomou and P. Kebarle, *Int. J. Mass Spectrom. Ion Processes*, **101**, 325 (1990).
37. F. Y. Saleh, G.E. Mbamalu, Q.H. Jaradat and C.E. Brungardt, *Anal. Chem.*, **68**, 740 (1996).
38. R.K. Tandon, P.T. Crisp, J. Ellis, and R.S. Baker, *Talanta* , **31**, 227 (1984).
39. T. Shen-Yang, and L. Ke-An, *Talanta* , **33**, 775 (1986).
40. G. Michel, and R. Machiroux, *J. Raman Spectrosc.*, **14**, 22 (1983).
41. G. Michel, and R. Cahay, *J. Raman Spectrosc.*, **17**, 79 (1986).

## **Chapter 5**

### **Sulfur Speciation**

## 5.1 Introduction

The chemistry of sulfur is quite complex as it may exist in several different forms. In aqueous inorganic solutions sulfur commonly exists in anionic form, which may be as simple as sulfide or as complex as one of the numerous oxo or peroxy acid forms. Sulfur species are present in many different aqueous systems such as ground and surface waters as well as biological fluids. In ground water samples, complex sulfur species probably originate as a result of sulfide mineral oxidation at low to neutral pH's [1]. Therefore the reaction products can give some indication as to the mechanisms involved in this process and therefore the determination of such species is desirable for environmental reasons as well as from the point of view of understanding general inorganic sulfur chemistry. In biological samples such as urine, the determination of sulfate is quite useful [2]. Sulfate derivatives may also exist in many different organic molecules such as sulfonated azo dyes, as well steroidal complexes [3].

Over the years sulfur species and inorganic anions in general have been determined for the most part by chemical, chromatographic and spectrochemical techniques. For example oxo-sulfur species have been determined by ion exchange chromatography [4,5], ion pair chromatography[6-9], capillary electrophoresis [10] and spectrophotometry [11-14]. For the most part these studies have focused on such species as sulfate, sulfite, thiosulfate, and polythionate species ranging up to thirteen sulfur atoms. In some cases however these types of techniques are inadequate as they are unable to provide the desired degree of selectivity or sensitivity. As a result researchers



have moved toward developing chromatographically coupled mass spectrometric techniques such as HPLC-ICP-MS, and CE-ICP-MS in attempts to improve inter-element speciation [15-17]. These techniques are fine for differentiating between different oxidation state metal ion species and different molecular ion species such as arsenite, monomethyl arsonic acid (MMAA) and dimethylarsinic acid (DMAA), but are not entirely effective at differentiating sulfur species [15].

More recently a relatively new technique, electrospray ionization mass spectrometry (ESMS), has been used successfully to determine inorganic cations and anions in solution samples [18-19]. In particular *Agnes et al* [18] have shown that it may be successfully used to directly determine sulfur anion species in solution. A variation of electrospray, "ion spray" has also been coupled to capillary electrophoresis for the mass spectrometric determination of inorganic cations and anions [20], which is desirable when examining complex samples.

The technique has been described extensively in the literature [21-23] and so only a qualitative description will be given here. Simply put, electrospray is an electrostatic spraying process, where a liquid surface becomes disrupted when an intense electric field is applied resulting in a spray of charged droplets. In the case of electrospray a solution of some minimum conductivity (typically a methanolic electrolyte solution on the order of  $10^{-5}\text{M}$  -  $10^{-3}\text{M}$ ) is pumped (  $\sim 1\text{-}10\mu\text{L}/\text{min.}$ ) through a stainless steel capillary ( $\sim 100\mu\text{m}$  i.d.,  $200\mu\text{m}$  o.d.) which is held at some high potential relative to a counter electrode ( the mass spectrometer sampling orifice ). This spraying phenomena at the capillary tip affords the transfer of solution

ions to the gas phase where they may be sampled by a mass spectrometer. A negatively biased capillary results in negatively charged droplets and ultimately negative gas phase ions, the opposite is true for a positively biased capillary. The formation of the spray, the charging of the droplets and formation of gas phase ions from such droplets are described in some detail in the literature [22,23].

The focus of this paper is on ESMS's effectiveness in investigating inorganic sulfur species in solutions, and is presented in part as a continuation of previous work [18]. In particular the paper will discuss some background on the generation and sampling of gas phase sulfur ions. A variety of solutions will be investigated ranging from standard laboratory solutions to reaction mixtures to real samples. Although the focus is on the qualitative aspects some preliminary data on the quantitation of sulfur species will be presented.

## **5.2 Experimental**

The electrospray source and mass spectrometer have been previously described [23]. The high pressure sampling region of the modified Sciex/Perkin-Elmer ELAN Model 250 ICP-MS mass spectrometer, is based on a sampling plate/skimmer configuration. There have, however, been some modifications inside the mass spectrometer; the shadow or first photon stop in the ion optics as well as the second stop located in the bessel box have been removed. This has led to an increase in sensitivity of one to one and a half orders of magnitude. As anions are being studied the mass spectrometer was operated in

negative ion mode. For these studies the ES tip was typically biased at -3000V, the front plate at -600V, the sampling plate was varied to minimize or maximize collisionally induced dissociation (CID) in the high pressure region (typically between -2 and -60V) and the skimmer was held at -2V. As the skimmer potential is held constant, the potential drop and hence energy is proportional to the sampling plate voltage (see ref. 24 for discussion). The curtain gas used for these experiments was nitrogen at a flow rate of about 1.3 L/min. The ES needle tip had a 100 $\mu$ m i.d. and was operated at a flow rate of 1.0-2.0 $\mu$ L/min via a syringe pump ( Sage Instruments model 341A ). The tip position although optimized for each set of experiments was usually set 5 mm from the front plate and 1 mm off axis. It was found that careful selection of flow rate (usually a low flow rate) and applied capillary potential, led to stable signals without the use of discharge suppressing gases.

For quantitative investigations two different procedures were employed. In one, a normal electrospray setup was used where sample solutions are run in a sequential manner. The samples are prepared to contain the analyte in varying concentrations and a known constant concentration of internal standard. The flow rate was typically 2.00  $\mu$ L/min. In the second a Valco high pressure injection valve, with a 0.50  $\mu$ L internal sample loop was used. The samples were prepared to include the internal standard, and were injected into a flowing stream of internal standard in methanol. The flow rate of the carrier/internal standard solution was 2.50  $\mu$ L/min. Selected ions were monitored as a function of time.

All solutions were prepared by dissolving the ACS grade salts in distilled deionized water to form a stock solution. Aliquots of the stock solution were then diluted with HPLC-grade methanol to the desired concentration. This procedure was modified for the quantitative experiments where the methanol was distilled and the reagent salt was oven dried. These procedures result in the solution being primarily methanol with water content in the range of 1-3% by volume.

### 5.3 Results and Discussion

#### 5.3.1 General

Preliminary studies of inorganic sulfur species were carried out by Agnes *et al* [18] using electrospray mass spectrometry. It was shown that a wide range of anionic sulfur species could be examined. For the most part anionic sulfur species are quite amenable to electrospray and it is generally the case that if a species exists in an ionic form in solution and is stable in an electrospray solvent it may be observed by ESMS. These two stipulations may obviously pose some limitations. In addressing the first point; take sulfide for example, its reactive solution form is typically  $S^{2-}$  although this species is difficult to observe by electrospray. This is due primarily to the fact that simple sulfides such as  $H_2S$  are only partially ionized in aqueous solutions. The first and second dissociations constants are  $pK = 6.8$  and  $pK = 14.15$  respectively [25], which means that for an initial solution of  $1 \times 10^{-4}M$  only about  $3.6 \times 10^{-6}M$  exists as  $HS^-$  and there is virtually no  $S^{2-}$  ion present. In addition the equilibrium may be even further

shifted to the left when the sample is diluted in methanol, which has a much lower relative dielectric constant than water, ~33 as opposed to ~78.

One other concern is the stability of the species both in aqueous solution and the electrospray solvent. For the most part the common sulfur anions especially the oxo-sulfur species are quite stable in solvents like methanol, however some species such as sulfite ( $\text{SO}_3^{2-}$ ) are not, this example will be addressed later in the discussion.

Although the generation of gas phase ions from the droplets is still a controversial subject in the electrospray literature it is evident that ions tend to leave the droplet with a stabilizing solvation sphere of some size. It is these well solvated ions that are sampled by the mass spectrometer and Fig. 5.1 will be used to illustrate the processes involved in sampling a solvated anion and stripping it down to a bare molecular ion via high pressure CID at the interface.

Figure 5.1 shows a variable high pressure CID plot of ammonium persulfate ( $10^{-4}\text{M}$  in MeOH), where different "CID energies" are plotted as a function of intensity and  $m/z$ . It is important to note that these are not actual "collision energies" but are just the potential differences between the sampling plate and skimmer which will be related to the collision energy. This may be simply understood by considering the fact that the greater the electric field in this region the greater the acceleration of an ion relative to the neutral nitrogen curtain gas (or other neutral gasses in the expansion). This will in its simplest interpretation result in a greater collisional energy. The nature of the expansion will further complicate this as gas density and hence collisional frequency is a decreasing function of distance from

the sampling orifice. The energy of collisions which occur in the later part of the expansion may conversely increase as a result of greater mean free path and hence longer acceleration times between collisions. Whether the relationship between potential difference and CID energy is a strictly linear relationship is unknown, however the net result in all cases is that a greater potential difference affords a greater amount of stripping. Looking first at the low CID potential (10V) we see a low (relatively) intensity distribution at high  $m/z$ , these are peroxodisulfate water cluster species with distributions ranging from four water ligands to 11 water ligands, the most intense peak in this distribution seems to be persulfate with seven water molecules at  $m/z$  159. As these species are  $2^-$  anions the distribution separation is 9  $m/z$  units ( $18/2$ ). As the potential difference is increased in increments of 5V the distribution makes an obvious shift to lower  $m/z$  values and eventually at a CID value of 30V yields primarily a desolvated bare persulfate anion at  $m/z$  96. There is a minor peak at  $m/z$  105 due to the singly-hydrated peroxodisulfate species. Past this point the energy supplied goes into molecular fragmentation and various decomposition products are formed. The actual process for the persulfate ion has been described in some detail by Agnes *et al.*[18]. It is interesting to note the increase in signal intensity going from CID 10V to CID 30V. It would be expected that the total ion current should remain somewhat constant, regardless of energy, but this was not observed. One probable explanation for this is that ions leave the expansion region with greater velocities for higher potential differences and thus they have a much more efficient transmission through the ion optics and quadrupoles.

Figure 5.1 illustrates the different types of information that may be obtained and that it is important to be aware of sampling conditions while interpreting the mass spectrum. At potentials differences greater than 30V molecular fragmentation occurs and species such as  $\text{HOSO}_4^-$ ,  $\text{HSO}_4^-$ ,  $\text{SO}_3^-$  and  $\text{SO}_2^-$  may be observed, all of which are clearly not present in the original solution. These harsher condition spectra will be discussed in an appendix at the end of the chapter and will not be discussed here. Therefore great care must be taken when interpreting spectra.

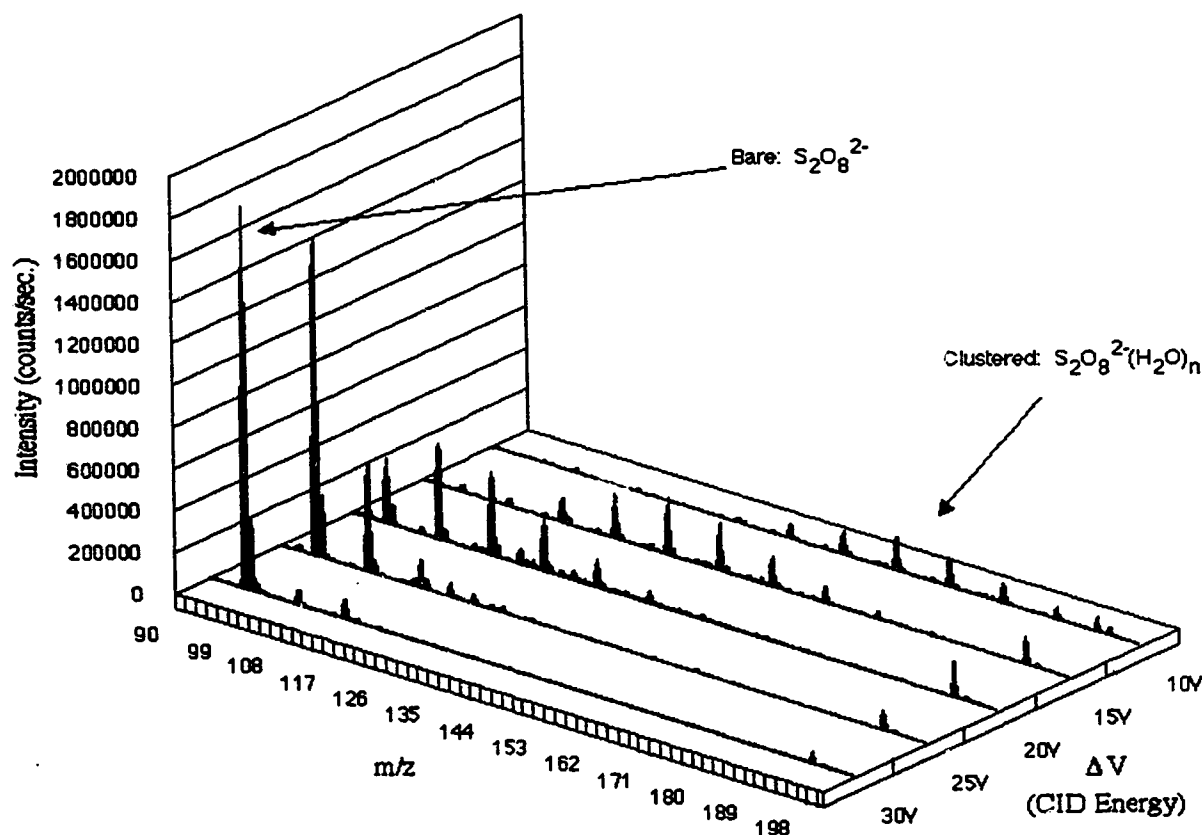
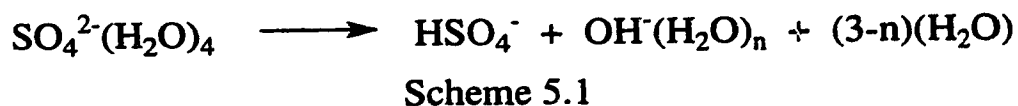


**Figure 5.1** 3D CID spectra of ammonium persulfate ( $1.0 \times 10^{-4}\text{M}$ ) in methanol. The plot illustrates the change in the solvated distribution of the persulfate ion going from -10V potential difference to a -30V potential difference.

Depending on the nature of the anion it may or may not be possible to 'strip' its solvation sphere down to a 'bare' molecular form. In the case of the persulfate ion above, it is large enough to stabilize its bare gas phase charge, however other smaller anions may not be able to support multiple charges and therefore will seek to reduce their charge and this is usually achieved by fragmentation. Sulfate and thiosulfate are two such multiply charged ions that undergo charge reduction reactions in the gas phase.

The sulfate anion which is perhaps the most common of the sulfur-oxygen anion species can exist in solution in several different forms;  $\text{H}_2\text{SO}_4$ ,  $\text{HSO}_4^-$  and  $\text{SO}_4^{2-}$  depending on the solution pH. For the most part it exists almost entirely as the  $\text{SO}_4^{2-}$  ion in neutral solutions. Electrospray mass spectra of vanadyl sulfate in methanol are given in Figure 5.2. The figure consists of two spectra: a mild (relative) CID condition spectrum in Fig. 5.2(a), and a harsher CID spectrum in Fig. 5.2(b).

Figure 5.2(a) shows the distribution of solvated sulfate ions and as well a certain amount of the protonated equilibrium species  $\text{HSO}_4^-$ . The  $2^-$  water solvated species are separated by 9 m/z units corresponding to differences of one water ligand. It is observed that the sulfate anion requires at least four water ligands to stabilize its 2 charges. Once this species is reached it will not simply lose another water ligand rather it will charge separate as shown in Scheme 5.1 below due to charge instability:





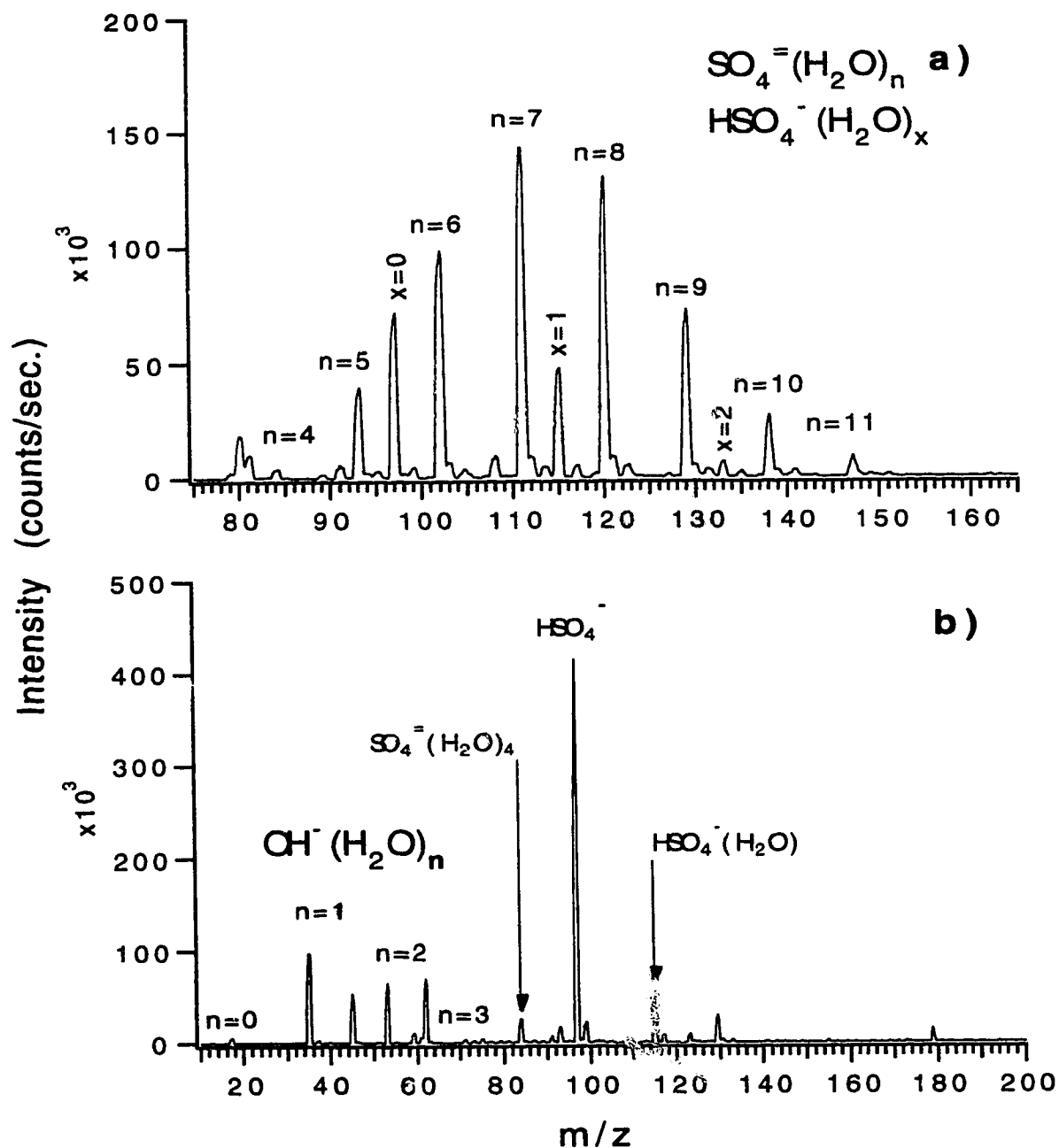
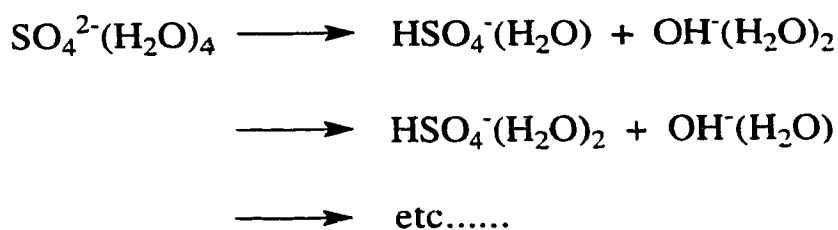


**Figure 5.2** Mass spectrum of vanadyl sulfate ( $1.0 \times 10^{-4} \text{M}$ ) in methanol. The spectra were acquired at two different sampling plate to skimmer potential differences a)  $-12.5 \text{V}$  and b)  $-22.5 \text{V}$ .

Although it seems clear that when sampling with high pressure CID that the minimum water ligand number for sulfate is four, the charge separation reactions may also occur to a lesser degree in the more solvated species ( i.e.. 5 water ligands). The charge separation itself is not straight forward as it may occur with some variation and some possibilities are presented in Scheme 5.2



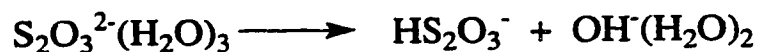
Scheme 5.2

The above reactions probably account for the presence of the  $\text{HSO}_4^-$  species observed in Fig. 5.2(a). At extremely mild sampling conditions the  $\text{HSO}_4^-$  species contribution is greatly reduced. Sulfate with less than four water ligands is not observed using the high pressure CID interface. The above studies have also been observed using low pressure CID by Blades and Kebarle [26].

Figure 5.2b shows a spectrum acquired under harsher CID conditions, where all the sulfur species have essentially been converted into one species ( $\text{HSO}_4^-$ ) prior to mass analysis. Note also the presence of various solvated hydroxide species characteristic of the charge separation step. It is possible however to have distributions due to basic ions such as  $\text{OH}^-$  under gentler CID conditions and so the origin of these species may be viewed with caution. However as a consequence of CID if they did exist from other sources such as free  $\text{OH}^-$  they would exist primarily as the bare  $\text{OH}^-$  ion at  $m/z$  17

exclusively. Therefore the distribution observed in Fig. 5.2b would most likely be a result of the fragmentation of the solvated sulfate ion. Also note the peaks at  $m/z$  129.5 and  $m/z$  179 which have not been definitely assigned but may be assigned with caution to vanadyl ( $\text{VO}(\text{SO}_4)_2^{2-}$ ) and vanadate species ( $\text{VO}_2(\text{SO}_4)^-$ ) respectively.

Thiosulfate, although not as stable and somewhat more reactive in solution than sulfate also exists primarily as the  $2^-$  ionic species in solution. Figure 5.3 contains three sodium thiosulfate spectra: each acquired under different CID region conditions. Under fairly gentle conditions (Fig. 5.3(a)) where  $\Delta V = 14\text{V}$  a distribution of solvated thiosulfate ions with a solvation distribution ranging from three to nine water molecules is observed. A distribution maximum is noted at  $m/z$  101 corresponding to the  $\text{S}_2\text{O}_3^{2-}(\text{H}_2\text{O})_5$  species. Under gentler conditions the distribution maximum shifts to higher values. Similar to the sulfate anion, a minimal solvation sphere must be maintained by the thiosulfate anion in order to stabilize its charge. For thiosulfate it is found that at least three water ligands are required corresponding to an  $m/z$  of 83, any number less than this leads to some interesting results. Intuitively one might expect a charge separation similar to that of sulfate to occur as in the scheme below:



Scheme 5.3

This is not strictly observed. Figure 5.3b shows a spectrum acquired under slightly harsher conditions ( $\Delta V = 19\text{V}$ ), where the solvated distribution shifts to a maximum at  $m/z = 83$  and decomposition products resulting from the continued stripping

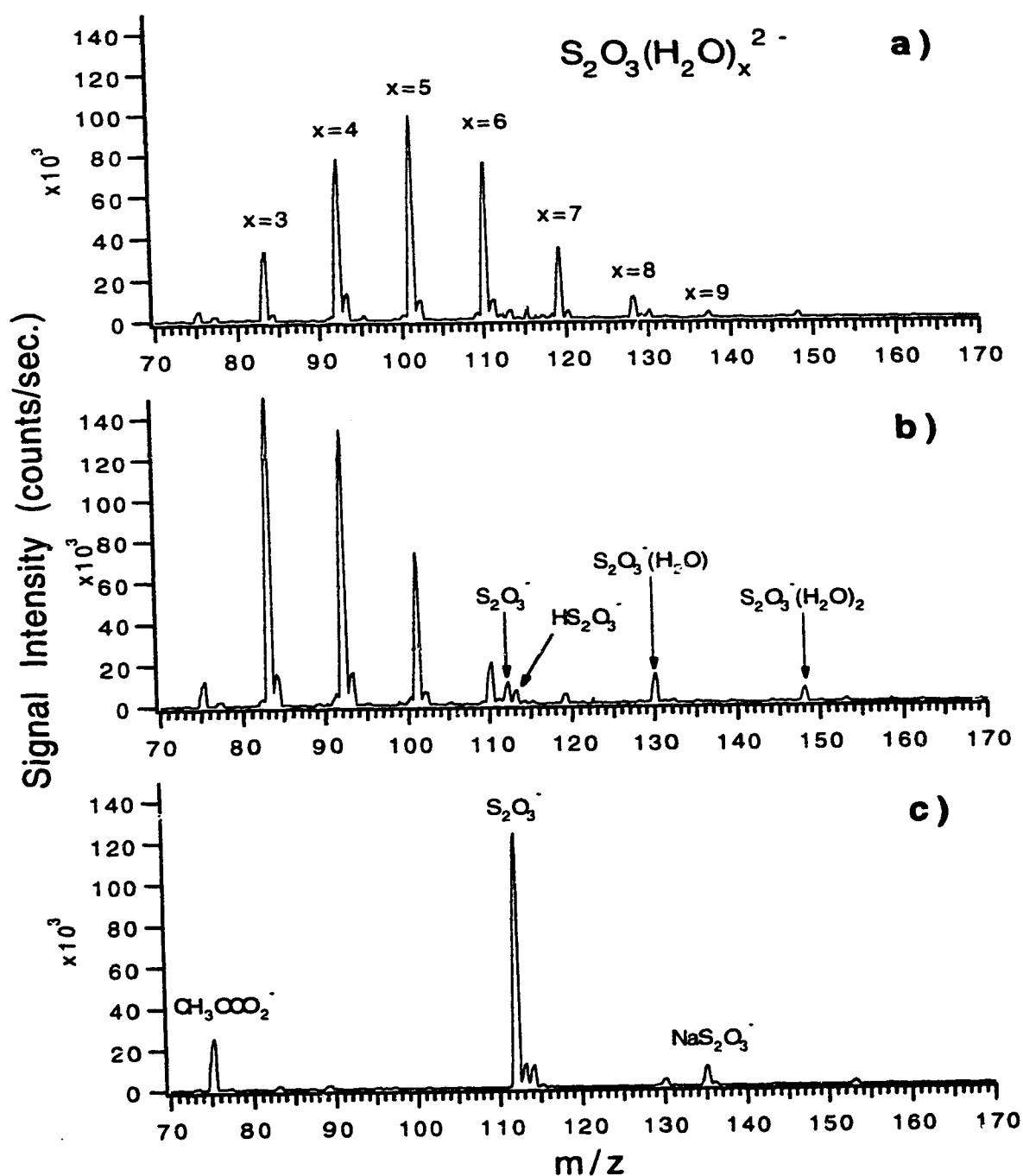


**Figure 5.3** Mass spectra of sodium thiosulfate ( $1.0 \times 10^{-4} \text{M}$ ) in methanol. The spectra were acquired at different sampling plate to skimmer potential differences; a) -14V, b) -19V and c) -24V.

of this species are observed. Although there is evidence for the expected  $\text{HS}_2\text{O}_3^-$  anion at ( $m/z = 113$ ), it is not the dominant ion formed. The dominant species formed is based on the  $\text{S}_2\text{O}_3^-$  ( $m/z = 112$ ) ion and its solvated precursors  $\text{S}_2\text{O}_3^-(\text{H}_2\text{O})$  and  $\text{S}_2\text{O}_3^-(\text{H}_2\text{O})_2$  at  $m/z$  130 and 148 respectively. It is unclear how this product forms, however an electron must be lost in coincidence with a loss of water ligand. Examination of the third spectrum in the series (Fig. 5.3(c)) illustrates that the solvated species can be stripped down to the bare molecular ion:  $\text{S}_2\text{O}_3^-$  at  $m/z$  112. The exact nature of the process going from the solvated 2- molecular ion to the 1- bare ion is currently under investigation. The formation of the  $\text{S}_2\text{O}_3^-$  species is a consistent product when sampling with the high pressure CID source, however it is unknown whether this species forms in the same dominant manner under the conditions of low pressure CID.

From the above discussion it is apparent that some ions cannot be stripped down to their 'true' molecular ions, however they may be stripped down to characteristic molecular ions as indicators. In the above case the characteristic ions are  $\text{HSO}_4^-$  ( $m/z = 97$ ) for sulfate and  $\text{S}_2\text{O}_3^-$  ( $m/z = 112$ ) for thiosulfate.

It is clear that with some background knowledge of the sampling behavior of these species by high pressure CID it should be possible to differentiate between the various anions in solution. A test sample was prepared of equal molar concentrations of ammonium persulfate, sodium sulfate and sodium thiosulfate where each was  $10^{-4}\text{M}$  in methanol. Figure 5.4 contains two spectra, where spectrum (a) was acquired under fairly harsh CID conditions ( $\Delta V = 30\text{V}$ ) and spectrum (b) was acquired under gentler conditions ( $\Delta V = 10\text{V}$ ). Based on the

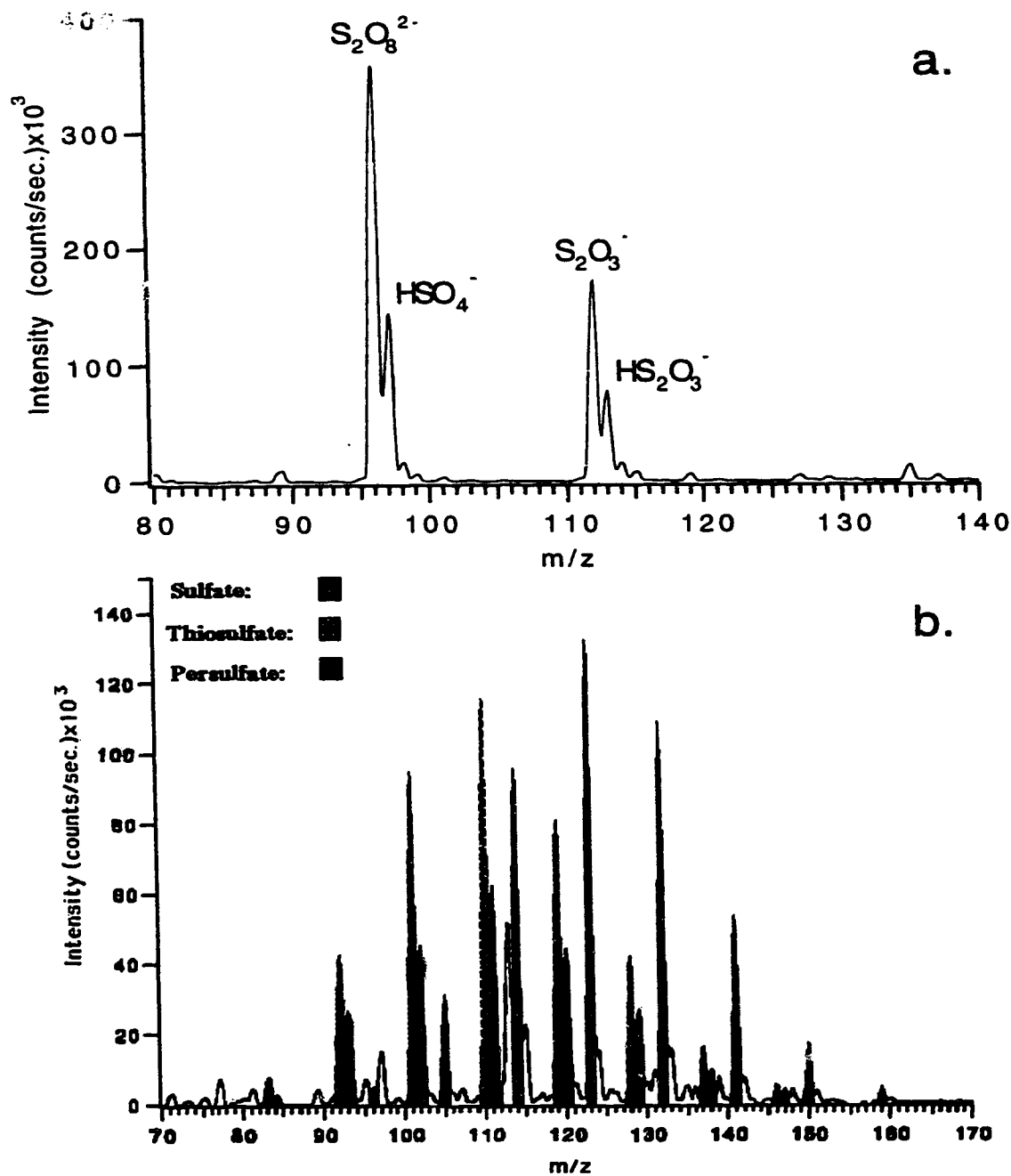
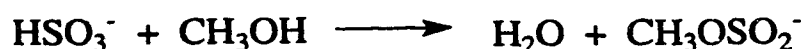


**Figure 5.4** Mixture of oxo-sulfur species; ammonium persulfate, sodium thiosulfate and sodium sulfate each  $1.0 \times 10^{-4} M$  in methanol. Spectrum a) was acquired with a sampling plate to skimmer potential difference of  $-30V$  and spectrum b) was acquired with a sampling plate to skimmer potential difference of  $-10V$ .

knowledge of the potential difference and characteristic peak assignments spectrum (a) indicates that the persulfate anion, the sulfate anion and the thiosulfate anion may be present, however the assignment may be ambiguous at best. It is not until the ions are sampled under gentler conditions (spectrum b) that this is confirmed. Examination of Fig. 5.4b illustrates the presence of the three distinct distributions of persulfate, sulfate, and thiosulfate, each highlighted in its own pattern. Not all species are stable in electrospray solvents let alone in aqueous solutions. One such species is the sulfite ion, which is only finitely stable in aqueous solutions, and is reactive in methanol solutions. Upon dilution of freshly prepared aqueous sulfite solution in methanol, the species:  $\text{CH}_3\text{OSO}_2^-$  is readily observed by electrospray. This is illustrated in Fig. 5.5, where in addition to the  $\text{CH}_3\text{OSO}_2^-$  species ( $m/z = 95$ ) being observed the presence of the minor species  $\text{HSO}_4^-$  is also detected. The origins of the  $\text{HSO}_4^-$  species is unclear however the ester may be formed via the scheme:



Scheme 5.4

When an aqueous sulfite solution is allowed to age (~ 1 month) the only observable species when diluted by methanol is sulfate. This indicates that sulfite slowly decomposes in aqueous solution to yield sulfate. Other species such as dithionite ( $\text{S}_2\text{O}_4^{2-}$ ) are also fairly unstable in aqueous solutions, and may decomposes rapidly depending on the pH [25]. Its decomposition products if stable in solution may of course be detected by ESMS.

From the above discussion it is obvious that the chemical character of the species is critical when obtaining information on them by ESMS. It was shown that large multiply charged anions are able to stabilize the charge internally, whereas smaller multiply charged ions need a supporting solvation sphere to be stable. If the ion gets to the point where it no longer has the necessary solvation, then charge separation reactions occur. It is important to be able to understand these processes in order to properly interpret the resulting mass spectra.

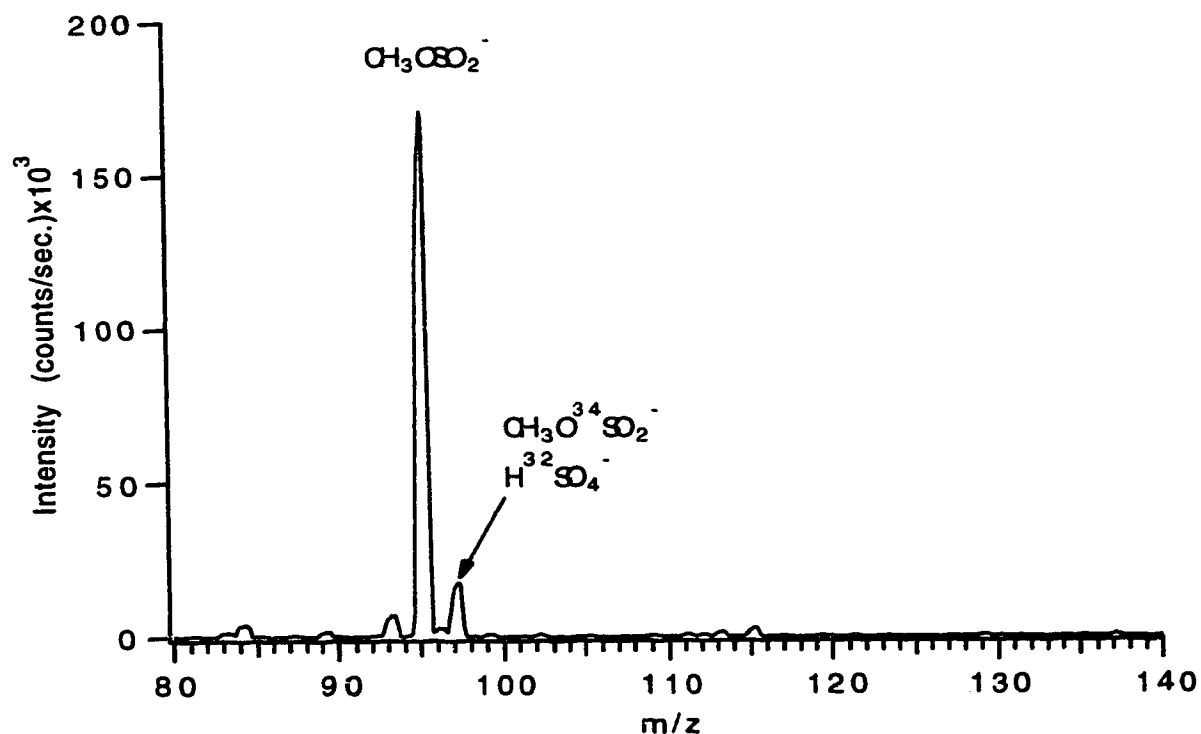


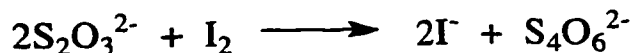
**Figure 5.5** Mass spectrum of sodium sulfite ( $1.0 \times 10^{-4}\text{M}$ ) in methanol. The spectrum was acquired with a sampling plate to skimmer potential difference of  $-20\text{V}$ .



### 5.3.2 Interpreting Reaction Mixtures

Sulfur ions in solution, especially various oxo-anions can be quite reactive. They can act both as reducing agents and oxidizing agents of various strengths in solution. For instance the thiosulfate and sulfite ions are known to have a moderate reducing character, whereas the peroxodisulfate ion is known to be a powerful oxidizing agent. This characteristic may be quite useful analytically, for example Koh *et al* [11-14] have determined many sulfur species spectrophotometrically based on the redox chemistry of these species.

Perhaps one of the most well known reactions is the use of thiosulfate in the volumetric determination of iodine, which proceeds according to the reaction:



Scheme 5.5

where the products are iodide and tetrathionate ions. This simple reaction system was examined by electrospray. The mixture consisted of  $1.02 \times 10^{-2}\text{M}$  iodine and  $2.23 \times 10^{-2}\text{M}$  thiosulfate in aqueous solution. Upon mixing and dilution the dark purple iodine solution immediately became clear, which is characteristic of its reduction to iodide. The solution after standing for two hours was then diluted with methanol (100X) and the resulting solution was electrosprayed. Figure 5.6 contains two spectra acquired under different sampling conditions; Fig. 5.6(a), at a potential difference of 15V and Fig 5.6(b), at 27V. Examination of Fig 5.6(a) reveals two distributions; the tetrathionate distribution stripped down to the bare tetrathionate ion at  $m/z$  112, and accompanying hydrates, as well as a distribution of thiosulfate species,

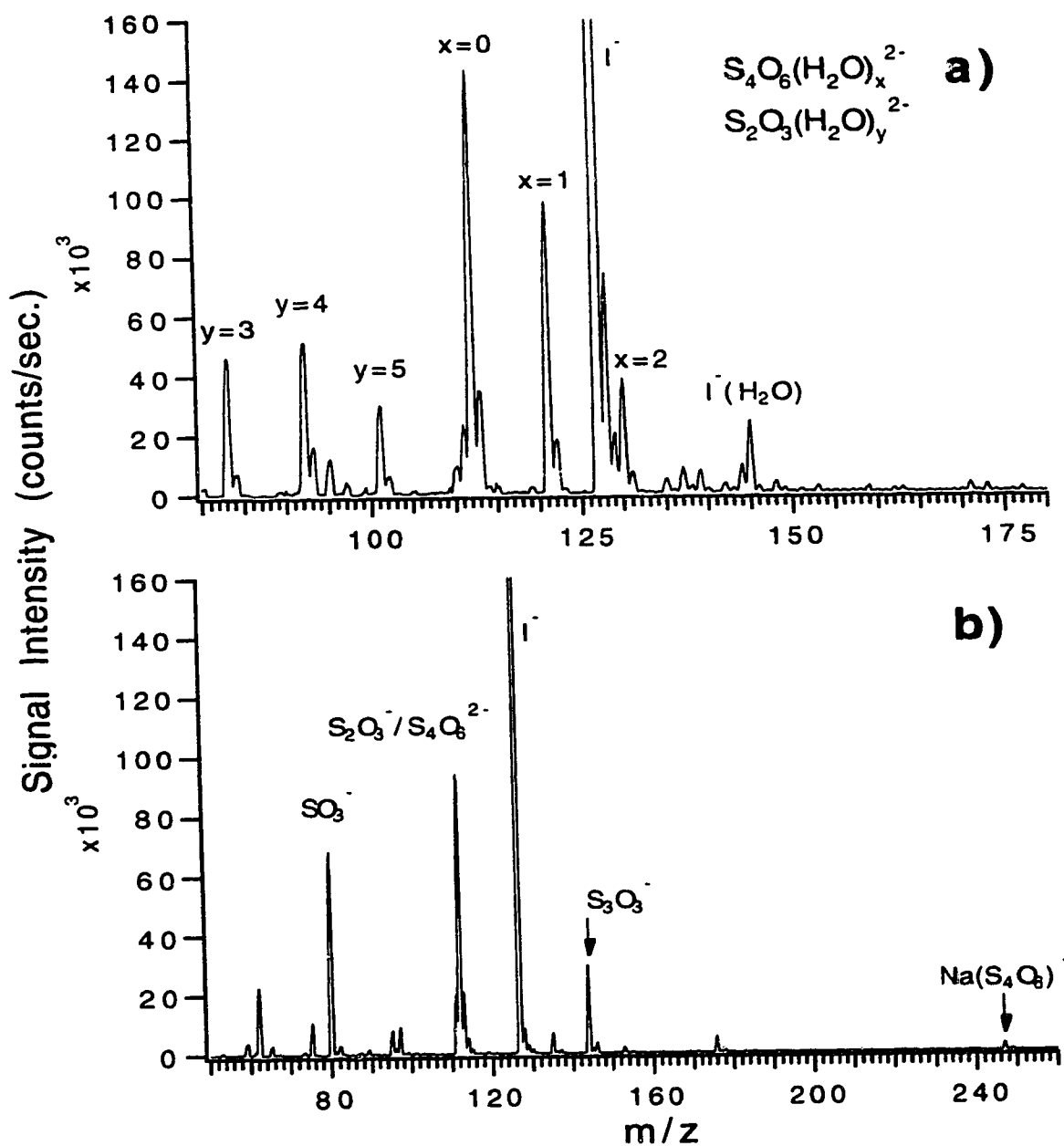
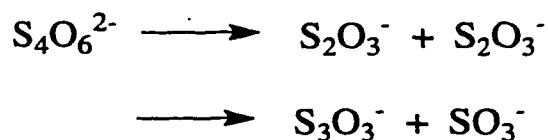


**Figure 5.6** Mass spectra of the reaction products from a solution of iodine ( $1.0 \times 10^{-2} M$ ) and sodium thiosulfate ( $2.0 \times 10^{-2} M$ ) diluted in methanol 100X. The spectra were acquired at a sampling plate to skimmer potential differences of a) -22V, and b) -27V.

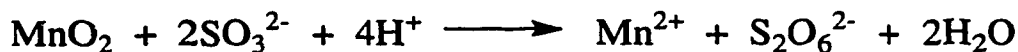
which was present in excess. The spectrum just highlights the hydrated species, however there are species such as  $\text{S}_4\text{O}_6^{2-}(\text{CH}_3\text{OH})$ ,  $\text{S}_4\text{O}_6^{2-}(\text{CH}_3\text{OH})_2$  and  $\text{S}_4\text{O}_6^{2-}(\text{CH}_3\text{OH})(\text{H}_2\text{O})$  present at  $m/z$  128, 144, and 137 respectively. The iodide ion is also present at  $m/z$  127. If the spectrum is acquired at a greater potential difference (Fig. 5.6(b)) ambiguous products shown below:



Scheme 5.6

are formed, which would not normally be found in solution. The tetrathionate ion because of its size can be stripped down to its bare form, at  $m/z$  112, however increasing the CID energy leads to the decomposition products as described above and as observed in Fig. 5.6(b). Although this is a relatively simple reaction system, the product ion, tetrathionate is readily observed by ESMS.

A second redox mixture system that was studied by ESMS is given in the scheme below:



Scheme 5.7

where sulfite is oxidized by manganese (IV) oxide, yielding the dithionate ion ( $\text{S}_2\text{O}_6^{2-}$ ). The reaction mixture consists of  $\text{MnO}_2$  (0.087g in 100mL volume total),  $2.05 \times 10^{-2}\text{M}$   $\text{SO}_3^{2-}$  and  $4 \times 10^{-2}\text{M}$   $\text{HNO}_3$ . The reaction mixture was allowed to stand for one day to ensure complete reaction upon which time it was diluted with methanol (100X) and then examined by electrospray. The results are

given in Fig. 5.7, the spectrum was acquired under fairly harsh stripping conditions in order to illustrate that the dithionate ion may be stripped down to its bare molecular ion. This is observed at  $m/z$  80 and is confirmed by its isotopic packet and in addition there is some residual hydrate at  $m/z$  89. If the CID energy is greatly increased the dithionate ion decomposes according to the following scheme:

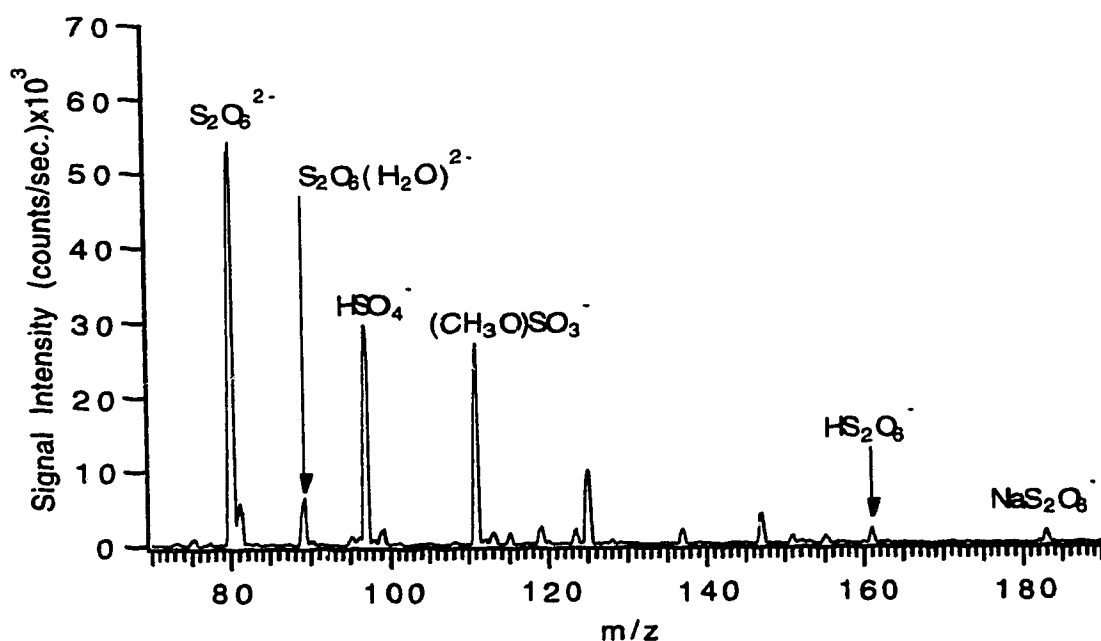


**Figure 5.7** Mass spectrum of the reaction products from a solution of  $\text{MnO}_2$  ( $1.0 \times 10^{-2}\text{M}$ ), Sodium sulfite ( $2.0 \times 10^{-2}\text{M}$ ) and nitric acid ( $4.0 \times 10^{-2}\text{M}$ ) diluted in methanol 100X. The spectrum was acquired with a sampling plate to skimmer potential difference of -22V.

In addition to the  $2^-$  species the protonated and sodiated adducts are also observed at higher  $m/z$ . The spectrum also shows two other ions of interest, those at  $m/z$  97 ( $\text{HSO}_4^-$ ) and  $m/z$  111 ( $\text{CH}_3\text{OSO}_3^-$ ), there

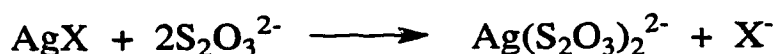
are however two possible explanations; the first being the oxidation of sulfite by Mn (IV) both in aqueous and methanolic solutions to yield the two products, the second is the reaction of the dithionate ion with methanol via the following scheme:



Scheme 5.9

It is unlikely that the above scheme occurs on its own in solution and may be acid or manganese (IV) catalyzed, or may be occurring as a result of some gas phase chemistry.

Sulfur species are also useful complexing agents and for example thiosulfate is used in the photographic processes. Thiosulfate solutions are typically used to complex unphotolyzed silver bromide from a photographic emulsion. In fact thiosulfate is able to complex with most silver ions in solution provided it is added in excess. When silver is the dominant ion a  $\text{Ag}_2(\text{S}_2\text{O}_3)$  precipitate will form which then gradually decomposes to  $\text{Ag}_2\text{S}$ . However in the case of thiosulfate being used in the dissolution and complexation of silver halides it is typically added in excess to ensure the reaction:



Scheme 5.10

The above reaction holds for any of the insoluble silver halides as the net stability constant for the above complex is on the order of  $5 \times 10^{13}$ . To examine this system a solution was prepared where  $\text{AgCl}$  (0.1433g in a total volume of 100mL) was dissolved in excess  $\text{S}_2\text{O}_3^{2-}$  ( $2.5 \times 10^{-2}$  M). The solution was allowed to sit for one day and then diluted 100X

in methanol and then examined by ESMS. The results are shown in Fig. 5.8. Figure 5.8(a) was acquired under fairly gentle conditions and the spectrum shows the distribution of solvated thiosulfate, as expected being added in excess and as well a second distribution of solvated  $\text{Ag}(\text{S}_2\text{O}_3)_2^{3-}$  species. This distribution ranges from 5 water ligands ( $m/z$  140.3) to 11 water ligands ( $m/z$  176.3) and species are separated by 6  $m/z$  units ( $18/3 = 6$ ). The  $\text{Ag}(\text{S}_2\text{O}_3)_2^{3-}$  species is only stable down to 5 hydrates. The spectrum in Fig. 5.8b is a high resolution spectrum and was acquired under slightly harsher sampling conditions. Some of the isotopic fine structure due primarily to the silver and sulfur isotopes, which becomes compressed three fold as it is a  $3^-$  species can be seen. The spectrum in Fig 5.8c was acquired under fairly harsh conditions and shows what happens when the  $\text{Ag}(\text{S}_2\text{O}_3)_2^{3-}$  is stripped lower than the minimum stabilizing ligand number (i.e. 5 water ligands). Consistent with the previous discussion on thiosulfate one of the thiosulfate ligands loses an electron in some unknown manner to form an electron deficient species as shown at  $m/z$  165.5 ( $\text{Ag}(\text{S}_2\text{O}_3)_2^{2-}$ ). The complex further decomposes to the  $\text{Ag}(\text{S}_2\text{O}_3)^-$  species as observed at  $m/z$  219, with increased CID energy. The above species isotopic abundance's are consistent with the calculated values as shown by the two examples given in Fig. 5.9.

The above discussion illustrates electrosprays' strength as an investigative probe into solution chemistry. Where reaction mixtures or complex mixtures of species may be investigated and meaningful results obtained. In some cases however the sample may be too complex and therefore separation techniques must be used in order to properly evaluate a sample. The use of ESI or ion spray-coupled

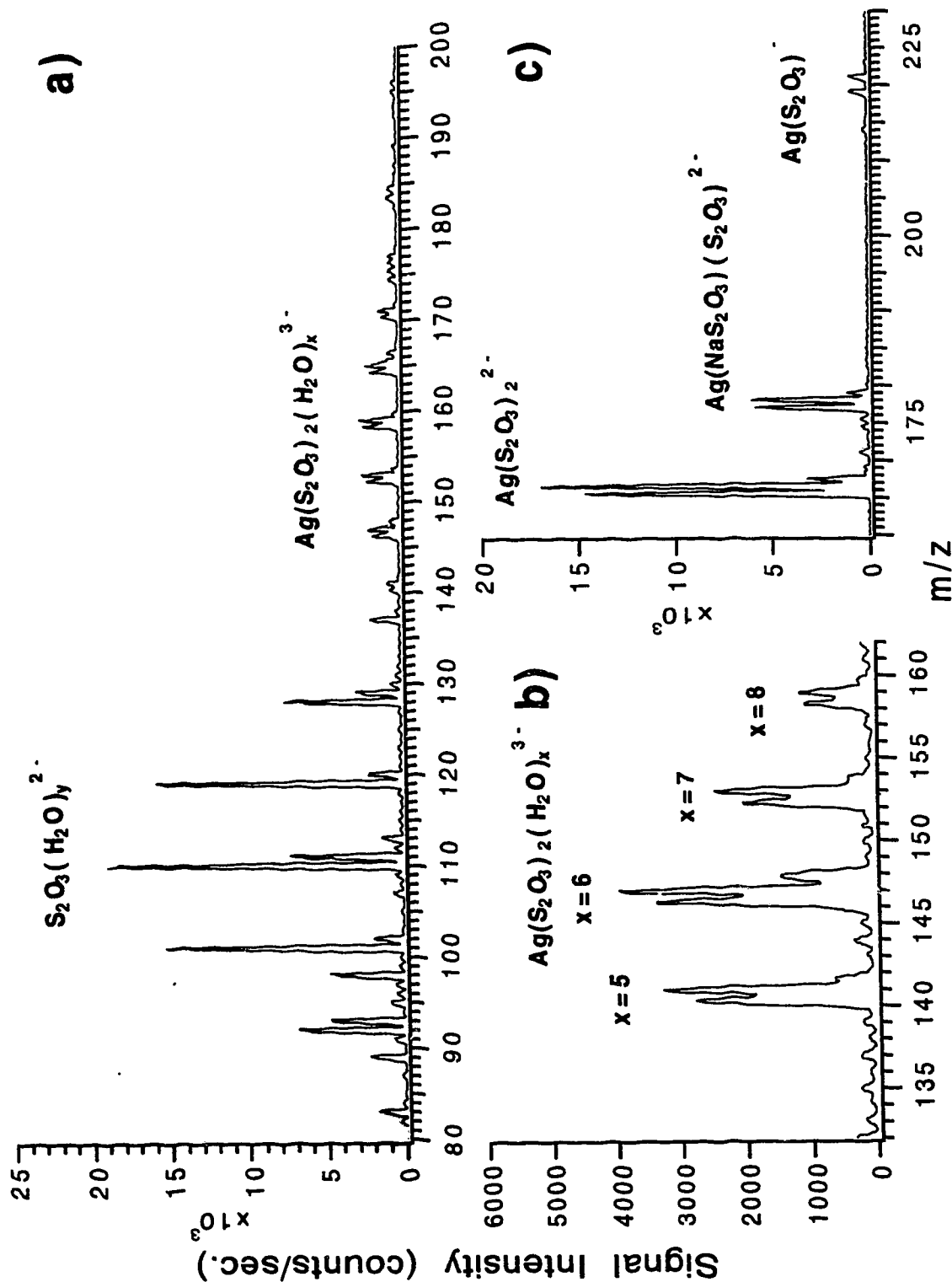


**Figure 5.8** Mass spectra of the reaction products from a solution of silver chloride ( $5.0 \times 10^{-3} M$ ), dissolved by sodium thiosulfate ( $2.5 \times 10^{-2} M$ ) in aqueous solution. The sample was then diluted 100X in methanol. The spectra were acquired at different sampling plate to skimmer potential differences; a) -9V, b) -14V (high resolution) and c) -24V.

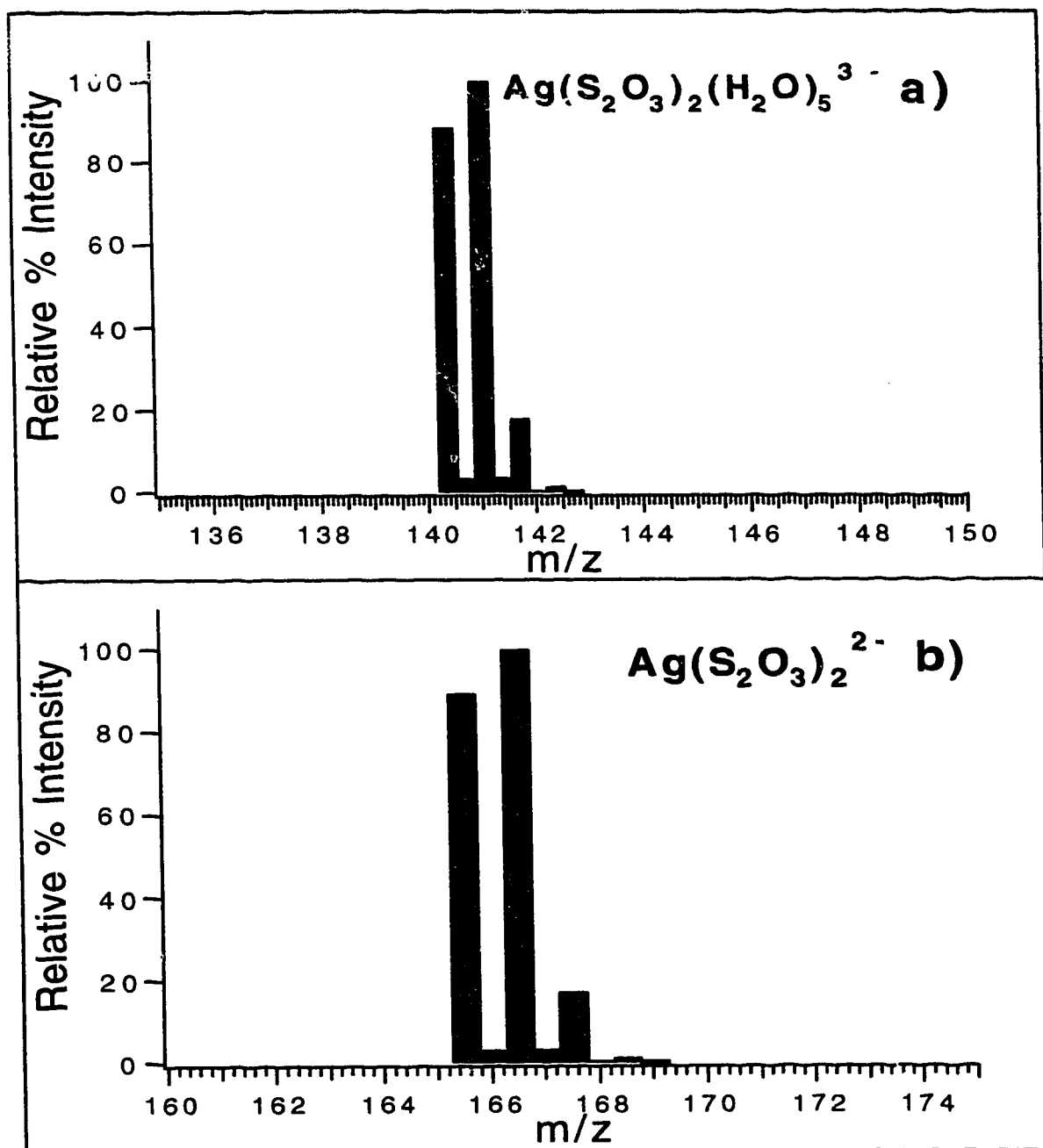


**Figure 5.9** Relative isotopic abundance's silver thiosulfate complexes; a)  $\text{Ag}(\text{S}_2\text{O}_3)_2(\text{H}_2\text{O})_5^{3-}$ , b)  $\text{Ag}(\text{S}_2\text{O}_3)_2^{2-}$ .

techniques has focused for the most part on biological compounds [27-28] however some groups have investigated inorganic systems [20]. It



is clear that ESMS can be a powerful probe of inorganic solution species.

### 5.3.3 Quantitative Studies: Preliminary Data

To date there has been a decided lack of information regarding the quantitative aspects of electrospray mass spectrometry. This is probably because of the subtle complexity of the technique. The concentration response is inherently non-linear and has been described by Agnes *et al* [29]. There is also a lack of standard reference materials for many anionic compounds such as sulfur species. As a result there is a real challenge to find ways to accurately quantitate samples by electrospray mass spectrometry. This work is currently being investigated in our laboratory and an in depth study will be presented in a future paper. Some preliminary results of that study which are encouraging but by no means definitive, are presented here. To achieve linearity in the calibration curve the analyte signal is typically ratioed against an internal standard or an electrolyte buffer. In addition to account for matrix affects, which can be quite severe in some cases, the preferred method of quantitation is standard addition.

A calibration curve for sulfate is presented in Fig. 5.10. Harsh CID conditions were utilized, thus the signal measured was that for  $\text{HSO}_4^-$  at  $m/z$  97 (see Fig. 5.2(b)). Iodide ( $\text{I}^-$  at  $m/z$  127) was used as the internal standard and was present in all solutions at a level of  $1 \times 10^{-4}\text{M}$ . The response was linear over the two orders of magnitude shown with the slope of the log-log plot being  $1.01 \pm 0.02$ . The correlation coefficient was 0.998. The detection limit for sulfate

based on three times the standard deviation of the background at  $m/z$  122 was 1 ppb. The background position at  $m/z$  122 was selected as there is not an ion present at this point under the conditions sampled, and thus this value should reflect the detection limit of a sample not contaminated by sulfate. Sulfate is a fairly common anion and may be present as an impurity in reagents or solvents. Therefore great care must be taken in sample and standard preparation. As an example, a sample was run consisting of just  $10^{-4}$ M iodide in methanol. The background sulfate concentration was found to be  $3.60 \pm 0.26$  ppb based on the above plot. In either case the above results indicate the types of sensitivities obtainable by electrospray and detection limits may be blank limited and thus higher than the 1ppb indicated above.

The applicability of this technique to a real life sample was investigated. A waste water sample was examined using electrospray mass spectrometry. The sample was originally collected to look at a series of cations and anions in a waste water sample collected from a landfill site. Sulfate was determined to be present at  $6.10 \pm 0.61 \times 10^{-3}$  M in the sample by an independent laboratory using ion chromatography.

A mass spectrum of the sample was obtained (see Fig. 5.11) by diluting the sample 100X in methanol and the mass spectrum was acquired with a sampling plate to skimmer potential difference of 40V. Note the presence of  $\text{CH}_3\text{O}^-$  ( $m/z = 31$ ), and  $\text{CH}_3\text{OCO}_2^-$  ( $m/z$  75) which are typical negative background ions indicative of basic solutions. The presence of sulfate in the sample is indicated by the signals for  $\text{HSO}_4^-$  and  $\text{NaSO}_4^-$  at  $m/z$  97 and 119. Other anions observed include  $\text{F}^-$ ,  $\text{Cl}^-$ ,  $\text{NO}_2^-$ , and  $\text{NO}_3^-$ .

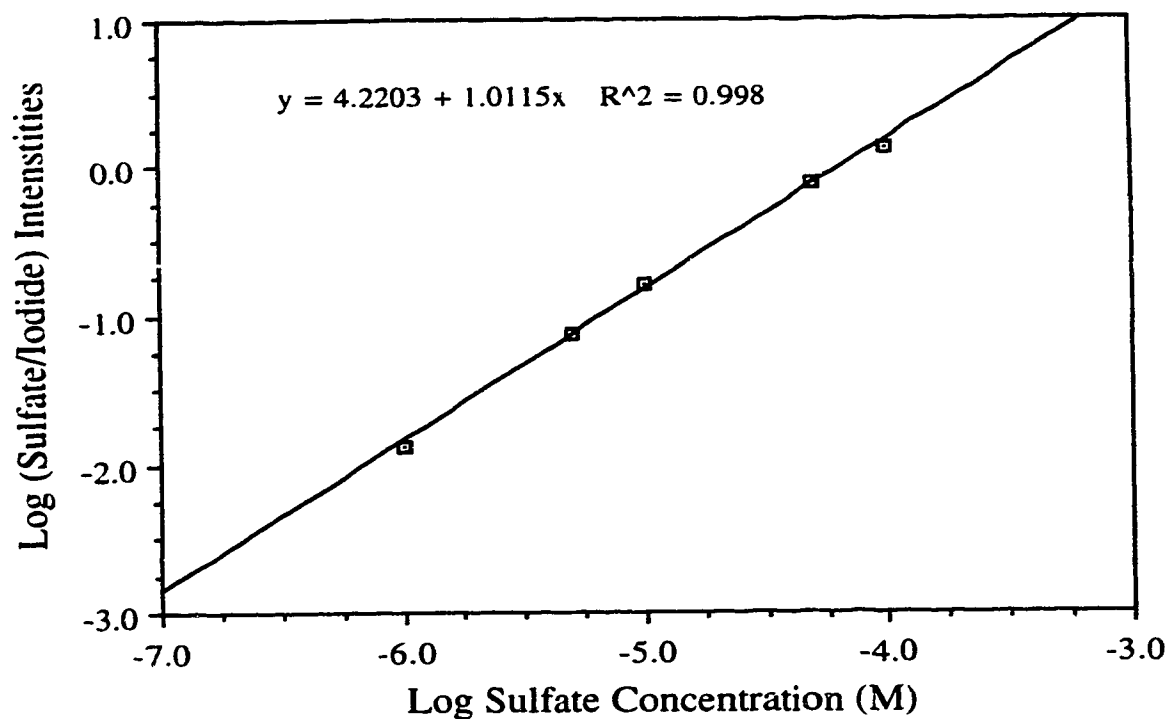


**Figure 5.10** Log-log calibration curve for sodium sulfate in methanol by ESMS the log of the sulfate intensity as ratioed against a  $1.0 \times 10^{-4}$  M KI internal standard response is plotted versus the log of the sulfate concentration.

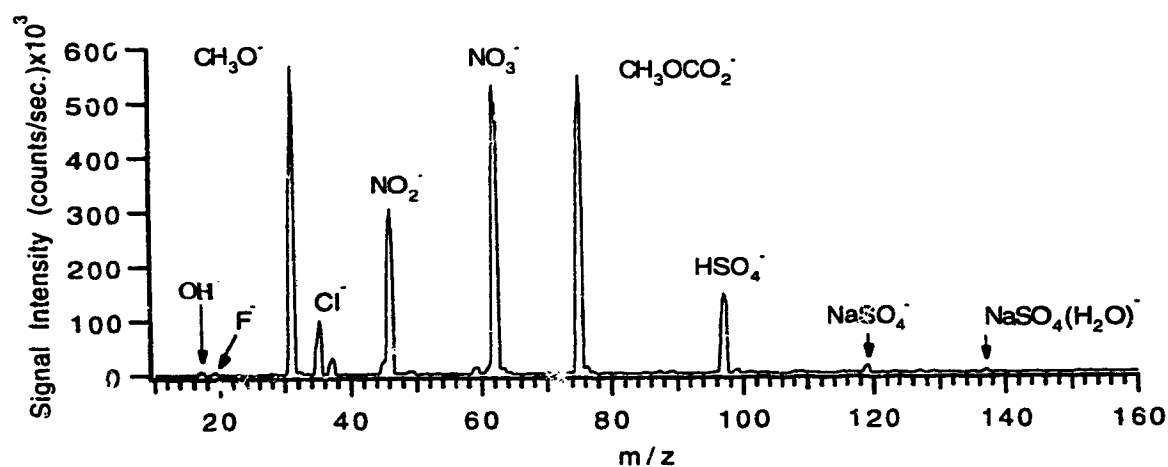


**Figure 5.11** Mass spectrum of a waste water sample. The sample was diluted 100X in methanol and acquired with a sampling plate to skimmer potential difference of -40V.

A major problem associated with quantitation by electrospray is that the response of the analyte and internal standard may not behave similarly upon addition to or variation of the sample matrix. Variation in an ions intensity with concentration has been discussed in the literature [23]. It is therefore desirable to match the matrix as closely as possible to minimize these effects. The standard addition technique should allow for this.

Sample preparation involved diluting 0.33 mL of the sample with KI internal standard ( $KI = 1.0 \times 10^{-4} M$ ). Prior to dilution, aliquots of a standard  $Na_2SO_4$  were added to the sample to afford the standard addition. The samples were then injected from a  $0.50 \mu L$  sample loop into a flowing stream of internal standard ( $KI = 1.0 \times 10^{-4} M$ ) solution. The standard addition calibration curve is shown in Fig. 5.12. The signal level used for sulfate was the sum of the intensities for  $HSO_4^-$  and  $NaSO_4^-$  and five replicates were used for each point. Using least squares calculations the sulfate concentration was determined to be  $4.87 \pm 0.33 \times 10^{-3} M$ . This of course gives the combined total concentration of  $H^{97}SO_4$  and  $Na^{97}SO_4$  observed mass spectrometrically, therefore to calculate the the total sulfate one needs to incorporate the other isotopes. Table 5.1 below gives the relative isotopic abundances for sulfate species as a function of sulfur isotope.

**Table 5.1:** Relative isotopic abundance of various sulfate species.

isotope S	$SO_4^{2-}$	$HSO_4^-$	$NaSO_4^-$	$\%SO_4^{2-}$
32	100	100	100	93.72
33	0.96	0.98	0.96	0.90
34	5.25	5.25	5.25	4.92
35	0.01	0.02	0.01	0.01
36	0.06	0.06	0.06	0.06

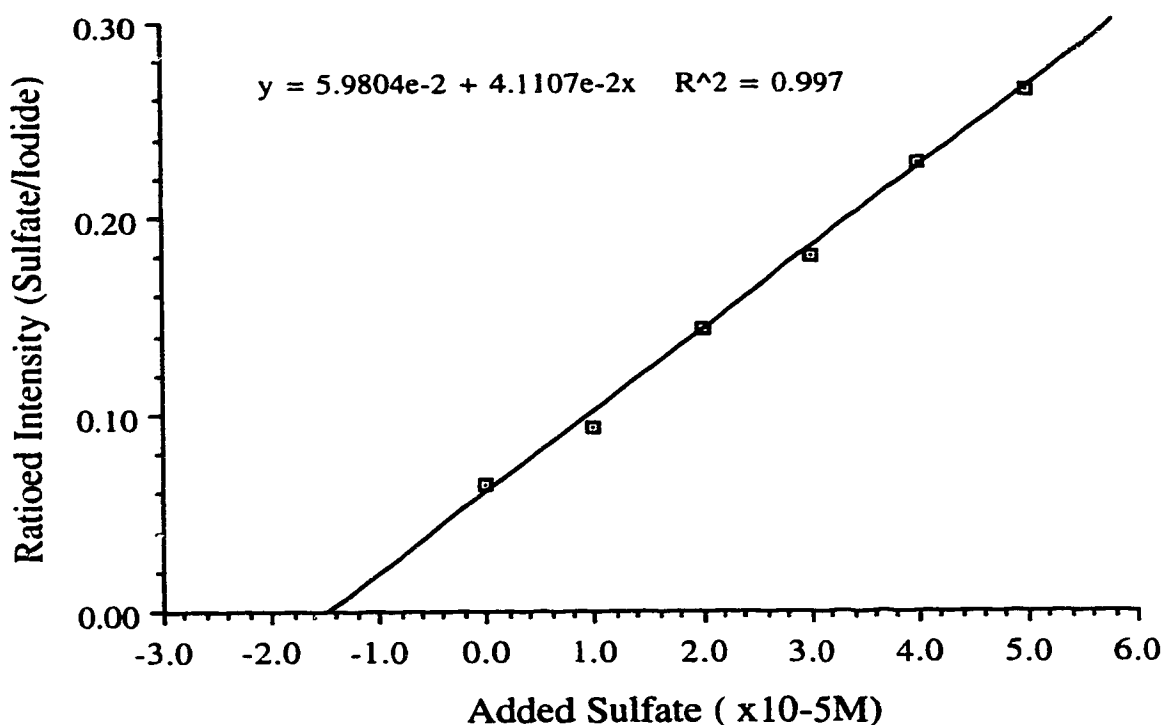


**Figure 5.12** Standard addition calibration curve for sulfate ion in a waste water sample by ESMS the total sulfate intensity is ratioed against a  $1.0 \times 10^{-4}\text{M}$  KI internal standard response and plotted versus added sodium sulfate concentration.

Therefore the reported value of  $4.87 \pm 0.33 \times 10^{-3}\text{M}$  is actually only 93.72% of the total value. The total sulfate in the sample is then actually  $5.20 \pm 0.35 \times 10^{-3}\text{M}$ . If this value is then compared to the reported value of  $6.10 \pm 0.61 \times 10^{-3}\text{M}$  (determined earlier from an independent laboratory) it is found to be 14.8% lower than expected. There is however overlap within the two limits of error associated with each number. The difference is however quite significant and may be due to several factors such as; the original sample analysis may have been inaccurate, the sample which was run 1 month after collection may have had its speciation altered in this time, or the

response or activity of the sulfate ion or adduct ions in methanol may not be the same as in aqueous solutions. The fact that the isotope ratio was assumed constant and therefore only the major isotope needed to be monitored may also have contributed to error in no small amount. Although the results are not accurate enough to seem analytically useful, they are promising especially as these are only preliminary results.

## 5.4 Conclusions

The ability of electrospray to generate intact gas phase ions representative of solution ions opens up a whole new avenue for speciation work. In many ways it is an ideal source to couple to mass spectrometry as it retains key chemical information about the nature of the elements in a sample that mass spectrometry is capable of determining (i.e., molecular form and charge state), information that, for example, is generally destroyed when using inductively coupled mass spectrometry. The sampling of these ions is for the most part understood however there are avenues open for further fundamental studies which may concentrate on energy deposition in the desolvation process (e.g., ion kinetic energies as a function of CID energy and state of desolvation and fragmentation on the resultant energies). However, it is also clear from this study that for every determination considerable work must be done to properly understand the qualitative results of ESMS and in particular more work is required to define the concentration response of ions by electrospray in order to properly and accurately quantitate them.

## 5.5 Appendix: Existence of the Bare Peroxodisulfate Ion

The solvated peroxodisulfate anion spectrum (gentle conditions) is shown in Fig. 5.13a. The solvation distribution ranges from 1-7 water molecules. As the potential difference at this stage is on the order of 20V the actual ions sampled will have solvation spheres much greater than this, probably on the order of 15-20 water molecules. When the potential difference is increased to 25V the distribution shifts from 1-7 down to 0-5 water molecules as shown in Fig. 5.13b. At this point the peak at  $-m/z$  96 is probably the bare  $S_2O_8^{2-}$  anion as the energy provided via CID seems to be consumed primarily by declustering collisions rather than fragmentation of the molecular ion. Note too, in both spectra, the species  $HS_2O_8^-$  is observed at  $-m/z$  193.

The spectra in Fig. 5.14 illustrate the probable turning point, ie. where the energy provided by CID exceeds that required to completely decluster the solvated ions being sampled by the mass spectrometer. Therefore the additional energy is probably imparted into the fragmentation of the molecular ion. The two spectra in Fig. 5.14 correspond to potential differences of 35V(a) and 40V(b). In Fig. 5.14a the bare molecular species at  $-m/z$  96 as well as small contributions by the mono and di solvated species at  $-m/z$  105, 112, and 114 can be seen. When the potential difference is increased to 40V (Fig. 5.14b) there are two important points to note; the first being a doubling of the intensity of the peak at  $-m/z$  98 and the formation  $HSO_5^-$  at  $-m/z$  113.

With regards to the first point there is a minor increase in the overall peak intensity at  $-m/z$  96 of ~5% (~60000 counts/second) with

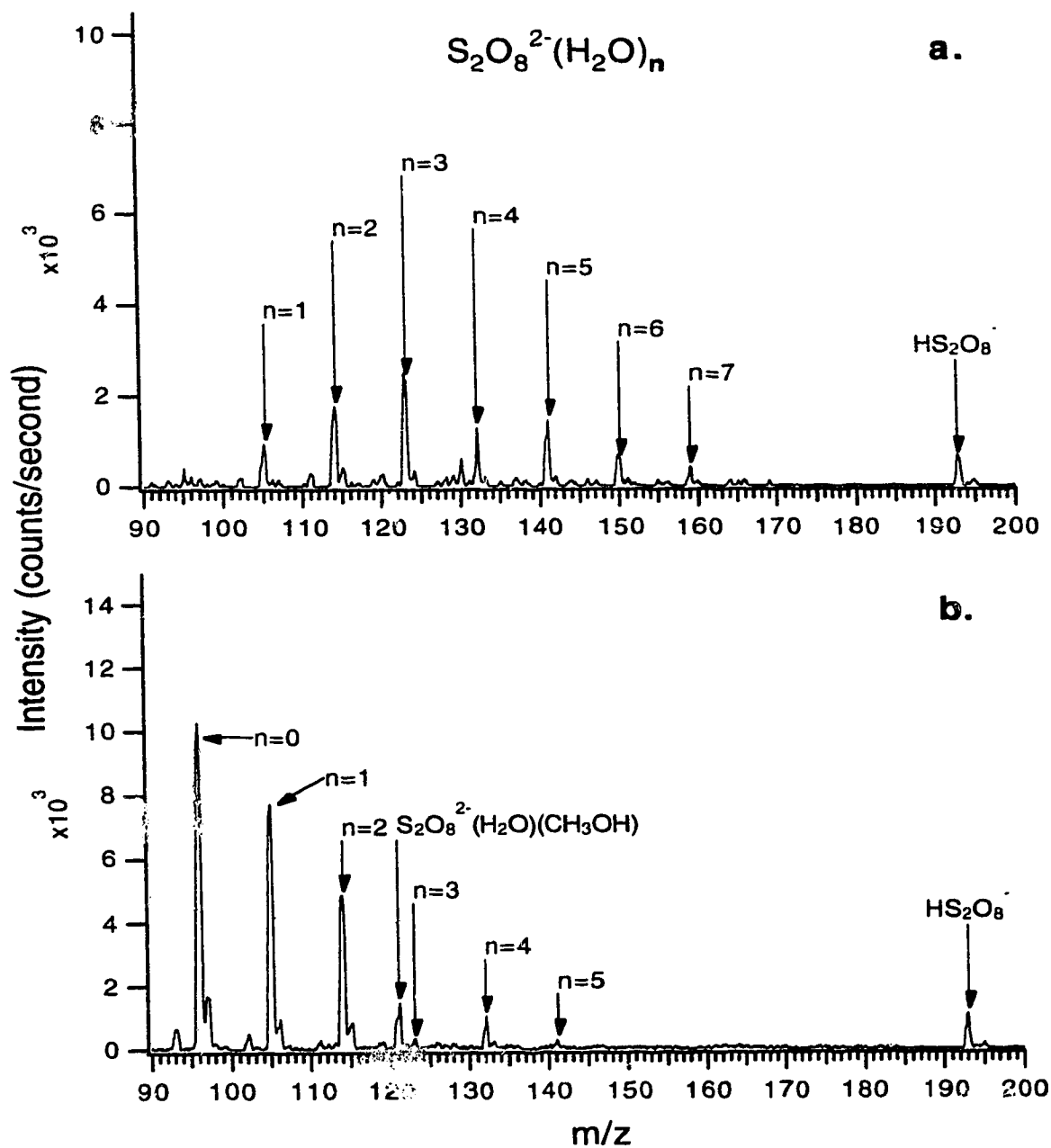
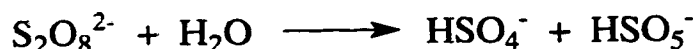


**Figure 5.13** Negative ion mass spectra of  $2.0 \times 10^{-4}\text{M}$  ammonium persulfate in methanol obtained with a sampler to skimmer potential difference of **a.**; 20V, and **b.**; 25V.



a corresponding doubling of the peak at  $-m/z$  98 (~2500 counts/second). This large increase at  $-m/z$  98 is probably due to the start of the formation of  $\cdot\text{SO}_4^-$ , as a result of molecular fragmentation (see Fig. 5.16).

The second point indicates that a hydrolysis reaction is occurring between the last water ligand and the peroxodisulfate anion. This suggests a second pathway for the decomposition of the solvated peroxodisulfate anion as shown in the scheme below:



Scheme 5.11

If the formation of peroxomonosulfate is quantitative then the formation of  $\text{HSO}_4^-$  must also be quantitative. This is difficult to see as there is only ~ 1000 counts per second produced. However it does seem that once a certain energy barrier is overcome there is portion of peroxodisulfate that is converted to peroxosulfate in preference to further ligand loss. This fraction increases as the potential difference is increased (70V) as shown by the spectrum given in Fig. 5.15.

The isotopic distribution at  $-m/z$  96 shown in the spectrum (Fig. 5.15) is that primarily of the singly charged sulfate radical anion (see Fig 5.16). Thus as one increases the potential difference to 70V it seems obvious that the peroxodisulfate anion is being converted into the sulfate radical ion of the same  $-m/z$  as the isotopic ratio pattern changes. The increased energy has also led to the formation of more peroxomonosulfate at  $-m/z$  113 as well as a decomposition product  $-m/z$  80 corresponding to  $\text{SO}_3^-$ .

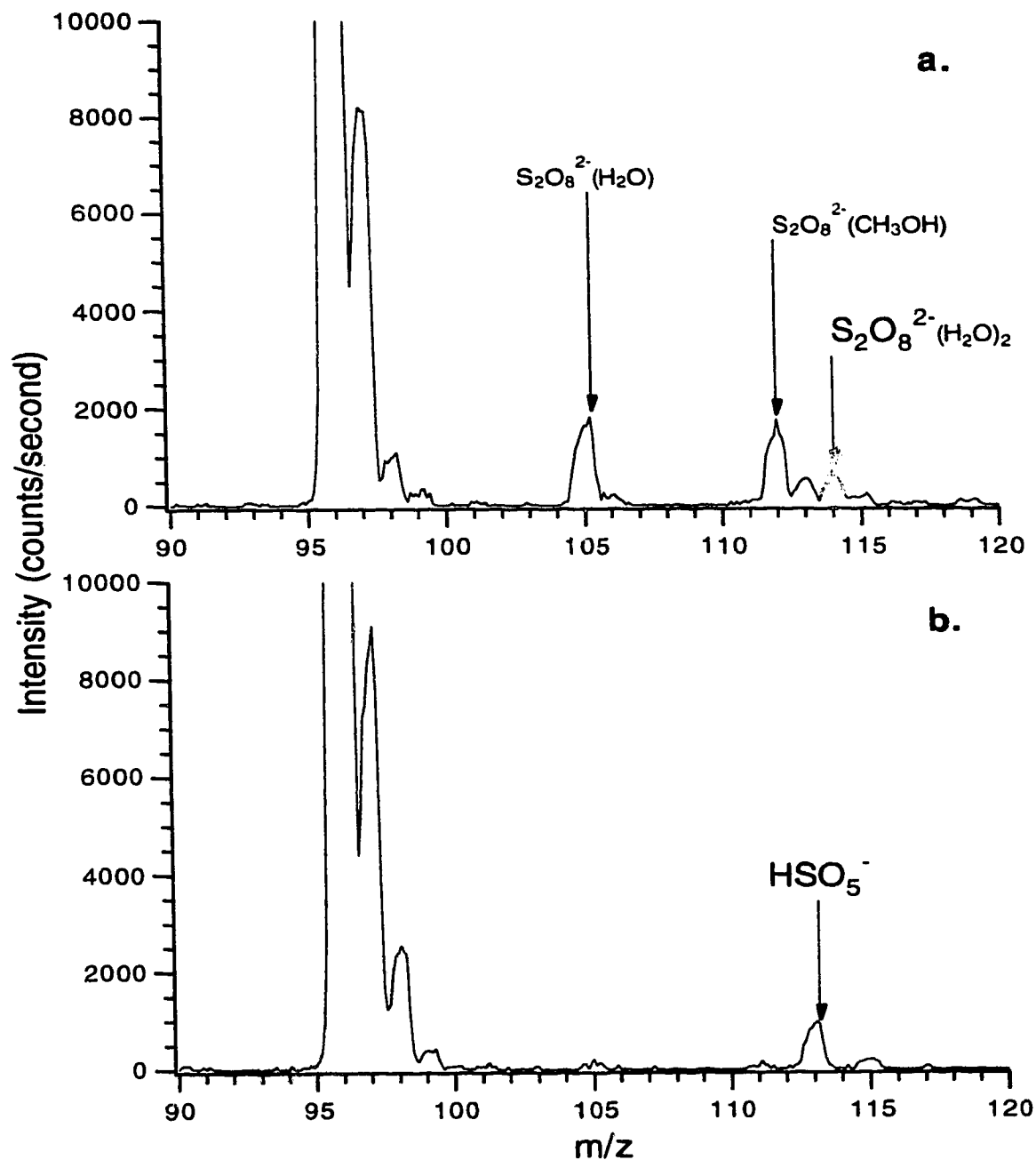
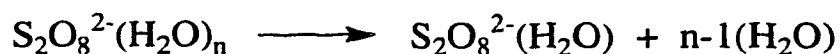
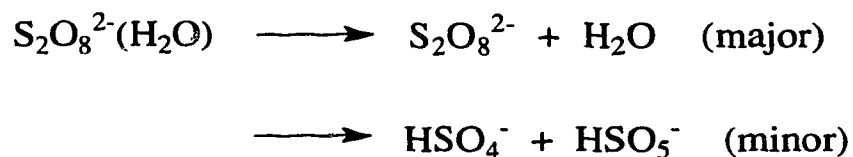


**Figure 5.14** Negative ion mass spectra of  $2.0 \times 10^{-4}M$  ammonium persulfate in methanol obtained with a sampler to skimmer potential difference of a); 35V, and b); 40V.

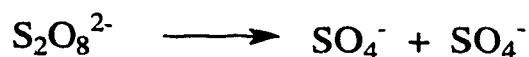
Based on these spectra it seems reasonable to conclude that peroxodisulfate does exist under 'gentle' CID conditions. Once a certain CID energy threshold is exceeded  $\text{S}_2\text{O}_8^{2-}$  is ultimately converted into the radical sulfate anion. Based on the CID spectral evidence obtained a proposed series of events is illustrated in the following schematic:



Scheme 5.12



Scheme 5.13



Scheme 5.14

The mechanism responsible for formation of the sulfite anion at  $-m/z$  80 is still unclear. Its origin may stem from the fragmentation of several possible parent ions:  $\text{S}_2\text{O}_8^{2-}$ ,  $\text{HS}_2\text{O}_8^-$ ,  $\text{HSO}_5^-$  or  $\cdot\text{SO}_4^-$ . It seems most plausible that energetic collisions with one of the first two ions with nitrogen could lead to the formation of  $\text{SO}_3^-$ . A decomposition of  $\text{S}_2\text{O}_8^{2-}$  could yield  $\cdot\text{SO}_3^-$  and  $\cdot\text{SO}_5^-$  however there is no  $\cdot\text{SO}_5^-$  present in the spectra. This may be due to the fact that as it is formed it picks up a proton via a gas phase transfer.

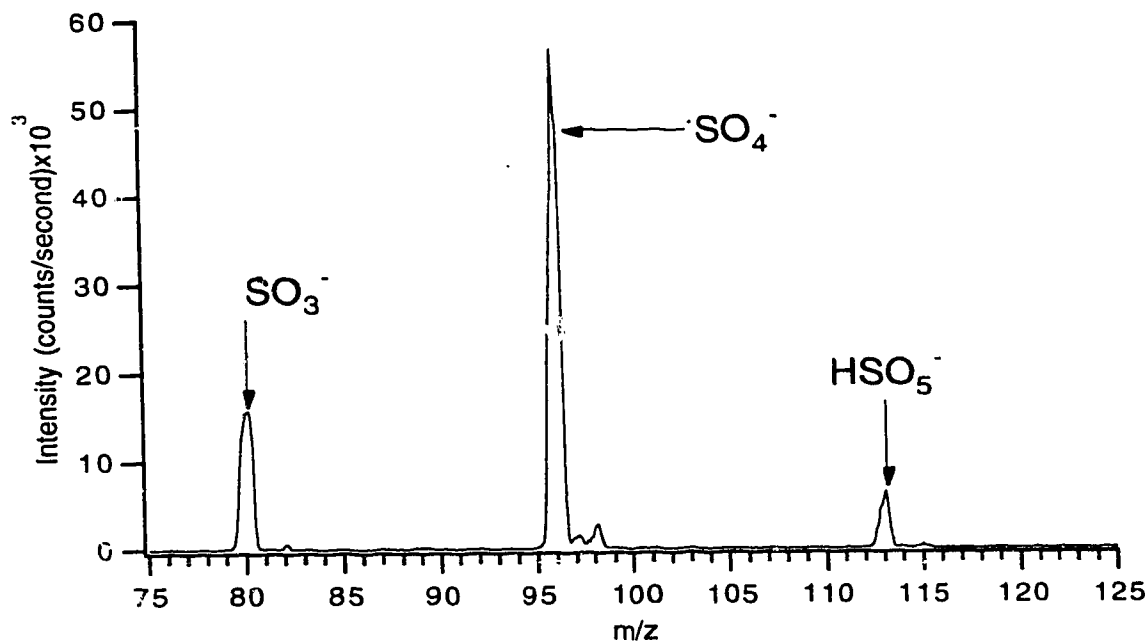
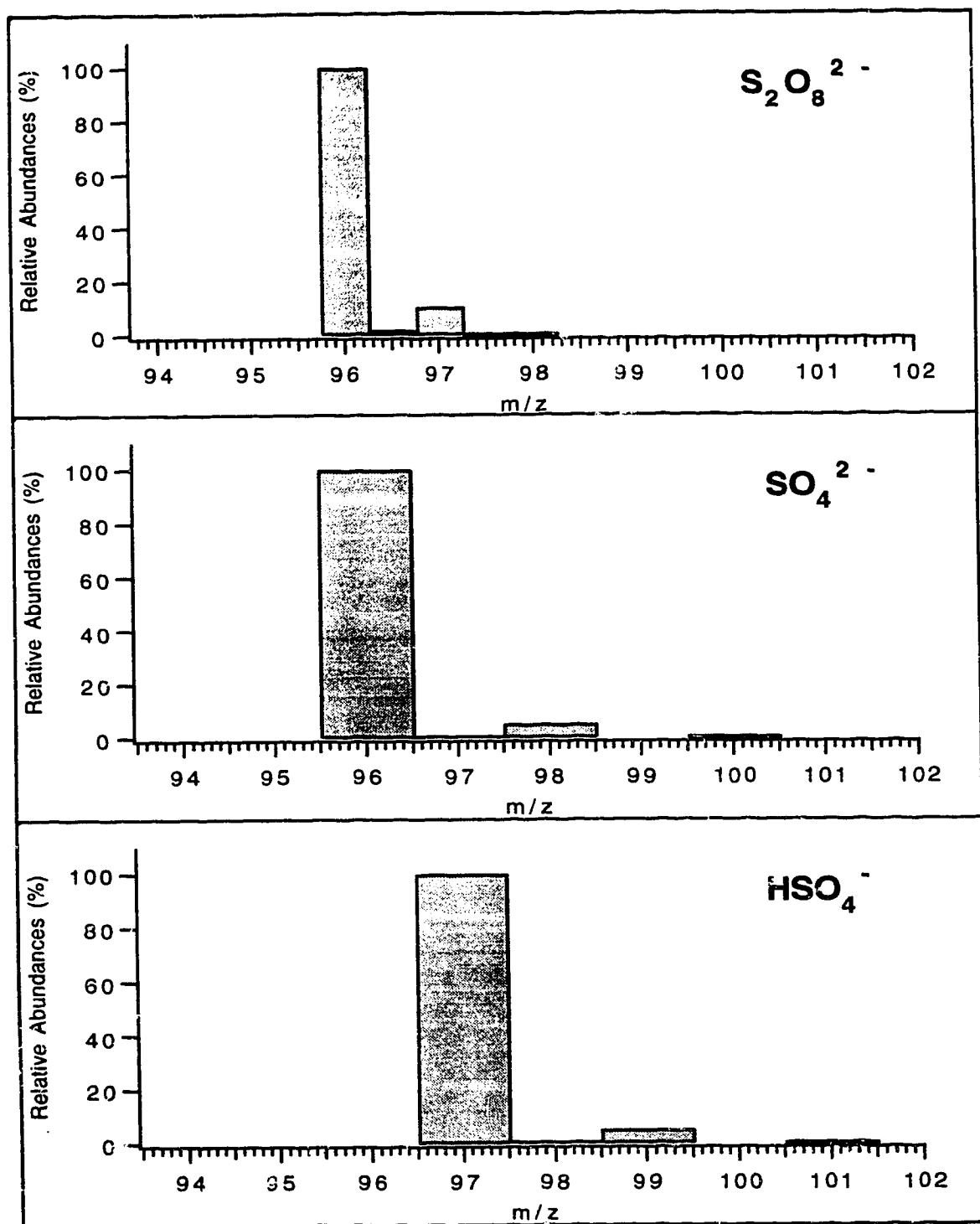


Figure 5.15 Negative ion mass spectra of  $2.0 \times 10^{-4}$  M ammonium persulfate in methanol obtained with a sampler to skimmer potential difference of 70V.

With this knowledge in mind it would seem likely that the species observed at  $-m/z$  96 in Figure 4e of the recent report [30, 18] was probably for the most part the radical sulfate anion with some peroxodisulfate anion present as well. The use of frame by frame CID work shows quite well how one is able to identify peaks of questionable origin that are present in ES-MS spectra. It also highlights the abundance of qualitative information that may be obtained from an electrosprayed solution. Similar results have also been observed by Blades and Kebarle [26].



**Figure 5.16** The relative isotopic abundance of  $S_2O_8^{2-}$ ,  $SO_4^{2-}$  and  $HSO_4^-$

## 5.6 References

1. M.B., Goldhaber, *Am. J. Sci.*, **283**, 193 (1983).
2. R.P. Singh, R.P. and G.H. Nancollas, *J. Chromatog.*, **433**, 373 (1988).
3. A.P. Bruins, T.R. Covey, and J.D. Henion, *Anal. Chem.*, **59**, 2642 (1987).
4. B. Takano, M.A. McKibben, and H.L. Barnes, *Anal. Chem.*, **56**, 1594 (1984).
5. Y. Miura, M. Tsubamoto, and T. Koh, *Anal. Sci.*, **10**, 595 (1994).
6. R. Steudal, and G. Holdt, *Chrom.*, **651**, 379 (1986).
7. S.B., Rabin, and D.M. Stanvury, *Anal. Chem.*, **57**, 1130 (1985).
8. B.L., De Backer, L.J. Nagels, F.C. Alderweireldt and P.P. Van Bogaert, *Anal. Chim. Acta*, **273**, 449 (1993).
9. M. Geissler, and R. Van Eldik, *Anal. Chem.*, **64**, 3004 (1992).
10. B.J. Wildman, P.E. Jackson, W.R. Jones, and P.G. Alden, *J. Chromatog.*, **546**, 459 (1991).
11. T. Koh, and K. Taniguchi, *Anal. Chem.*, **46**, 1679 (1974).
12. T. Koh, Y. Miura, M. Suzuki, M., *Anal. Sci.*, **4**, 267 (1988).
13. T. Koh, Y. Miura, M. Ishimori, and N. Yamamuro, *Anal. Sci.*, **5**, 79 (1989).

14. T. Koh, N. Takahashi, and K. Yokoyama, *Anal. Sci.*, **10**, 765 (1994).
15. K.E., LaFreniere, V.A. Fassel, and D.E. Eckels, *Anal. Chem.*, **59**, 879 (1987).
16. D.T. Gjerde, D.R. Weiderin, F.G. Smith, B.M. Mattson, *J. Chromatogr.*, **640**, 73 (1993).
17. J.W. Olesik, J.A. Kinzer, and S.V. Olesik, *Anal. Chem.*, **67** 1 (1995).
18. G.R. Agnes, I.I. Stewart and G. Horlick, *Appl. Spectrosc.*, **48**, 1347 (1994).
19. G.R. Agnes and G. Horlick, *Appl. Spectrosc.*, **48**, 655 (1994).
20. T.G. Huggins, and J.D. Henion, *Electrophoresis*, **14**, 531 (1993).
21. M. Yamashita and J.B. Fenn, *J. Phys. Chem.*, **88**, 4451 (1984).
22. I. Hayati, A.I Bailey, and TH. F. Tadros, *J. Colloid. Interface Sci.*, **117**, 205 (1987).
23. P. Kebarle and L. Tang, *Anal. Chem.*, **65**, 972A (1993).
24. I.I. Stewart and G. Horlick, *Anal. Chem.*, **66**, 3983 (1994).
25. F.A. Cotton, and G. Wilkinson, "*Advanced Inorganic Chemistry. A Comprehensive Text*" Fifth Edition, Interscience, New York N.Y., p.687, 1988.
26. A.T. Blades, and P. Kebarle, *J. Am. Chem. Soc.*, **116**, 10761 (1994).

27. R.D. Smith, J.H. Wahl, D.R. Goodlett, and S.A. Hoftstadler, *Anal. Chem.*, **65**, 574A (1993).
28. R.D. Smith, C.J. Barinaga, and H.R. Udseth, *Anal. Chem.* , **60**, 1948 (1988).
29. G.R. Agnes and G. Horlick, *Appl. Spectrosc.*, **48**, 649 (1994).
30. G.R. Agnes, Doctoral Thesis; "*Elemental Electrospray Mass Spectrometry*", chapter 7, spring (1994).



## **Chapter 6**

### **Electrospray: Current Implications**

## 6.1 Introduction

The electrostatic spraying of liquids or "electrospray" is a complex phenomenon. Much of the early fundamental work on electrospray was carried out during the past century by Zelany [1]. This work was continued by other researchers, for example, Vonnegut and Neubauer [2], Taylor [3,4], and Pfeifer and Hendricks [5]. The technique quickly found application in a wide variety of fields such as paint spraying, electrostatic printing, fuel atomization, and crop spraying. In 1968, *Dole et al.* [6] showed that the technique was useful in generating large intact gas phase macroions (polymers), a task which was notoriously difficult without sample degradation. It was not until the 1980's when Yamashita and Fenn [7,8] successfully coupled the technique to mass spectrometry that it really attained attention from the scientific community. Since then, there has been a literal explosion of applications. Biological applications dominate this technology, ranging from molecular weight determinations of large biological ions, to potential sequence information from peptides, to metal complexes with proteins, peptides and amino acids. The technique is also used in numerous studies of inorganic and organometallic solution systems. A number of researchers performed investigations on inorganic solutions with both complexed [9-14] and uncomplexed metal ions [15-18]. This led to the investigation of inorganic solutions for the purpose of elemental analysis and speciation work [19-28].

The successful coupling of electrospray with mass spectrometry and the resultant explosion of applications raised a number of fundamental questions regarding certain aspects of the mechanisms

associated with the electrospray phenomena. To properly evaluate, interpret and plan experiments it is important to understand from a very basic level the normal operation of the technique as it pertains to mass spectrometry. It should be clarified at this point that the 'normal operation' refers to electrospray with methanol solutions. A brief discussion of operating modes of electrospray is provided. Aspects of the ion-current generation and sampling by a mass spectrometer from such modes will be discussed. The reader should then be provided with a very clear pictorial representation of the electrospray phenomena generated by electrolytes in methanol. There are a number of recent fundamental research papers on the subject to which reference will be made[29-38].

## **6.2 Experimental**

The electrospray source and mass spectrometer have been previously described [20] (as well chapter 2 of this thesis). The high pressure sampling region of the modified Sciex/Perkin-Elmer ELAN Model 250 ICP-MS mass spectrometer, is based on a sampling plate/skimmer configuration. The electrospray tip is typically biased to either +/- 2.5-3.0 kV relative to the front plate which is held at +/- 600V depending on whether positive or negative ion mode is used. The tip is typically positioned around 5-10mm relative to the counter electrode and will be indicated where required. The sampling plate to skimmer voltage difference will be given as required and is typically between 10-60V, depending on the amount to CID required. The solution flow rate is

typically 1.00-2.00  $\mu\text{L}/\text{min}$ . as supplied by a Harvard Apparatus 22 syringe pump. A picture of the capillary used is given in Fig. 6.1.

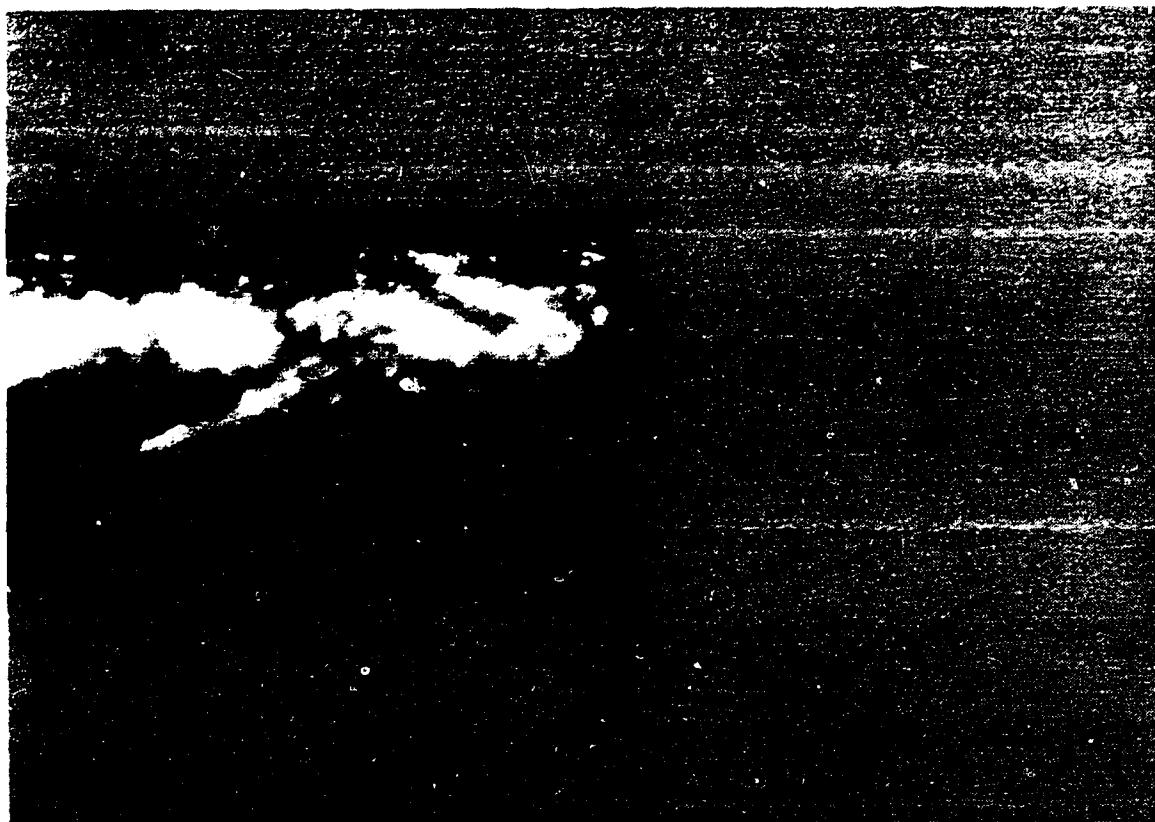


**Figure 6.1** CCD image of the stainless steel electro spray capillary tip.  
O.D. = 200 $\mu\text{m}$ , I.D. = 100  $\mu\text{m}$ .

Conductivity measurements were conducted on a YSI Model 33 conductivity meter with a 0.58 cm cell constant.

Figure 6.2 gives the schematic diagram of the system used to acquire the CCD images and simultaneously monitor the electro spray current. The electro spray current is monitored by placing an electrometer (Princeton Applied Research; PAR Model 135 electrometer) between the counter electrode (ground plate) and ground, thus monitoring the total ion current or charge striking the counter electrode for a given set of electro spray conditions.

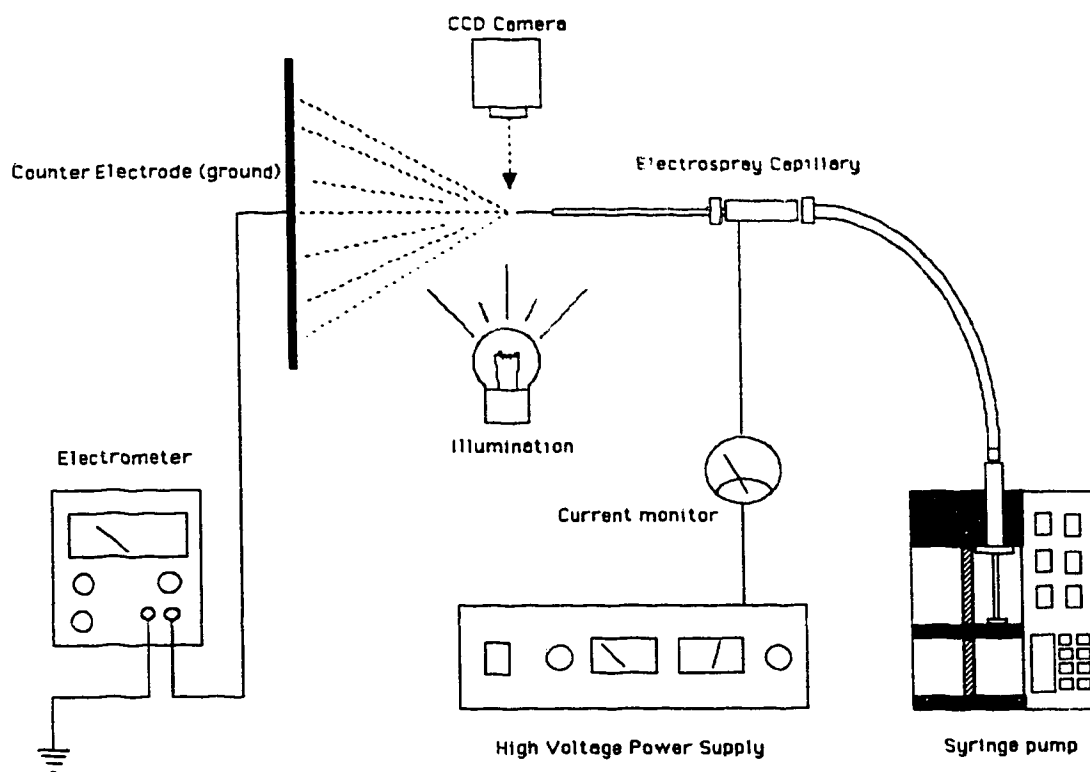


**Figure 6.2** Schematic of the system used to collect the images as well monitor the spray current.

The typical operating conditions for electrospray in Fig. 6.2 is a capillary to plane separation of 5mm, a solution flow rate of  $2.00\mu\text{L}/\text{min.}$ , a capillary o.d of  $200\mu\text{m}$  and i.d. of  $100\mu\text{m}$ .

The images were acquired on either a COHU high performance CCD camera, or on a Sony, XC-73 CCD camera. The images were magnified by a Leica Wild M3B microscope, with a 1.5X front lens. The microscope has a magnification of either 6.4X, 16X and 40X giving an overall magnification of 9.6X, 24X, and 60X. At maximum magnification for the Sony Camera this led to a pixel resolution of  $\sim 1\mu\text{m}$ , and for the COHU camera of  $\sim 1.6\mu\text{m}$ . The resolution was determined by comparing a grid of known spacing to the pixel distance

of the grid, multiple grids were measured for both horizontal and vertical separation. The results were consistent, and gave good agreement with the capillary outer diameter, which was measured as  $216\mu\text{m}$  for both cameras. Unless indicated all images were acquired in maximum resolution settings. A Sun Sparc 10 workstation was used to capture and digitize the images. The camera and microscope mount were positioned in a horizontal manner to observe the electrospray capillary from the side. This viewing position was selected as it was felt it would best capture the capillary operating in its normal position.

Solutions used in these experiments were prepared from distilled H.P.L.C grade methanol, and reagent grade salts. Typically a stock solution of  $10^{-2}\text{M}$  electrolyte was prepared and then diluted appropriately with methanol. The stock solutions were prepared by dissolving the appropriate amount of electrolyte in methanol, and in some cases ultrafiltered distilled water. The methanol stock solutions were used when control of the solution conductivity and surface tension was important.

## **6.3 Results and Discussion**

### **6.3.1 Electrospray formation**

On first inspection electrospray appears conceptually to be a relatively simple ion source and in many respects it is. Closer inspection however, will reveal that several complex phenomena are occurring to eventually yield the gas phase ions recorded by a mass spectrometer. These phenomena are divisible into two main processes; the formation of charged droplets at the capillary tip and the liberation of gas phase

ions from such droplets. Charged droplets under normal operating conditions originate from a fine filament jet that extrudes from the apex of a "Taylor cone" [3] (see Fig. 6.3). At some critical distance the jet breaks apart to form the charged droplets from which gas phase ions are the eventual product. The generation of gas phase ions from the charged droplets is quite a complex and little understood process. A recent review of the current thoughts on this aspect is discussed by Kebarle and Tang,[40] this however is not the focus of this paper.

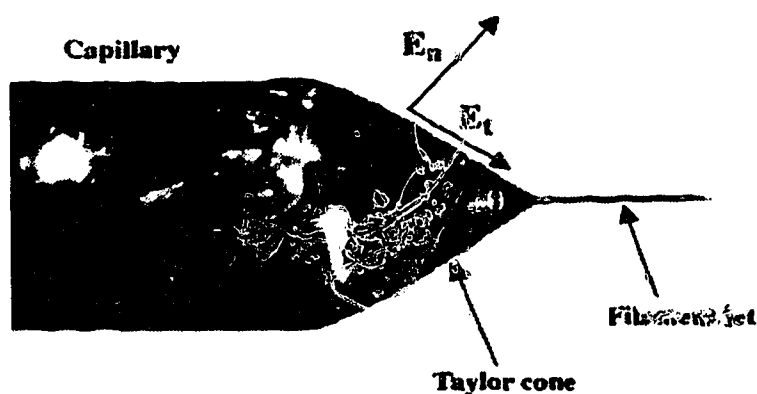


**Figure 6.3** A CCD picture of the "Taylor cone" (60X, pixel resolution of  $1\mu\text{m}$ ).  
Solution: KCl at  $1.0 \times 10^{-4}\text{M}$  in MeOH. Flow rate:  $2.00\mu\text{L}/\text{min.}$ ,  
Capillary Voltage:  $-2.00\text{kV}$ , Capillary to plane separation:  $5\text{nm}$ .

The normal operating mode of electrospray is the "Taylor cone" mode. This name refers to the shape a liquid meniscus may assume under the influence of an applied electric field as studied by G.I Taylor in 1964 [3]. The formation of such a cone is actually quite complex. The formation of axisymmetric motion in the cone is the result of interfacial electric shear stresses at the surface of the liquid

which in consequence yield its conical shape.<sup>4</sup> The effect of shear stresses is described at some length by Smith [29] and Hayati *et al.* [31,38] and although it is probably not the quintessential description it agrees with observation. The following discussion is modeled after this thought. For the typical methanol liquid/gas interface of electrospray to experience a shear stress two criterion must simultaneously be fulfilled:

- 1) It must have a net surface charge.
- 2) It must experience a tangential electric field.

The first point may be satisfied by electrolyte present in the methanol either as analyte or impurity. An applied electric field drives free charges in the liquid to the surface of the cone, in effect a sort of charge separation occurs near the surface of the liquid where the field penetrates. For a field created by a positive potential difference the positive ions are driven towards the surface and the negative ions are driven away from the surface (this point will be discussed in more detail later) and vice versa. Thus the surface will acquire a net charge. The accumulation of net charge at the surface creates a normal electric field of magnitude (Fig. 6.3);

$$E_n = q / \epsilon_0 \quad (6.1)$$

where  $q$  is the surface charge density and  $\epsilon_0$  is the permittivity of free space. The normal field acts against the binding forces of the liquid surface tension and will tend to pull the charged surface in the direction of the field that results in a net destabilizing effect. In the normal direction at the meniscus a pressure balance must exist between



the internal pressure, surface tension pressure and a normal component of stress, as given by equation (6.2) below [29];

$$\Delta p = \frac{\gamma \cot \theta_0}{r} - \left[ \frac{\epsilon_0 E_n^2}{2} - \frac{(\epsilon_0 - \epsilon) E_t^2}{2} \right] \quad (6.2)$$

where  $\epsilon$  is the dielectric constant of the liquid, and  $E_t$  is the tangential field which will be defined below,  $r$  refers to the radial distance,  $\theta_0$  refers to the cone half angle and  $\gamma$  is the surface tension.

For a curved surface or drop like liquid profile, when sufficient potential is applied the meniscus or charged surface is 'pulled' down field and the charged surface tends toward zero radius of curvature or in simpler terms the liquid is pulled to a point. This event becomes very important based on Rayleighs equation as given below [39];

$$Q^2 = 64\pi^2 \epsilon_0 \gamma R_r^3 \quad (6.3)$$

where  $Q$  refers to the surface charge present at the meniscus of radius  $R$ . This equation suggests that a surface of some curvature is only able to support a maximum amount of charge before it becomes unstable. The unstable surface will expel this destabilizing charge usually in the form of a jet of liquid. Therefore as the charged liquid meniscus is pulled towards a point of minimum curvature, it will experience surface instability and act to extrude the destabilizing charge. This act is crucial in the formation of an electrospray as it serves to initiate the charge flow at the surface. A stable "Taylor cone" formation is only maintained when the flow of liquid leaving the cone due to charge flow balances the flow of solution delivered to the capillary tip or

cone base as determined by a mechanical pump or some other form of hydrostatic pressure.

The second point is satisfied by the very nature of the liquid. Typically most common electrospray solvents exhibit a semi-insulating nature or low relative dielectric constant (methanol ~33). The effect of the dielectric is to maintain a potential drop between the liquid at the base of the cone and its apex. This field is not very large and at the methanol liquid apex the potential may have a value <1% different from the capillaries' potential. This will impart a tangential electric field in the direction of flow at the interface of magnitude;

$$E_t = \Delta\phi / l \quad (6.4)$$

where  $\Delta\phi$  is the potential drop along length  $l$  of the cone. The tangential electric field is directly proportional to the potential drop along the surface and may be deduced at any spherical radius of the cone  $r$  by equation 6.5 [31]:

$$E_t = \frac{I}{2\pi\kappa(1-\cos\theta) r^2} \quad (6.5)$$

where  $\kappa$  is the solution conductivity and  $I$  is a conduction current which flows in the cone to compensate for the current flowing from the cone or loss of charge. The above equation may be integrated over  $r$  to yield the potential drop at any location along the cone. The tangential field then serves to accelerate the surface charge layer down field towards the apex. The movement of this layer of surface liquid

(of some thickness) relative to the bulk results in a tangential shear plane.

The shear ( $T_t$ ) and normal ( $T_n$ ) stresses are calculated from equations (6.6) and (6.7) given below

$$T_t = \epsilon_0 E_t E_n \quad (6.6)$$

$$T_n = 1/2 \epsilon_0 E_n + 1/2 (\epsilon - \epsilon_0) E_t^2 \quad (6.7)$$

From the above equations it may become apparent that the solution conductivity is very important, where poorly conducting or insulating liquids (such as pure methanol) will not have the free charges necessary to supply a sufficient surface charge. The overall effect is that the  $E_n$  term in equations (6.6) and (6.7) tends to zero and hence the shear stress will also approach zero. As well, the normal stress becomes dominated by the second term on the right  $1/2(\epsilon - \epsilon_0)E_t^2$  and results in solvent polarization which drives the solvent to regions of high field intensity ( the capillary tip ) [31]. In the case of conductive solutions such as methanol containing sufficiently high levels of electrolyte, equation (6.5) will tend toward zero and hence the shear stress (equation (6.6)) will also tend toward zero. Equation (6.7) will become dominated by the first term to the right;  $1/2\epsilon_0 E_n$ . This then leads to surface instability and in some regions the surface charge may accumulate in excess of the Rayleigh limit [39] which may result in secondary jet formation. Figure 6.4 is an example of this sort of phenomena where instability is observed in the vicinity of the apex of the Taylor cone, where instead of a well defined cone tip with a filament as in Fig. 6.3, here the apex appears diffuse in appearance.

The accumulation of such charge in this region would yield large normal fields and consequently the stabilizing effect by the tangential shear stress is diminished. A stable Taylor cone configuration may be achieved for the same solution (Fig. 6.4) by changing the operating conditions and will be discussed later.

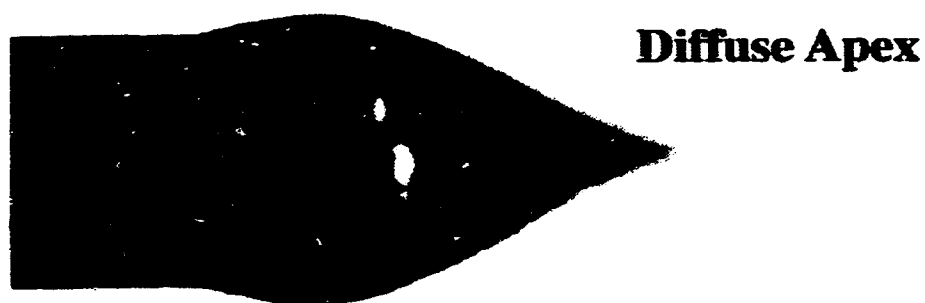


**Figure 6.4** Unstable Taylor cone profile of; KCl:  $3.0 \times 10^{-4} \text{M}$ , Flow rate  $1.50 \mu\text{L}/\text{min.}$ , Electrospray tip biased to  $-1.90 \text{kV}$ , held 5mm from counter electrode.

The above discussion has indicated the necessary criterion to form a stable jet. In particular the solution must contain sufficient electrolyte to charge a surface under a given set of operating conditions. A sufficiently non conducting liquid must be used for a potential gradient to be established across the cone. If conditions are selected (flow rate, voltage, separation, etc..) to satisfy the above

stipulations, a stable Taylor cone may be observed, once outside the limits, instability of one sort or another will set in.

With this information, the actual generation of an electrospray as a function of potential will be described. The applied potential is the only variable with the capillary to counter electrode separation of 5mm, flow rate of 2.00 $\mu$ L/min. and a KCl solution concentration of  $1 \times 10^{-4}$ M all being fixed. Figure 6.5 is a sequence of 12 pictures going from low applied potential (Fig. 6.5b) to high applied potential (Fig. 6.5l). The pictures were acquired at a magnification of 60X.

Examining Fig. 6.5b first, the liquid under an applied potential (-1.55kV) is being pulled towards the counter electrode however the field is not strong enough at this point to actually deform the drop. At this potential the droplet just grows until its weight is no longer supported by the capillary and it drops off and so the only effect here is a seeming droplet polarization.

If the voltage is turned up (Fig. 6.5c and 6.5d) to -1.60kV, -1.70kV the profile takes on what will be referred to as a "Pulsed Droplet" mode. In this mode the meniscus is pulled to a point and extrudes a jet of charged liquid and then collapses or 'falls back' to an initial state. Upon collapse the meniscus will charge up and deform again repeating the process. The result of such events being the time averaged pictures as observed in Fig. 6.5c and Fig. 6.5d. These observations are in agreement with Cloupeau and Prunet-Foch, who refer to this mode as a "spindle mode"[33]. This particular mode will be discussed in more detail later.

Figs. 6.5e and 6.5f, are also considered to fall into the "spindle mode"[33] and result by increasing the potential to -1.80 and -1.90kV

respectively. This will be referred to as the "Rapid Pulsed Droplet" mode. The difference between the Pulsed and Rapid Pulsed Droplet modes is apparent visually where the later seems to adopt more of a cusp form. Inspection of the time averaged figures (Figs. 6.5e and 6.5f) reveals that like the Pulsed Droplet mode there are extended and relaxed meniscus shapes and that as the potential is increased the extended form seems to pull back towards the capillary tip. This may be understood by the fact that with the increased potential the surface is charging up and deforming faster and therefore will not extend as far (as a result of liquid flow) before sufficient charge is present to emit a jet. This is discussed in more detail later.

Increasing the potential from -1.90kV to -1.95kV results in a sharp transition and a "Taylor cone" is formed (Fig. 6.5g). The position of the cone apex appears to 'shrink' or move towards the capillary with a further increase in potential as illustrated in Figs. 6.5g-6.5i. As the conical surface tends towards a flat surface ( or  $\theta = 180^\circ$ ) the filament assumes a non-symmetric orientation (Fig. 6.5j). At some potential a condition is reached where increased normal forces acting to destabilize the surface overcome the shear forces necessary to stabilize a single jet and thus multiple jets may be formed at the meniscus. This is observed in Figs. 6.5k and 6.5l, where two and multiple filaments are visible respectively. The bifurcated cone observed in Fig. 6.5k appears quite stable and probably may be used as a stable operating mode for electrospray. The multifilament conical meniscus (Fig. 6.5l) however was not stable and was prone to discharge (current monitored).

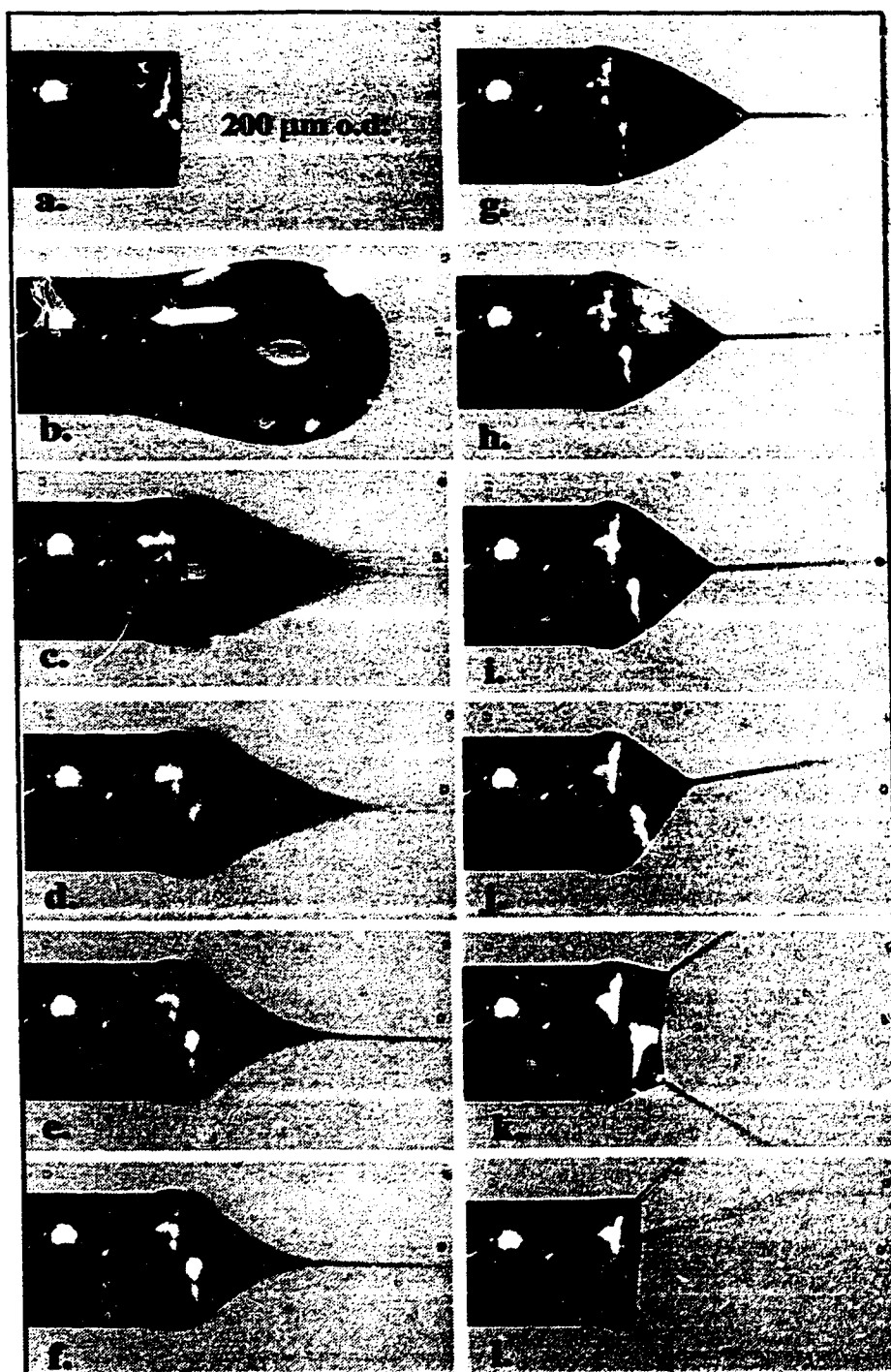


**Figure 6.5** The visual response of the electrospray as a function of applied voltage for  $1.0 \times 10^{-4} \text{M}$  KCl in MeOH. a.) 0V, b.) -1.55kV, c.) -1.60kV, d.) -1.70kV, e.) -1.80kV, f.) -1.90kV, g.) -1.95kV, h.) -2.00kV, i.) -2.10kV, j.) -2.20kV, k.) -2.30kV, l.) -2.40kV. Flow rate: 2.00uL/min., Electrode Spacing: 5.0mm

To attain a clearer understanding of the Pulsed and Rapid Pulsed Droplet modes a stroboscopic study was undertaken to isolate discrete events occurring in these modes. It became immediately apparent that these processes are not time consistent and therefore one stroboscopic frequency was never able to illuminate the mode in a constant position for any significant length of time. The strobe could be used to 'slow' the events so that discrete events could be observed and recorded to deduce their progression.

The Pulsed Droplet mode was studied and the results are presented in Fig. 6.6 which consists of eight pictures in chronological order acquired at a strobe frequency of 125Hz. The picture in Fig. 6.6a is formed as a result of a charged meniscus being 'pulled' down by the electric field as a result of normal forces. At the apex the meniscus is pulled to a point of minimal curvature from which a thin jet emerges and acts to carry away charge. This jet is maintained by the flow of surface charge along the conical surface towards the apex. If the loss of liquid at the apex is equal to the flow of liquid in the capillary then a "steady state" is maintained. If the loss of liquid at the apex occurs at a rate slower than the supply rate then the cone will extend until it can no longer maintain its shape and thus collapse. These events are depicted in Figs. 6.6b-6.6f. The end result of the collapse is that droplets on the scale of 10's of microns are produced (Fig. 6.6h) at some frequency. The size of the droplets formed as a result of the collapse of the cone may vary due to flow inconsistencies or temporary instabilities leading to volume fluctuations.



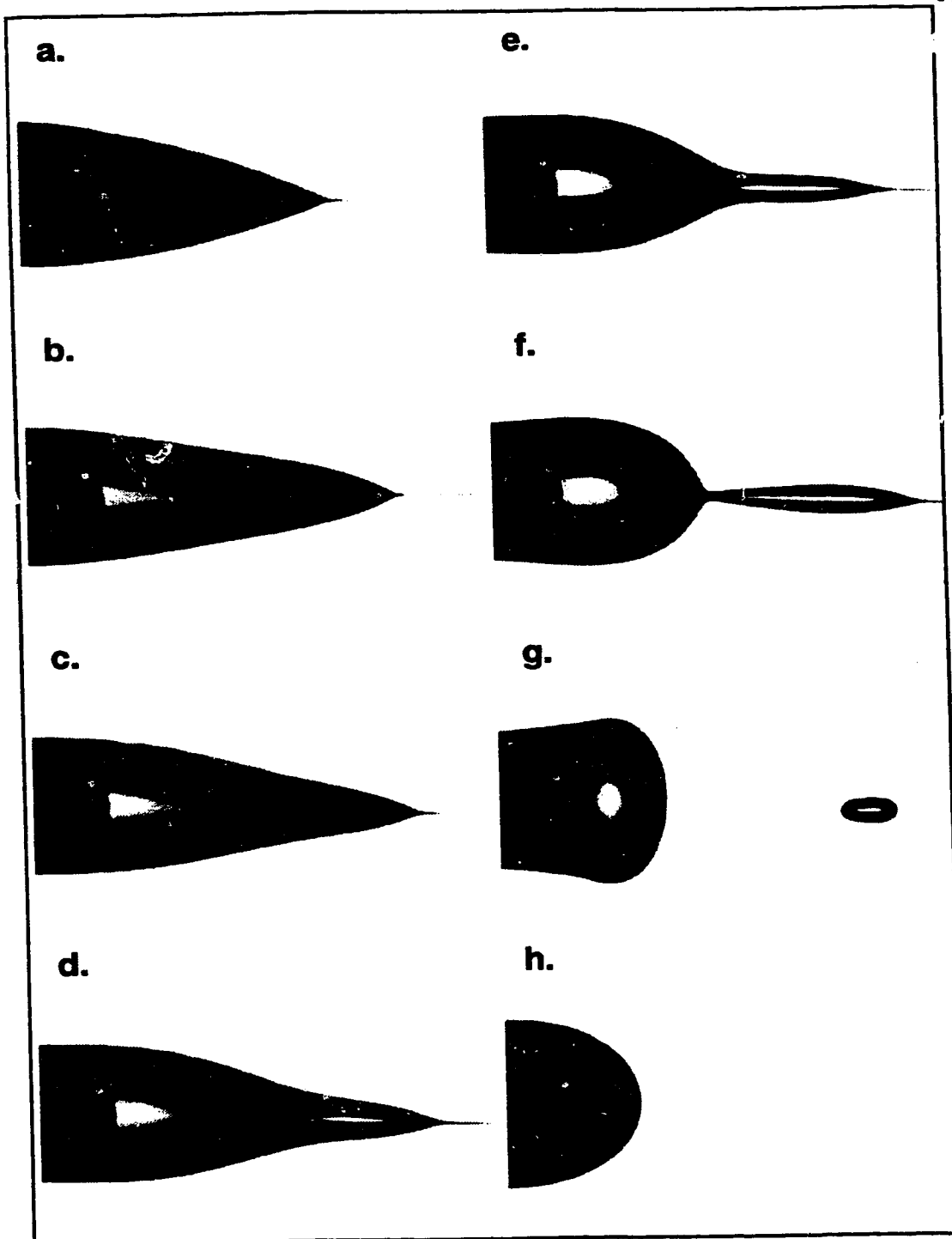


**Figure 6.6** The chronological sequence of events in the "Pulsed Droplet" mode. Going from an extended form to a relaxed form.

The second mode, the Rapid Pulsed Droplet mode consists of a rapid switching between a tight meniscus (Fig. 6.7a) and an elongated cone terminating in a filament or jet (Fig. 6.7b) these pictures were acquired using a frequency of 66Hz. In this mode the charged surface is rapidly 'pulled' to a point which elongates into a filament from which the charge flows and terminates in a spray as seen in Fig. 7b. Once some critical amount of charged liquid is expelled, the cone is no longer able to maintain its shape and collapses to a meniscus form, upon which the process repeats. This process is fast compared to the Pulsed Droplet mode. Some interesting phenomena known as "kink instabilities" may also be observed in this mode as shown at the end of the filament in Fig. 6.7c [32,33]. The Rapid Pulsed Droplet mode produces small droplets at fairly high frequency. Both modes produce droplets of different size, where droplets formed in the Pulsed Droplet mode are the result of the collapse of an extended cone whereas those formed in the Rapid Pulsed Droplet mode are due to the collapse of a hyper extended cone or filament.

Time averaged pictures of the above modes give the impression that they are quite consistent. Stroboscopic studies have revealed that they are somewhat erratic and are prone to fluctuation. As mentioned above these are the result of flow inconsistencies which may be attributed to fluctuations originating at the pump or other forms of temporary instability caused by undefined or external processes. The act of surface wetting is very important when considering processes that lead to instabilities. The stainless steel surface provides a wettable surface for methanol and as such there will be a certain volume of liquid that covers a portion of the capillary tip. This is illustrated

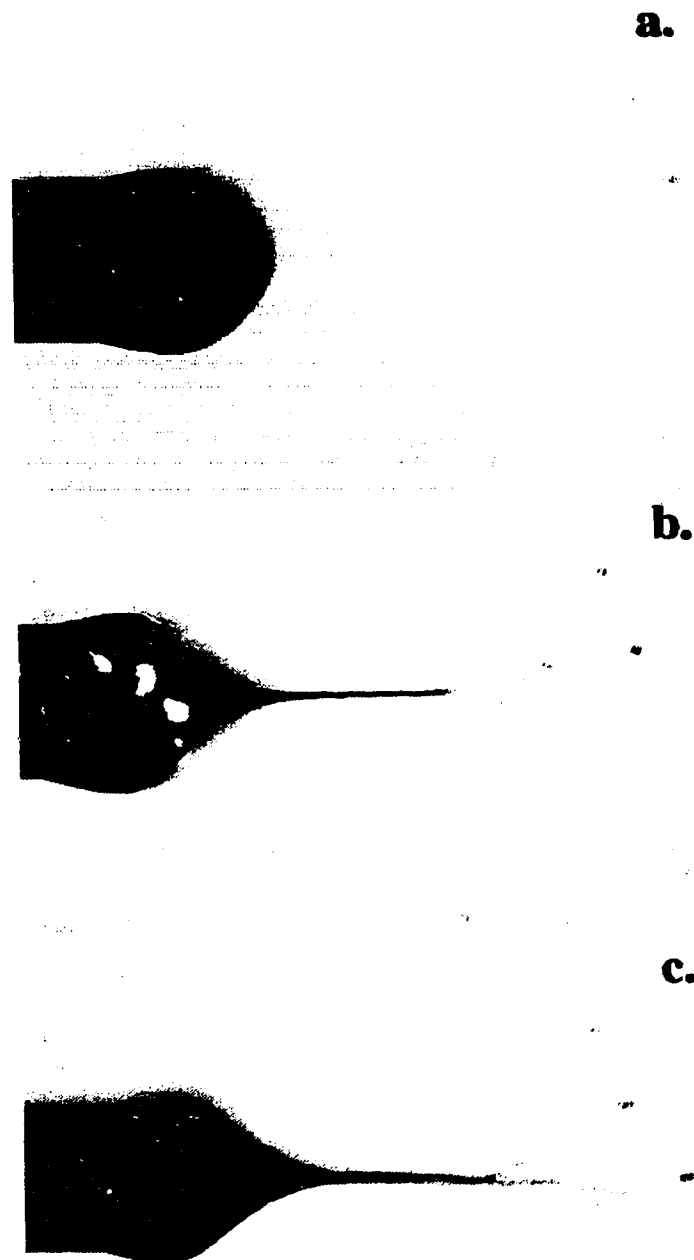


**Figure 6.7** The main functioning modes of the "Rapid Pulsed Droplet" mode. a.) is the relaxed form and b.) is the extended spray form and c.) reveals some of the fine structure of the spray, 'kink instabilities'.

(under close inspection) in Fig. 6.5, as well in Figs. 6.6 and 6.7. This surface liquid can distort the flow profile at times and, depending on the particular operating mode, its volume may change significantly. Surface wetting appears to be most significant in the Pulsed droplet mode and least significant in the multifilament modes. Changes in the surface wettable volume affect the volume of liquid in the cone and ultimately lead to fluctuations in the electrospray current. In a stable Taylor cone operating mode this excess liquid (residual from a previous mode) is quickly lost and a steady state flow is achieved with a stable current. If an electrospray tip suffers from jagged edges or metal burrs its ability to achieve a steady consistent flow is hampered.

From Fig. 6.5 it appears that the transition between the modes is somewhat smooth and consistent, which it was for this particular study, however at different concentrations intermediate modes may form. For instance at higher concentrations, the "Pulsed Mode" has been observed to switch directly into the cone mode, for a short period of time (visible to the eye) and then switch back to the "Pulsed Mode", this intermediate mode appears as a sort of switching mode. This is not to be confused necessarily with being right on the verge of switching from the "spindle mode" to a Taylor cone as in Figs. 6.5f and 6.5g as increasing the voltage somewhat in this mode does not always create the Taylor cone. It would seem that the increased concentration allows the formaton of shortlived (longlived cones as compared to those of Fig. 6.5c, 6.5d) cones which can probably not meet the current or charge demands to maintain their shape. Again this mode might be caused in some part by flow oscillations or irregularities.

From the above discussion a steady state is only achieved in the Taylor cone mode (and possibly the bifurcated cone mode). To balance the two flow rates (i.e. in versus out), it is obvious that there are a number of important parameters to be considered. Of these the filament diameter is critical, as it determines the velocity at which the liquid must travel to maintain this state (the converse may of course be true). Consider a simple example; for a liquid flow rate of  $2.00\mu\text{L}/\text{min.}$ , the flow velocity through a  $100\mu\text{m}$  diameter capillary is  $0.42\text{ cm}/\text{sec.}$ , whereas through a diameter of  $4\mu\text{m}$  (approximate diameter of filament in Fig. 6.5g) the average flow velocity becomes  $264.3\text{ cm}/\text{sec.}$  This velocity is dictated by the experimental conditions. The scaling of the jet diameter is quite complex, and not wholly defined, however the filament diameter is thought to scale with conductivity and flow rate [29,32,33]. Fernandez de la Mora and Loscertales[36] have studied the formation of filament jets in some detail especially with regards to its diameter.

The stable ion current generated in the Taylor cone mode is desirable for mass spectrometric studies. Understanding the current response as a function of many variables in this mode then becomes very important as will be discussed in the following section.

### **6.3.2      Electrospray Current**

The events pictured in Fig 6.5 are presented in a plot of observed current versus applied potential and is given in Fig. 6.8. For a  $1 \times 10^{-4}\text{M}$  solution of KCl in methanol run in negative ion mode at a flow rate of  $2.00\mu\text{L}/\text{min.}$  and a capillary to plane separation of  $5\text{mm}$  the forward increase in potential (going from low potential to high) reveals three

main current generating regions. Starting at about -1.60kV, the current response is due to that of the Pulsed Droplet mode and as the potential is increased there is a transition to the Rapid Pulsed Droplet mode (-1.85kV). A further increase in potential at this point yields the Taylor cone with a corresponding rapid increase in current. As the potential is increased still further the Taylor cone profile changes, with a slight but minimal increase of current. This region may be classified as a sort of current plateau. Although some researchers report a greater relative increase in current in this region [29,32] this was not normally observed under the conditions of the experiment. The current generated in the Taylor cone mode as observed by the counter electrode in this system is approximately 62nA. If it is assumed that in the negative ion mode the only charge carrier is the chloride ion (neglect impurity, auto solvolysis products, etc.) then the total charge striking the counter electrode is calculated to be  $3.88 \times 10^{11}$ /sec. There is a second increase of current as the Taylor cone switches to a bifurcated cone (this is usually preceded by a region of instability as the modes switch) which may be anticipated due to two current carrying filaments. This region seems stable, however by increasing the voltage the bifurcated cone then switches to a multifilament (three or greater filaments) mode which is unstable and is often characterized by wandering filaments and large current fluctuations associated with discharge.

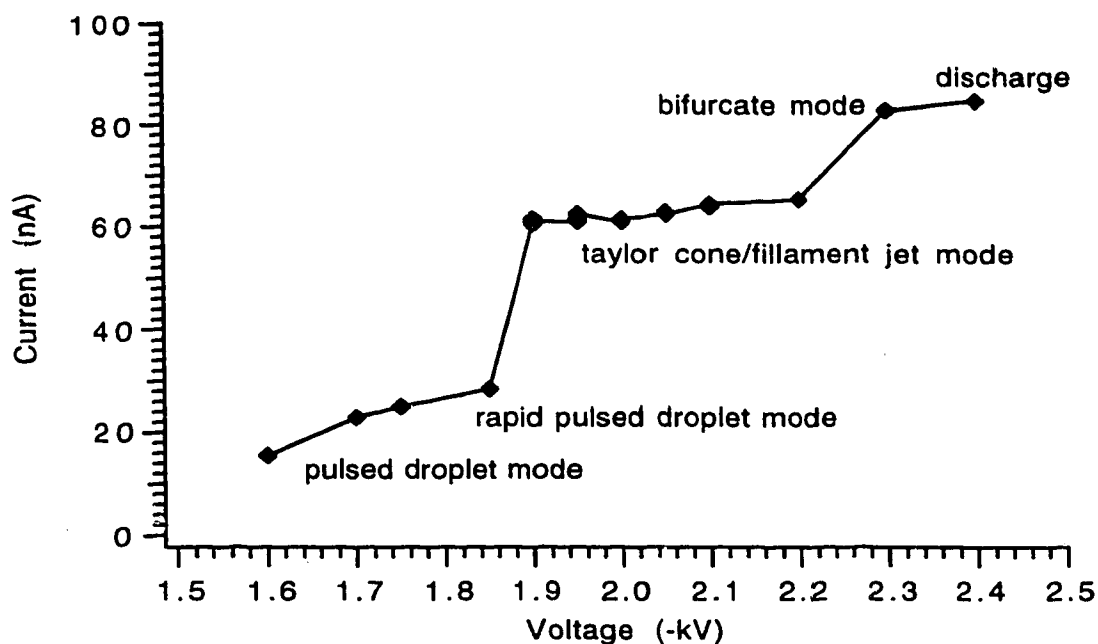


**Figure 6.8** The observed current response as a function of applied potential. KCl:  $1.0 \times 10^{-4} \text{M}$  in methanol, Flow rate;  $2.00 \mu\text{L}/\text{min.}$ , capillary to plane separation; 5mm.

Close examination of the Taylor cone (Figs. 6.5g-6.5i) shows that the cone appears to 'shrink' as was discussed previously, however the filament length in this region seems to maintain a constant length. This is illustrated graphically by Figs. 6.9a and 6.9b. During the course of the experiment three pictures were acquired for each voltage step and were digitized (pixel resolution =  $1.0 \mu\text{m}$ ). From these pictures the cone and filament were characterised. The length of the filament jet was measured from cone apex to the border between the dark and gray regions which represents the end of the bulk liquid flow. These end points are somewhat arbitrary and will have error associated with them. The cone height was measured from the capillary tip to the cone apex. The filament diameter was about  $4 \mu\text{m}$  consistently. This measurement was however difficult because it

approaches the limit of resolution and measurement at the filament edges were subjective due to optical effects and should be viewed with some caution. If anything this number might be high. When the various filaments were magnified and compared they seemed quite similar and any change in diameter would be less than  $1\text{ }\mu\text{m}$ . Similar filament lengths and diameters imply that the charging process was consistent because the filaments seem to break up (or form a spray fan) at around the same length. Therefore, if these filaments were carrying the same charge and volume and thus breaking up at the same length, then the observed current should be more or less the same. This agrees fairly well with what is observed in Fig. 6.8.

The decreasing cone height observed in Fig. 6.9b may be understood as a result of the cone trying to maintain a steady state. By increasing the potential at the capillary there will be a greater potential drop through the cone assuming the same shape is maintained. This would imply that the Tangential field would also increase as dictated by equation (6.4). If this happens then the steady state becomes perturbed and the cone appears to shrink, which in effect results in a decrease to the denominator of equation (6.4). Therefore as the voltage is increased the cone length shrinks proportionally in order to maintain a constant Tangential field and so maintain a steady state. This implies that the normal field remains constant.



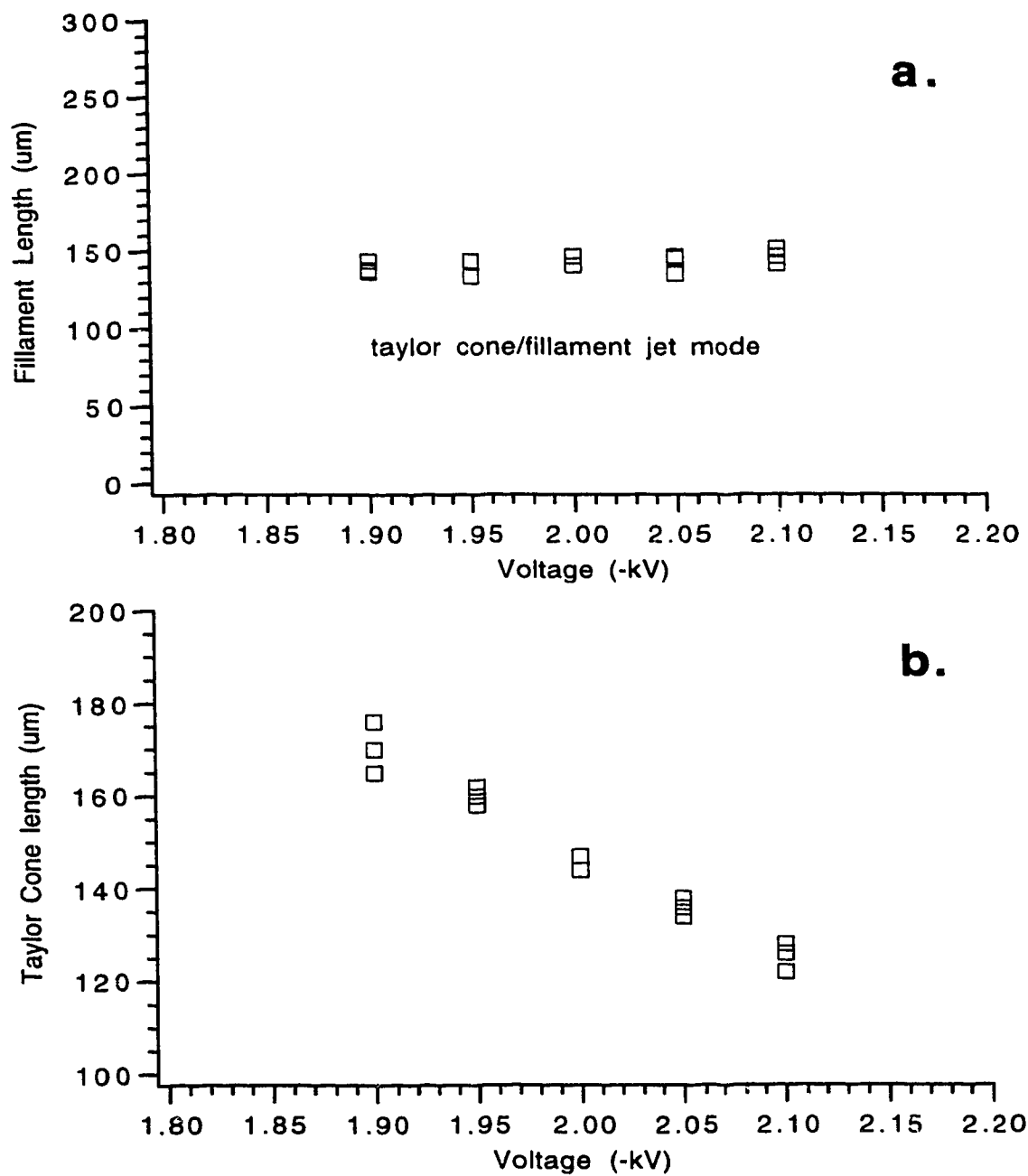


**Figure 6.9** The observed cone-jet coordinates as a function of applied potential, a.) filament length b.) cone length. KCl:  $1.0 \times 10^{-4} \text{M}$  in methanol, Flow rate;  $2.00 \mu\text{L}/\text{min.}$ , capillary to plane separation; 5mm.

The above discussion was focused on the current response as a function of forward increase of applied potential. It is a fairly well known fact that there are hysteresis effects which occurs at the cone. Going from high potential to low potential typically seems to extend the potential at which the cone is stable (lowers the lower limit). This is illustrated in Fig. 6.10. It is sometimes advantageous to raise the voltage higher than that necessary to form a stable cone and then lower it until a stable cone is observed.

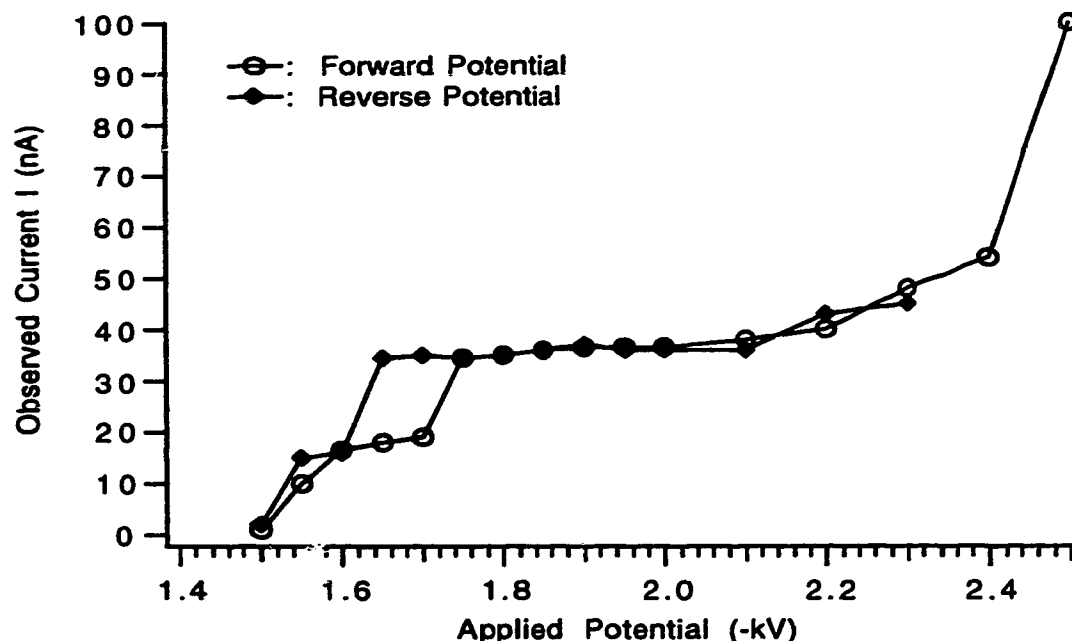


**Figure 6.10** The effect of hysteresis on the onset potential for a KCl solution of  $1.0 \times 10^{-4} \text{M}$  in methanol, Flow rate;  $2.00 \mu\text{L}/\text{min.}$ , capillary to plane separation; 5mm.

A series of concentrations are examined (typical of running a calibration curve) and the results are plotted in Fig. 6.10. The concentration of KCl is varied and examined under identical conditions and the current is recorded as a function of decreasing potential (i.e. going from high to low potential). Examination of Fig. 6.10 reveals

that the voltages required to achieve the stable Taylor cone mode varies with concentration, and what might not be immediately obvious is that the voltage range where a stable Taylor cone mode can exist decreases for fixed conditions. This is especially true for concentrations above  $2 \times 10^{-4} \text{M}$  KCl where in some cases stability can only be achieved in a narrow potential range and eventually it becomes unattainable. This is to be expected as the increase in conductivity should lead to a decrease in cone stability for a fixed set of conditions. In addition for concentrations greater than given in Fig. 6.10 the current jump from the Rapid Pulsed Droplet mode to the Taylor cone mode diminishes and appreciable currents may be sustained in the Rapid Pulsed Droplet mode. In this mode the current does not necessarily translate into the gas phase ion equivalent unless the electrospray tip is positioned far enough from the counter electrode to allow complete evaporation from the larger droplets which are created.

From Fig. 6.11 a voltage where all of the concentrations have stable Taylor cones is  $-1.95 \text{kV}$ , and a plot of observed current vs concentration is given in Fig. 6.12. The plot shows a linear response in current with increased concentration, however the plot has a non-zero intercept. This non-zero intercept is to be expected based on the nature of the technique, as there is a certain electrolyte concentration required to give the minimum conductivity necessary to form a stable electrospray.

The current versus concentration calibration curve given in Fig. 6.12 has assumed that the dissolution of strong electrolyte like KCl in methanol was complete for dilute samples. To confirm this and rule out any nonlinearity effects the conductivity of solutions used for Fig.

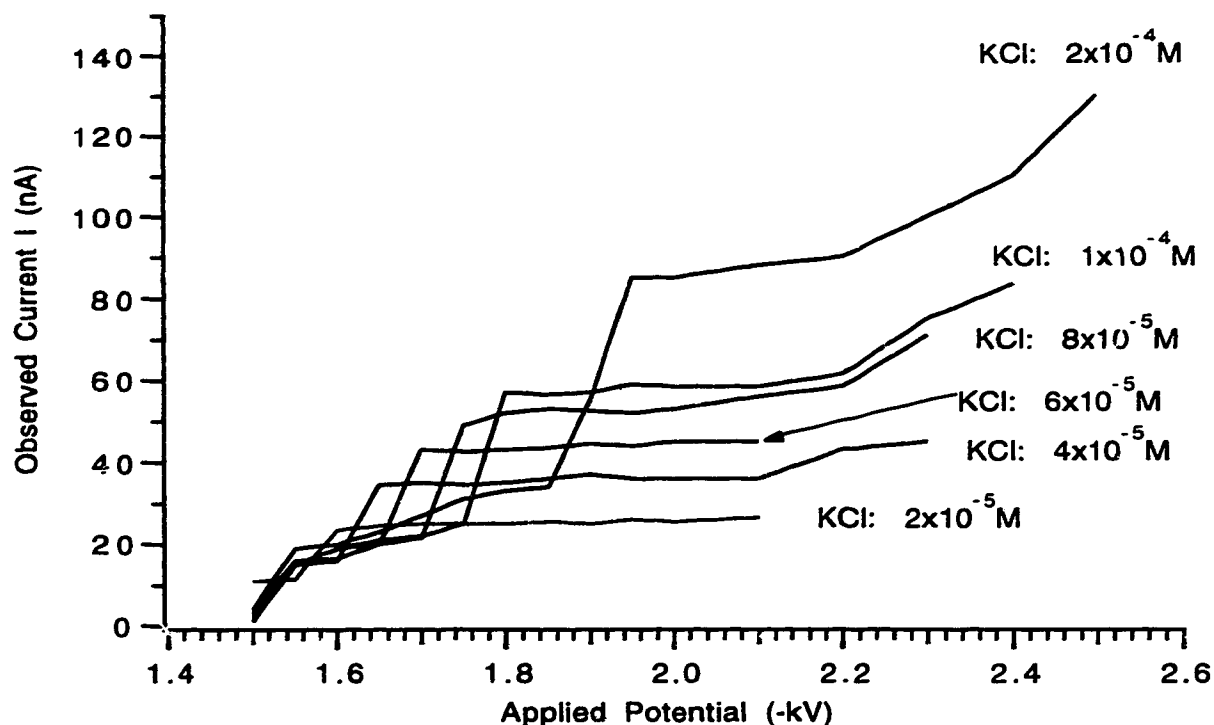


**Figure 6.11** The current vs applied potential plot for a series of KCl concentrations. Ranging from  $2.0 \times 10^{-5}$  M– $2.0 \times 10^{-4}$  M KCl in methanol at a Flow rate;  $2.00 \mu\text{L}/\text{min.}$ , capillary to plane separation; 5mm.

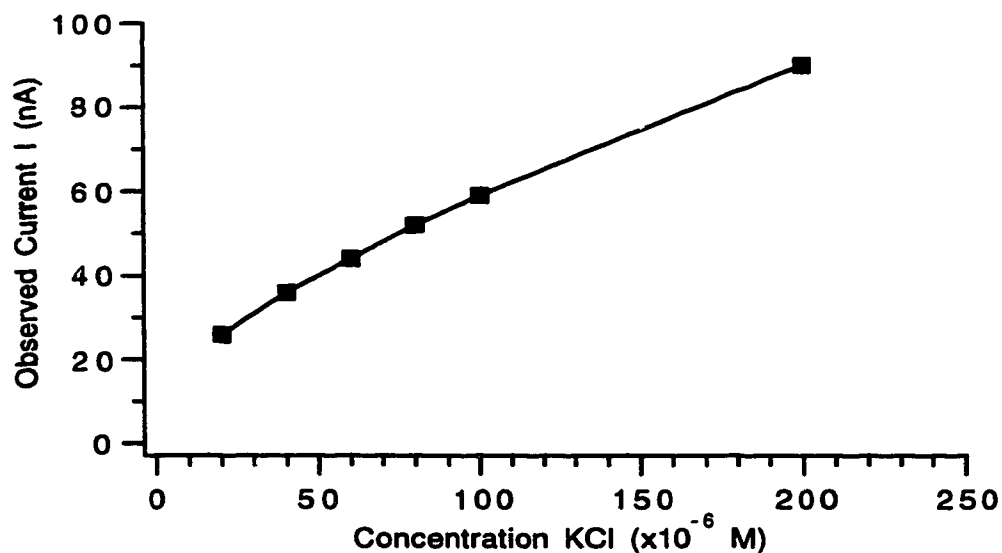


**Figure 6.12** The current vs concentration profile of KCl in methanol. Acquired at a potential of  $-1.95$  kV, with a flow rate of  $2.00 \mu\text{L}/\text{min.}$ , and a capillary to plane separation of 5mm.

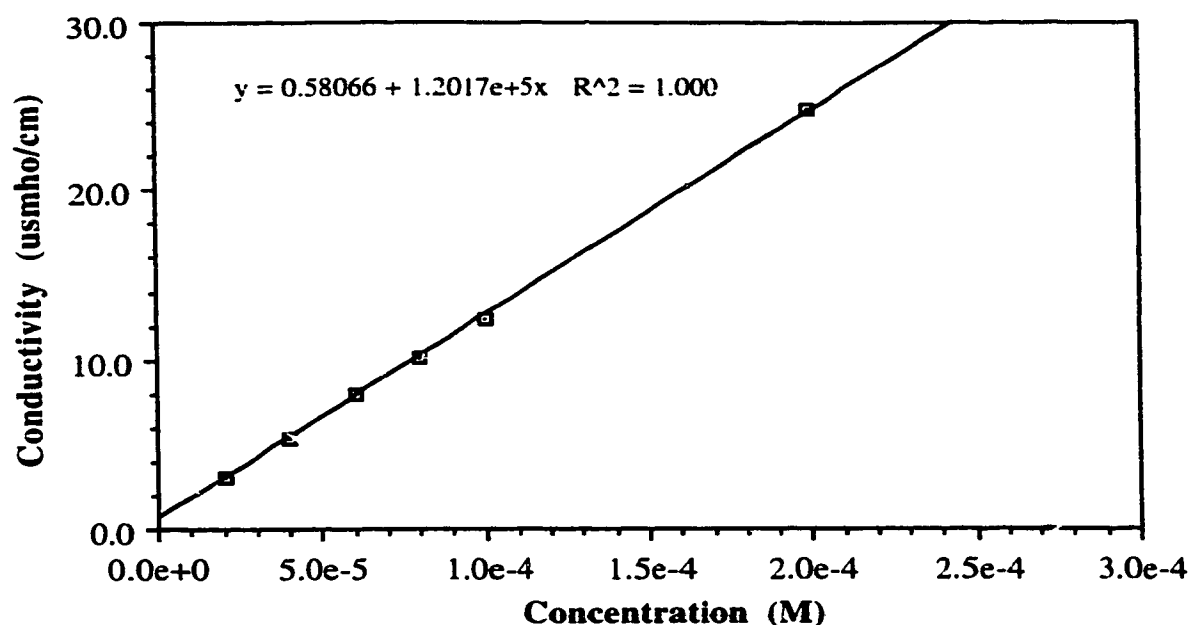


**Figure 6.13** A conductivity vs concentration plot for KCl in methanol.

6.11 were measured. The results are plotted in Fig. 6.13 and exhibit a linear response over the concentration range measured.

To further characterize the response observed in Fig. 6.11 for the various concentrations examined the cone angles at various voltages were plotted as a function of applied potential (Fig. 6.14a). From this plot it appears that the formation of a Taylor cone with the same cone angle increases with concentration. A point was selected arbitrarily where all the cones had the same geometry. It was found that at a full cone angle of  $\sim 72^\circ$  there seemed to be maximum agreement with the collected data points and so this angle was selected. The potential at which this cone angle was achieved and the resultant current observed are plotted in Fig. 6.14b as a function of concentration. Both seem to be increasing as a function of concentration. The current output as a function of concentration increases as would be expected. The increase

in potential necessary to achieve the same cone geometry for increasing concentrations is not expected. The onset of the Taylor cone mode or onset potential has been approximated in the literature, and is thought to be a function of the capillary geometry and the electric field. Smith has deduced from the literature the onset potential to be of the form [29];

$$V_o = A_1 \left[ \frac{2 \gamma r_c \cos \theta_o}{\epsilon_o} \right]^{1/2} \ln (4 h / r_c) \quad (6.6)$$

where  $r_c$  is the radius of the capillary,  $\epsilon_o$  is the permittivity of free space,  $h$  is the spatial separation between the capillary and counter electrode,  $A_1$  is an empirical constant, and  $\gamma$  is the surface tension of the liquid. Forms of this equation have been presented in a current review of the mechanism of electrospray by Kebarle and Tang [40]. The onset potential as illustrated in Fig. 6.11 is a function of concentration and therefore the voltage required to form a specific cone angle for all the solutions must also be a function of concentration. The data exhibited in Fig. 6.14 were acquired under identical conditions, and the same cone angle was achieved as a function of potential. Therefore, if the constant  $A_1$  is constant for all concentrations, then this implies that the roughly linear increase in potential is due to a square root increase in surface tension. For electrolytes in solution there is a tendency to increase surface tension with increased concentration, Weissenborn and Pugh report a  $d\gamma/dC$  of 1.85 for KCl in water at 25°C [41]. This implies a linear increase in surface tension with concentration however it is doubtful that the

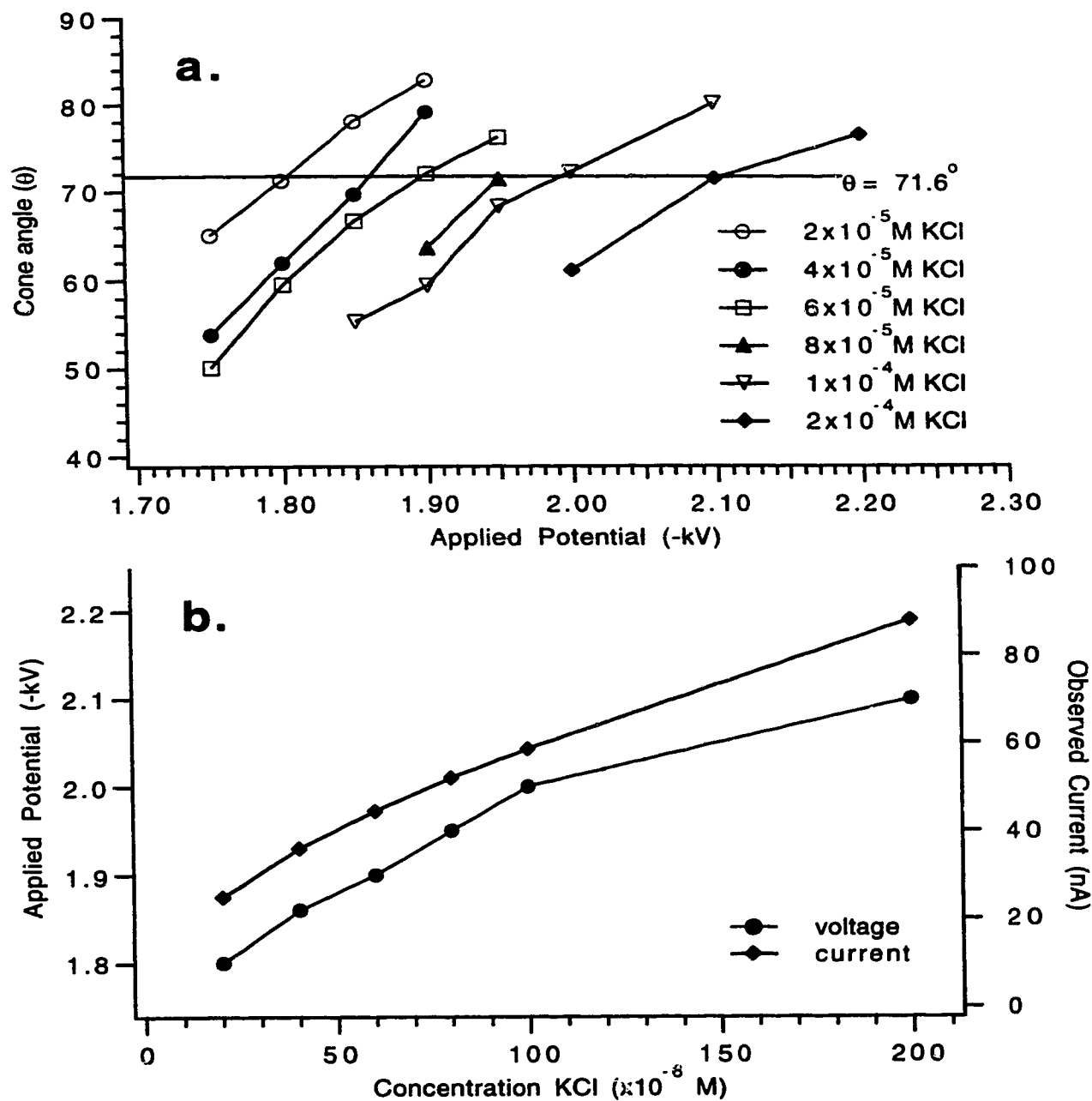


**Figure 6.14** a.) Plot of cone angle vs Applied potential for various concentrations of KCl in methanol. b.) The applied potential and observed current at  $\theta = 71.6^\circ$  for various concentrations of KCl in methanol. Acquired at a flow rate of  $2.00 \mu\text{L}/\text{min}$ . and a capillary to plane separation of 5mm.

magnitude of the change is enough to account for the potential difference alone. At best equation (6.5) can only be considered a rough calculation, however as it is based on certain physical relationships it should scale properly. This is not entirely observed. Smith did not find this dependence [29] however Hayati *et al.* found some dependence in the same conductivity range of this study [30]. In addition to this it was found that for higher concentrations, where it was difficult to form a stable spray, a diffuse apex could be focussed (brought together to form one distinct jet) by increasing the potential relative to a lesser concentrated solution. Increasing the potential in this case had the effect of stabilizing the cone. At extreme concentrations this seemed only to buy momentary stability however in less extreme concentration ranges a stability could be achieved.

There is a dependence of the filament diameter on the solution conductivity, where increased conductivities result in decreased filament diameters, as was mentioned previously. When the filament diameter for the various concentrations were examined there seemed to be an overall decrease, however these values were difficult to quantitate and so should be viewed with caution. Ultimately a decrease in filament diameter with the same cone geometry implies that the average liquid velocity must increase in the filament (and consequently its supply) in order to maintain a steady state. An increase in the potential drop down the cone would yield the increased velocities which are necessary to account for this, and will help minimize the effects of instability due to increases in the normal field. This in effect provides increased stability through increased shear stress. There is of



course an upper limit to the amount of stabilization which may be achieved.

There appears to be only a narrow or limited concentration range of about 1-2 orders of magnitude where a stable electrospray can exist, under constant conditions. By changing the operating conditions however it is possible to extend the concentration range in which a stable Taylor cone configuration may be obtained. Although there appears to be a minimum concentration requirement (minimum conductivity) necessary to form a stable electrospray some sources suggest that there is no upper limit in conductivity [29] and that it becomes defined by the operating conditions. In the normal operating mode of this paper (see experimental) the upper limit of KCl appears to be about  $5.0 \times 10^{-4} \text{M}$  in methanol, above which a stable Taylor cone cannot be achieved. When the solution flow rate is reduced to  $1.5 \mu\text{L}/\text{min}$ , a stable Taylor cone is achieved. Figure 6.15 illustrates the affect of flow rate on the observed current as well its effect on the cone angle or shape. This figure is modeled after a  $1.0 \times 10^{-4} \text{M}$  KCl solution under fixed conditions where the potential remained fixed at  $1.90 \text{kV}$  and the flow rate was varied. From Fig. 6.15a it is obvious that there is a net increase in current with flow rate and Fig. 6.15b illustrates changes in the cone profile. In this experiment a stable Taylor cone was not achieved at flow rates above  $2.60 \mu\text{L}/\text{min}$ , and at best profiles like that shown in Fig. 6.4 were obtained. No measurements were taken at values less than  $1.00 \mu\text{L}/\text{min}$ , because of noticeable pump oscillations. For a constant applied potential a 'shrinking' cone results in a smaller potential drop which should roughly scale with the decrease in cone length (eqn. (6.4)) to provide the necessary Tangential

field to stabilize the cone. Considering that the filament radius scales with the flow rate [36,37] the steady state is maintained under conditions of changing flow rate through a varying filament diameter. As the filament diameter increases the average liquid velocity must then decrease. Thus if surface charging is deemed to be time dependant then a slower moving surface should allow for a greater charge density, which would then be reflected in the observed current. This is illustrated in Fig. 6.15a. If too great a surface charge is attained then surface instability will occur at the apex as illustrated in Fig. 6.4. Therefore flow rate adjustment may be used to extend the concentration range of solutions studied, this is however at the expense of current and therefore net ion flow. Concentration studies then become limited in range without the incorporation of a calibrant or internal reference ion [22] to account for current differences in mass spectral analysis. This will be elaborated on in the next section.

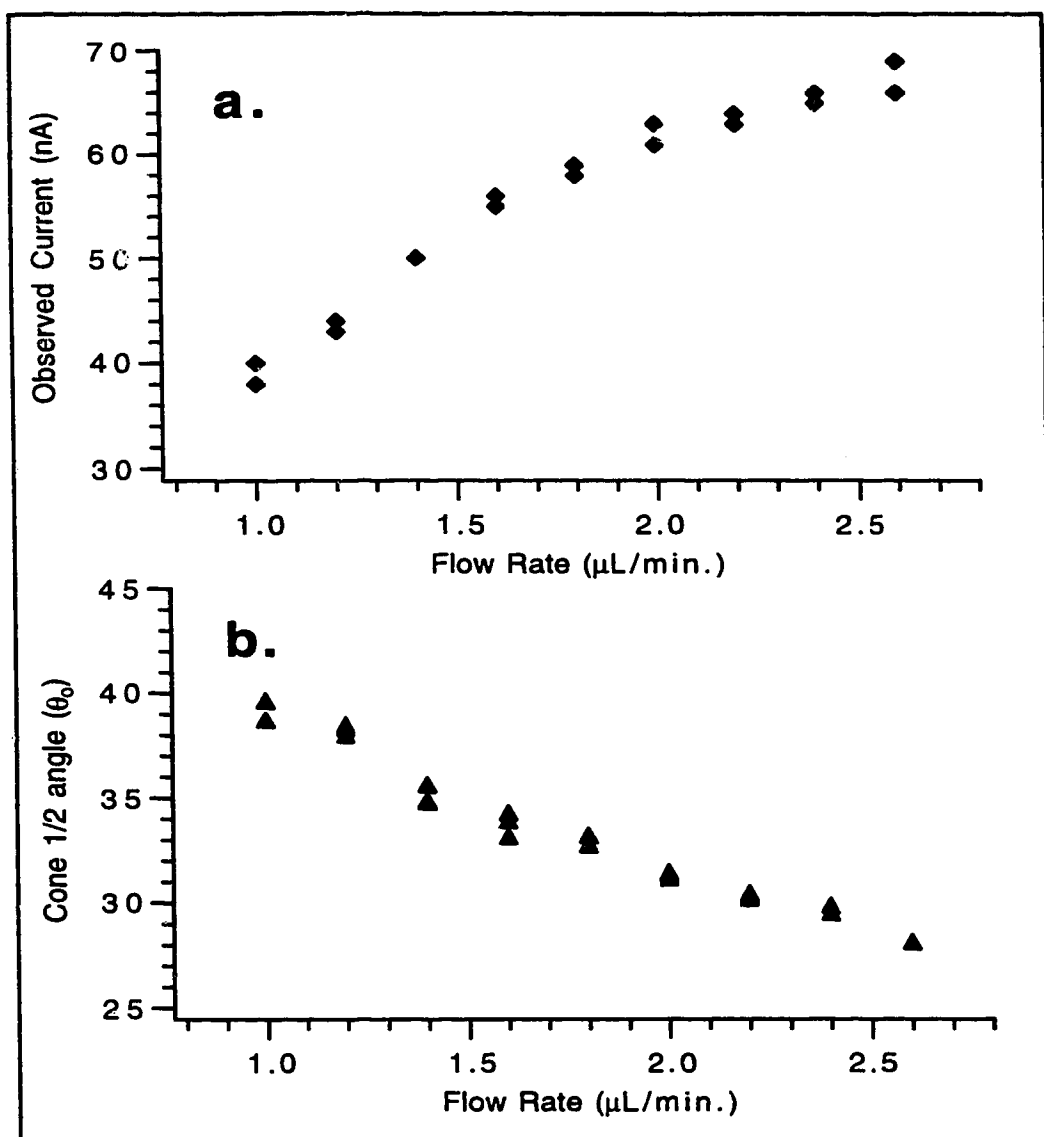


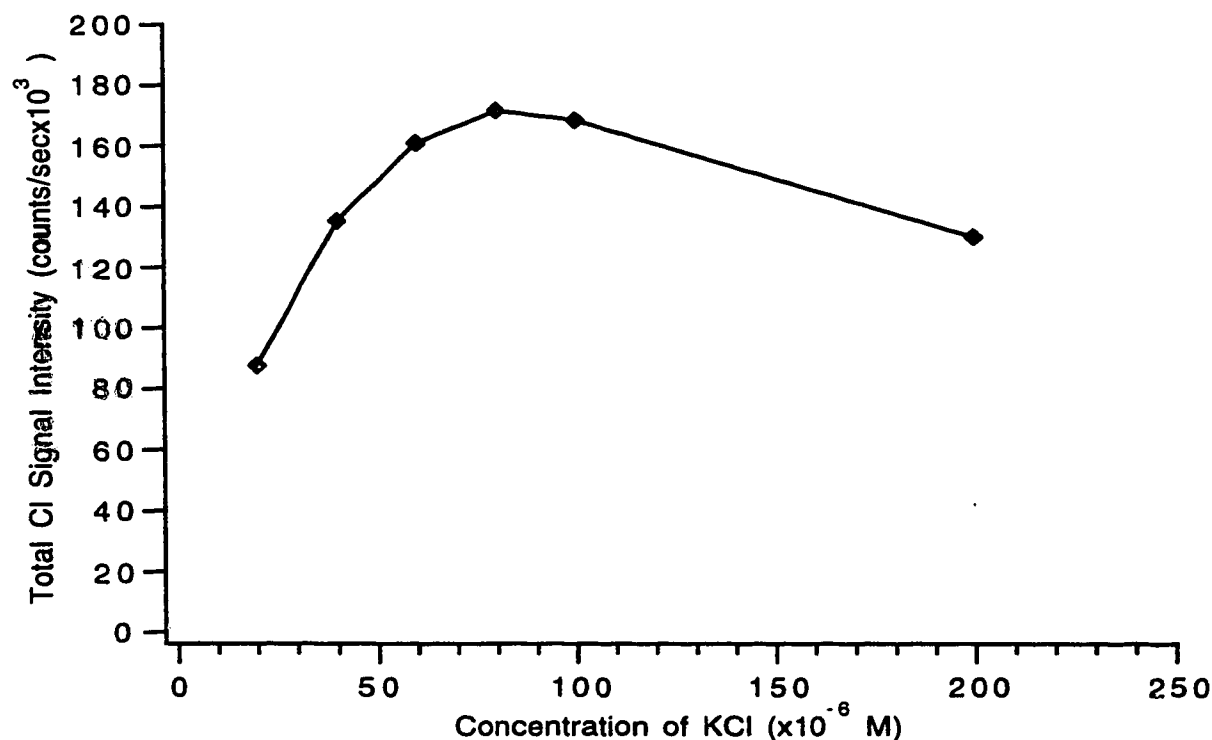
**Figure 6.15** The effect of flow rate on the a.) observed current and the b.) observed cone 1/2 angle. The solution is KCl:  $1.0 \times 10^{-4}\text{M}$  in methanol, the capillary tip is held at a potential of 1.90kV, and at a separation of 5mm.

### 6.3.3 Mass Spectral Consequences

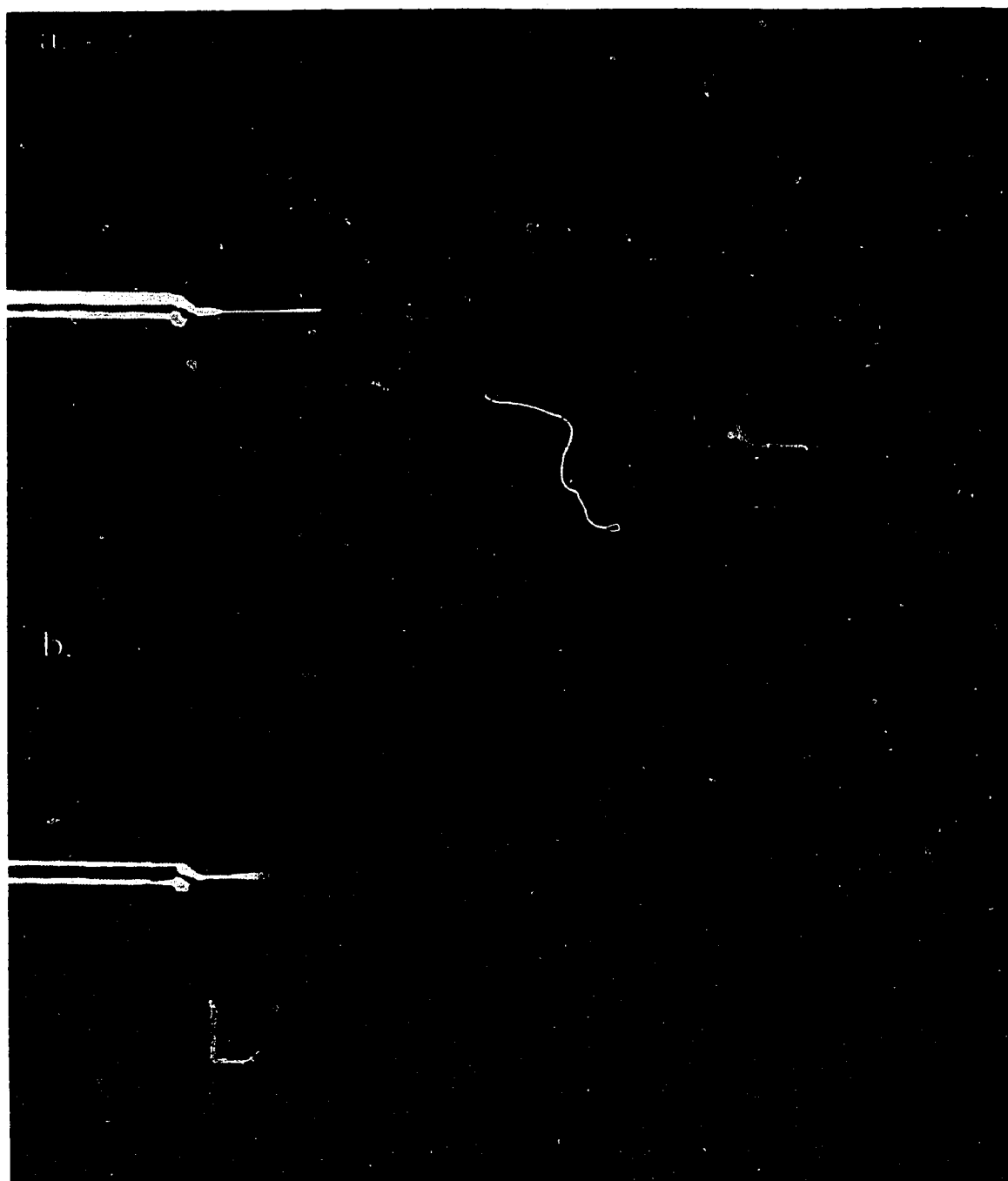
From the current vs concentration plot of Fig. 6.12, it would be expected that an ion current vs concentration plot as obtained on a mass spectrometer would yield approximately the same response. The mass

spectrometric response is illustrated in Fig. 6.16. Unlike the response observed in Fig. 6.12, the ion intensity increases until it reaches a maximum and then it starts decreasing. This may be understood by considering the sampling process in a mass spectrometer. The sampling orifice, which is typically located in a position directly in front of the electrospray capillary, is only  $\sim 100\mu\text{m}$  in diameter, however due to the vacuum it probably engulfs a much larger area than its diameter would suggest. In order to achieve the same linear response as in Fig. 6.12 the charge density of the ion in the ambient atmosphere directly in front of the orifice must increase in proportion to the concentration. Based on Fig. 6.16 this is not strictly observed especially for higher concentrations. The reason for this may be understood by examining the spray profile of the various concentrations. Figure 6.17 shows the spray profiles of  $2.0 \times 10^{-5}\text{M}$  and  $2.0 \times 10^{-4}\text{M}$  KCl in methanol, under normal conditions. The hazy vertical line on the extreme right of both pictures is caused by the counter electrode which is 5mm distant. Examination of Fig. 6.17 reveals obvious differences in the spray profile. There is a marked spray volume difference between the spray profile of the lesser concentrated spray profile (Fig. 6.17a) and the more concentrated spray profile (Fig. 6.17b). The spatial location of the start of the spray fan is different for both concentrations where the more concentrated profile starts at a position much closer to the cone than the lesser concentrated profile. This implies that the filament is carrying a greater amount of charge and so the resulting initial droplets will have a higher charge to mass ratio than the lesser concentrated ( $2.0 \times 10^{-5}\text{M}$ ) KCl solution. Of course this may be anticipated because the mass flow

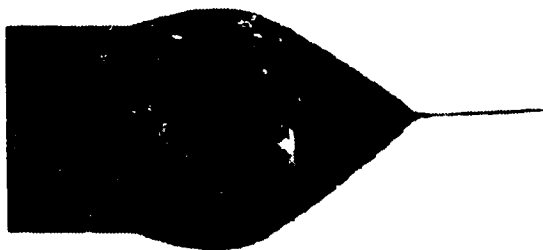
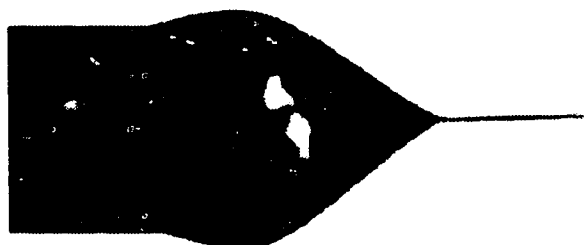
remains constant whereas the observed current changes. Figure 6.18 presents the same pictures acquired through backlighting and illustrates the differences in filament structure. The lesser concentrated sample (Fig. 6.18a) has an extended filament where the grey or diffuse portion is probably a rapid stream of droplets rather than actual bulk liquid. Figure 6.18b is the profile of the  $2.0 \times 10^{-4} \text{ M}$  KCl solution which has no extended filament. The bulk liquid seems to terminate promptly and most likely coincides with the start of the spray.



**Figure 6.16** The total mass spectral ion intensity of chloride vs concentration plot for KCl in methanol. The capillary to front plate separation is 5mm, the flow rate is  $2.00 \mu\text{L}/\text{min}$ . and the sampling plate to skimmer potential was 35V.



**Figure 6.17** Pictures acquired of the electro spray phenomena for KCl at a.)  $2.0 \times 10^{-5} \text{M}$  and b.)  $2.0 \times 10^{-4} \text{M}$ . The hazy vertical illuminate at the right of each image is the counter electrode (out of focus) at 5mm separation. The flow rate was  $2.00 \mu\text{L}/\text{min.}$  in both cases.

**a.****b.**

**Figure 6.18** Pictures acquired of the electrospray phenomena for KCl at a.)  $2.0 \times 10^{-5} \text{M}$  and b.)  $2.0 \times 10^{-4} \text{M}$ . The figures are backlit and were acquired at a capillary to counter electrode separation of 5mm at a flow rate of  $2.00 \mu\text{L}/\text{min}$ .

The other implication is indirect, however, it is to be expected that the charge concentration becomes more dilute as one travels further from the point of jet rupture as a result of coulombic repulsion between the charged droplets in the spray core. This may be understood by considering the apex of the fan to be the point of greatest charge density, and the base of the cone therefore encompassing a much larger area will consequently have a smaller charge density. Examination of each of the spray profiles especially Fig. 6.17b reveals that the inner core of spray is surrounded by a

'shroud' or outer core, which seems to have its origins at the point of filament rupture. Tang and Gomez [34] have described the structure of the electrospray at some length. They found that the sprays lateral spreading was dominated by space charge effects (coulombic repulsion), whereas a charged droplet's forward or axial motion is driven primarily by the applied electric field and is typically an order of magnitude greater than the space charge or repulsive field. Space charge effects are more dramatic at the boundaries of the spray profile (shroud region) than in the core. Tang and Gomez [34] were able to conclude that the core (arbitrarily defined) carried the bulk of the flow and total current, whereas the shroud only comprised about 3% of the flow and 15% of the charge

The above discussion implies that the lesser concentrated spray may experience a lesser degree of charge dilution by the time it reaches the counter electrode, whereas the more concentrated spray will have a greater degree of charge dilution when it reaches the same point. Therefore these effects result in non-linear effects as observed by a mass spectrometer and may be further complicated with the introduction of counter flowing curtain gas. It therefore becomes important to consider effects occurring at the interface or sampling region of the mass spectrometer especially for current versus concentration responses.

To explore the mass spectral spray profile in terms of intensity and homogeneity, a sample solution of  $1.4 \times 10^{-4} \text{M}$  KI and  $0.5 \times 10^{-4} \text{M}$   $\text{KClO}_4$  was prepared (the significance of the concentrations will be discussed shortly) and its response as a function of radial distance from central axis was monitored. It was found that, when the capillary tip



was placed 5mm from the front plate and the solution flow rate was  $2.00\mu\text{L}/\text{min.}$ , the maximum intensity was found at 0.0 mm off the central axis. The spray capillary was then moved incrementally in the radial direction and the total isotope intensities of  $\text{I}^-$  and  $\text{ClO}_4^-$  were monitored. The results are given in Fig. 6.19 where the total intensities are a decreasing function of radial distance from the central axis. An intensity ratio of the two ions appears constant throughout implying a spray homogeneity. A noticeable hump at about  $r = 1.8\text{mm}$  occurs and may be due to either temporary instability or an actual aspect of the spray profile. Such spray profiles have been studied in the literature [42]. The ion intensity as a function of capillary to front plate separation decreases with increasing separation.

The homogeneous profile observed over the radial distances covered and the conditions with which it was acquired indirectly allow for a linear plot of analyte intensity versus concentration to be obtained. Figure 6.19 is a linear calibration plot where an increasing concentration of iodide ion is plotted as a function of the ratio of the observed intensities of iodide over the total intensities of the perchlorate ion isotopes. Perchlorate is then present in the solution to act as an internal standard and is present in this experiment at  $0.5 \times 10^{-4}\text{M}$ . This method seems to circumvent the problem associated with charge dilution in front of the mass spectral sampling orifice and in effect allows differences in solution (i.e. concentration differences) to be tracked in a linear manner. This is critical for quantitative studies and has been discussed in some detail by Agnes and Horlick [22].

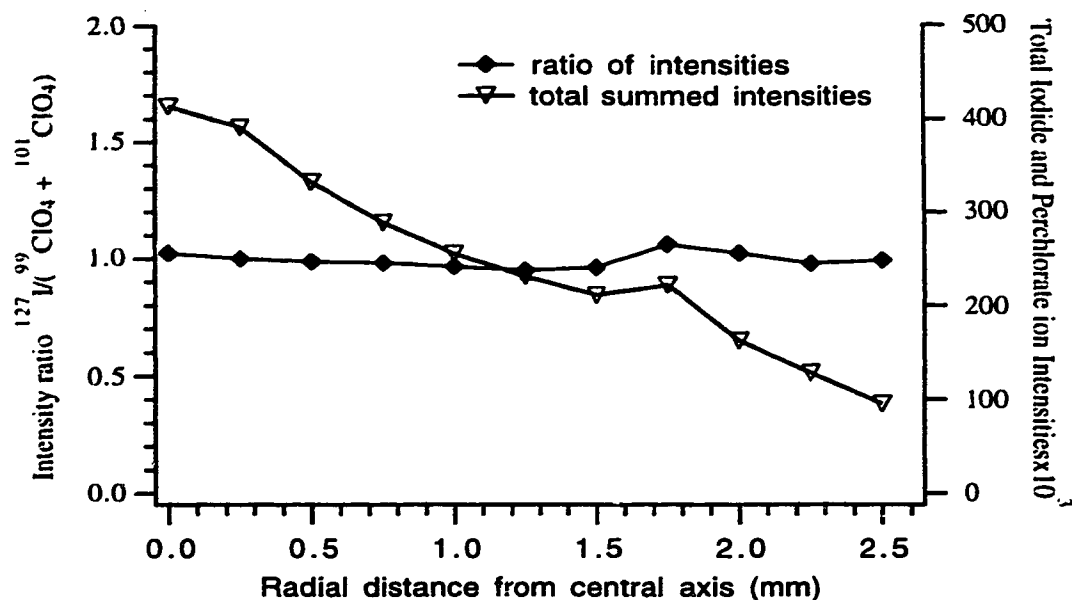


**Figure 6.19** Total intensity and ratioed intensity of  $\text{KClO}_4$  ( $0.5 \times 10^{-4} \text{M}$ ) and  $\text{KI}$  ( $1.4 \times 10^{-4} \text{M}$ ) in methanol. Capillary to front plate separation of 5mm, flow rate of  $2.00 \mu\text{L}/\text{min.}$ ,  $V_{\text{tip}}$  of  $-2.70 \text{kV}$ , front plate voltage of  $-600 \text{V}$ , sampling plate potential of  $40 \text{V}$  skimmer potential of  $-5 \text{V}$ .

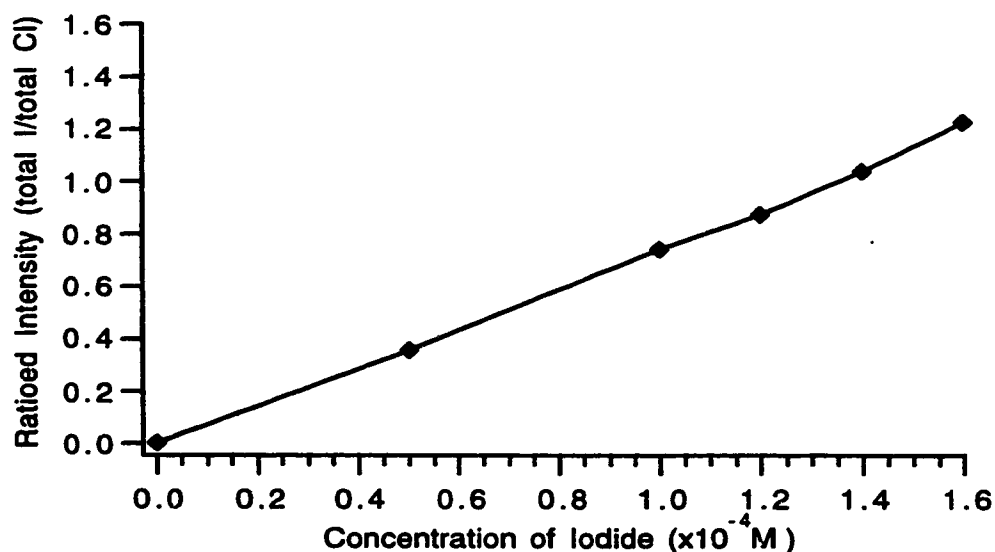


**Figure 6.20** The ratioed response calibration curve for varying concentrations of  $\text{KI}$  in the presence of  $0.5 \times 10^{-4} \text{M}$   $\text{KClO}_4$ . Capillary to front plate separation of 5mm, flow rate of  $2.00 \mu\text{L}/\text{min.}$ ,  $V_{\text{tip}}$  of  $-2.70 \text{kV}$ , front plate voltage of  $-600 \text{V}$ , sampling plate potential of  $40 \text{V}$  skimmer potential of  $-5 \text{V}$ .

From the above plot the intensity ratio obtains a value of  $\sim 1$  for a concentration ratio of  $1.4 \times 10^{-4} \text{M}$  to  $0.5 \times 10^{-4} \text{M}$  or  $\sim 3:1$  and it is because of this that it was selected for the experiment presented in Fig. 6.19. The fact that there is such a marked intensity difference between two seemingly strong electrolytes will be discussed in the next section.

#### **6.3.4 Surface Charging**

If it is assumed that the above model for the generation of the electrospray is for the most part correct then the charging or the conductive transport of charge to the surface becomes quite important. In fact the transport of charge must then be considered a current limiting step. For instance increasing the concentration of electrolyte will typically increase the observed current, the important question then becomes; why? Initially this question may seem straightforward enough however upon consideration it becomes quite complex owing to the amount of variables that may come into play. It is first important to redefine some of the key aspects of current generation; the first is the creation of a charge density (it is assumed that free charges relax to the surface) and the second is the transport of such charge. The latter has already been discussed in terms of the cone surface and the filament jet. The filament jet not only carries the charge but it is also responsible for the bulk transport of the liquid and variation in the filament diameter can lead to differences in the velocity of the jet and therefore in the filament current. Similarly the flow velocity at the cone surface is also important and has been described by Hayati [38] and Fernandez De la Mora and Loscertales [36]. If the charge density

is considered constant regardless of conductivity then the velocity profiles become critical in determining the current. Therefore in considering the discussion concerning Fig. 6.15, a decrease in current should be observed for a larger flow rate. The opposite is observed.

The charging of the liquid surface is probably the more important of the two, this seems to be supported in the literature, where some authors suggest; "Charge separation effects become then current limiting" [43]. There is however minimal information on this particular aspect of the process and for the most part it is referred to in passing only.

If we consider the process to be a steady state one, then as the convective charge current travels down the cone to the filament and then out to form the spray it must be continually resupplied at the base of the cone by a conduction current. The supply of ions is thought to be based on an electrophoretic or charge separation model [44,45], where in the case of a negatively biased capillary the negative ion will migrate towards the surface under the influence of an external field whereas the counter ion will migrate away from it, and eventually to the counter electrode where it is presumably discharged. There must then be a time dependent supply of ions to the surface by conduction, dictated by the flow and loss of charge at the filament. In addition this would imply that the discharge of counter ion must be efficient in that it matches the current requirements if not dictating it.

For a set of conditions, where for example a  $1 \times 10^{-4} \text{M}$  solution of KCl is electrosprayed, fluctuations or perturbation of the steady state system are uniquely reflected in the observed current. For example the observed current for this particular experiment was  $\sim 60 \text{nA}$ ,

oscillations caused by the pump will be reflected at the cone where the flow rate appears to increase and decrease in a regular fashion. The flow of liquid to the cone thus fluctuates and manifests itself into an observed current oscillation of 1-2 nA depending on the severity of the oscillation. The oscillation leading towards increased flow rate yields a high swing in current and vice versa, if the charge conduction process is static then the filament diameter must increase to accommodate the excess liquid which should result in a decrease in current, the opposite is observed as implied in the discussion of Fig. 6.14.

For higher concentration samples ( $\text{KCl} \geq 3 \times 10^{-4} \text{M}$ ) it is noted that there is a time dependence on stability. A cone may appear unstable (as in Fig. 6.4) however after a period of time the cone may stabilize itself and form a steady state. This phenomena is little understood and is obviously the result of an equilibration process. However whether it is the result of a net decrease in charge supplied to the surface or change in the amount of counterion discharged at the electrode surface is little understood. Other processes could be occurring.

If the current was based on a time dependant supply of ions to the surface, then individual properties of the ions should reflect this. For instance if a particular ion had a greater relative mobility than a second ion (where both ions had the same counter ion) under the influence of an electric field, than it should reach the interface faster. All things considered equal then in a given time period more of the faster ion should accumulate at the interface. Therefore the surface charge density becomes based on the initial concentration and the movement of the ion to the surface. Two ions of equal concentration

but of differing relative mobilities may then exhibit different overall currents in the Taylor cone mode.

To explore the above thought a series of simple potassium salts (KCl, KI, KClO<sub>4</sub> and K<sub>2</sub>SO<sub>4</sub>) were selected for study. The experiment consisted of acquiring current versus voltage curves for the above solutions run in negative ion mode. As all the ions have the same counter ion it was then assumed that the current would be due the various anions alone. The results are presented in Fig. 6.21, where Fig. 6.21a is the current versus voltage profile and Fig. 6.21b is the observed current versus electrolyte in the Taylor cone mode. The plots indicate a different current response for each of the anions.

To better understand this, the conductances of the various solutions must be considered. The molar conductivities may be calculated using the Fouss-Onsager conductance equation [46]. The form of the equation for unassociated electrolytes is given by:

$$\Lambda = \Lambda_0 C - SC^{1/2} + EC \log C + JC \quad (6.7)$$

where  $\Lambda$  is the molar conductance and  $\Lambda_0$  is the limiting molar conductance,  $C$  is the electrolyte concentration,  $S$  is the Onsager limiting slope,  $E$  is a constant and  $J$  is a coefficient where both are functions of the solvent properties. These values along with other physical data on methanol are given in Tables 6.1 and 6.2. The unassociated form of the equation was chosen

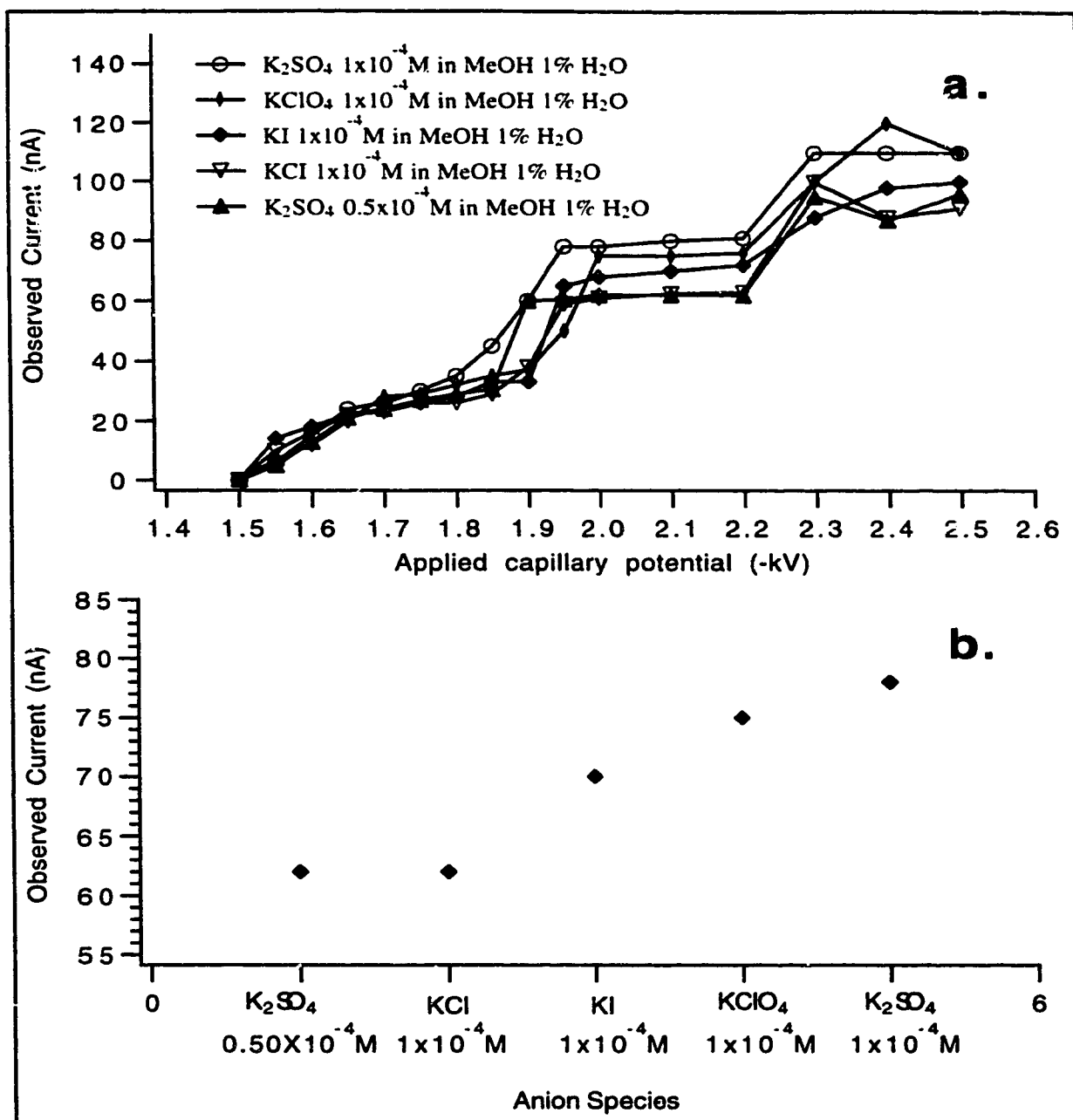


**Figure 6.21** Observed current profiles for various electrolytes ( $\text{KCl}$ ,  $\text{KI}$ ,  $\text{KClO}_4$ ,  $\text{K}_2\text{SO}_4$ ) in methanol. a.) current versus applied potential and b.) current versus electrolyte.

Table 6.1: Physical Properties and Theoretical Constants of Methanol<sup>a</sup>.

Dielectric constant	$\epsilon$	32.64
Viscosity	$100\eta$	0.5445
Density	$d$	0.78665
Fouss-Onsager constants:	$S$	243
	$E$	576
	$J$	1270

a. Kay R.L., J. Am. Chem. Soc. 82, (1960), 2099-2105.

Table 6.2: Physical Parameters of Electrolytes in Methanol<sup>a,b,c</sup>.

Electrolyte	$\Lambda_0^{a,b}$ $\Omega^{-1}\text{cm}^2\text{M}^{-1}$	$\lambda_{-o}^c$ $\Omega^{-1}\text{cm}^2\text{M}^{-1}$	$K_a^d$ M	$r^e$ $10^{-10}\text{m}$
KCl	107.9	52.3	0 (5)	1.81
KBr	108.9	56.5	0	1.96
KI	115.2	62.8	0	2.20
KClO <sub>4</sub>	123.1	71.0	11	2.40 <sup>f</sup>

a. Kay R.L., J. Am. Chem. Soc. 82, (1960), 2099-2105.

b. Conti, F., and Gianfranco, P., J. Phys. Chem., 72, (1968), 2245-2248.

c. B. Kratochvil and H.L. Yaeger, "Conductance of Electrolytes in Organic Solvents" in *Topics in Current Chemistry*, Vol. 27, pp. 1-58 (1972).

d. Association constant.<sup>a,c</sup>

e. Ionic radii, CRC Handbook of Chemistry and Physics, R.C. Weast ed., M.J. Astle Assoc. Ed., 61st ed., CRC Press Inc., Boca Raton, (1980-1981).

f. W.E. Dasent, "Inorganic energetics An Introduction", Cambridge University Press, Cambridge, 1982 2nd ed., pp. 78.



because of the relatively small values of the association constants and dilute conditions.

Table 6.2 lists the limiting ionic conductivities as given by Kratochvil and Yaeger [47]. A first approximation of the differences in ion mobilities may be observed in Fig. 6.21 where the limiting single ion mobility-viscosity product is plotted as a function of the estimated crystallographic radii of the various anions. There is obviously a trend, where the 'larger' ions seem to have higher mobilities. This reverse size-mobility dependence is probably the result of the smaller less polarizable ions having a greater solvent affinity. Thus for ions of similar size but greater charge (i.e. 1<sup>-</sup> and 2<sup>-</sup> ions) solvation may become more important, resulting in a larger solvent sphere being associated with the ion as it travels through the medium. Conductance data was not available for the sulfate anion, and so it cannot be compared to the singly charged anions with any confidence. For the sulfate di-anion it is thought that solvation is important and hence will have an affect on its relative mobility.

Figure 6.21b shows an increase in observed current going through the series from chloride to perchlorate, which seems to correlate well with the conductance data. Although the sulfate data cannot be compared as directly to the singly charged anions, it reveals several interesting aspects of the charging process. The  $0.50 \times 10^{-4} \text{M}$   $\text{K}_2\text{SO}_4$  solutions exhibits a similar current response as the  $1 \times 10^{-4} \text{M}$   $\text{KCl}$  solution, although their concentration ratios are 1:2 respectively there charge ratios are 1:1. A  $1 \times 10^{-4} \text{M}$   $\text{K}_2\text{SO}_4$  solution on the other hand has a 1:1 concentration with a corresponding 2:1 charge ratio with  $\text{KCl}$ , the resultant current is obviously higher. Without further

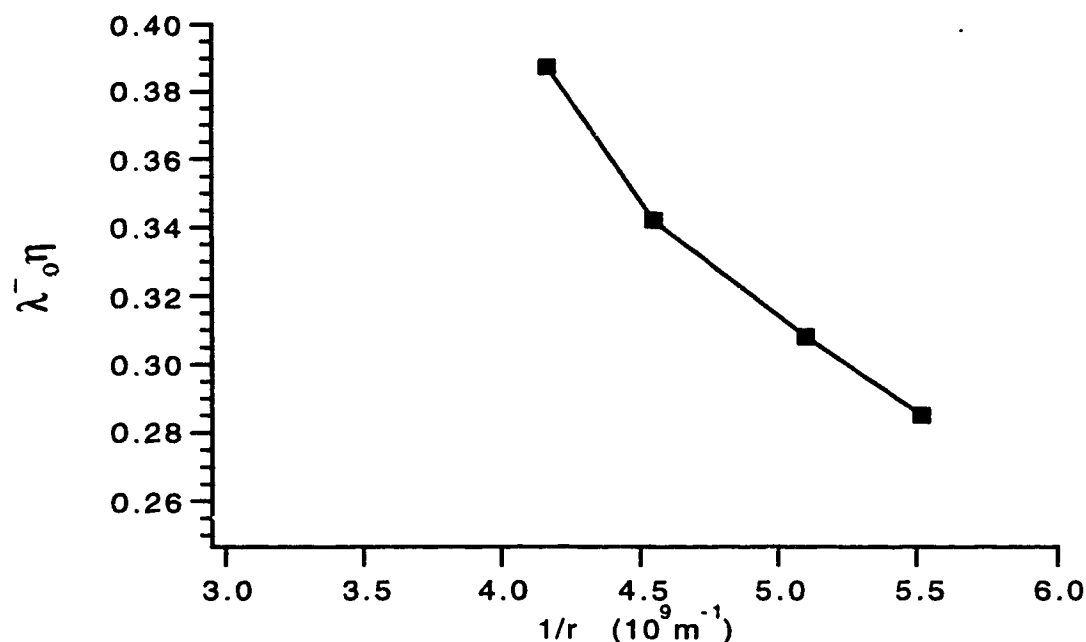
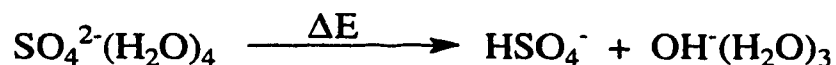


**Figure 6.22** Limiting single ion mobility-viscosity product versus the reciprocal of the estimated crystallographic radii for various anions in methanol.

data, it is difficult to compare these two species. However, what is revealed is that at the mass spectrometer, obvious intensity differences should be observed. For example, if it is assumed that sulfate exists almost entirely as the  $2^-$  species in dilute solution, then the actual numbers observed due to a current of  $\sim 60\text{nA}$  will appear to be that of a  $30\text{nA}$  signal acquired from a singly charged species. Likewise, the signal from the  $1 \times 10^{-4}\text{M}$   $\text{K}_2\text{SO}_4$  solution will give rise to an actual ion number  $1/2$  of the current ( $\sim 39\text{nA}$ ). This only considers processes occurring at the Taylor cone and when processes occurring in the charged droplets are considered interpreting mass spectrometrically observed ion intensities may become more complicated [48]. Processes occurring in the droplet refer to charge equilibration where an excess

of one ion may be enriched at the surface to exchange with ions in the bulk and its relative affinity for the surface larger relative to the bulk. These processes are however not the focus of this paper.

If solution mixtures of the various electrolytes are sampled by the mass spectrometer then to a first approximation these intensity differences should be observed. Three spectra are presented in Fig. 6.23 to exemplify this: Fig. 6.23a contains  $\text{KClO}_4$  and  $\text{KI}$ , Fig. 6.23b contains  $\text{K}_2\text{SO}_4$  and  $\text{KI}$  and Fig 6.23c contains  $\text{KCl}$ ,  $\text{KI}$  and  $\text{K}_2\text{SO}_4$  where all electrolyte is present in equal molar concentrations at  $1 \times 10^{-4} \text{M}$ . Each spectrum is acquired under identical conditions, with a sampling plate to skimmer potential difference of 35V. This potential difference effectively strips all the solvent from the gas phase ions and results in 'bare' gas phase ions being detected. In particular it results in solvated sulfate being stripped down to  $\text{HSO}_4^-$  via collisionally induced dissociation or CID as described by the following basic mechanism.



The  $\text{HSO}_4^-$  is created in the expansion region primarily and this particular reaction has been discussed in detail in the literature [28].

Examination of Fig. 6.23a-c reveals obvious differences in the equal molar ion signal intensities. The results typically reflect the relative intensities as would be expected from Fig. 6.21, especially

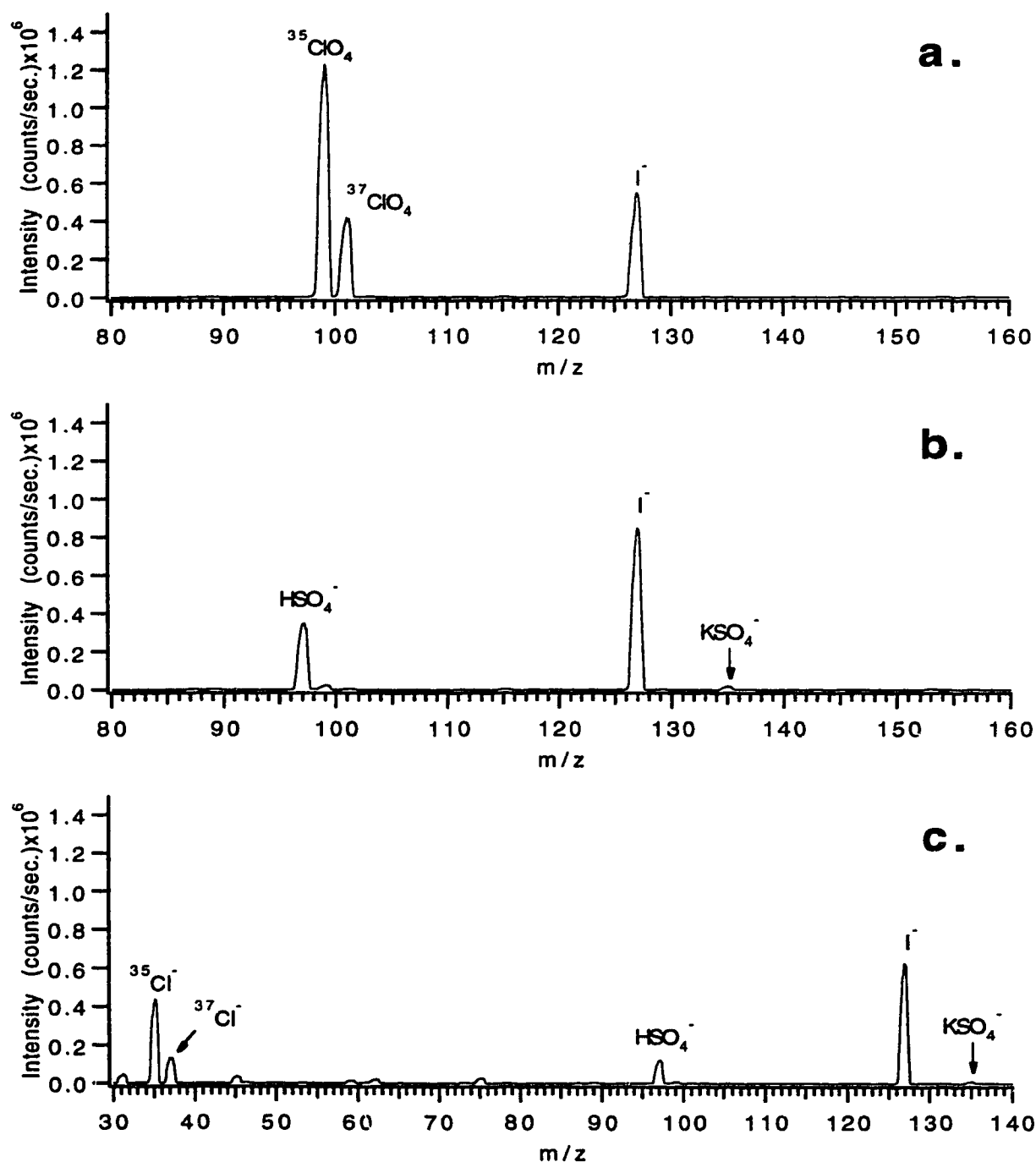


**Figure 6.23** The electrospray mass spectra of three different solutions acquired at a capillary to front plate separation of 5mm, flow rate of 2.00  $\mu\text{L}/\text{min.}$ , and a sampling plate to skimmer potential difference of 35V. All electrolyte is present at  $1.0 \times 10^{-4}\text{M}$  in methanol. a.)  $\text{KClO}_4$  and  $\text{KI}$ , b.)  $\text{K}_2\text{SO}_4$  and  $\text{KI}$  and c.)  $\text{KCl}$ ,  $\text{K}_2\text{SO}_4$  and  $\text{KI}$ .

with regards to the sulfate intensities which seem to be much lower than any of the singly charged anions. As well perchlorate which is thought to have the greatest mobility exhibits an extremely strong signal.

It should be noted that this relationship should not be over interpreted as other effects are thought to occur in the charged droplets which may serve to enhance or subtract from the eventual ion intensity as observed by the mass spectrometer. Tang and Kebarle have reviewed this subject in some detail [48]. Therefore the observed intensities in Fig 6.21 may be the product to some degree of these effects.

The results shown above do seem to correlate well with those proposed and that in part the charging process at the cone may have direct consequences in the observed mass spectra. It does seem that based on the current intensities of Fig. 6.21 that there is an obvious difference in the charging of an interface by different electrolytes. Thus the chemical nature of a particular ion (strong electrolyte) must have some effect on its observed ion intensity and cannot simply be thought of as a 'strong electrolyte' with only a generic character typical of a class of ions. These differences are probably also observed in process occurring in the droplet, which may lead to a net increase or decrease in surface concentration and ultimately change the ion intensities observed.

## 6.4 Conclusions

As was implied at the beginning of this paper electrospray is quite a complicated ion source. As a result there are several complex processes which occur to generate the gas phase ions as recorded on a mass spectrum. In order to better understand these processes a thorough investigation of the phenomena was undertaken and the results were presented both pictorially and through discussion. The discussion it should be stressed is based on the author's observation and interpretation of such events with support from the literature. As an ion source, electrospray's ability to generate a stable signal or current is determined primarily by its ability to maintain a stable Taylor cone. From this mode it is able to uniquely generate gas phase ions which more or less reflect the solution composition as is observed in Fig. 6.23 and countless application papers devoted to the subject. There is however no complete or near 100% conversion of solution ions to the gas phase and as a result there is a seeming 'competition' to achieve a 'free' gas phase ion state. The competition seems to start in the cone and is transferred right through to the smallest of droplets. In addition the formation of the spray which is critical to the formation of gas phase ions becomes at the same time counter productive to signal intensity due to dilution of charge. As an ion source however its uniqueness has been realized and its contribution has been invaluable. With further study its applications can only increase.

## 6.5 References

1. J. Zelany, *Phys. Rev.*, **3**, 69, (1914).
3. B. Vonnegut and R.L. Neubauer, *J. Colloid Sci.*, **7**, 616, (1952).
3. G.I. Taylor, *Proc. Roy. Soc. A.*, **280**, 383, (1964).
4. J.R. Melcher and G.I. Taylor, *Annu. Rev. Fluid Mech.*, **1**, 11, (1969).
5. R.J. Pfeifer and C.D. Hendricks, *Phys. Fluids*, **10**, 2149 (1967).
6. M. Dole, L.L. Mack, R.L. Hines, R.C. Mobley, L.D. Ferguson and M.B. Alice, *J. Chem. Phys.*, **49**, 2240 (1968).
7. M. Yamashita and J.B. Fenn, *J. Phys. Chem.*, **88**, 4451 (1984).
8. M. Yamashita and J.B. Fenn, *J. Phys. Chem.*, **88**, 4671 (1984).
9. V. Katta, S.K. Chowdhury and B.T. Chait, *J. Am. Chem. Soc.*, **112**, 5348 (1990).
10. X. Xu, S.P. Nolan and R.B. Cole, *Anal. Chem.*, **66**, 66 119 (1994).
11. C.L. Gatlin, F. Turecek and T. Vaisar, *Anal. Chem.*, **66**, 712 (1994).
12. R. Arakawa, T. Matsuo, H. Ito, I. Katakuse, K. Nozaki, T. Ohno and M. Haga, *Org. Mass Spectrom.*, **29**, 289 (1994).
13. J.M. Curtis, P.J. Derrick, A. Schnell, E. Constantin, R.T. Gallagher, and J.R. Chapman, *Inorg. Chim Acta*, **21**, 197 (1992).
14. A.M. Bond, R. Colton, J.C. Traeger, and J. Harvey, *Inorg. Chim Acta*, **212**, 233 (1993).
15. A.T. Blades, P. Jayaweera, M.G. Ikonomou and P. Kebarle, *Int. J. Mass Spectrom. Ion Processes*, **101**, 325 (1990).

16. A.T. Blades, P. Jayaweera, M.G. Ikonomou and P. Kebarle, *Int. J. Mass Spectrom. Ion Processes*, **102**, 251 (1990).
17. Z.L. Cheng, K.M.W. Siu, R. Guevremont and S.S. Berman, *Org. Mass Spectrom.*, **27**, 1370 (1992).
18. Z.L. Cheng, K.M.W. Siu, R. Guevremont and S.S. Berman, *J. Am. Soc. Mass Spectrom.*, **3**, 281 (1992).
19. G.R. Agnes and G. Horlick, *Appl. Spectrosc.*, **46**, 401 (1992).
20. G.R. Agnes and G. Horlick, *Appl. Spectrosc.*, **48**, 655 (1994).
21. G.R. Agnes, I.I. Stewart and G. Horlick, *Appl. Spectrosc.*, **48**, 1347 (1994).
22. G.R. Agnes and G. Horlick, *Appl. Spectrosc.*, **48**, 649 (1994).
23. G.R. Agnes and G. Horlick, *Appl. Spectrosc.*, **49**, 324 (1995).
24. I. I., Stewart and G. Horlick, *Trends in Anal. Chem.*, **15**, 80 (1996).
25. I.I. Stewart and G. Horlick, *Anal. Chem.*, **66**, 3983 (1994).
26. J.J. Corr and D.J. Douglas, "Elemental Ion Spray-Mass Spectrometry: Analysis of Solutions of Metal Salts", in *Abstracts and Index of Authors of the 41 st ASMS Conference of Mass Spectrometry and Applied Topics*, San Francisco, p.202 (1993).
27. I. I., Stewart and G. Horlick, *J. Anal. At. Spectrom.*, submitted (1996).
28. I. I., Stewart, D. Barnett and G. Horlick, *J. Anal. At. Spectrom.*, in press (1996).
29. D.P.H. Smith *IEEE Trans. Ind. Appl.*, **63**, 527 (1986).
30. I. Hayati, A.I Bailey, and TH. F. Tadros, *J. Colloid. Interface Sci.*, **117**, 205 (1987).
31. I. Hayati, A.I Bailey, and TH. F. Tadros, *J. Colloid. Interface Sci.*, **117**, 222 (1987).



32. M. Cloupeau and B. Prunet-Foch, *J. Electrostatics*, **22**, 135 (1989).
33. M. Cloupeau and B. Prunet-Foch, *J. Electrostatics*, **25**, 165 (1990).
34. K. Tang and A Gomez, *Phys. Fluids*, **6**, 2317 (1994).
35. J. Fernandez De La Mora, *J. Fluid Mec.*, **243**, 561, (1992).
36. J. Fernandez De La Mora and I.G. Loscertales, *J. Fluid Mec.*, **260**, 155, (1994).
37. J. Rossell-Lompart and J. Fernandez De La Mora, *J. Aerosol Sci.*, **25**, 1093, (1994)
38. I. Hayati, *Colloids and Surfaces*, **65**, 77, (1992).
39. Lord Rayleigh, *Philos. Mag.*, **14**, 184 (1882).
40. P. Kebarle and L. Tang, *Anal. Chem.*, **65**, 972A (1993).
41. P. K. Weissenborn and R.J Pugh *Langmuir*, **11**, 1422 (1995).
42. K. Hiraoka, K. Murata and I. Kudaka, *Rapid Commun. Mass Spectrom.*, **7**, 363 (1993)
43. A. Gomez and K. Tang, *Phys. Fluids*, **6**, 404 (1994).
44. M.G. Ikonomou, A.T. Blades and P. Kebarle, *Anal. Chem.*, **62**, 957, (1990).
45. M.G. Ikonomou, A.T. Blades and P. Kebarle, *Anal. Chem.*, **63**, 1989, (1991).
46. R.L. Kay, *J. Am. Chem. Soc.*, **82**, 2099 (1960).
47. B. Kratochvil and H.L. Yaeger, "Conductance of Electrolytes in Organic Solvents" in *Topics in Current Chemistry*, Vol. **27**, pp. 1-58 (1972).
48. L. Tang and P. Kebarle, *Anal. Chem.*, **65**, 3654 (1993).

## **Chapter 7**

### **Surface Tension Gradients**

## 7.1 Introduction

It has been long realized by researchers who use Electrospray Mass Spectrometry (ESMS) to study of gas phase ions that there is a discrepancy between the relative concentration of electrolytes in solution and what is recorded in a mass spectrum. It was this discrepancy which probably led to the formulation of Iribarne and Thompsons' ion evaporation model in the 1970's when they were investigating the mechanism of ion production from evaporating charged droplets [1,2]. Although they used an atomizer/induction electrode to produce a fine mist of charged droplets [2] rather than the charged electrospray capillary, the process of 'liberation' of gas phase ions from the charged droplets must be similar. It was not until the mid 1980's that the successful coupling of the electrospray source to a mass spectrometer was achieved by Yamashita and Fenn [3,4]. With this coupling a literal explosion of applications found their way into the literature, and consequently a number of fundamental questions were raised. It rapidly became obvious that although the technique could generate intact gas phase ions from solution the exact mechanism of such was little understood. As a result numerous investigations were undertaken by the mass spectrometry community (far too many to properly reference here) in order to further define the technique and propose explanation to account for the little understood aspects of this phenomena. Although a lot has been learned there is still much to learn and in a recent review of the current thought on ESMS by Kebarle and Tang the authors preface this up by saying: " Readers of

this report will learn about current ideas but will not find certainty" [5].

Perhaps one of the most intriguing and revealing aspects about electrospray is the nonlinear relationship between the observed intensity and the solution concentration of ions. This dependence has been studied in some detail by Tang and Kebarle [6]. In particular the overall ion intensity of one species may vary widely depending on which other ions are present. This may be traced to "surface activity", which when broadly applied refers to an ions preference to be at the surface rather than in the bulk and thus have a higher relative concentration in this phase rather than the bulk.

If one considers a charged droplet originating from a filament jet issuing from a Taylor cone as discussed in chapter 6, then depending on the experimental conditions ( i.e., concentration, flow rate, etc.) it will be created with some initial charge to liquid mass or droplet size ratio. If the liquid is methanol then it will evaporate from the droplet and this typically occurs until a critical droplet radius is achieved upon which the droplet becomes unstable. This critical point may be evaluated in terms of Rayleighs criterion for droplet instability as given below[7];

$$Q^2 = 64\pi^2 \epsilon_0 \gamma R_r^3 \quad (7.1)$$

where Q refers to the surface charge present at the meniscus of radius R,  $\epsilon_0$  is the permittivity of free space and  $\gamma$  is the liquid surface tension. It has actually been observed that the fission process occurs at a value some 80% less than that predicted by equation (7.1) [8,9]. The

fission process is characterized by the droplet expelling excess charge in the form of a jet of liquid from the surface which serves to carry away ~ 2% of the droplet mass and ~15% of the charge in the form of multiple droplets. This process of evaporation-fission is thought to cycle in the droplets down to some critical size at which point the gas phase ions are 'liberated' through some little understood process [6]. If these process are occurring prior to the 'liberation' of gas phase ions then the droplet environment cannot be considered static in that any charge originally present at the surface will remain there 'locked' in position as it were. This is important because during this time electrolyte in the bulk may exchange with electrolyte at the surface of the droplet thus enhancing the surface population of one ion relative to others. The amount of exchange then becomes dependent on the evaporation rate of the droplet relative to the time of diffusion for a particular ion. Tang and Kebarle express the time of diffusion of an ion to the surface as;

$$t_{\text{diff}} = R^2/\pi D \quad (7.2)$$

where R is the radius of the ion and D is the diffusion coefficient of the ion. For non 'surface active' ions there will be a non discriminating partition between the bulk and surface and so it should not serve to enhance or decrease the net surface concentration. If however there is 'surface activity' or specific adsorption at the interface then there may be a net accumulation of one ion at the interface relative to another ion depending on there relative 'surface activities'. It was thought that strong electrolytes such as the alkali metals have no 'surface activity'

and as a result they do not accumulate at the surface as other surface active ions do [6]. It has been observed that strong electrolytes do exhibit a relative ion intensity difference for equal solution concentrations and therefore this chapter is dedicated to exploring this. This chapter is based on uncompleted work, and therefore is written accordingly. This chapter will highlight the observed mass spectrometric results which led to the initiation of the research and the experimental procedure that would be initiated to investigate such observations focusing on the procedures and the importance of the results.

## **7.2 Experimental**

All mass spectra are recorded using an in house electrospray source and a modified PE/SCIEX ELAN 250 ICP-MS. These have been described previously in the thesis especially chapters 1 and 2 and will not be discussed further here.

The measurement of surface tension was performed using the hanging pendant drop method and will be described later in the text in detail.

Solutions used in these experiments were prepared from distilled H.P.L.C grade methanol, and reagent grade salts. Typically a stock solution of  $1.0 \times 10^{-2} \text{M}$  electrolyte was prepared and then diluted appropriately with methanol. The stock solutions were prepared from dissolving the appropriate amount of electrolyte in methanol, and in some cases ultra filtered distilled water.

### 7.3 Discussion

#### 7.3.1 Mass Spectral Ion Intensity

When solutions containing a mixture of strong electrolytes are electrosprayed the mass spectrometric response of each ion may be quite different depending on the nature of the ion. This behavior has been observed for ions which are typically not considered to be 'surface active'. An example of this is given in Fig. 7.1a below. The solution contained KCl, KClO<sub>4</sub> and KI, each 1.0x10<sup>-4</sup>M in methanol. The spectrum was acquired in negative ion mode with a sampling plate to skimmer potential difference of 35V which resulted in stripping CID conditions. From the spectrum (Fig. 7.1a) it is obvious that there is a difference in intensity between the electrolytes. For the most part the halides have similar total (isotopic) intensity responses however perchlorate also regarded a fairly strong non-complexing electrolyte has a much greater intensity response than the halides. This was somewhat unexpected. The response difference between the halides from this spectrum is difficult to discern however upon closer inspection is on the order of ~22% less than the iodide ion signal. The chloride ion response compared to iodide is consistently lower from solution to solution and mixture to mixture. These results or numbers should be viewed with caution however as an ion transmission curve was never evaluated and so differences at this level (~20%) may be due to some extent to different transmission efficiencies of the ions. As a rough guide however a quadrupole transmission curve is given in Fig. 1 in

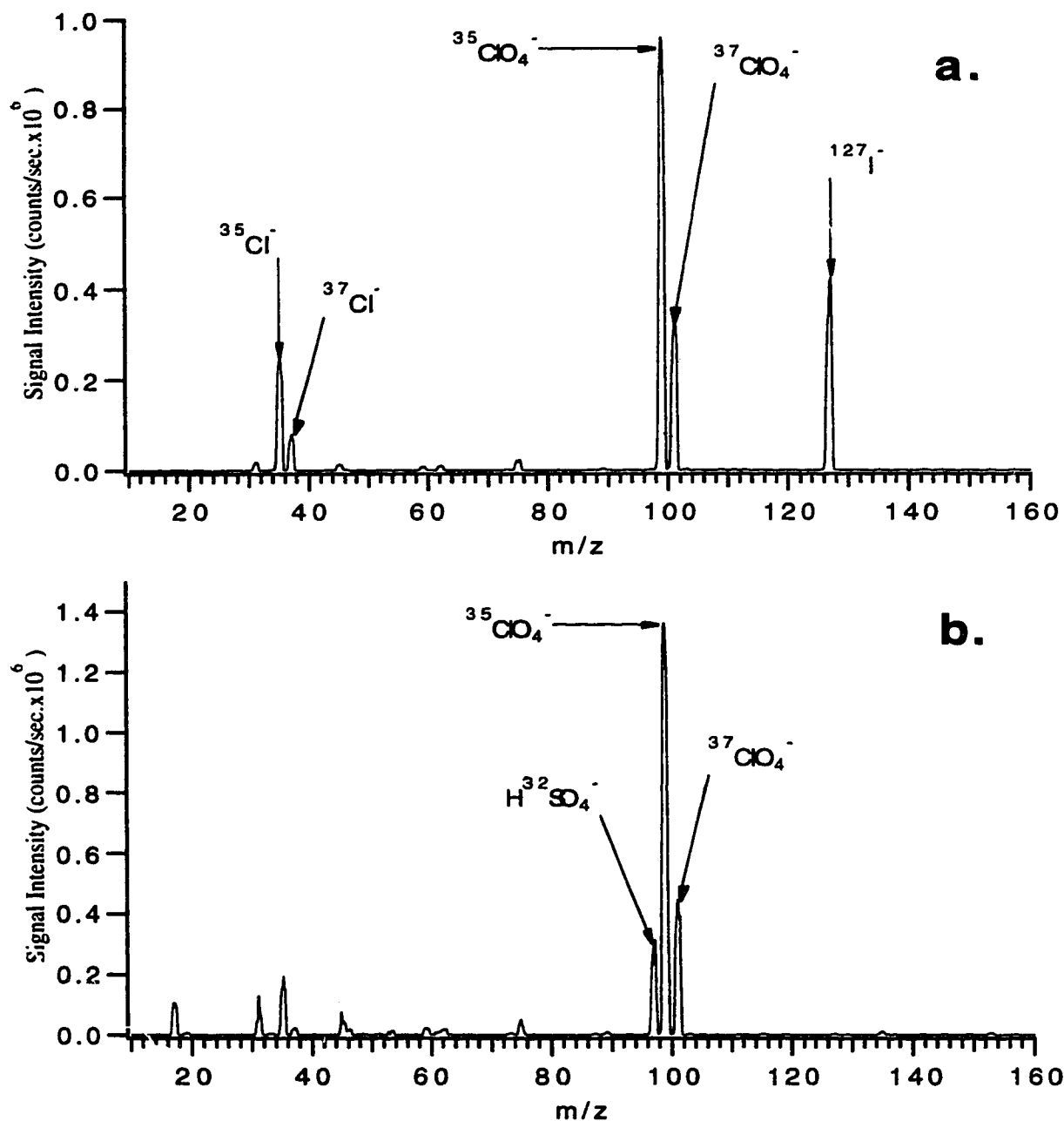


**Figure 7.1** The electrospray mass spectra of a) KCl, KClO<sub>4</sub> and KI and b) KClO<sub>4</sub> and K<sub>2</sub>SO<sub>4</sub> each at  $1.0 \times 10^{-4}$  M in methanol. The spectra are acquired in negative ion mode with a sampling plate to skimmer potential difference of 35V, at a flow rate of 2.00  $\mu\text{L}/\text{min}$ .



a paper by Tang and Kebarle [6]. From this curve there does not appear to be a great transmission difference between an ion of  $m/z$  35 and one of  $m/z$  127. Again this may be only used as an example or rough guide in assessing the intensity difference. Despite this, the authors feel that there is a real intensity difference between the two halides.

Figure 7.1b is the mass spectrum of  $\text{KClO}_4$  and  $\text{K}_2\text{SO}_4$  each  $1 \times 10^{-4}\text{M}$  in methanol, collected under the same conditions as Fig. 7.1a. The spectrum in this case highlights a real intensity difference where the perchlorate although overlapping isobarrically with the  $\text{H}^{34}\text{SO}_4^-$  isotope at  $m/z$  99 is  $\sim 4\times$  more intense. Based on the discussion in Chapter 7 of this thesis, one may expect this intensity difference. However based on ion currents alone one may anticipate that the intensity difference would be on the order of  $\sim 2:1$  rather than the observed  $\sim 4:1$  ratio. Consider also that the  $\text{HSO}_4^-$  ion is initially formed as a solvated  $\text{SO}_4^{2-}$  ion and therefore reflects the later's gas phase ion intensity rather than the former. The fact that the solvated sulfate may be stripped down to the  $\text{HSO}_4^-$  ion precludes any mass dependent transmission losses through the quadrupole as both ions have will have nearly the same  $m/z$ , and so the intensity differences in this case may be viewed as real.

Although the above figure presents only two examples of this sort of behavior it is readily observed with other ions. The above example does illustrate an obvious intensity difference between strong electrolytes. It therefore becomes advantageous to anticipate these differences as it enables the researcher to properly interpret and plan experiments. This becomes especially important when

investigating quantitation by ESMS as a selected buffer analyte may serve to either enhance a particular sample ions intensity or reduce it. The next section discusses one possible method to achieve this.

### 7.3.2 Surface Tension Gradients

It is well known that the surface tension of a liquid at constant temperature may vary significantly with the addition of organic or inorganic solutes. For example the addition of sodium chloride to water serves to increase the surface tension, while the addition of propionic acid serves to decrease the surface tension. A correlation between the concentration of a solute in a solvent and the resultant surface tension was derived by Gibbs over a century ago;

$$d\gamma = - \Gamma_j d\mu_j \quad (7.3)$$

where  $\Gamma_j$  is the surface excess of the solute  $j$  adsorbed per unit surface area at the liquid-air interface,  $\gamma$  is the surface tension and  $\mu_j$  is the chemical potential of the solute. For dilute solutions  $d\mu_j = RT d(\ln C_j)$  where  $C_j$  is the concentration of solute  $j$ . This leads to the simplified form;

$$d\gamma = - (RT/C_j)\Gamma_j dC_j \quad (7.4)$$

which may be re expressed in terms of surface excess;

$$\Gamma_j = - (C_j/RT)(d\gamma /dC_j)$$

It then becomes obvious that a plot of surface tension versus concentration yields the slope in the above equation which then

ultimately determines whether or not the surface excess is positive or negative. Returning to the original example of sodium chloride in water where surface tension increased as a function of increased concentration, the slope is positive and hence there is a negative excess or negative adsorption at the surface. The reverse is true for propionic acid. From the above example it may be concluded that the propionic acid is "surface active" whereas sodium chloride is non "surface active".

To understand this it must be understood that the liquid in the surface phase exhibits properties different from that of the bulk phase. For a given gas liquid interface such as a liquid drop, the liquid behaves as if it is surrounded by an elastic skin with a tendency to contract. Consider now a freshly formed droplet that is free of stress, the molecules of liquid at the surface would then have a higher chemical potential than that of molecules in the bulk. Therefore there would be a net movement of some of the molecules from the surface towards the bulk (i.e to a position of more favourable chemical potential) resulting in an increase in the molecular spacing in the surface layer. This of course will lead to an extra attractive tension between the molecules in the surface layer, reducing their chemical potential. The net desorption of liquid from the surface continues until a tension is achieved such that the chemical potential of the two phases is balanced. It is at this point that the number of molecules entering and leaving the surface layer is equal. Therefore in considering propionic acid and sodium chloride, it is obvious that their chemical potentials in the two phases

governs their respective net surface absorption or excess to some degree.

Consider solutions of two non "surface active" ions with the same counter ion, each of the electrolytes will have different surface tension gradients ( $d\gamma/dC_j$ ). Therefore even though they are both considered non "surface active" they will have different relative surface absorbances. Therefore large relative differences in  $d\gamma/dC_j$  should yield large differences in the surface concentration whereas small differences will yield little or no differences in the surface concentrations. The implications of this will be discussed in section 7.3.4.

### 7.3.3 Surface Tension Measurements

In order to calculate the surface tension gradient a method of evaluating the surface tension must be used of which there are many. The method of choice (based on availability) in this chapter would have been the pendant drop method. If a droplet of liquid is suspended from a rod or a small capillary it will take on an equilibrium shape. This shape may be related to Laplace's equation, which is the mechanical equilibrium condition for two homogeneous fluids separated by a curved interface. In essence this equation relates the pressure difference across a curved interface to the surface tension and the curvature of the interface and is given below;

$$\frac{2\gamma}{b} - \sigma_{gz} = \gamma \left[ \frac{1}{r_1} + \frac{1}{r_2} \right] \quad (7.5)$$

where;  $\gamma$  is the surface tension,  $\sigma$  is the density of the liquid,  $z$  is the access of symmetry,  $b$  is the radius of curvature at the droplet tip,  $g$  is the acceleration constant and  $r_1$  and  $r_2$  are the two principle axis of symmetry. The density of the liquid may be determined prior to analysis. Therefore the remaining variables may be measured from a picture taken of the droplet and the surface tension determined. Figure 7.2 gives a schematic representation as to how this is achieved. Backlighting is used to provide a silhouette image of the droplet, this image is then acquired by a CCD camera, digitized and then sent to a computer. A software program (ADSA-P: Axisymmetric Drop Shape Analysis-Profile) is then used to solve for  $\gamma$  based on the droplet shape. The ADSA-P technique has been described in the literature [10]. The technique should then be capable of tracking the change in surface tension as a function of concentration.

#### **7.3.4 Implications of the Surface Tension Gradient Measurements**

It is obvious that events which occur at the gas liquid interface in electrospray are of critical importance. For events which occur at the Taylor cone such as surface charging it is seen that the movement of charge to the interface is very important as was discussed in chapter 6 of this thesis. However for a charged droplet the movement of charge (ions) between the bulk and the interface is typically driven by diffusion rather than the influence of an electric field.

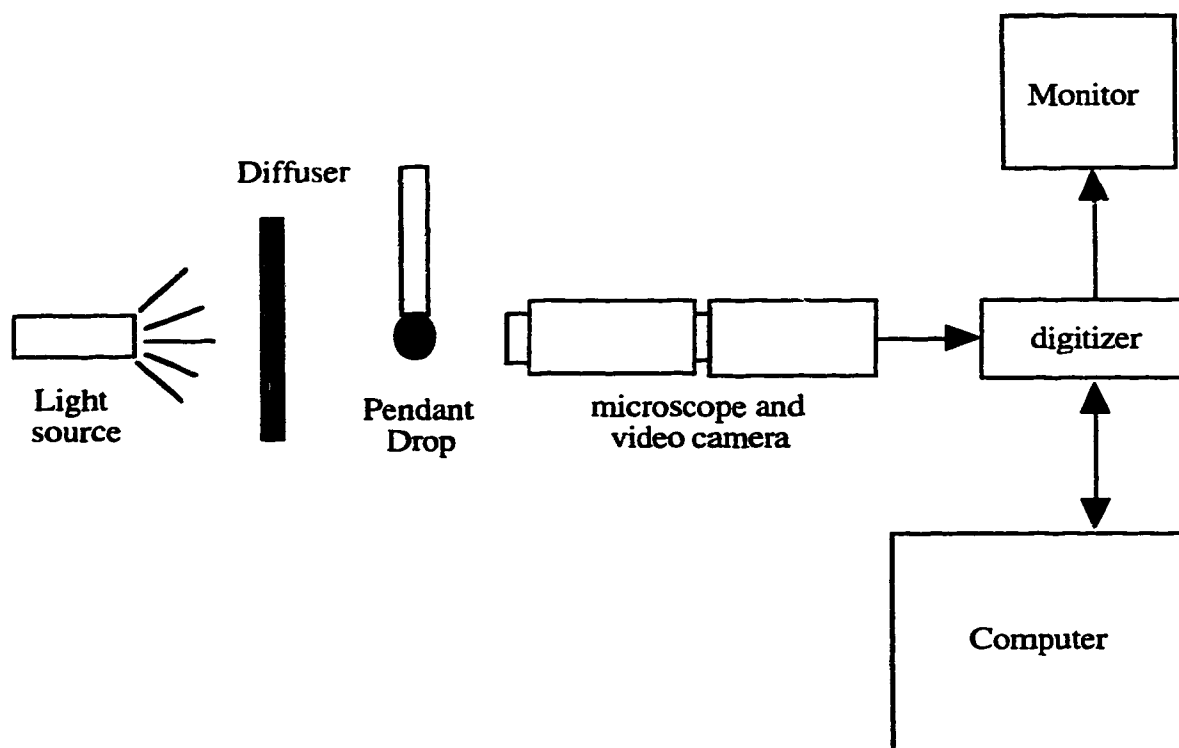


**Figure 7.2** The schematic representation of the system proposed to acquire surface tension measurements.

Consider an uncharged droplet containing two equal molar salts, where both cations are the same but the anions are different. In the uncharged state (i.e. no excess anion in the droplet) an equilibrium will exist for both species between the bulk and the interfacial region where depending on the value of the surface tension gradient a net positive or negative surface excess will occur. If the two salt species yield two different but positive surface tension gradients then at equilibrium the surface of the droplet will contain different concentrations of the two anions of an amount dictated by equation (7.4). If this droplet was then allowed to evaporate to some degree there will also be an accompanying increase in bulk

concentration and a net change in the surface tension which results or occurs as a result of changes in the relative surface concentrations.

If the above scenario is considered in terms of charged droplets formed as a result of the electrospray process then an excess of charge must then exist in a given droplet. This charge will be accounted for by the two anions in solution present at the surface in some ratio. If for simplicities sake equal concentrations are assumed initially and the time for evaporation before a fission process occurs is much greater then the time it takes of a particular anion to diffuse to the surface, then exchange may occur between the bulk and the surface. Therefore based on the fact that the two anions have different affinities for the surface layer at some time later it would seem obvious that the ratio of anion surface concentration will change to reflect this. In effect there will be a partitioning of the anions between the surface and the bulk where the ion with the lower chemical potential in the surface layer will or should have an increased concentration in this phase.

The situation may become further complicated if the process responsible for the formation of the charged droplets results in a net excess of one anion over the other. For example an ion that has a higher relative mobility may give rise to a higher surface concentration in the droplet charging process as discussed in Chapter 6. If this ion also has a greater affinity for the surface layer than the other then an even larger excess of this ion at the surface may be realized.

To summarize it was felt that if an ion had a greater relative affinity for the surface layer than a second ion it, then it would be

reflected in the relative surface populations of the two ions. This is only relevant however if the mechanism for the formation or 'liberation' of gas phase ions is directly reflective of the surface population of the ions.

It is difficult to evaluate this thought without the relevant surface tension gradients of strong electrolytes in methanol. However Weissenborn and Pugh have recently published a series of values for several electrolytes in water at 298K [11]. A selection of such surface tension gradients is presented in Table 7.1 for a variety of electrolytes. Weissenborn and Pugh were then able to classify various anions and cations as being either positively or negatively absorbed at the interface based on intercomparison between a whole range of electrolytes and the classification of selected anions is presented in Table 7.2. From Table 7.1 it is seen that for the same cation (sodium) salts there are obvious differences in the surface tension gradients which must be related to relative absorption of the various anions at the interface. In particular notice the relative differences between the sodium salts of chloride, iodide, perchlorate and sulfate. If these gradients held their relative values in methanol then we would expect that the observed ion intensities should reflect this in some part. For example the surface tension gradient differences between sodium sulfate and sodium perchlorate is quite large and as well perchlorate is thought to have a net positive surface absorption. From this it would be expected that the relative surface populations would be quite different. This difference is observed in the relative ion intensities of perchlorate and sulfate as seen in Fig. 7.1b.



**Table 7.1** Literature values<sup>a</sup> of  $dy/dc_j$  for a variety of electrolytes in water at 298K.

Electrolyte	$dy/dc_j$
NaCl	$2.08 \pm 0.08$
NaI	$1.23 \pm 0.06$
NaClO <sub>3</sub>	$0.89 \pm 0.05$
NaClO <sub>4</sub>	$0.22 \pm 0.06$
Na <sub>2</sub> SO <sub>4</sub>	$2.90 \pm 0.08$
KCl	1.85, 1.65
KBr	1.97

a. P.K. Weissenborn and R.J. Pugh, *Langmuir*, 11, 1422 (1995)

**Table 7.2** Anion Adsorption classification<sup>a</sup> for various anions in water at 298K.  
Positively adsorbed (+) and Negatively adsorbed (-).

Anion	Classification
F <sup>-</sup>	-
Cl <sup>-</sup>	-
Br <sup>-</sup>	-
I <sup>-</sup>	-
NO <sub>3</sub> <sup>-</sup>	-
ClO <sub>3</sub> <sup>-</sup>	+
ClO <sub>4</sub> <sup>-</sup>	+
SO <sub>4</sub> <sup>2-</sup>	-

a. P.K. Weissenborn and R.J. Pugh, *Langmuir*, 11, 1422 (1995)

tension gradients which must be related to relative absorption of the various anions at the interface. In particular notice the relative differences between the sodium salts of chloride, iodide, perchlorate and sulfate. If these gradients held their relative values in methanol then we would expect that the observed ion intensities should reflect this in some part. For example the surface tension gradient differences between sodium sulfate and sodium perchlorate is quite large and as well perchlorate is thought to have a net positive surface absorption. From this it would be expected that the relative surface populations would be quite different. This difference is observed in the relative ion intensities of perchlorate and sulfate as seen in Fig. 7.1b.

Examining the intensity response difference of a system containing two different electrolytes where one is held constant and the others concentration is varied should also yield responses reflective of the anions surface affinity. With this in mind the response of chloride was observed as a ratio of both iodide and perchlorate where each was held constant at  $0.5 \times 10^{-4} \text{M}$ . For the chloride ( $\text{Cl}^-$  and  $\text{ClO}_4^-$ ) species the total intensity due to the major isotopes was summed prior to ratioing. The results are presented in Fig. 7.3. From the plot it is seen that the points where the ratio is unity or equal intensities are observed is quite different for each system and hence the various slopes or responses are also different. For the chloride and iodide system equal intensities are achieved at a concentration ratio of  $\sim 2:1$ , whereas it is  $\sim 4:1$  for the chloride/perchlorate system. Referring to Table 7.1 and assuming that the relative surface tension gradient is similar or at least

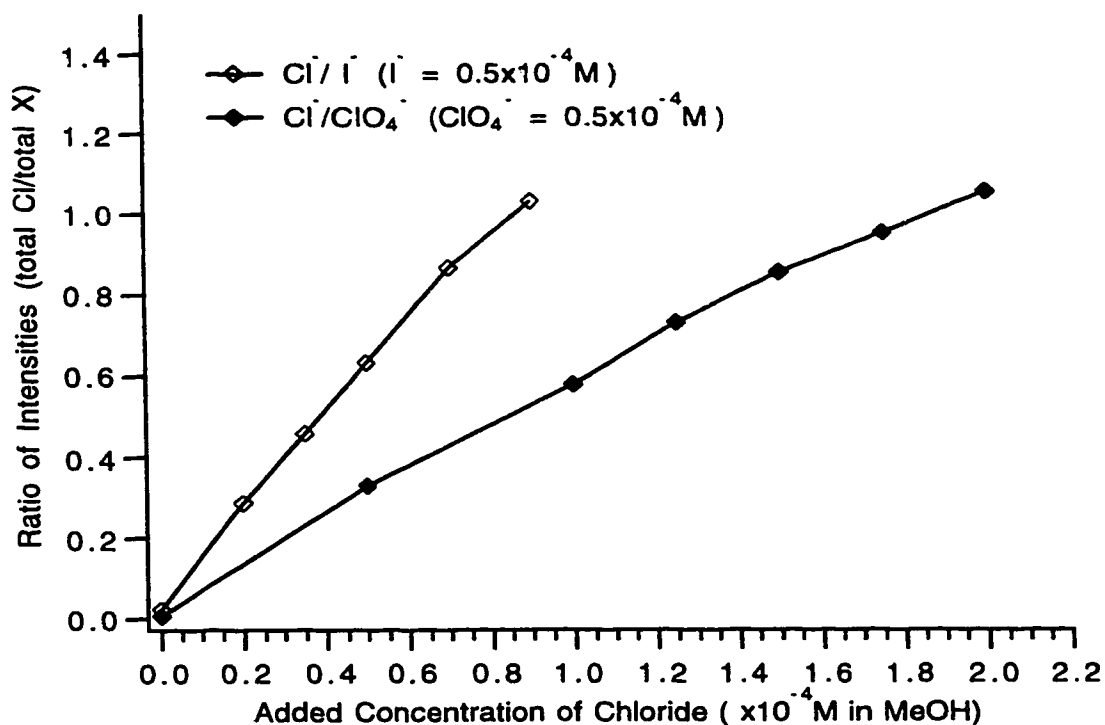


**Figure 7.3** Ratioed response curves for varying chloride concentrations in the presence of constant concentrations ( $0.5 \times 10^{-4}$  M) of iodide and perchlorate.

reflective of systems of potassium salts in methanol then the relative differences in the surface tension gradients should reflect this. This is observed where the difference between the chloride and iodide salts is markedly different than the chloride and perchlorate salts. Referring to Fig 6.20 of this thesis it is also observed that the ratio of iodide to perchlorate is  $\sim 3:1$  which is less than that of the chloride to perchlorate intensity as expected. From the above discussion it would seem likely that the relative surface affinities of the various anions would lead to surface enrichment and hence the relative intensities observed.

## 7.4 Conclusions

It is thought that surface enrichment does occur in a charged droplet with the net result being a greater concentration of the more "surface active" species. The expression "more surface active" does not necessarily imply that the ion must be "surface active" but just that it may have a larger surface excess and hence a greater relative affinity for the surface. The above discussion was only intended to characterize the thought behind the experiment and possible implications of the results which was partially supported by the literature [11]. Although the author believes there is a strong correlation between the surface tension gradient and the observed relative ion intensities of various species it must still be viewed with caution as the precise mechanism for formation of gas phase ions from the charged droplet surface is yet unresolved. If the mechanism was such that there was a direct correlation between surface concentration and gas phase ion production then knowledge of the surface tension gradient would be quite useful especially in planning out experiments of a quantitative nature. If the mechanism was such that the gas phase ion population was related to the relative evaporation rates of ions as suggested by Iribarne and Thomson [1,2], then knowledge of the surface tension gradient becomes less important. Tang and Kebarle in a detailed investigation of this problem were not able to conclude in favor of any one theory completely [6]. Regardless of which mechanism for ion production is correct the knowledge of the surface tension gradient is still an

important parameter in understanding and characterizing the events which occur at the interface.

## 7.5 References

1. J.V. Iribarne and B.A. Thomson, *J. Chem. Phys.*, **64**, 2287 (1976).
2. B.A. Thomson and J.V. Iribarne, *J. Chem. Phys.*, **71**, 4451 (1979).
3. M. Yamashita and J.B. Fenn, *J. Phys. Chem.*, **88**, 4451 (1984).
4. M. Yamashita and J.B. Fenn, *J. Phys. Chem.*, **88**, 4671 (1984).
5. P. Kebarle and L. Tang, *Anal. Chem.*, **65**, 972A (1993).
6. L. Tang and P. Kebarle, *Anal. Chem.*, **65**, 3654 (1993).
7. Lord Rayleigh, *Philos. Mag.*, **14**, 184 (1882).
8. D.C. Taflin, T.L. Ward and E.J. Davis, *Langmuir*, **5**, 376 (1989).
9. A. Gomez and K. Tang, *Phys. Fluids*, **6**, 404 (1994).
10. Y. Rotenburg, L. Boruvka and A.W. Neumann, *J. Colloid Interface Sci.*, **93**, 169 (1983).
11. P.K. Weissenborn and R.J. Pugh, *Langmuir*, **11**, 1422 (1995).

## **Chapter 8**

## **Conclusions**

## 8.1 Summary

The pursuit of different and hopefully better methods to obtain chemical information from solutions is an ongoing process. There are countless techniques which exist and are accessible to the analytical chemist in order to obtain this information. The fact that there exist so many different techniques is a testament to the fact that there is no one universal technique which is capable of providing the 'ultimate' analysis. The recent development of Electrospray Mass Spectrometry (ES-MS) has ushered in the potential to look at solution speciation from a different vantage point, one giving the possibility of unambiguous determination of solution ions, where both molecular form and oxidation state may be realized.

From the introduction this point was emphasized in particular for inorganic solutions. The solution species could be either metal ions in solvated or complexed form or inorganic molecular ions such as oxo-halides or oxo-sulfur ions. The thesis was then written to explore in some detail the ability of Electrospray to achieve this.

It became obvious from the beginning that in order to interpret the mass spectra recorded from electrospray a clear picture of the sampling process must be obtained, in particular the effect of high pressure collisionally induced dissociation (CID) on the observed mass spectrum. The effect of CID of positive metal ions in solution was discussed in some detail in Chapter 3 highlighting decomposition or fragmentation patterns. Fragmentation of anionic species was described in some detail in Chapters 4 and 5. With a

clear understanding of the sampling process it then becomes easier to interpret the results and analyze their significance.

Chapter 4 of the thesis presents the investigation of chromium solution ions by ES-MS where species of different form and oxidation states were determined. The technique shows great promise especially in the investigation of Cr(VI) species such as chromate and dichromate where molecular ions may be observed directly in the gas phase.

A detailed investigation of an inorganic molecular ion system was presented in chapter 5. In particular a whole range of sulfur species was investigated and it was found that with proper interpretation and selection of conditions they could be determined individually when present in the same solution.

It was felt over the course of this investigation that there were results obtained and aspects of electrospray that were poorly understood and with that in mind more thorough investigations into the fundamentals of electrospray were undertaken. The results of the investigation were presented in Chapters 6 and 7 of the thesis. Chapter 6 was a detailed investigation into the actual spray process and its implication towards general determinations and quantitative work. As well a real understanding of the conditions necessary to achieve a stable 'electrospray' was realized. Chapter 7 although incomplete presents thought on the subject of the differences in the relative ion intensities of various species. This becomes important in assessing the significance of peak intensities of various species. Knowledge of this nature becomes critical when looking at equilibrium species such as chromate and dichromate as discussed in



chapter 4. It would help determine or reflect the significance of relative intensities and so provide a more reliable relation to the actual solution equilibrium concentrations of the various species.

## 8.2 Assessment

From the body of the work, it should have been evident that electrospray could be used to determine solution species quite effectively. The technique is however limited to solution ions and non labile species. As well solution information is less easily obtained from samples of complex matrices where for example a target analyte may be present at trace concentrations in a highly concentrated electrolyte background. It is obvious that electrospray does suffer from numerous shortcomings, all of which can be traced back to the processes involved in generating a stable 'electrospray' or fundamentals of the technique. Some of these problems may be overcome with greater knowledge or awareness of these basic processes at a fundamental level. In particular knowledge of the behavior of ions at a charged interface must be understood especially in terms of their relative affinities for the interface and how differences may influence or affect quantitation. Despite all the shortcomings its usefulness as a technique to generate gas phase ions representative of the solution composition should not be overlooked. A very simple but effective example of this is given below in Fig. 8.1, which is a mass spectrum of a solution containing only dichromate and nitric acid. The nitric acid is present to ensure a equilibrium distribution between chromate and dichromate both

dichromate and nitric acid are present at  $10^{-4}\text{M}$  in acetonitrile. The main anionic solution species that should be present under these conditions are then  $\text{HCrO}_4^-$  and  $\text{Cr}_2\text{O}_7^{2-}$  and  $\text{NO}_3^-$ . Figure 8.1 exhibits this quite effectively where the spectrum is essentially bare except for these species. This type of information cannot be obtained by other energetic or destructive techniques such as ICP-MS and it becomes obvious that it is here that ES-MS will find its niche.

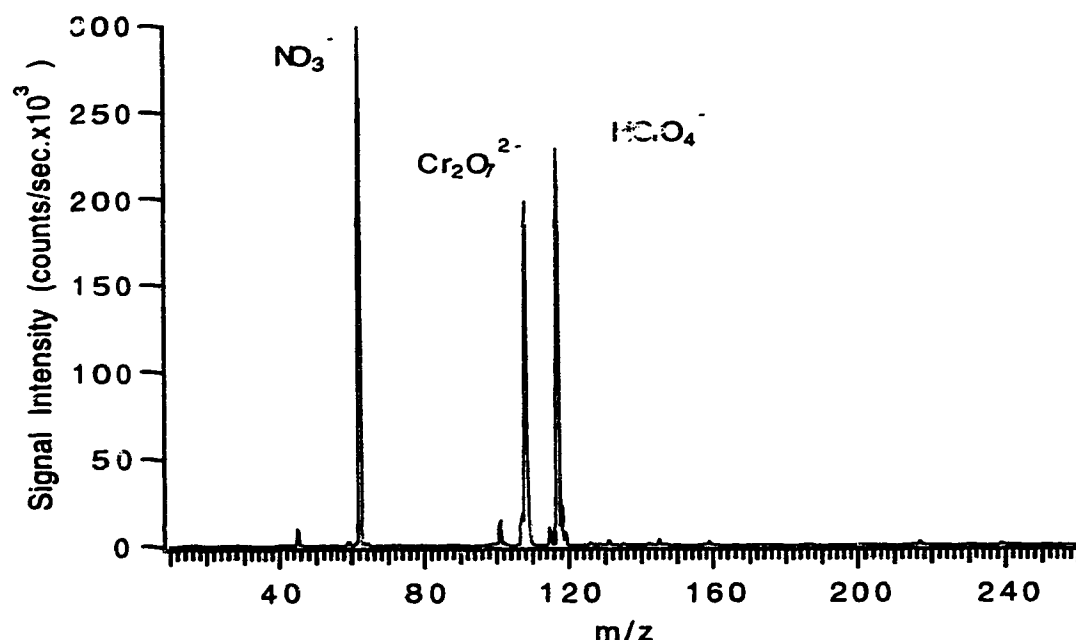


**Figure 8.1** The electrospray mass spectrum of sodium dichromate and nitric acid each  $1.0 \times 10^{-4}\text{M}$  in acetonitrile.

### 8.3 Future Improvements and Recommendations

As of the beginning of these investigations there were numerous modifications to the instrumentation and operating systems. They entailed modification of the ion optics as well the placement of a plenum chamber on the front end, both of which are described in

some detail in chapter 2. In terms of further improvements the changing of the front end ion optics to an rf quadrupole rather than electrostatic lens system would be more suited to the electrospray source. As well improvements in the electrospray needle in terms of plumbing and design could be achieved to yield more reproducible and stable signals, the need for a well constructed needle or capillary tip was illustrated in chapter 6. Perhaps one of the greatest improvements will come through fundamental studies not directly related to the actual electrospray process. One of the biggest problems and perhaps most frustrating as a result of its contradictory nature is the fact that electrospray is being used to probe the solution chemistry however its effectiveness cannot be fully realized because the initial solution chemistry is little understood or poorly characterized. This is especially true when considering various equilibria in a given electrospray solvent rather than water. As well to what degree do interfacial phenomena affect the observed relative ion intensities observed. It does seem obvious and unfortunate that the chemistry must first be known before it may be properly understood.